An Integrated Metabolic Model for Microbial Internal Carbon Driven Post-Anoxic Biological Nutrient Removal

A Thesis

Presented in Partial Fulfillment of the Requirements for the

Degree of Master of Science

with a

Major in Civil Engineering

in the

College of Graduate Studies

University of Idaho

by

Jason James Mellin

Major Professor: Erik R. Coats, P.E., Ph.D.

Committee Members: James Moberly, Ph.D.; Richard Nielsen, Ph.D., P.E.

Department Administrator: Patricia J. S. Colberg, Ph.D., P.E.

August 2017

Authorization To Submit Thesis

This thesis of Jason James Mellin, submitted for the degree of Master of Science with a major in Civil Engineering and titled "An Integrated Metabolic Model for Microbial Internal Carbon Driven Post-Anoxic Biological Nutrient Removal," has been reviewed in final form. Permission, as indicated by the signatures and dates given below, is now granted to submit final copies to the College of Graduate Studies for approval.

Major Professor _____Date_____
Erik R. Coats, P.E., Ph.D.

Committee Members _____Date_____
Richard Nielsen, Ph.D., P.E.

_____Date_____
James Moberly, Ph.D.

Department Administrator _____Date_____
Patricia J. S. Colberg, Ph.D., P.E.

Abstract

Conventional post-anoxic denitrification can produce lower effluent nitrate concentrations than preanoxic configurations, but at the expense of either large tank volumes (associated with endogenous decay) or external carbon substrate addition such as methanol. Recent research has indicated that when post-anoxic denitrification is coupled with EBPR, the denitrification process can be driven by glycogen and PHA carbon polymers stored within the cells of denitrifying bacteria, thereby eliminating the need for carbon substrate addition. Moreover, denitrification kinetics are enhanced vs. endogenous decay. Collectively, very low effluent ammonia, nitrate, and phosphorous concentrations are achievable. A metabolic model is developed to simulate this internal carbon driven post-anoxic EBPR process (hereby termed Biopho-PX) with specific focus on anoxic glycogen degradation and evaluation of the overall model through lab scale and pilot scale testing on municipal wastewater.

Acknowledgments

I would like to thank my major professor, Dr. Erik Coats, for his untiring assistance and excellent mentoring during this endeavor. I would also like to thank my committee members, Dr. James Moberly and Dr. Richard Nielsen, for their input and for providing valuable insight regarding potential directions for future work. Special thanks need to go to my lab mates, especially Felicity Appel, Derek Probst, Ben Carleton, and Eric Huges, for their assistance, company, and patience. Finally, of course, I can't thank my wife, Joanna, enough for her love and support through this adventure.

Dedication

For Mary

Table of Contents

List of Tables

List of Figures

Abbreviations

AE	aerobic
AMO	*ammonia monooxygenase*
AN	anaerobic
AOB	ammonia oxidizing bacteria
ASM	activated sludge model
ATP	adenosine triphosphate
AX	anoxic
BNR	Biological Nutrient Removal
BOD	biochemical oxygen demand
COD	chemical oxygen demand
dGAO	denitrifying glycogen accumulating organism
DO	dissolved oxygen
dPAO	denitrifying phosphorus accumulating organism
EBPR	enhanced biological phosphorus removal
ED	Entner-Doudoroff
EMP	Embden-Meyerhof-Parnas
EPA	Environmental Protection Agency
FAD	flavin adenine dinucleotide (oxidized form)
$FADH_2$	flavin adenine dinucleotide (reduced form)
GAOs	glycogen accumulating organisms

G6P	glucose-6-phosphate
GTP	*guanosine triphosphate*
HAc	acetic acid
HRT	hydraulic residence time
IR	internal recycle
ITP	*inosine triphosphate*
IAWPRC	International Association on Water Pollution Research and Control
IWA	International Water Association
MLE	Modified Ludzack Ettinger
MLSS	mixed liquor suspended solids
Nap	*nitrate reductase* (periplasmic)
Nar	*nitrate reductase* (membrane bound)
NAD^+	nicotinamide adenine dicnucleotide (oxidized form)
$NADH_2$	nicotinamide adenine dicnucleotide (reduced form)
$NADP^+$	nicotinamide adenine dicnucleotide phosphate (oxidized form)
$NADPH_2$	nicotinamide adenine dicnucleotide phosphate (reduced form)
Nir	*nitrite reductase*
NOB	nitrite oxidizing bacteria
Nor	*nitric oxide reductase*
Nos	*nitrous oxide reductase*
OHOs	ordinary heterotrophic organisms
PAOs	phosphorus accumulating organisms
PEP	phoenolpyruvate

PHA polyhydroxyalkanoate

PHB poly-β-hydroxybutyrate

PHV poly-β-hydroxyvalerate

PH2MV poly-β-hydroxy-2-methylvalerate

Pit phosphate inorganic transporter

polyP polyphosphate

PQQ pyrroloquinoline quinine

Pst phosphate specific transporter

qPCR quantitative polymerase chain reaction

RAS return activated sludge

redox oxidation-reduction

SBR sequencing batch reactor

SDNR specific denitrification rate

SFE standard free energy

SRT solids retention time

TCA tricarboxylic acid cycle (citric acid cycle)

TUDP Technical University of Delph Phosphorus (activated sludge model)

VFA volatile fatty acid

WAS waste activated sludge

WRRF water resource recovery facilities

Nomenclature

C	number of carbon atoms in biomass
C-mol	carbon mole
$COD_{inf.sol}$	soluble influent COD
$COD_{eff.sol}$	soluble effluent COD
$COD_{inf.tot}$	total unfiltered influent COD
C_x	active biomass concentration
e^-	electron
f_{gly}	fraction of glycogen to active biomass
f_{eo}	fraction of electrons going to energy production
f_{so}	fraction of electrons going to cells
K	half-saturation coefficient, ATP requirement for biomass synthesis, electron transfer efficiency for catabolic reaction, limit of population
MW_x	molecular weight of biomass
m_{ATP}	ATP requirement for maintenance
m_{pha}	maintenance coefficient on PHA
m_s	specific rate of substrate degradation for maintenance
m_x	specific rate of biomass degradation for maintenance
P	phosphorus, population
P/O	ATP produced per mole of $NADH_2$
pH_{in}	pH inside the cell
pH_{out}	pH outside the cell
r_{atp}	ATP conversion rate
r_{g6p}	glucose-6-phosphate conversion rate
r_{gly}	glycogen conversion rate
r_{h2o}	water conversion rate
r_{no3}	nitrate conversion rate

r_{o2}	oxygen conversion rate
r_{phb}	PHB conversion rate
$r_{p.in}$	phosphate inside the cell conversion rate
$r_{p.out}$	phosphate outside the cell conversion rate
r_{pp}	polyphosphate conversion rate
r_s	substrate conversion rate
r_x	biomass conversion rate
Y_{ATP}	yield coefficient for biomass cells on ATP
$Y_{gly,pha}$	yield coefficient for PHA on glycogen
$Y_{pha,x}$	yield coefficient for biomass on PHA
$Y_{pha,pp}$	yield coefficient for polyphosphate on PHA
$Y_{pha,gly}$	yield coefficient for glycogen on PHA
$Y_{pp,pha}$	yield coefficient for PHA on polyphosphate
Y_{sp}	yield coefficient for product p on substrate s
Y_{sx}	yield coefficient for biomass x on substrate s
$Y_{x,gly}$	yield coefficient for glycogen per biomass
$Y_{x,pp}$	yield coefficient for polyphosphate per biomass
α_1	amount of ATP required for uptake of 1 mole of acetate accross the cell membrane
α_2	ATP produced from 1 mole of polyphosphate hydroloyzed
α_3	ATP required to synthesize 1 mole of polyphospahte
α_m	ATP required for synthesis of biomass monomers on G6P
α_x	ATP required for polymerization of biomass monomers
$\Delta G_a^{0'}$	SFE for electron acceptor reduction
$\Delta G_{\mathrm{ATP.HYD}}^{0'}$	SFE for ATP hydrolysis and cell yield on ATP
$\Delta G_{cells}^{0'}$	SFE for synthesis of biomass macromolocules
$\Delta G_{\mathrm{CS}}^{0'}$	Gibbs energy for carbon source oxidation
$\Delta G_d^{0'}$	SFE for electron donor oxidation

$\Delta G_p^{0'}$	Gibbs energy for conversion of carbon source to pyruvate
$\Delta G_r^{0'}$	SFE for overall redox reaction
$\Delta G_{syn}^{0'}$	SFE for synthesis of biomass cells
δ_o	ATP produced per mole of $NADH_2$ with oxygen as the electron acceptor
δ_n	ATP produced per mole of $NADH_2$ with nitrate as the electron acceptor
ϵ_o	Amount of phosphate uptake per $NADH_2$ oxidized in an aerobic environment
ϵ_n	Amount of phosphate uptake per $NADH_2$ oxidized in an anoxic environment
η	CO_2 released from synthesis of one C-mol biomass
γ_{nadh}	degree of reduction of $NADH_2$
γ_s	degree of reduction of substrate
γ_x	degree of reduction of biomass w/NH_3 as N source
$\gamma_{x.\varphi}$	degree of reduction of biomass w/NO_3 as N source
κ	electron transfer efficiency for biomass synthesis
σ_c	average carbon fraction of biomass
μ	biomass specific growth rate
ν_i	internal flux rate for metabolite i

Note: Model state variables, stoichiometric parameters, and kinetic parameter definitions are presented in Appendix A.

Chapter 1: Introduction

Municipal wastewater contains high concentrations of organics and nutrients that need to be removed in order to protect public health and the environment prior to its discharge into the water environment. Spurred by a federal shift in water quality regulations, recent years have seen regulatory authorities require many communities to remove constituents, particularly the nutrients nitrogen and phosphorus, to extremely low limits, in order to provide greater protection of receiving water bodies. Increased treatment requirements demand the expansion of existing treatment processes and greater energy input into the treatment train. This has required many communities to increase expenditures of capital, operational, and maintenance resources to meet these new effluent discharge limits, placing a significant strain on their finances.

In the face of strict wastewater treatment limits, many communities are struggling. The ability to produce clean water in a sustainable way, while minimizing energy and financial costs, is clearly imperative and much work has been undertaken to develop systems that realize this aim. One class of treatment systems that takes a sustainable approach to treatment and that has been proven in many full scale applications is a class of systems termed Biological Nutrient Removal (BNR). BNR systems leverage the metabolisms of microorganisms within bioreactors to remove organics and nutrients from the wastewater. The post-anoxic denitrification process is one example of a BNR system. A schematic of this process is presented in Section 2.3.5 where the process is described in more detail. This process consists of an aerobic bioreactor followed by an anoxic bioreactor (which has no dissolved oxygen but significant levels of nitrate in solution). Within the aerobic reactor, nitrifying bacteria convert ammonia nitrogen to nitrate. In the anoxic zone, denitrifying bacteria convert the nitrate to nitrogen gas which off-gases to the atmosphere, thereby removing nitrogen from the system. In this process, organics within the wastewater are depleted by the microorganisms within the aerobic reactor. With no carbon remaining in solution to feed the denitrifying metabolism of the denitrifiers in the anoxic reactor, the denitrifiers must rely upon their endogenous metabolism. This results in much lower denitrification rates and impractically large bioreactor volumes to obtain adequate nitrogen removal from the system. In practice, an external carbon substrate is almost always added to the anoxic reactor to achieve sufficiently high denitrification rates and maintain reasonable

anoxic tank volumes.

Another type of BNR system, termed enhanced biological phosphorus removal (EBPR), uses an anaerobic bioreactor followed by an aerobic and/or an anoxic bioreactor, depending on the specific type of system employed. The anaerobic bioreactor induces the required metabolisms of phosphorus accumulating organisms (PAOs) necessary to achieve EBPR. In the aerobic and anoxic zones of EBPR systems, PAOs uptake phosphorus from bulk solution into their cells. Subsequent removal of a portion of these phosphorus rich PAOs from the system results in a net removal of phosphorus from the wastewater.

Recent research has shown that when post-anoxic denitrification is coupled with EBPR, the denitrification process appears to be driven by glycogen and polyhydroxyalkanoate (PHA) carbon polymers stored within the cells of the denitrifying bacteria, thereby eliminating the need for carbon substrate addition in the anoxic reactor.[12,48,106,113] This process has been shown to produce denitrification rates significantly greater than typical endogenous denitrification rates while producing very low effluent ammonia, nitrate, and phosphorus concentrations. The objective of the research presented in this thesis was to examine this process in more detail and to produce a metabolic model that can be used to simulate the observed internal carbon driven denitrification process for the purposes of process optimization and design.

Chapter 2: Background

2.1 Effects of Excess Nitrogen and Phosphorus on Surface Water

Untreated municipal wastewater contains organics, nutrients (nitrogen and phosphorus), pathogens, and a variety of other constituents that can be detrimental to public health, if the wastewater is discharged to the environment without treatment. Furthermore, when untreated wastewater is discharged to a receiving water body, aerobic heterotrophic microorganisms will degrade the organics for energy and growth, using dissolved oxygen (DO) within the water in the process. This can decrease the DO in the waterbody and create a significant threat to aquatic life.

Beyond impacts associated with organics, extensive surface water degradation by advanced eutrophication can occur in the presence of excess nitrogen and phosphorous. The excess of these nutrients can dramatically increase the growth of nuisance organisms, such as algae and cyanobacteria, within the water body. When this organic matter decays, it can cause a depletion of dissolved oxygen and a release of toxic constituents and phosphates that were previously bound in sediments, which in turn increases the mortality of aquatic life.[9] Eutrophication can also pose a threat to human health through the production and release of cyanotoxins by cyanobacteria which then enter drinking water supplies.[9,85] While water bodies are naturally eutrophic, many waters realize advanced, or accelerated eutrophication, due to human activity. This occurs principally by nutrients entering the water body by way of agricultural runoff and water resource recovery facilities (WRRF), formally known as wastewater treatment plant, discharges. Surface water quality deterioration by eutrophication is both a global and a local issue. Examples of algae blooms caused by eutrophication within the Pacific Northwest are shown in Figure 2.1.

In addition to contributing to eutrophication, high aquatic concentrations of nitrogen can result in additional undesirable consequences. The oxidation of nitrogen in the form of ammonia by autotrophic bacteria will consume oxygen and further contribute to the hypoxia of a water body. Moreover, ammonia is known to be toxic to aquatic life, and the consumption of high levels of nitrogen in the form of nitrate has been identified as causing methemoglobinemia in

(a) Fernan Lake, Kootenai County, ID[1]

(b) Lake Spokane, Stevens County, WA[73]

(c) Odell Lake, Klamath County, OR[72]

(d) Battle Ground Lake, Clark County, WA[74]

Figure 2.1: Examples of eutrophication in the Pacific Northwest

infants and other negative health effects in humans. For these reasons, a large effort has been expended by public agencies, engineers, and the public in controlling the discharge of excess nitrogen and phosphorus into aquatic ecosystems.

2.2 Nitrogen and Phosphorus Limits on WRRF Discharges

The most common forms of nitrogen in typical domestic wastewater are ammonium (60%) and organic nitrogen (40%).[107] Ammonium (NH_4^+) is the protonated form of ammonia which is in equilibrium with free ammonia (NH_3) in solution. At a pH of 7, virtually all of the ammonia is in the ammonium form with the equilibrium shifting toward greater free ammonia concentration with increasing pH. Nitrate concentrations in domestic wastewater are typically insignificant, although some industrial effluent streams contain appreciable amounts of nitrate. Organic nitrogen is largely composed of amino groups (NH_2^-) such as arise from amino acids

and proteins and which are easily biologically degraded to ammonium.[107] Phosphorus exists in wastewater in the forms of orthophosphates and organic phosphate. Depending upon pH, orthophosphates will exist as H_3PO_4, $H_2PO_4^-$, HPO_4^{2-}, or PO_4^{3-}. Sources of organic phosphorus include organic phospholipids and nucleotides.[107]

Nitrogen and phosphorus concentration limits in WRRF discharge streams are regulated based on the existing water quality and associated beneficial uses designation of the receiving waters. Stricter limits are placed on discharges to receiving waters of low water quality and on effluent streams intended for indirect or direct reuse applications. In addition, the regulation of nutrients in wastewater has traditionally been based on the concept that controlling the limiting nutrient available in the receiving waterbody will reduce the availability of this nutrient to plant life, thereby reducing the growth of organic matter in the system and preventing eutrophication.

While nitrogen and phosphorus are both needed to support organic growth, the control of phosphorus has received a greater emphasis in the past by many regulators as it was believed to be the limiting nutrient that controls eutrophication and algae blooms in fresh waters. This belief was due, in part, to the ability of many cyanobacteria to fix nitrogen from the atmosphere. There is evidence, however, that nitrogen fixation does not completely make up the total amount of nitrogen required for growth in many aquatic systems and that nitrogen can be a limiting nutrient in many areas. In addition, nitrogen and phosphorus concentrations can vary significantly across the same watershed and the diverse variety of aquatic plants and flora in surface waters have different nitrogen and phosphorus requirements for growth. Due to these reasons, the U.S. Environmental Protection Agency (EPA) currently advocates the regulation of both nitrogen and phosphorus in WRRF discharges to protect receiving waters.[96]

Nevertheless, given that phosphorous levels below 0.1 mg/L have been shown to produce cyanobacteria blooms[9] and that even low levels of phosphorus can contribute toward low dissolved oxygen in fresh waters, regulatory limits for phosphorus concentrations in WRRF discharges are becoming increasingly strict in many areas in order to provide greater protection to receiving waters. Within the U.S., several WRRF discharge limits have reached as low as 0.05 mg/L.[94] Consistently achieving effluent phosphorus concentrations at this level currently requires the addition of chemicals to precipitate phosphorus from the wastewater, which can

significantly increase the cost of treatment. This issue is impacting not only WRRF facilities across the country, but local facilities as well. Table 2.1 lists several WRRF facilities within the state of Idaho which have recently had low phosphorous discharge limits imposed on their discharge streams.

Table 2.1: Idaho WRRF facilities with low phosphorus limits.

WRRF Facility	Avg. Monthly Limit	Avg. Weekly Limit	Seasonal Avg. Limit[a]
Boise, Lander St.	0.07 mg/L	0.931 mg/L	-
City of Coeur d'Alene	-	-	0.076 mg/L at 6 mgd
HARSB[b]	-	-	0.066 mg/L at 2.4 mgd
City of Moscow	0.136 mg/L	0.27 mg/L	-
City of Plummer	0.050 mg/L	0.131 mg/L	-
City of Post Falls	-	-	0.076 mg/L at 5 mgd

[a] February 1 to October 31
[b] Hayden Area Regional Sewer Board

Several of the WRRF facilities listed in Table 2.1 are facilities that serve small communities and therefore have limited resources and funds to implement extensive treatment regimes. The development of low cost, sustainable treatment systems that can meet these new low phosphorus discharge limits and be incorporated by small facilities is imperative. BNR systems can help to fill this need in many instances. When properly incorporated, BNR systems can be less expensive to operate and more environmentally sustainable then traditional physiochemical treatment methods. Indeed, a study by Coats et al. using Environmental Life Cycle Cost Analysis has shown that BNR treatment methods, either alone, or in tandem with traditional physiochemical treatment methods can provide a lower environmental cost then traditional physiochemical methods alone.[13]

2.3 Biological Removal of Nitrogen from Wastewater

2.3.1 Nitrification

Several physiochemical methods can be employed to remove nitrogen from wastewater, including the oxidation of ammonia by chlorine, use of ion-exchange systems, and chemical precipitation of

ammonium from solution. Most commonly, however, engineers employ BNR systems to remove nitrogen from wastewater through the use of the nitrification and denitrification processes.

Nitrogen can be present in wastewater under several different species, according to its oxidation state. The biochemical conversion pathways that are active within BNR processes to convert nitrogen between its different species are shown in Figure 2.2.

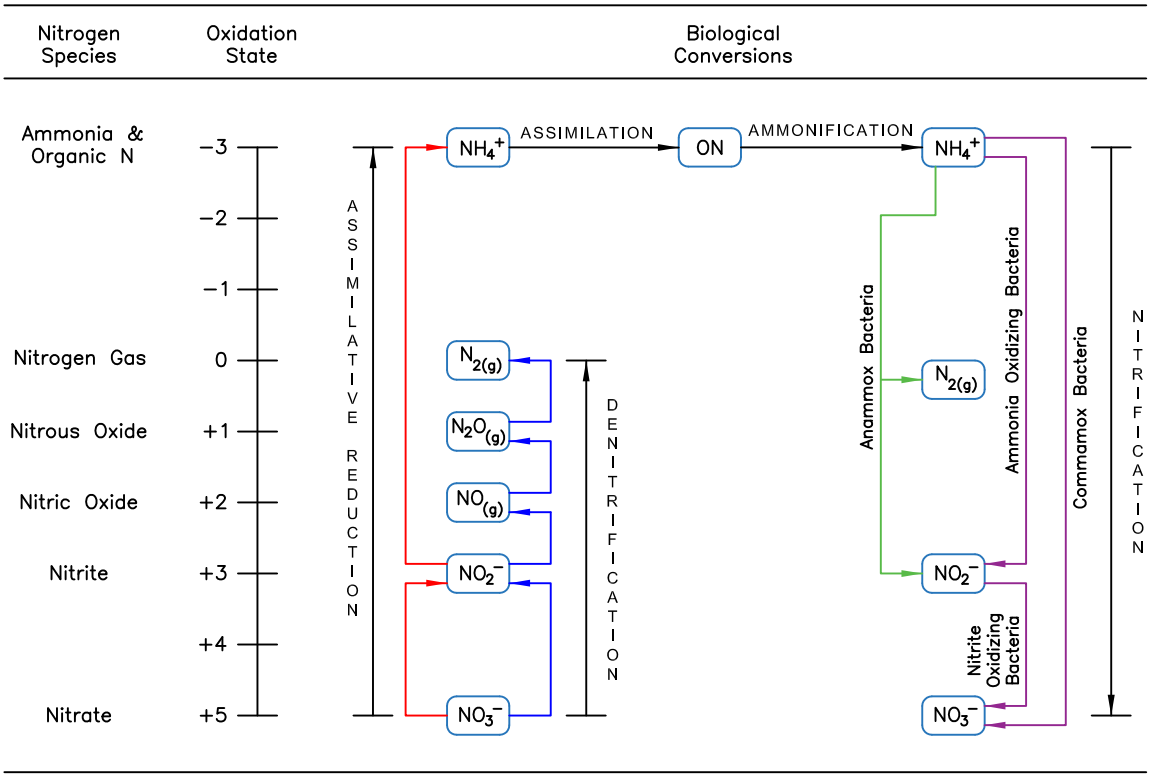

Figure 2.2: Biological conversions of nitrogen within BNR processes (adapted from Water Environment Federation[23] and Grady et al.[29]).

Two-Step Nitrification. Biological nitrification of ammonia to nitrate has conventionally been held to be completed in two separate steps, with each step completed by two different groups of microorganisms. In the first step, ammonia oxidizing bacteria (AOB) oxidize ammonia to nitrite (NO_2) for cellular energy using dissolved oxygen as the terminal electron acceptor. In the second step, nitrite oxidizing bacteria (NOB) use oxygen as the terminal electron acceptor to oxidize nitrite to nitrate (NO_3).

Known AOBs consist of bacteria and archea and exist across several phylogenic genera and

sublineages. The most common AOBs in wastewater treatment are aerobic chemoautotrophs, which use carbon dioxide as their carbon source and oxygen as the terminal electron acceptor. Oxidation of ammonia to an intermediate compound, hydroxylamine (NH_2OH), occurs through a membrane bound enzyme, *ammonia monooxygenase* (AMO). Subsequent oxidation of hydroxylamine to nitrite then occurs through the periplasmic enzyme *hydroxylamine oxidoreductase*. *Ammonia monooxygenase* has been found to have the ability to oxidize other compounds besides ammonia including several organic compounds. This ability opens up intriguing opportunities for alternative uses of AOBs, including the oxidation of methane to methanol, which is commonly used as a carbon source to to drive conventional post-anoxic denitrification processes.[93] While there are many types of AOBs, the AOBs that are perhaps most reported to be active in activated sludge BNR systems are of the genus *Nitrosomonas* and *Nitrosospira* within the *β-proteobacteria* subclass.

The known NOBs are all within the genera *Nitrobacter*, *Nitrospira*, *Nitrococcus*, and *Nitrospina*.[20] NOBs active within wastewater systems are chemoautotrophs which oxidize nitrite to nitrate in a single step. As with AOBs, oxygen is used as the terminal electron acceptor and carbon dioxide as the carbon source for cellular synthesis. The specific enzymes used by each species of NOBs to oxidize nitrite have not been fully elucidated but it is known that *Nitrobacter* of the *α-proteobacteria* subclass oxidizes nitrite through use of the enzyme *nitrite oxidoreductase*.[20] More research into the enzymatic machinery of the other NOB species is needed. Interestingly, early research indicated that *Nitrobacter* were the main NOBs active in wastewater systems but recent research has indicated that *Nitrospira* of the *β-proteobacteria* subclass can be dominant, depending on growth conditions.[94] Again, more research is needed to define the relative contribution of NOB species that prevail under different operating conditions.

AOBs and NOBs can be further classified according to ecological r/K selection theory as either r-strategists or K-strategists. The terms come from the Verhulst model for population growth:

$$\frac{dP}{dt} = rP(1 - P/K) \tag{2.1}$$

Here, r is the population growth rate, P is the population size, and K is the limit of P (the maximum population that can be sustained). The effect of the term $(1-P/K)$ is to introduce a decay, or death rate into the equation which moderates the otherwise unimpeded growth rate of the initial term, rP. As the population size increases, the decay rate predicted by the equation increases. An r-strategist is an organism which places a high priority on growth and reproduction and typically predominates in less dense but unstable environments. K-strategists, on the other hand, place a low priority on growth but are well adapted to living in dense but stable conditions that are close to the population carrying capacity of the environment. The K-strategists have a higher affinity for substrate than r-strategists at low substrate concentrations and will therefore outcompete the r-strategists under this condition. Conversely, r-strategists have a high maximum specific growth rate and an overall higher rate of substrate utilization at high substrate concentrations and will outcompete the K-strategists when substrate concentrations are high. The common AOB *Nitrosospira* and NOB *Nitrospira* are generally considered to be K-strategists while the common AOB *Nitrosomonas Europea* and the NOB *Nitrobacter* are considered to be r-strategists.[94]

Since the nitrifying AOBs and NOBs are autotrophic bacteria that use oxygen as the terminal electron acceptor, the nitrification process must occur within an aerobic environment. The overall reactions for both steps of the nitrification process are shown below:[94]

$$\text{Nitritation:} \qquad 2\,NH_4^+ + 3\,O_2 + 2\,H_2O \longrightarrow 2\,NO_2^- + 4\,H^+ + 2\,H_2O \tag{2.2}$$

$$\text{Nitratation:} \qquad 2\,NO_2^- + O_2 \longrightarrow 2\,NO_3^- \tag{2.3}$$

Incorporating alkalinity and omitting cell synthesis from the reaction, the overall nitrification process can be represented as:

$$NH_4^+ + 2\,HCO_3^- + 2\,O_2 \longrightarrow NO_3^- + 2\,H_2CO_3^- + H_2O \tag{2.4}$$

The reaction produces carbon dioxide, which exists as $H_2CO_3^-$ in the liquid medium. A portion of the carbon dioxide in solution will be incorporated into the cell mass during cell synthesis, which is not shown in the above reaction. Alkalinity is consumed by the hydrogen

atoms liberated from ammonia, which can cause a decrease in pH and a suppression of the nitrification rate. Alkalinity addition to the bulk solution is required if the incoming influent alkalinity concentration is not sufficient to feed the nitrification reaction with enough residual alkalinity to buffer a pH change. Peak nitrification rates are considered to occur within a pH range of 7.5 to 8.0 with nitrification rates dropping significantly as pH declines below 7.0. Generally, maintaining an alkalinity concentration of 50-60 mg/L as $CaCO_3$ in the bulk solution is considered sufficient to maintain a pH of 6.8 or larger in order to sustain reasonable nitrification rates.[94]

Single-Step Nitrification. Recently, the discovery of bacteria that can oxidize ammonia directly to nitrate, a process termed comammox (complete ammonia oxidation), has been reported. Due to the more favorable energetics of this process over two-step nitrification, this speculative bacteria had been theorized to exist for several years and was hypothesized to have a competitive advantage particularly within biofilms and aggregated clusters, such as flocs, which have environments characterized by low substrate incursion and favor low growth rates but high growth yields.[15] This is the type of environment that a K-strategist, such as *Nitrospira*, would find favorable. In 2015, two independent research groups reported their identification of a comammox bacteria in the same issue of the scientific journal *Nature*. Daims et al. enriched an AOB culture over a period of four years which was seeded by a biofilm that was growing on a pipe under flowing hot water in a 1,200 meter deep oil extraction well.[19] The enriched culture contained no known AOBs but contained a bacterium of the genus *Nitrospira* which was found to oxidize ammonium to nitrate. Genomic analysis revealed that the organism's genome contained the genes necessary for ammonia and nitrite oxidation. Moreover, these genes were shown to be expressed during the bacteria's growth on ammonia which was being oxidized to nitrate. The authors subsequently analyzed metagenomic data sets from several engineered systems with floc or biofilm processes and found a relatively high presence of the identified comammox genes for ammonia and nitrite oxidation in several of the locations. Indeed, the presence of comammox in an Austrian nitrifying activated sludge plant was estimated to be between 43% to 71% of the total *Nitrospira* population.

In separate work, Van Kessel et al. obtained an enriched nitrifying culture seeded by a biofilm growing in the anaerobic zone of a trickling filter connected to a recirculating aquaculture system.[97] Two species of the genus *Nitrospira* were found in this culture that could oxidize ammonia directly to nitrate under very low oxygen (<3.1 µM) conditions. Genomic analysis and feeding of the culture with ^{15}N-labeled ammonium verified the comammox metabolism of the identified species. Furthermore, when samples of the culture were fed a fluorescently labeled ammonia analogue that binds to the AMO enzyme, fluorescently labeled *Nitrospira* was subsequently detected, which reinforced the evidence of the presence of a comammox metabolism in the bacteria. Additionally, a search by the authors of existing public sequence databases found evidence that comammox bacteria may have previously been misidentified as nitrite or methane oxidizing bacteria and that the presence of comammox bacteria is likely present within many environments and engineered systems.

The discovery of the existence of comammox opens up a new field of research into our understanding of the nitrification cycle, and many questions remain to be answered such as their specific metabolism, growth kinetics, growth inhibitions, and interactions with other microbial species. Much research will occur in the future into these organisms as their existing and potential contribution to nitrification within the environment and engineered systems such as WRRF facilities is elucidated.

2.3.2 Denitrification

Depending on the quality of the receiving water body, a WRRF may be required to remove a significant portion of the nitrogen present in its process streams prior to discharge into the environment. Nitrogen can completely removed from wastewater through several denitrification processes as explained below.

Ammonification and Assimilation. Nitrogen is primarily present in wastewater in its most reduced state as either ammonia or organic nitrogen. Heterotrophic bacteria within BNR systems act to hydrolyze organic nitrogen within the reactor thereby releasing ammonia into the solution in a process termed ammonification. Ammonification is an important process in

BNR treatment since it liberates nitrogen from organic matter for subsequent oxidation by bacteria, which do not have the ability to oxidize nitrogen in the organic form.[29]

The concentration of ammonia in BNR reactors is also affected by microbial assimilation. Microbial cells assimilate nitrogen, in the form of ammonia, into their cells during cell synthesis, accounting for 10 to 30 percent of nitrogen removal alone in the treatment of domestic wastewater.[94] While most municipal wastewater contains sufficient ammonia to support biological growth, the potential for ammonia depletion in the process stream must be accounted for in the design and operation of the treatment process. In the absence of ammonia, bacteria will reduce available nitrate and nitrite to ammonia for assimilation in a process called assimilative reduction. This process requires a transfer of electrons from carbon substrate to the nitrate/nitrite species in order to reduce nitrogen from an oxidation state of +5 (for nitrate) or +3 (for nitrite) to -3 (for ammonia). The process of reducing nitrate for assimilation effectively reduces the overall energy otherwise available in the system and leads to lower cellular growth yields. These lower yields must be accounted for in the design and operation of systems that have the potential to be depleted of ammonia. It should be noted that some prokaryotes have the ability to reduce nitrogen gas to ammonia for subsequent assimilation into their cellular structure. Most prokaryotes do not have this ability, however, and the assimilation of nitrogen gas is considered to be insignificant in BNR systems.[20,29] While assimilation of nitrogen can provide a significant contribution to the removal of nitrogen from wastewater, other methods must be employed to meet strict WRRF nitrogen discharge limits. The most common method applied is the use of biological denitrification.

Metabolisms of Biological Denitrification. Biological denitrification refers to the biological removal of nitrogen from solution. This occurs primarily through the reduction of the oxidized nitrogen species, nitrate and nitrite, to nitrogen gas. Nitrate and nitrite act as terminal electron acceptors in the denitrifier's respiratory metabolism as the denitrifiers catabolize substrate for energy and growth. In addition to nitrate and nitrite, the other oxidized nitrogen species, nitric oxide and nitrous oxide, can serve as electron acceptors in the process. However, nitrate is the most stable and the most prevalent of the oxidized nitrogen species in the bulk

solution of conventional WRRF denitrification systems and nitrate is generally considered to be the predominant nitrogen species acting as the electron acceptor in these systems. It should be kept in mind, however, that nitrite, nitric oxide and nitrous oxide will also be utilized as electron acceptors when available.

Denitrifying bacteria obtain electrons for transfer to the available electron acceptor by oxidation of either inorganic or organic substrates. A wide variety of microorganisms are capable of performing denitrification, including heterotrophic and autotrophic organisms. The vast majority of denitrifiers in conventional BNR systems are facultative heterotrophs which can oxidize organic carbon substrate with either oxygen or the oxidized nitrogen species as the terminal electron acceptor. The use of oxygen as a terminal electron acceptor produces more energy than the use of oxidized nitrogen, and denitrifiers will preferentially use oxygen when it is available. This can lead to a depression in denitrification rates when DO is present within the anoxic zone.

In an aerobic reactor, the simultaneous presence of DO and oxidized nitrogen species in the same reactor can result in the phenomena of simultaneous nitrification and denitrification if a significant DO concentration gradient exists between the bulk solution and the interior of the microbial flocs. Outside of the floc mass, DO concentrations are highest and nitrifying organisms within the bulk solution can utilize the available DO to oxidize any ammonia present in the solution to nitrate. Within the floc structure, DO concentrations can be significantly lower then the concentrations in the bulk solution. If the DO concentration is sufficiently low within the floc, denitrifying organisms will reduce available nitrate to nitrogen gas. Simultaneous nitrification and denitrification can also be achieved if the bioreactor is operated such that regions of high DO and regions of low DO develop spatially within the reactor. In order to achieve nitrification in these systems, however, WRRFs must be operated at a solids retention time (SRT) significantly larger than that normally required to achieve nitrification. These types of treatment systems can be engineered to achieve simultaneous nitrification and denitrification through the careful design and control of the aeration system.

More conventionally, the denitrification process relies on denitrifying facultative heterotrophic bacteria oxidizing organic carbon substrate in solution in an anoxic reactor. Electrons are trans-

ferred to the electron transport chain where nitrate is reduced through a series of intermediates as follows:[20,94]

$$\underset{\text{nitrate}}{2\,NO_3^-} \xrightarrow{\text{Nar/Nap}} \underset{\text{nitrite}}{2\,NO_2^-} \xrightarrow{\text{Nir}} \underset{\substack{\text{nitric}\\\text{oxide}}}{2\,NO_{(g)}} \xrightarrow{\text{Nor}} \underset{\substack{\text{nitrous}\\\text{oxide}}}{N_2O_{(g)}} \xrightarrow{\text{Nos}} \underset{\text{dinitrogen}}{N_{2(g)}} \tag{2.5}$$

The enzyme *nitrate reductase* transfers electrons to nitrate, which reduces it to nitrite. Depending on the specific denitrifer, *nitrate reductase* is either membrane bound (Nar) or periplasmic (Nap). Denitrifiers contain one of two types of the enzyme *nitrite reductase* (Nir). Both types of the enzyme reduce nitrite to nitric oxide but contain cofactor and structural differences. Following the reduction of nitrite to nitric oxide, the membrane bound *nitric oxide reductase* (Nor) and the periplasmic *nitrous oxide reducatase* (Nos) reduce nitric oxide to nitrous oxide and nitrous oxide to dinitrogen, respectively.[20]

Several aspects of this reaction pathway should be mentioned which have been found to contribute to a WRRF's negative impact on the environment and are currently the focus of ongoing research. Depending on the microbial community and conditions within the denitrifying reactor, the process may not always proceed to dinitrogen, and considerable nitric oxide and nitrous oxide may be produced.[20] The production and release of nitric oxide and nitrous oxide from a WRRF can be problematic. Nitric oxide is quickly converted to the toxic pollutant nitrogen dioxide in the atmosphere while nitrous oxide has been identified as a potent greenhouse gas. In fact, nitrous oxide is estimated to be 300 times more potent than carbon dioxide.[94] In addition to production during denitrification, nitrous oxide is also produced by AOBs in the oxidation of ammonia. The total production of nitrous oxide from wastewater treatment is potentially considerable. Indeed, in 2006, WRRFs were estimated to contribute three percent of the total amount of global nitrous oxide emitted.[94] Research is currently ongoing to address the environmental impact of nitrous oxide from wastewater treatment and to identify potential strategies for reducing this impact.

The stoichiometry of the denitrification process depends on the specific carbon substrate oxidized. If the common assumption that wastewater is composed of the elements $C_{10}H_{19}O_3N$ is invoked, denitrification can be described by the following equation:[94]

$$C_{10}H_{19}O_3N + 10\,NO_3^- \longrightarrow 5\,N_2 + 10\,CO_2 + 3\,H_2O + NH_3 + 10\,OH^- \quad (2.6)$$

In the denitrification process, approximately 3.57 grams as $CaCO_3$ of alkalinity is produced per gram of nitrate reduced. This partially offsets the 7.14 grams of alkalinity as $CaCO_3$ consumed in the oxidation of ammonia to nitrate in the nitrification process. For this reason, it is common for a BNR system to include denitrification in the design even if nitrate is not specifically required to be removed from the discharge stream. To take advantage of the alkalinity created in the denitrification zone, a preanoxic denitrification process configuration is commonly employed, as will be described later.

2.3.3 Nitritation and Denitritation

When incorporating BNR, a large portion of a WRRF's energy expenditure consists in providing aeration for carbon oxidation and nitrogen removal. The nitritation and denitritation processes have been shown to be able to provide significant aeration savings for certain BNR process streams. In the nitritation process, nitrification can be intentionally interrupted after the oxidation of ammonia to nitrite, through careful control of DO and other operating conditions within the reactor. Microbial denitritation can then be utilized to reduce nitrite to nitrogen gas. The process, also referred to as shortcut nitrogen removal, is illustrated in Figure 2.3 which compares the process schematically to the conventional nitrification/denitrification processes.

Shortcut nitrogen removal has been used effectively to treat wastewater streams with high ammonia concentration (above 100 mg-N/L), such as anaerobic dewatering effluent streams, and requires less oxygen and carbon substrate than the use of conventional nitrification and denitrification.[29] As shown in Figure 2.3, 8 electrons are transferred from ammonia to oxygen when it is oxidized to nitrate. In the nitritation process, ammonia is oxidized to nitrite, which only requires the transfer of 6 electrons. This results in 3/4 of the electrons transferred and a 25% savings in the oxygen required to oxidize ammonia when nitritation/denitritation is employed. Similarly, denitrification requires the transfer of 5 electrons from the carbon substrate

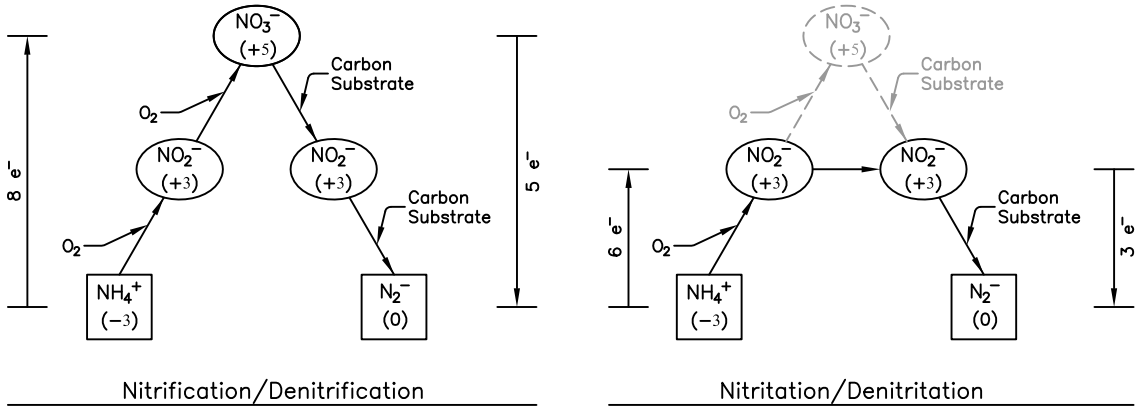

Figure 2.3: Schematics of the nitrification/denitrification and nitritation/denitritation processes. Oxidation state is shown with the species name. Number of electrons (e^-) transferred is shown adjacent to each transformation (adapted from Daigger[18])

to nitrate as nitrate is reduced to dinitrogen gas. Nitrite reduction only requires the transfer of 3 electrons from the carbon substrate. This results in only 60% of the electrons required for reduction of nitrite to nitrogen gas compared to the reduction of nitrate to nitrogen gas. A 40% savings in the amount of carbon substrate required for nitrogen removal is therefore realized.

As Diagger notes, however, while oxygen savings are realized and less carbon is required in shortcut nitrogen removal, no savings in oxygen will be realized if the carbon substrate that was saved is required to be subsequently oxidized in the treatment system (to meet effluent BOD requirements, for instance).[18] This can be seen by noting that the net change in the oxidation state of nitrogen is the same when ammonia is oxidized to nitrogen gas through either nitrification/denitrification or nitritation/denitritation. Referring to their oxidation states, it is noted that when nitrite is oxidized to nitrate, 2 electrons are required to be transferred to oxygen and when nitrate is reduced to nitrite, 2 electrons are required to be transferred from the carbon substrate. Therefore, the oxygen saved in nitritation is the same amount of oxygen required to oxidize the carbon substrate that was saved by employing denitritation.

If the carbon substrate that would be saved can be diverted upstream of the biological process in a sidestream to be beneficially utilized in another process (e.g. for anaerobic conversion to biogas), then the oxygen saved by the nitritation/denitritation process can be fully achieved. Additionally, a direct benefit can be realized by employing the nitritation/denitritation process in a post-anoxic denitrification configuration. These systems almost always require the

addition of carbon substrate to the post-anoxic reactor since a large portion of the influent carbon substrate is oxidized with the ammonia in an upstream aerobic zone. By employing nitritation/denitritation, less carbon substrate is required to reduce the oxidized nitrogen to nitrogen gas which will correspondingly reduce the amount of carbon substrate required to be added to the post-anoxic reactor. Additionally, the reduced oxygen required in the nitritation process allows for smaller aeration rates to be applied to the aerobic reactor. This can lead to easier control and optimization of aeration rates and less oxygen wasted through over aeration and savings in the plant's aeration costs.

2.3.4 Anammox

A significant discovery occurred in the 1990s with the identification of a class of AOBs termed anammox (anaerobic ammonium oxidation) bacteria, which have the ability to anaerobically oxidize ammonia directly to nitrogen gas with nitrite as the electron acceptor, thereby providing substantial savings in aeration costs. Anammox bacteria are autotrophic and their ability to fix carbon from CO_2 also results in a significant reduction in carbon substrate required for the removal of nitrogen from the wastewater. Their practical use in mainstream wastewater treatment is currently limited, however, due to their slow growth characteristics among other challenges. In addition, their use has not been shown to provide a vast improvement in effluent nitrogen over conventional denitrification systems. Anammox systems have principally found successful application in the treatment of wastewater streams with high concentrations of ammonia such as found in filtrate from dewatered digester sludge. Research is ongoing to expand the use of anammox to conventional wastewater streams and advances in this area may occur as more knowledge is gained.

2.3.5 Conventional Preanoxic and Post-Anoxic Denitrification

Conventional Preanoxic Denitrification. Most common denitrification processes use preanoxic configurations in which an anoxic reactor is placed upstream of an aerobic reactor as shown in Figure 2.4

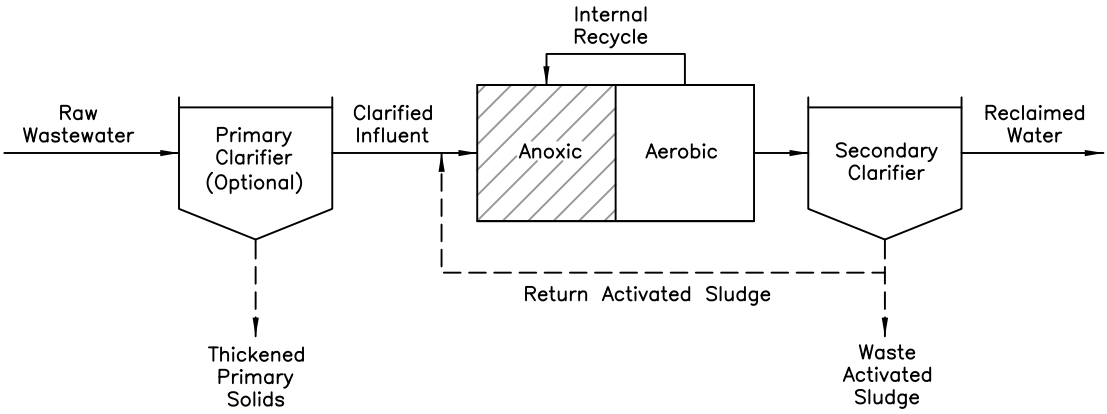

Figure 2.4: Preanoxic denitrification process schematic.

Figure 2.4 is a schematic of the Modified Ludzack Ettinger (MLE) process, which is the most common type of preanoxic process employed. Within the downstream aerobic reactor of this process, AOBs oxidize ammonia within the bulk solution to nitrite and NOBs oxidize nitrite to nitrate. An internal recycle (IR) stream high in nitrate is pumped from the aerobic reactor to the upstream anoxic reactor. Within the anoxic reactor, denitrifying bacteria reduce nitrate to nitrogen gas, using readily biodegradable organic carbon in the incoming influent as the electron donor and nitrate as the electron acceptor. The IR pumping rate controls the amount of nitrate entering the anoxic zone and thus controls the amount of nitrogen that can be removed in the system. Maximum practical IR pumping rates are generally limited to approximately 400% of the influent flow. As noted by Grady et al., feasible pumping rates limit nitrogen removal within MLE preanoxic systems to 60% to 85% of the influent nitrogen concentration.[29]

Conventional Post-Anoxic Denitrification. While preanoxic denitrification configurations are most often used in WRRFs, post-anoxic designs are also employed to provide greater nitrate and total nitrogen removal. A conventional post-anoxic denitrification configuration is shown in Figure 2.5.

Influent flows into the upstream aerobic reactor, where ammonia is oxidized to nitrite and then to nitrate. Nitrate-rich effluent flows from the aerobic reactor into the downstream anoxic reactor, where denitrifying bacteria reduce nitrate to nitrogen gas; denitrifiers quickly consume any remaining carbon substrate to provide reducing equivalents and energy to drive their

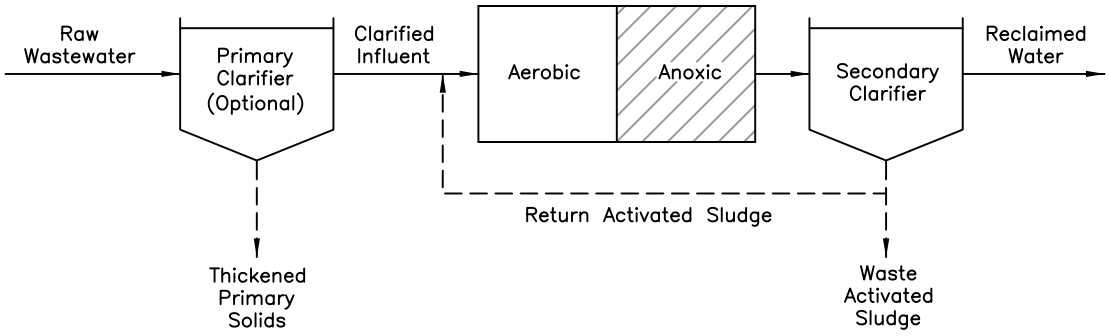

Figure 2.5: Post-anoxic denitrification process schematic.

metabolisms. In the absence of available exogenous carbon substrate, the denitrifiers will engage in endogenous respiration to drive their metabolism, which results in a substantially lower specific denitrification rate (SDNR) than obtained when external carbon substrate is available. Typical post-anoxic SDNRs relying on endogenous decay are 3 to 6 times lower than SDNRs experienced in preanoxic systems.[94] The resultant large anoxic volumes required to obtain adequate denitrification under the low SDNRs experienced under endogenous respiration can inhibit the nitrifying ability of the biomass and are often unfeasible for typical facilities. Due to this, external carbon substrate (typically methanol) is almost always added to the anoxic basin to increase the SDNR and to reduce the required size of the anoxic basin.[106] While the addition of carbon substrate increases the cost of operation of a post-anoxic system, these types of systems have the benefit of achieving substantially greater nitrogen removal then preanoxic configurations. In a post-anoxic configuration all of the nitrate produced in the aerobic zone flows to the anoxic reactor. Given an adequate reactor volume and carbon substrate, the system is theoretically able to achieve complete denitrification, and thus near-complete nitrogen removal. Practical limits to the size of the anoxic reactor and the cost of adding external carbon will limit the achievable effluent nitrogen concentration in a particular system, however.

Four-Stage Bardenpho Process. The four-stage Bardenpho process, developed in South Africa, adds a post-anoxic zone to an MLE configuration, as shown in Figure 2.6. The process is used to achieve lower effluent nitrate concentrations than can be obtained with the MLE process alone. Denitrification in the post-anoxic tank can be driven by endogenous decay or an external carbon source can be added. In addition, an aerobic tank is added at the end of

the process to polish the treated wastewater prior to its discharge to the clarifier. This step is used to prevent denitrification of the remaining nitrate from occurring in the clarifier which can upset the settling characteristics of the clarifier as nitrogen gas bubbles rise up through the clarifier contents. Typically, greater than 75% of the influent nitrate is removed prior to the wastewater entering the post-anoxic tank with final effluent nitrogen concentrations of 3 mg/L achievable.[94] The system has the disadvantage of requiring a larger overall tank volume than the MLE and conventional post-anoxic systems.

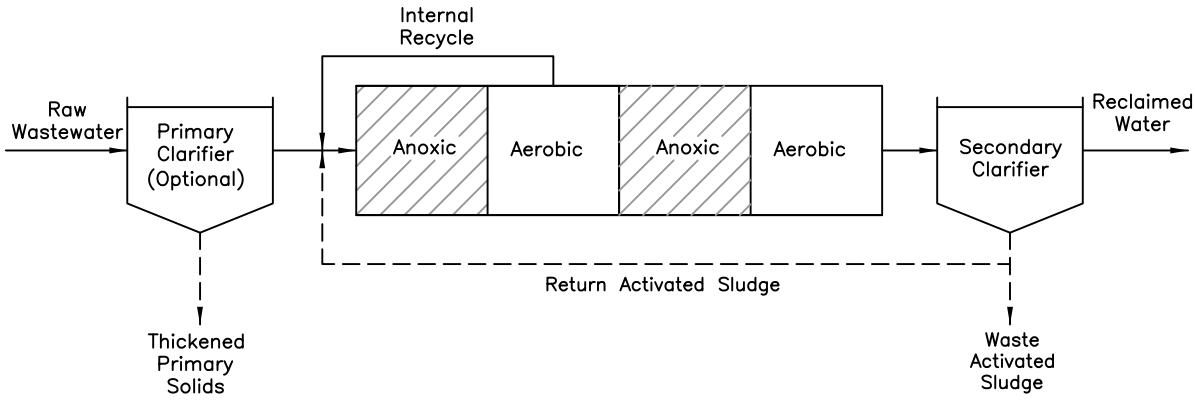

Figure 2.6: Four-stage Bardenpho process schematic.

2.4 Phosphorus Removal from Wastewater

2.4.1 Natural Phosphorus Removal

Biological Assimilation of Phosphorus. Phosphorus is removed from wastewater by several biological means. One important means of removal in biological treatment systems is through biological assimilation. Bacteria in the reactor will uptake phosphorus into their microbial mass to support cellular synthesis and associated metabolisms. In conventional biological treatment systems that are used for stabilization of influent carbon, biological assimilation of phosphorus by ordinary heterotrophic organisms can result in a removal of 10% to 20% of the influent phosphorus.[94]

Microbial Induced Precipitation of Phosphorus. Another mechanism that will remove phosphorus from bulk solution is microbial induced precipitation of phosphorus, mainly in the form of calcium phosphate. This has been hypothesized to occur through three processes, as identified by Baetens:[5]

1. Precipitation of phosphates in an aerated plug flow reactor due to microbial induced changes in pH.
2. Precipitation of phosphates in biofilms due to changes in pH caused by denitrifiers.
3. Anaerobic precipitation of phosphates due to high orthophosphate concentrations in EBPR.

The first such process was described in 1970 by Menar and Jenkins.[65] According to their description, near the inlet of an aerobic plug flow reactor, microorganisms oxidizing carbon substrate will uptake oxygen and release CO_2 resulting in low DO and high CO_2 concentrations near the inlet of the reactor. The high CO_2 concentration causes a drop in the pH of the solution which can cause phosphorus compounds to solubilize. Near the end of the reactor, most of the substrate has been utilized, which results in an increased DO and lower CO_2 concentration. This results in a corresponding rise in the pH of the bulk solution, causing calcium phosphate to precipitate. While the hypothesis is feasible, it should be noted that the work of Menar and Jenkins was based on field observations and lab studies of activated sludge prior to the elucidation of present day EBPR theory. In this regard, the contribution of EBPR to the author's observed decrease in soluble phosphorus concentrations when the sludge transitions from a zone of low DO concentration to a zone of high DO concentration within the reactor is possible. Indeed, the author's observation of very high phosphorus removal at a point 3/4 along the length of a 300 foot aeration basin at the former Rilling Roads treatment facility in San Antonio, Texas is interesting. At this point within the reactor the DO concentration rose from a level of 1.2 mg/L to 5 mg/L with a corresponding large decrease in orthophosphate concentration in the bulk solution. The authors observed that the pH in the reactor ranged from an influent value of 7.3 to an effluent value of 7.9 which they considered to contribute to a precipitation and the observed decrease in phosphorus in solution. As will be discussed

in Section 2.4.3, conventional EBPR theory indicates that phosphorus accumulating organisms will release internally stored phosphate to bulk solution in an anaerobic zone and uptake more phosphorus than originally released in a subsequent aerobic zone. Considering that at a DO value of 1.2 mg/L at the beginning of the reactor, the DO concentration within the floc structure could approach anaerobic conditions prior to being exposed to oxygen as it flows into an area of high DO (where a drop of phosphorus in solution was observed), a contribution of EBPR bacteria to the observed phosphorus removal in this plant cannot be discounted.

The second process of microbial induced precipitation of phosphorus can occur within biofilms supporting denitrification. Here, the denitrification process produces alkalinity which will cause the interior pH of the biofilm to increase with a corresponding precipitation of calcium phosphate.[5] This potential precipitation needs to be accounted for in the design and operation of fixed film wastewater treatment processes such as trickling filters and submerged biofilm reactors.

The third process occurs in the presence of high phosphate and calcium concentrations in solution. Maurer et al. observed precipitation of calcium phosphate at a pH between 7.0 and 8.0 and at phosphorus levels of about 30 mg P/L and calcium concentration of about 60 mg/L.[54] To clarify, typical domestic wastewater influent contains phosphate concentrations on the level of 3.6 mg/L[38] and calcium concentrations on the level of 20 mg/L[54] which are much lower than that observed for the precipitation of phosphorus. Phosphate and calcium concentrations in certain wastewaters may reach these levels, however, particularly within the anaerobic zone of EBPR systems where phosphate is released from phosphorus accumulating organisms. Even so, the overall situation in a treatment system can be complex since a change in conditions (such as pH and calcium activity) within the subsequent aerobic zone of an EBPR system can also redissolve phosphorus.[5]

2.4.2 Chemical Phosphorus Removal

While some natural phosphorus removal will occur as described, WRRFs more commonly achieve phosphorus removal for discharge permit requirements through either chemical or EBPR

processes. Chemical phosphorous removal is typically accomplished by precipitating phosphorous from the wastewater through the addition of metal salts containing aluminum, ferrous iron, ferric iron, or calcium, followed by filtration.[94] Chemical phosphorous removal can consistently provide effluent phosphorous levels below 0.05 mg/L, but the process has the disadvantage of the high cost that comes with chemical addition and the processing of large amounts of sludge with low agronomic value that results from the precipitation process. Several strategies and configurations are employed in the design of chemical phosphorus removal systems which are covered in standard wastewater treatment texts, such as by Tchobanoglous et al.[94]

While chemical phosphorus removal is an important tool that is available for WRRF facilities to achieve strict phosphorus removal limits, the work in this thesis is centered on the modeling of the removal of phosphorus and nitrogen from wastewater in a particular BNR process. An emphasis is therefore placed on understanding the EBPR process over chemical phosphorus removal in the following narrative.

2.4.3 Enhanced Biological Phosphorus Removal: Process and Metabolisms

Phosphorus Accumulating Organisms. The EBPR process leverages the metabolism of certain, potentially unique microorganisms to remove phosphorus from wastewater streams. EBPR is driven by a specific population of chemoheterotrophic microorganisms, termed phosphorous accumulating organisms (PAOs), which will uptake and internally store excess phosphorous from wastewater when they are subjected to an anaerobic environment followed by either an aerobic or anoxic environment. Subsequent removal of a portion of the PAOs with their internal stores of phosphorous through the waste activated sludge (WAS) stream results in the net removal of phosphorous from the system. EBPR does not have the disadvantage of requiring continuous chemical addition or the increased sludge processing that is inherent in chemical phosphorus removal systems. The process is not without disadvantages, however. Full scale EBPR installations are able to produce effluent total phosphorus concentrations in the range of 0.1 to 0.2 mg/L but cannot consistently meet the same very low effluent total phosphorus concentrations that can be obtained by chemical phosphorous removal processes. EBPR is also known to be prone to biological upsets from such causes as dynamic influent

loading, introduction of DO or nitrate into the anaerobic zone of the process, and oftentimes unknown factors.[58] For this reason EBPR facilities are typically designed with the capability to provide chemical phosphorous removal in the event of an upset to the biological process. In addition, EBPR facilities are known to be associated with the precipitation of large amounts of struvite in downstream piping and anaerobic digesters which results in increased operation and maintenance costs.

The underlying metabolism of PAOs is still a subject of much research and debate, despite considerable effort and research that has been performed to elucidate the metabolism of PAOs over the last 20 plus years. Currently, a PAO has not been successively isolated in pure culture and the identification of which specific microorganisms are PAOs remains a subject of controversy. The majority of early studies on PAO cultures identified the dominant PAO as belonging to the genus *Acinetobacter* in the *γ-proteobacteria* class and much EBPR research effort was expended on this organism. Studies using florescent *in-situ* hydridisation (FISH) on 16S rRNA led to the current consensus that *Acinetobacter* in fact contributes little to EBPR. Seviour et al. notes, however, that the current state of knowledge cannot definitively rule out a significant contribution to EBPR by this organism.[85] More recent research has implicated the organism *Canditatus* Accumulibacter phosphatis (*Accumulibacter*) of the subclass 2 *β-proteobacteria* as a potential PAO.[71] The fact that this microorganism has been found to have a significant presence in both lab and full scale EBPR systems adds weight to this claim. Nevertheless, due to the very diverse microbial nature of EBPR sludge and the wide ranging results of numerous PAO microbial studies, it is highly likely that several different types of organisms contribute to the EBPR process as PAOs. Thus, there is still much research that is needed in this area.

Research into the underlying metabolic processes of PAOs has also been wide ranging. Several models have been proposed for PAO metabolisms, and various aspects of these models are still debated in the literature. A review of the literature shows continuing debate on numerous aspects of the PAO metabolism such as the type of transport process(es) used to uptake substrate by the PAO, which glycolytic pathways are active within the cell for generation of ATP and reducing power, the contribution of the TCA cycle in the anaerobic metabolism, and which metabolic pathways or partial pathways are active in the PAO.

PAO Anaerobic Metabolism According to the Modified Mino Model. The majority of conceptual models describing PAO metabolism are largely based on the theorized metabolism initially presented by Arun et al.[4] and which is frequently referred to as the modified Mino PAO model due to Mino's work on elucidating the behavior of intracellular glycogen in PAOs.[66] A schematic showing an adapted version of this model's description of the PAO's anaerobic metabolism is shown in Figure 2.7.

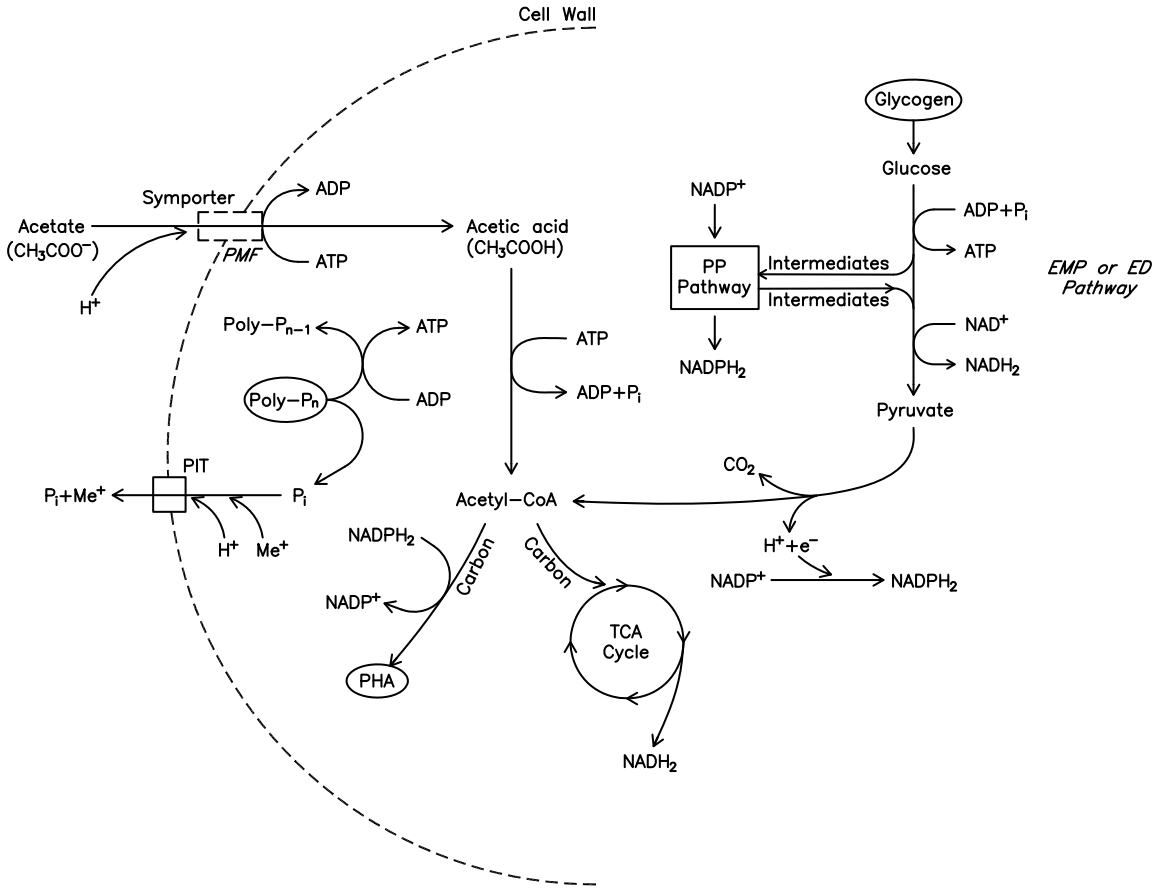

Figure 2.7: PAO anaerobic metabolism (adapted from Grady et al.[29] and Coats[10]).

The modified Mino conceptual model assumes that PAO metabolism is dependent upon an adequate supply of short chain fatty acids (VFAs) within the anaerobic zone. VFAs are largely fermented by non-PAO facultative heterotrophic organisms from readily biodegradable carbon sources within the influent if an adequate anaerobic environment and detention time is available. These conditions are often found in long sewer collection lines or purposely designed into an engineered EBPR system by using an appropriately sized anaerobic reactor. If an adequate

supply of VFAs is not available to support PAO metabolism, supplemental VFAs may be added. A common approach is to ferment primary solids on-site within a separate fermenter in which VFAs can be elutriated and added to the raw wastewater influent stream. Primary solids fermentation generally will produce a mixture of 50% acetate and 30% propionate with the residual being C_4 - C_6 VFAs.[94] Typically, the predominant VFA species in a raw wastewater influent is acetate, generally followed by propionate and butyrate. Since acetate is the most prevalent form of VFA species in wastewater, the vast majority of EBPR conceptual models use acetate as the model substrate and this assumption is adopted in this work. In reality other VFA species are present, and even prevalent, in full scale EBPR plants. In addition, the sludge in full scale plants is composed of mixed microbial communities which may consist of various PAO and PAO competitors (specifically GAOs, see Section 2.4.3) which will affect the rate and amount of VFA sequestration from solution by the PAOs. While these factors will affect the performance of the EBPR process, they can be successfully accounted for in the design of a specific EBPR facility through proper calibration of the design models used.

In an anaerobic zone that is rich in VFAs, PAOs are able to rapidly uptake acetate across their cell membrane using ATP. The exact mechanism used by PAOs to transport substrate across the cell membrane is still debated. Mino et al.[66] and Smolders et al.[89] both found strong evidence that acetate is transported across the cell membrane by an active transport process at the expense of ATP, in contradiction to the passive diffusion process proposed by the competing Comeau/Wentzel model.[14,110] Conversely, several other studies have shown evidence that a passive diffusion or a secondary transport process is the responsible uptake mechanism.[5,71] Nevertheless, once inside the cell, acetate is activated to acetyl-CoA using energy obtained through the hydrolysis of ATP. Acetyl-CoA is used to synthesize the cellular carbon storage polymer polyhydroxyalkanoate (PHA), which is used to store carbon and electrons for later use by the cell. Within the modified Mino model, ATP for acetate uptake and cell maintenance in the anaerobic zone is obtained primarily through the hydrolysis of the PAO's internal polyphosphate storage polymers with some contribution of ATP coming from the degradation of the cell's glycogen storage polymers through either the Embden-Meyerhof-Parnas (EMP) pathway or the Entner-Doudoroff (ED) pathway. Studies of PAO glycogen metabolism have

produced contradictory evidence as to whether the EMP or the ED pathway is used by PAOs in the anaerobic degradation of glycogen and the specific pathway employed remains a subject of controversy. It may be that the specific pathway used is dependent upon the type of PAO.[71] The ED pathway produces less ATP per mole of glycogen degraded which affects the system energy balance and thus the amount of required polyphosphate to be degraded to fuel the metabolism. Therefore, the pathway assumed in modeling the PAO and the EBPR process makes a difference.[58] Further research is required to settle this question. Lastly, the degradation of polyphosphate for ATP production releases orthophosphate and a metal cation, Me^+ (principally K^+ and Mg^{2+}), which are excreted from the cell through a phosphate inorganic transporter (Pit).[10,84] Due to this release, EBPR systems are characterized by relatively high levels of soluble phosphorus within the bulk solution of their anaerobic zones.

Cellular metabolisms primarily function through oxidation-reduction (redox) reactions in which electrons are taken from a substrate and directed through a metabolic pathway to reduce a substance in order to form a product. Due to the ubiquity of redox reactions within cellular metabolisms, a full description of the PAO metabolism requires an accounting of the flow of electrons and their carriers through the principal metabolic pathways. The electron carriers act as reducing agents and therefore are referred to as having reducing power. Bacterial cells contain several different carriers of reducing power, the three most prevalent of which are listed below (abbreviations are listed as oxidized form/reduced form):

1. Nicotinamide adenine dinucleotide: $NAD^+/NADH_2$
2. Nicotinamide adenine dinucleotide phosphate: $NADP^+/NADPH_2$
3. Flavin adenine dinucleotide: $FAD/FADH_2$

$NADH_2$ and $NADPH_2$ act as cofactors in a wide variety of enzymatic reactions. $NADH_2$ is principally used in catabolic reactions while $NADPH_2$ is primarily used in anabolic processes. Exceptions exist, however, as occasionally isoenzymes (different forms of the same enzyme) may be catalyzed by either $NADH_2$ or $NADPH_2$. $FADH_2$ is largely produced in the TCA cycle and plays an important role as a cofactor for the enzyme *ATP synthase* which produces ATP in the oxidative phosphorylation process. Other reducing power carriers are also used within

microbial metabolisms, such as pyrroloquinoline quinine (PQQ) which is used as a cofactor in methanol oxidation to formaldehyde.[69] The current consensus is that the *acetoacetyl-CoA reductase* enzymes that are used to produce PHA within the PAO require $NADPH_2$ as the reducing agent. $NADPH_2$ is primarily produced in the Pentose-Phosphate pathway but can also be generated from available $NADH_2$ through a transhydrogenase reaction.[10,84] The primary source of $NADH_2$, used in PAO catabolic reactions, is the EMP/ED pathways. Some evidence has also shown that the TCA cycle may also be active in the anaerobic environment, which can contribute to the supply of $NADPH_2$ and $NADH_2$ within the cell.[71,117] The amount of involvement of the TCA cycle in the anaerobic zone is unclear, however, and may be a function of specific environmental conditions and the type of PAO.[58]

PAO Aerobic/Anoxic Metabolism According to the Modified Mino Model. The PAO aerobic metabolism, following an anaerobic environment, can be described using an adapted version of the modified Mino model, as shown in Figure 2.8.

When the PAOs enter the aerobic reactor from the anaerobic zone, they have large PHA stores and low glycogen and polyphosphate reserves. Furthermore, most of the available readily biodegradable carbon substrate within the wastewater has been utilized in the anaerobic zone, and thus the concentration of carbon substrate within the aerobic reactor is low. In this environment, PAOs oxidize stored PHA to acetyl-CoA which enters the TCA cycle to produce $NADH_2$. $NADH_2$ is oxidized for ATP production through oxidative phosphorylation, with oxygen as the terminal electron acceptor. A portion of the stored PHA is also used to replenish the PAO's glycogen reserves through gluconeogenesis. In addition, PAO's will uptake inorganic phosphorus from the bulk solution for replenishment of their polyphosphate reserves. Transport of phosphorus into the PAO cell is generally believed to occur through two separate phosphorus transport mechanisms. Much of what we know about these systems in prokaryotes was derived from studies on non-PAO species, particularly *Escherichiacoli*. When phosphorus concentrations are high in bulk solution, a constitutively expressed low affinity phosphate inorganic transporter (Pit) will uptake phosphorus by use of the proton motive force. When phosphorus concentrations are low, a high affinity phosphate specific transporter (Pst) becomes active to

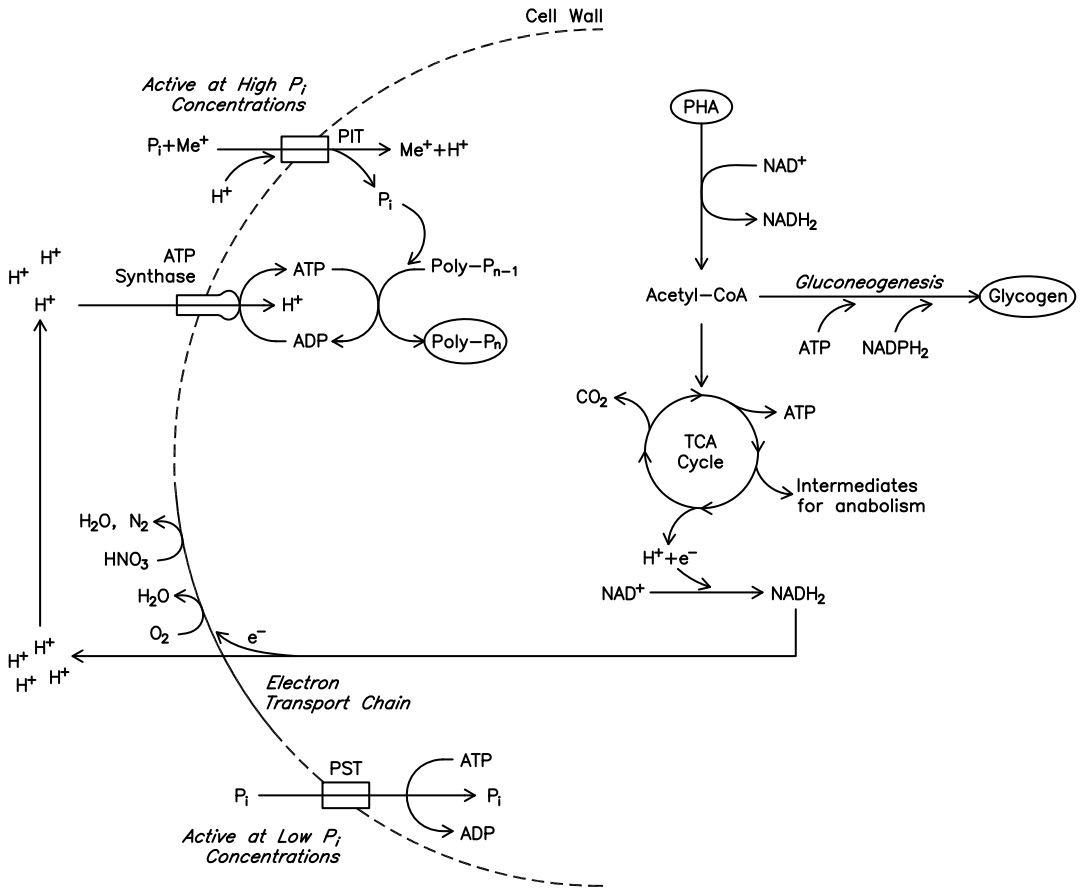

Figure 2.8: PAO aerobic metabolism (adapted from Grady et al.[29] and Coats[10]).

transport phosphorus into the cell at the expense of ATP. Repression of the Pst system in prokaryotes is generally believed to occur at phosphorus concentrations of about 4 µM (0.12 mg P/L).[111] Reinforcing the role of Pst and Pit in EBPR sludge, a recent metagenomic analysis of an *Accumulibacter* clade IIA dominated culture seeded by EBPR sludge found evidence that the Pst and Pit systems are present in this organism. The authors of this study postulated that the Pit system is operative at concentrations normally found in EBPR sludge while the Pst system is induced only at very low phosphorus concentrations.[53] There is some debate as to the what concentration of phosphorus will repress Pst in PAOs, however. He et al. notes that some studies have have indicated that the Pst system in PAOs may, in fact, also be active at high phosphorus concentrations, although the evidence for this is inconclusive.[34] This is another aspect of PAO metabolism that needs further research before definite conclusions can be drawn.

The large amounts of ATP generated in the aerobic zone allows for significant growth of PAOs. This growth increases the capacity of the PAO biomass to uptake and store phosphorus so that all of the inorganic phosphorus released in the anaerobic zone plus the concentration in the influent is able to be substantially reduced in bulk solution, with phosphorus stored as polyphosphate reserves in the PAO cells. Subsequent settling and wasting of a portion of the PAO biomass in the WAS stream results in a net removal of phosphorus from the system. The remaining biomass is returned to the anaerobic reactor through a recycle stream to repeat the process. The ability of PAOs to use an internal carbon source for growth in the aerobic zone, where exogenous carbon substrate has been depleted, gives PAOs a competitive advantage over ordinary heterotrophic organisms. This ability allows PAOs to grow and proliferate within the biomass which gives the biomass the ability to effectively remove phosphorus from the system.

Some types of PAOs, termed denitrifying PAOs (dPAOs), have the ability to use nitrate and/or nitrite as an electron acceptor in lieu of oxygen. Not all PAOs appear to be able to act as dPAOs and even dPAOs appear to differ in their ability to reduce nitrate and/or nitrite.[58] Kuba et al. found that dPAOs have the same PHA and glycogen metabolism as that of the Mino model.[43] Due to thermodynamic differences, however, less ATP is generated when nitrate or nitrite is used as an electron acceptor than when oxygen is used. Indeed, Kuba et al. estimated the amount of ATP produced per mol of $NADH_2$ supplied to the electron transport chain in enriched EBPR sludge to be 1.0 mol ATP/mol $NADH_2$ compared to 1.85 mol ATP/$NADH_2$ for oxygen that was previously determined by Smolders et al.[41,88] This lower ATP production efficiency results in less phosphorus uptake which can translate to higher effluent phosphorus concentrations compared to when oxygen is used as an electron acceptor.[71]

Practically, a denitrifying EBPR system requires an aerobic zone to nitrify ammonia to nitrate, which can then be reduced to nitrogen gas in an anoxic zone. Successful configurations that have been implemented include conventional preanoxic and post-anoxic denitrification systems preceded by an anaerobic zone to induce EBPR as well as dual sludge systems in which nitrifying sludge is kept completely separate from anaerobic-anoxic sludge but with nitrified supernatant cycled into the anaerobic-anoxic system for denitrification. Kuba et al. suggests that single sludge EBPR systems performing denitrification should be configured in a preanox-

ic configuration following the anaerobic zone (i.e. in an anaerobic-anoxic-aerobic configuration with internal recycle of nitrate rich wastewater from the aerobic to anoxic zone) rather than in a post-anoxic configuration.[42] The reasoning is based on the fact that in a preanoxic EBPR system, dPAOs have high levels of PHA as they leave the anaerobic zone and flow into the anoxic reactor. PHA is thus available to efficiently remove phosphorus and reduce nitrate simultaneously in the preanoxic reactor. In addition, PHA degradation was found by Smolders et al. to follow first order kinetics[88] Therefore, high levels of PHA result in a faster PHA metabolism, phosphorus uptake rate, and denitrification rate. Conversely, in a post-anoxic system, dPAOs flow into the anoxic reactor from the aerobic zone with low levels of PHA. The PHA consumed in the aerobic zone for phosphorus uptake with oxygen as the electron acceptor is not available to efficiently remove both phosphorus and nitrate simultaneously. It should be noted, however, that more recent studies have indicated that denitrifiers in a post-anoxic EBPR process appear to have the ability to utilize their glycogen reserves in the absence of PHA to drive the denitrification process at denitrification rates comparable to conventional preanoxic denitrification systems.[12,106,113]

Glycogen Accumulating Organisms

General Metabolism Several studies have noted the deterioration of EBPR systems with the prevalence of certain type of bacteria, termed glycogen accumulating organisms (GAOs). GAOs have a similar PHA and glycogen metabolism as PAOs in that they can uptake VFAs in an anaerobic environment for storage as PHA and then use their PHA reserves for energy in an aerobic environment. This ability allows them to aggressively compete with PAOs for VFA substrate and survive with PAOs in the downstream aerobic environment that is devoid of substrate. GAOs do not have the polyphosphate storage metabolism, however, and therefore do not uptake phosphorus for storage and use as an energy source. This metabolic deficiency makes GAOs undesirable in the EBPR process since their proliferation will decrease the amount of PAOs in the biomass and decrease the ability of the biomass to remove phosphorus from the wastewater. Research is ongoing to identify the specific species of microorganisms that are GAOs. Current organisms believed to be GAOs include, among others, *Candidatus*

Competibacter phosphatis, *Actinobacteria*, and *Defluviicoccus vanus*.[29]

GAO Anaerobic Metabolism According to the Filipe-Zeng GAO Model. The work of Filipe et al. and Zeng et al. resulted in a model of the GAO metabolism that is well accepted and, following Grady et al., is referred to here as the Filipe-Zeng GAO model.[25,29,114,115] Figure 2.9 shows a schematic of the GAO anaerobic metabolism based on a modified version of this model.

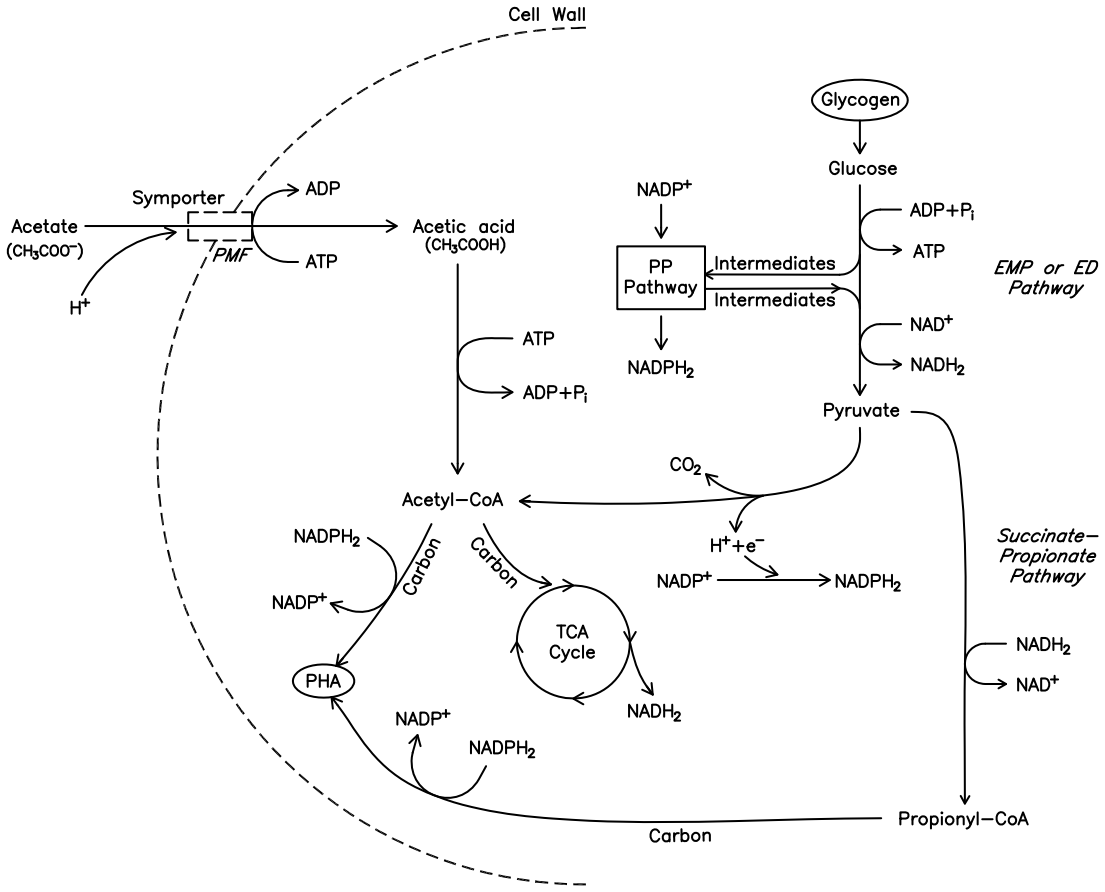

Figure 2.9: GAO anaerobic metabolism (adapted from Grady et al.[29]).

Briefly, the metabolism can be described as follows. In the anaerobic zone, glycogen is degraded to pyruvate through either the EMP or ED pathway, which produces all of the ATP required for the anaerobic metabolism. This includes the ATP required for the uptake of acetate, activation of acetate to acetyl-CoA, and the support of GAO maintenance activities. Reducing equivalents for synthesis of PHA are primarily produced by the degradation of glycogen. Some reducing

equivalents may also be produced by either a full or active TCA cycle[71] and potentially at least a partial pentose-phosphate pathway.[70] Residual reducing equivalents must be consumed in order to maintain an interior redox balance within the GAO, which is achieved by the reduction of pyruvate to propionyl-CoA which can be used to synthesize PHA. Propionyl-CoA mainly produces the PHA poly-β-hydroxyvalerate (PHV), whereas the PHA produced from acetyl-CoA is mainly poly-β-hydroxybutyrate (PHB). The significant amounts of propionyl-CoA within the GAO results in a significant fraction of the PHA produced by the GAO being of the PHV form. In fact, acetate fed GAOs synthesize about 75% PHB, 25% PHV, and a very small amount of PH2MV on a C-mole basis. By contrast, acetate fed PAOs are known to produce mostly PHB with typically less than 10% PHV.[71]

GAO Aerobic Metabolism According to the Filipe-Zeng GAO Model. Figure 2.10 presents a schematic of the aerobic metabolism of GAOs based on a modified Filipe-Zeng GAO model.

Aerobically, GAO metabolism is very similar to PAO metabolism with the exception that GAOs do not have a metabolism for polyphosphate synthesis and therefore uptake of excess inorganic phosphorus does not occur. PHA reserves are utilized to replenish glycogen reserves and to produce energy for cellular metabolism and growth. To accomplish this, PHA is degraded to both acetyl-CoA and propionyl-CoA according to the fractions of PHA that are of the PHB and PHV forms. A portion of acetyl-CoA undergoes gluconeogenesis to replenish glycogen reserves. Acetyl-CoA also enters the TCA cycle for production of reducing equivalents. In addition, a portion of propionyl-CoA is degraded to pyruvate, which is converted to aceytl-CoA through decarboxylation. Subsequent propionyl-CoA enters gluconeogenesis for replenishment of glycogen through conversion to either pyruvate or oxaloacetate. Large amounts of ATP are produced through oxidation of reducing equivalents by the oxidative phosphorylation process using oxygen as the electron acceptor.

Denitrifying GAOs (dGAOs) which can use nitrate/nitrite as their terminal electron acceptor are also known to exist, but dGAOs of different phylogeny are believed to have differing denitrification abilities. Zeng et al. found that an acetate fed dGAO enriched sludge containing

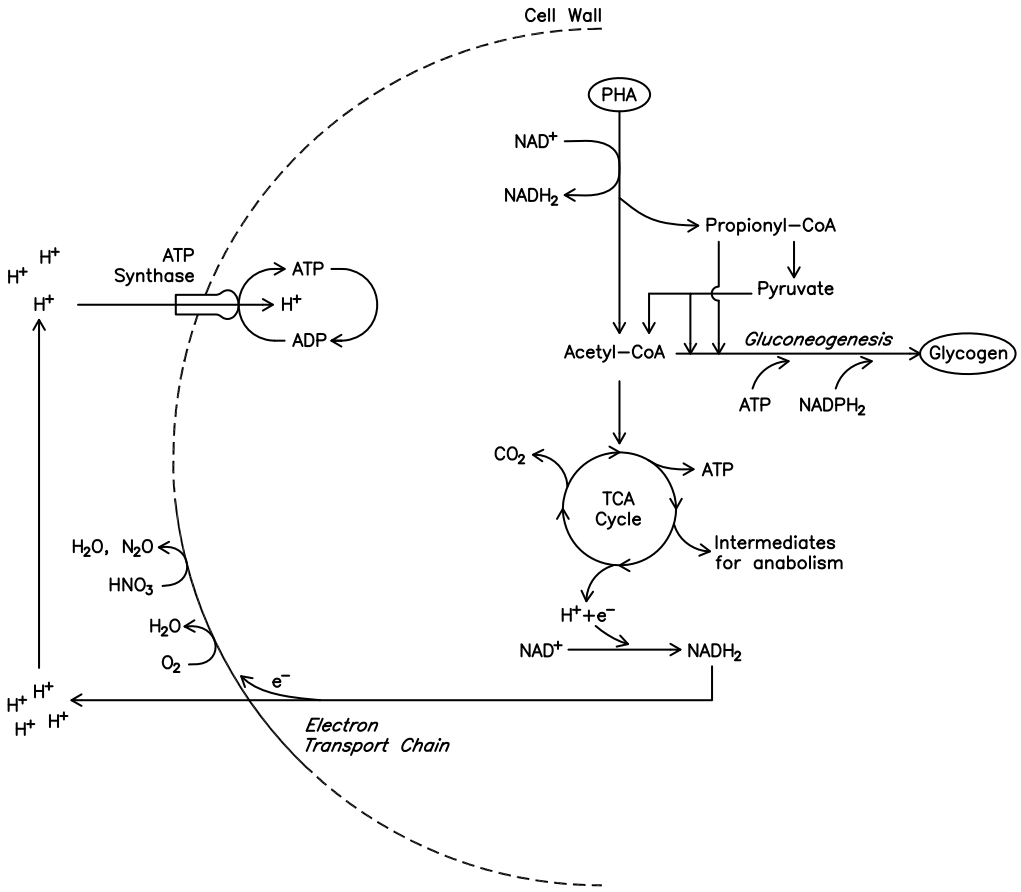

Figure 2.10: GAO aerobic metabolism (adapted from Grady et al.[29]).

mostly *Competibacter* had the ability to reduce nitrate to dinitrogen gas using internally stored PHA as the carbon substrate but that nitrous oxide was the main denitrification end product.[116] It was postulated that accumulation of nitrite within the reactor caused an inhibition of the nitrous oxide reductase enzyme which prevented further reduction to dinitrogen gas. Moreover, Wang et al. found that an acetate fed sludge enriched with cluster I *Defluviicoccus vanus*-related GAO could use acetate or internally stored PHA to reduce nitrate to nitrite but could not further reduce nitrite. Further studies have shown that other types of dGAOs have varying and different denitrification abilities.[58]

2.5 A New BNR Process: Internal Carbon Driven Post-Anoxic Biological Nutrient Removal (Biopho-PX)

2.5.1 Process Description

Recent research has indicated that EBPR coupled with post-anoxic denitrification can achieve SDNRs exceeding those typically associated with endogenous decay and has the potential to remove greater than 99% inorganic nitrogen and phosphorous removal without the addition of external carbon to the post-anoxic zone.[8,12,48,106,113] Denitrification in the post-anoxic zone appears to be driven by denitrifying PAOs and/or GAOs that are present within the EBPR process. Research strongly indicates that these organisms can use their internal glycogen reserves as a source of carbon and reducing equivalents to drive denitrification at higher than expected endogenous post-anoxic rates in the absence of exogenous substrate. The Coats' research group at the University of Idaho Department of Civil and Environmental Engineering is currently in the process of trademarking the term Biopho-PX to describe this process. In this work, the process is additionally referred to as an internal carbon driven post-anoxic biological nutrient removal (BNR) process. A schematic of this process under a continuous flow configuration is shown in Figure 2.11.

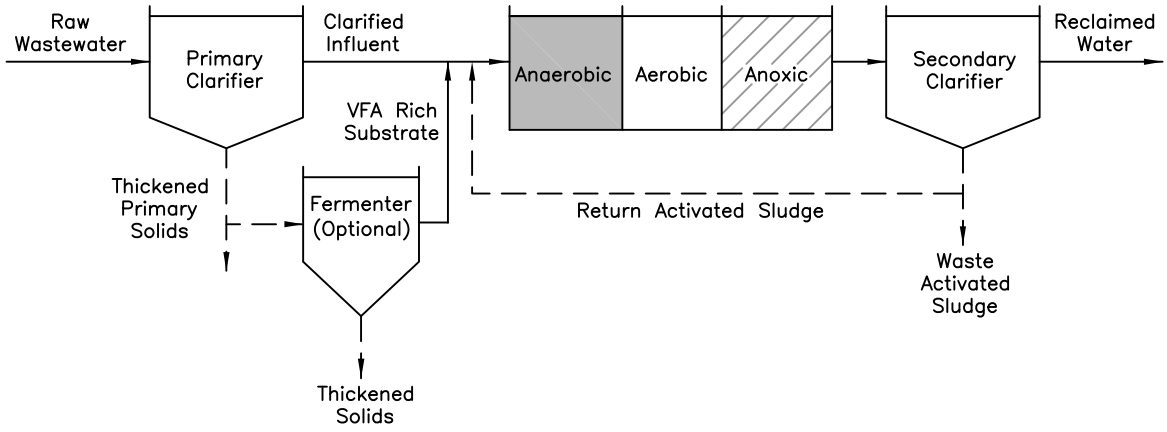

Figure 2.11: Post-anoxic BNR process flow schematic.

The configuration consists of an anaerobic zone followed by an aerobic and a post-anoxic zone. A fermenter to generate and supply VFAs to the anaerobic zone for PAO uptake may also be

required, depending on the influent wastewater VFA concentration. Return activated sludge (RAS) is cycled from the secondary clarifier to the anaerobic zone in order to maintain an adequate mixed liquor suspended solids (MLSS) concentration in the system and to maintain a consistent sludge blanket depth within the secondary clarifier. Within the anaerobic and aerobic zones, the sludge exhibits conventional EBPR metabolism. As PAOs uptake VFAs in the anaerobic zone, internal polyphosphate reserves are cleaved for energy to support the metabolism which results in the release of inorganic phosphorus into the bulk solution. The VFAs taken into the cell are converted to PHA which is stored for later use. In addition, PAOs utilize their internal glycogen stores to produce reducing equivalents and some ATP to support the anaerobic metabolism. As PAOs enter the aerobic zone, there is little external substrate in solution available but the PAOs have large PHA reserves which they degrade to produce large amounts of ATP to support growth and maintenance, using the oxygen in the solution as the terminal electron acceptor. Inorganic phosphorus is taken into PAO cells to replenish the PAO's polyphosphate stores and a fraction of the internal PHA is used to replenish the PAO's glycogen storage polymers. As the PAOs enter the anoxic reactor, they have little to no PHA left in reserve and exogenous readily biodegradable carbon substrate has been exhausted. Nevertheless, numerous studies have observed high denitrification rates within the anoxic zone concurrent with decreasing cellular glycogen levels under these conditions. It is hypothesized that dPAOs and/or dGAOs degrade internal glycogen stores to produce ATP to support their metabolism and potentially growth, through oxidative phosphorylation using nitrate and nitrite as the terminal electron acceptors.

It is currently unknown whether dPAOs or dGAOs or a combination of these organisms are responsible for the post-anoxic denitrification. Vocks et al. suggested that dGAOs may play a prominent role in the process since denitrification by dPAOs had so far been observed only with concurrent phosphorus uptake. In the post-anoxic BNR configuration, however, very little to no soluble phosphorus remains in solution after the aerobic zone and little to no phosphorus uptake is observed with denitrification. Glycogen levels within the biomass decrease with the nitrate and nitrite concentrations in the anoxic reactor, however, which suggests that organisms with a significant glycogen metabolism are oxidizing glycogen with nitrate and nitrite as the

electron acceptor. This points to a potential role for dGAOs in this process. Table 2.2 presents SDNRs observed with this process that were fed with real wastewater, compared to typical preanoxic and endogenous post-anoxic SDNRs.

Table 2.2: Typical preanoxic and post-anoxic SDNRs vs. observed SDNRs in post-anoxic BNR configurations with real wastewater.

Process	SDNR (mg N/g MLVSS-h)	Reference
Typical Preanoxic	1 - 3	Tchobanoglous et al.[94]
Typical Post-Anoxic (Endogenous)	0.2 - 0.6	Kujawa and Klapwijk[45]
Continuous Flow MBR[a]	0.47 - 2.6	Vocks et al.[106]
Nitrifying SBR	0.69 - 0.9	Coats et al.[12]
Nitrifying SBR	0.31 - 0.95	Winkler et al.[113]
Nitritating SBR	0.21 - 1.87	Appel[3]

[a] MBR=Membrane Bioreactor
[b] AN=Anaerobic, AE=Aerobic, AX=Anoxic

Table 2.2 indicates variability in the SDNR rates observed but that rates comparable to preanoxic configurations are achievable. Clearly, more research is needed to optimize this process. If full scale facilities can successfully implement this process, several benefits can be realized:

1. The process can achieve very low effluent nitrogen and phosphorous levels by leveraging microbial metabolisms and using influent BOD to efficiently remove both nitrogen and phosphorus. The removal of nitrogen from this process is expected to be higher than that achievable in preanoxic configurations.

2. External carbon is not required to be added to the post-anoxic reactor to fuel the denitrifying metabolism, resulting in cost savings. In addition, external carbon added to anoxic EBPR sludge can upset the EBPR process by inducing secondary phosphorus release from PAOs and encouraging proliferation and competition of ordinary heterotrophic organisms.

3. The process does not require MLR pumping as is required for preanoxic systems, resulting in lower energy demand.

4. For facilities that have phosphorous discharge limits, the process will remove both phosphorous and nitrogen biologically. Depending on the required effluent limits, chemical phosphorous removal and its associated increased costs for chemical addition and in-

creased sludge volume can be reduced or eliminated with this process.

2.6 Activated Sludge Modeling

Previous work on the internal carbon driven post-anoxic BNR process has shown that it has strong potential to become a viable and cost-effective process for obtaining low nitrogen and phosphorus effluent concentrations at full scale treatment facilities. A key component to advancing this process to the point where full scale installation is feasible is the optimization of the process operating parameters. Such optimization includes the selection of an appropriate SRT, optimal reactor hydraulic residence times (HRTs), recycle stream flow rates, etc. The use of a mathematical model that can be used to adequately simulate the process would be an invaluable tool in this optimization process, since model simulations can be used to save countless hours and effort in narrowing physical and operating alternatives prior to validation by lab and pilot scale studies. Recognizing this, an effort was made in this work to form such a model, as described later. In order to better understand the approach taken to derive this model, a review of the approaches that are commonly used to model activated sludge systems is needed.

2.6.1 General Activated Sludge Modeling Approaches

Process models can be classified into three general types based on what is known about the system that is being modeled; black box models, glass box models, and gray box models. In using a black box model, a macroscopic view of the system is taken and the system is considered solely in terms of its input and corresponding output response without consideration or knowledge of the specific internal reactions occurring within the system. Empirical or stochastic relationships are used to structure the model based on the input and output responses of the system. Traditional activated sludge design is based on this type of modeling. Indeed, until the early 1950s, the design of activated sludge systems relied largely on empirical relationships such as gross process loading factors and the aeration periods necessary to achieve adequate treatment.[51] Wastewater treatment standards up to this time focused only on BOD removal.

Such an approach has historically been able to produce well performing conventional activated sludge systems that meet their design intent even though the specific composition of the activated sludge remains undefined in the model.[100] A disadvantage of a black box approach is that the model is only valid within the range of the measurements used to create the model.[112]

A glass box model, also referred to as a white box model or an internal model,[51] refers to a model in which the internal reactions and processes are fully defined and all of the necessary information to fully describe the system are known *a priori*. Internal processes and reactions are described using first principles, based on physical, chemical, or biological insight and usually by a system of differential equations based on mass balances.[40] In practice, due to their complexity and the difficulty in obtaining all of the necessary information beforehand, true glass box models are rare. Van Loosdrecht et al. notes, however, that some activated sludge models have began to approach a glass box type of model, such as the ASM 3 model and the TUDP model which incorporate cycling of microbial storage products in order to better predict nutrient removal.[100]

A gray box model can be considered to consist of either a series of black box submodels or a combination of glass box and black box submodels.[40] As noted by Smolders et al., further investigation into a system that is modeled as a black box can result in insight which will allow mechanisms or processes within the system to be delineated and modeled as submodels within the main model.[91] These submodels are themselves viewed as black boxes. Such a model becomes mechanistic, in that underlying mechanisms that operate within the system begin to be defined. Here, the model begins to obtain predictive power and limited extrapolation becomes possible due to the model's theoretical underpinnings which describe the processes operating within the system.[112] Van Loosdrecht et al. notes that the main activated sludge models in use today (the International Water Association activated sludge models) take a gray box approach, where the sludge in the reactor is divided into individual fractions such as a readily biodegradable fraction, an inert particulate fraction, an ordinary heterotrophic bacteria fraction, a nitrifying bacteria fraction, a denitrifying bacteria fraction, etc.[100] Here, reactions between specific microbial communities and substrate fractions in the activated sludge are defined and incorporated into the model in order to refine the model predictions. Such models have proven to perform well for the simulation of nitrification and denitrification systems.

Although the predictive capacity of such models is increased, it does come at the expense of model complexity.

The approach taken to model activated sludge systems has largely evolved from a purely black box approach to an approach that attempts more of a glass box approach which incorporates microbial metabolisms into the model. Figure 2.12 illustrates how the refinement of activated sludge models has occurred.

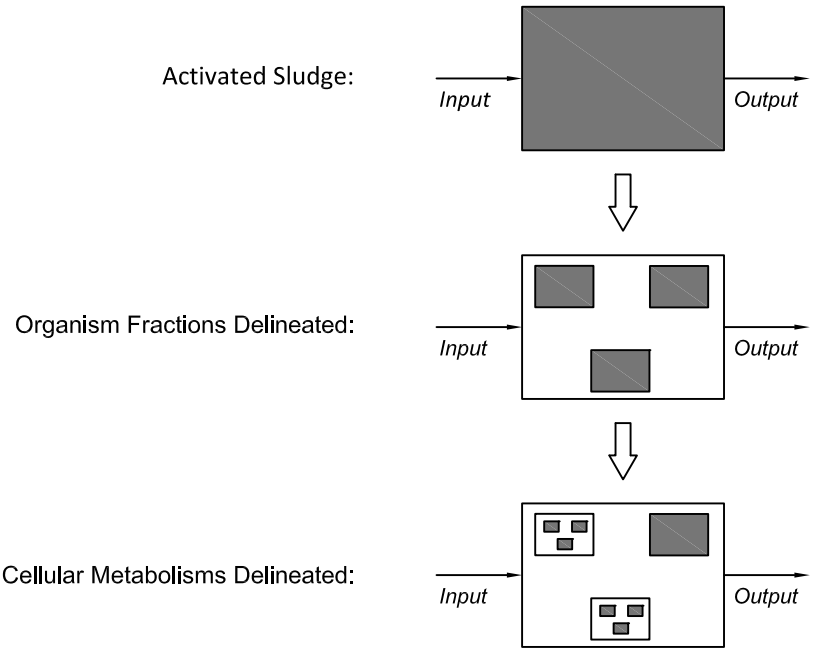

Figure 2.12: Refinement of an activated sludge model (adapted from Smolders[91], Meijer[62], and Van Loosdrecht et al.[100]).

Here the traditional activated sludge design approach, which incorporates empirical and stochastic relationships to describe the reactions and processes that occur within the activated sludge to transform the input (such as an F/M ratio) into the output response (such as effluent BOD), is represented as a black box. Investigation into the activated sludge process has allowed further refinement of activated sludge models by delineating the important classes of microorganisms within the sludge which act on substrate to oxidize carbon to carbon dioxide, oxidize ammonia to nitrate, and reduce nitrate to nitrite, etc. These processes are themselves modeled as a network of black box models within the main model to produce the model output (such as effluent BOD and nitrogen concentrations). Further refinement of activated sludge

models has been made possible by elucidation of the relevant microbial metabolisms of the microorganisms acting within the activated sludge. Here, a metabolic modeling approach is taken and the cycling of microbial storage products, such as PHA, glycogen, and polyphosphate are included within the overall model structure. Such a model has been shown to provide a substantial improvement in modeling EBPR processes although they have historically shown only a nominal improvement in the modeling of nitrification and denitrification. Therefore, whether the use of such a complex model is justified depends highly on the application.[100]

In the derivation or selection of an appropriate model, the engineer must choose a model that will appropriately describe the system for the specific application being considered. A balance must be made between the accuracy gained by a more complex model against the increased time and expense required (and implicit uncertainty) for parameter estimation. It is more advantageous to choose a simpler model over a more complex one, if the simpler model will provide an adequate enough description of the system under consideration. Two different fundamental approaches are currently used to model activated sludge systems today, the ASM (ASM 1, ASM2d, and ASM 3) models and metabolic models. The choice of which model to use depends upon the application.

2.6.2 Current Activated Sludge Models

IWA Activated Sludge Models. Prior to 1982, activated sludge models were developed independently by various research teams.[98] In 1986, the International Association on Water Pollution Research and Control (IAWPRC; now IWA) formed the "Task group on mathematical modeling for design and operation of biological treatment." The task group was composed of experts from various research groups and charged with developing a single activated sludge model to be used in the design of activated sludge systems. In 1982 the task group released the Activated Sludge System Model No. 1 (ASM 1) with a final form of the model released in 1987.[36] The ASM 1 model combines previously existing models and concepts into a single model that can be used to model carbon removal, nitrification, and denitrification. ASM 1 has gained wide acceptance in the engineering and wastewater industry and can be considered today as the standard reference model for activated sludge modeling and design.[27] In order to facilitate

the presentation of a large number of model parameters, the ASM 1 model components are arranged in the Gujer matrix form, in which state variables are displayed in the matrix columns and model processes are displayed in the matrix rows.[31,36]

In 1995 the IWA task group released the ASM 2 model, which is a heavily revised and expanded model capable of simulating carbon removal, nitrification, denitrification, chemical phosphorus removal, and EBPR.[37] The ASM 2 model was subsequently revised and released as ASM 2d to include denitrifying PAOs.[38] In 1999, IWA released ASM 3 which addressed several inadequacies that had been discovered in ASM 1, but does not include the ability to simulate phosphorus removal.[30] While ASM 1 remains the most popular of the Activated Sludge Models, both ASM 2d and ASM 3 have seen widespread use in the design of many activated sludge systems.

Metabolic Models. The ASM models primarily simulate the conversions and reactions occurring within a reactor, outside of the microbial cells. If the model incorporates the cycling of microbial storage products, as does ASM2d and ASM 3, they are accounted for only through the use of lumped storage variables.[51] Yield coefficients used within the model are largely empirically determined. In contrast, metabolic models account for the internal microbial reactions occurring within the microbial cells through known biokinetic stoichiometry and kinetic rates. All of the relevant metabolisms and reactions that occur within the cells are specifically incorporated into the model. Within EBPR, these metabolisms include the uptake of carbon substrate, the cycling of PHA, glycogen, and polyphosphate storage polymers, and the generation and use of ATP and reducing equivalents. Yield coefficients within metabolic models are derived directly from the stoichiometry of the internal conversions within the cell. While metabolic models are more complex than ASM type models, they usually require less calibration effort since a large portion of the variables in the model are stoichiometrically related and do not need to be explicitly determined or calibrated by the modeler.[51,85]

2.6.3 The Technical University of Delft Phosphorus Metabolic Model

History and Overview. The primary metabolic model used for modeling activated sludge facilities is the Technical University of Delft Phosphorus (TUDP) model developed by a working

group at the Delft University of Technology and which models PAO metabolism by incorporating the cyclic transformations of PHA, glycogen, and polyphosphate within the cell as the cell passes through anaerobic, aerobic, and anoxic zones. The current version of the model integrates the metabolic model of PAO metabolism into the ASM2d model structure such that the complete model is able to simulate phosphorus, nitrogen, and COD conversions. This model was developed primarily through the work of Smolders et al.,[86–90] Kuba et al.,[41,44] Murnleitner et al.,[67] Van Veldhuizen et al.,[102] and Meijer.[62] The model has been validated against several full scale BNR processes including mainstream EBPR,[59,102] EBPR process start-up,[61] EBPR limitations during wet weather flow periods,[63] and existing sidestream processes (Phostrip similar process for biological removal of phosphorus[7] and BABE process for nitrifying microorganism augmentation).[83]

Meijer provides a good summary of the history and structure of the model.[62] In brief, Smolders et al. developed the anaerobic and aerobic model kinetics and stoichiometry while Kuba et al. developed the anoxic parameters for the model. Murnleitner et al. modified the kinetic framework of Smolders to provide a better fit of the model under aerobic and anoxic environments. Van Veldhuizen et al. subsequently combined the metabolic model outlined by Murnleitner with the ASM 2d model. The combined model predicts phosphorous removal through the Murnleitner metabolic structure and predicts COD and nitrogen removal using the ASM 2d structure. Of note, Van Veldhuizen showed that this model could provide good prediction of full scale treatment plant effluent concentrations with the calibration of only 3 out of 60 of the model's parameters, together with adjustment of the unknown aeration input. The combined model was further refined by Meijer and was found to provide good results in modeling both lab scale and full scale facilities. Hauduc et al. subsequently corrected several typing errors in Meijer's version of the model.[32] The model developed in this thesis relies upon the TUDP model for conventional EBPR processes. It is important, therefore, to understand the underlying basis of the TUDP model and assumptions used in its derivation.

Representation of Reducing Power. The TUDP model represents all forms of reducing agents ($NADH_2$, $NADPH_2$, and $FADH_2$) as a single entity denoted as $NADH_2$. As noted by

Villadsen et al., this is valid when performing simple metabolic analysis on a metabolic process (such as when all anabolic reactions in the process are represented by a single stoichiometric equation).[105] In these cases, a unit of reducing power can be defined as a reducing equivalent, equal to one H^+ atom. Thus, the carriers $NADH_2$, $NADPH_2$, and $FADH_2$ all carry 2 reducing equivalents (two H compounds) and all $NADH_2$, $NADPH_2$, and $FADH_2$ generated and consumed in the metabolic reactions being analyzed may therefore be represented by the designation $NADH_2$. While different forms of reducing agent may be consumed and generated within a process, it takes the same amount of substrate to produce the net amount of reducing equivalents arising from the process. Therefore, the amount of reducing equivalents produced and the anabolic yields arising from the available reducing equivalents (and resulting ATP generation) will be the same whether the reducing agents are represented by a single designation or each individual agent is tracked separately through the calculations. Villadsen et al. notes, however, that for more complex metabolic analysis, such as the quantitative study of fermentative amino acid production, the tracking of the different reducing agents will be required.

Derivation of the TUDP Metabolic Model for Conversions by PAOs. The metabolic model component of the TUDP model was derived by utilizing a metabolic flux analysis procedure to determine the yield coefficients for the conversions of substrate and products (glycogen, PHA, and polyphosphate) that are induced by PAOs within EBPR. The yield coefficients were then coupled to appropriate kinetic rate equations which can be used to simulate the concentrations of the constituents within the reactor by forming mass balances. Both the anaerobic and aerobic conversions in the model are based on a Herbert-Pirt type relation that is expanded to include product formation. A general form of this relation, which describes the conversion rate of a substrate in solution by the biomass (r_s), is shown in equation 2.7.[81]

$$r_s = \frac{1}{Y_{sx}} r_x + \frac{1}{Y_{sp}} r_p + m_s C_x \tag{2.7}$$

The yield value Y_{sx} represents the production of biomass x on substrate, s, while Y_{sp} is the yield of end product (e.g. lysine or PHA), p, produced on the substrate. The variables r_x and r_p are the conversion rates of biomass and product, respectively. The coefficient m_s is the

specific rate of substrate degradation for maintenance and C_x is the concentration of biomass in the reactor. The derivation of the yield coefficients in equation 2.7 can be accomplished by taking advantage of the fact that a yield coefficient may be defined from the reaction rates of the consumed and produced components such that $Y_{ab} \equiv |r_b/r_a|$. A metabolic network analysis can be used to determine the rates of consumption of substrate and the production of products within the metabolism of an organism, from which the yield coefficients are determined. The general procedure will be illustrated in Chapter 3.7 where yield coefficients will be derived for PAOs under ammonia limited conditions within a post-anoxic EBPR process. For our current purpose of further understanding the underlying basis of the TUDP model, however, the specific metabolic processes that were assumed to occur in the anaerobic and aerobic metabolisms of PAOs for the derivation of the TUDP metabolic model are discussed below.

TUDP Model Anaerobic Reactions. The TUDP model uses four processes to simulate the PAO anaerobic metabolism:

1. Acetate transport across the cell membrane and subsequent conversion of acetate to PHB.
2. Hydrolysis of polyphosphate (polyP) and release of orthophosphate into bulk solution.
3. Generation of the reducing equivalent $NADH_2$ from glycogen degradation.
4. Anaerobic maintenance.

These processes can be visualized as shown in Figure 2.13.

Since the prevalent species of PHA synthesized when acetate is the sole substrate for PAOs is PHB, the TUDP model makes the simplifying assumption that all of the PHA species are of the PHB form. In addition, as shown in Figure 2.13, the TUDP model assumes that all reducing equivalents are $NADH_2$. This assumption can be justified in simple metabolic models, as previously discussed. As indicated in Figure 2.13, the model also assumes that all reducing equivalents are produced by glycogen degradation through the EMP pathway, as originally proposed by Mino et al.[66] Hence, the model does not include the TCA cycle in the anaerobic metabolism and all acetic acid is converted to PHB utilizing the $NADH_2$ formed from the

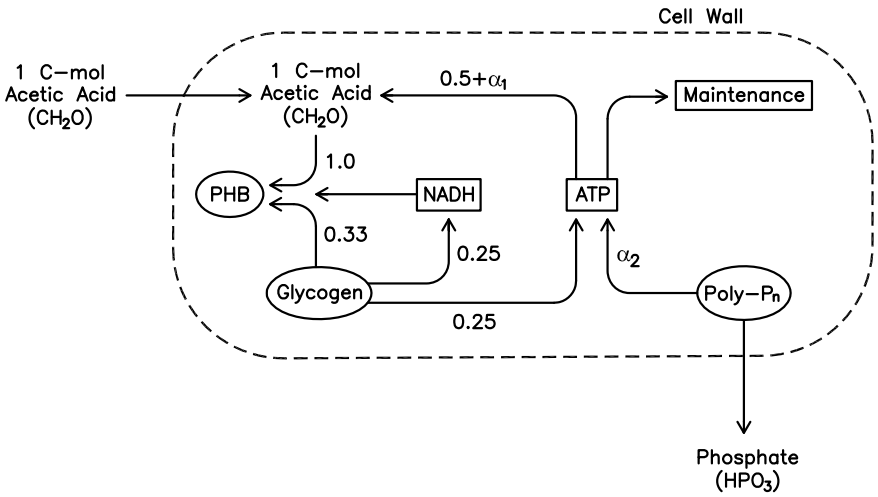

Notes: Stoichiometric coefficients refer to moles of substance (carbon compounds in C-mole). α_1=efficiency of acetate transport across the cell membrane. α_2=efficiency of ATP production from polyP hydrolysis.

Figure 2.13: PAO anaerobic metabolic conversions as modeled by the TUDP model (adapted from Smolders et al.[92] and Meijer[62]).

degradation of glycogen. As mentioned in Section 2.4.3, the role of the TCA cycle in the anaerobic metabolism of PAOs is still debated. The decision not to incorporate the TCA cycle into the anaerobic metabolism of PAOs in the TUDP model was based on experimental results obtained by Smolders et al. in which two pathways for the anaerobic production of reducing equivalents were considered.[89] The first pathway assumes all $NADH_2$ is produced by the degradation of a portion of acetic acid through the TCA cycle, which is in accordance with the metabolism proposed by Wentzel et al.[110] Glycogen is not involved in this pathway. The second pathway assumes all $NADH_2$ is produced by the degradation of glycogen through the EMP pathway. Smolders et al. measured the anaerobic acetate consumption of an enriched PAO culture against the corresponding CO_2 and PHB produced and the phosphorus released in a series of batch tests and an operating SBR. The results strongly indicated that glycogen was degraded through the EMP pathway without involvement of the TCA cycle as shown in Table 2.3.

The TUDP model combines the uptake of acetate, the subsequent conversion of acetate to acetyl-CoA, and the conversion of acetyl-CoA to PHB into a combined single reaction. Within this reaction, ATP created from the polyphosphate and glycogen degradation is used as an energy source to uptake acetate. The amount of ATP required for the uptake of acetate across

Table 2.3: Theoretical and measured conversion ratios for determination of the source of anaerobic reduction equivalents for the TUDP Model (adapted from Smolders et al.[89]).

	Theoretical		Measured	
Ratio	TCA	Glycogen (EMP)	Batch	SBR
CO_2/HAc	0.11	0.17	0.17	0.18-0.22
PHB/HAc	0.89	1.33	1.3	1.2
PO_4/HAc[a]	0.5-0.1	0.25-0.75	-	0.26-0.76

[a] Theoretical value depends on pH

the cell membrane, α_1, is pH dependent in the model and ranges between 0 moles ATP/C-mol at low pH (pH of 5.5) to 0.5 moles ATP/C-mol at high pH (pH of 8.5).[62,89] The conversion of 1 C-mol of acetic acid to 1 C-mol of acetyl-CoA is assumed to use 0.5 mole ATP/C-mol, while the conversion of acetyl-CoA to PHB is assumed to require 0.25 moles NADH/C-mol.

Smolders et al. found the actual composition of PAO cellular polyphosphate to be $Mg_{1/3}K_{1/3}PO_3$. Since the model does not consider magnesium or potassium species, the magnesium and potassium components are replaced with a proton to balance the charge on the phosphate group, resulting in polyphosphate being modeled as HPO_3. The quantity of ATP generated per mole of polyphosphate hydrolyzed, α_2, is suggested by Smolders et al. to be 1 mole ATP/P-mole. The hydrolysis of 1 mole of polyphosphate produces 1 mole of phosphate, which is released from the cell into bulk solution.

By assuming that the net accumulation of NADH and ATP within the cell are both zero, Smolders et al. obtained the following equation describing the anaerobic metabolism at a pH of 7:[89]

$$\underset{\text{acetate}}{CH_2O} + 0.5\,\underset{\text{glycogen}}{CH_{10/6}O_{5/6}} + 0.44\,\underset{\text{polyP}}{HPO_3} + 0.023\,H_2O \longrightarrow 1.33\,\underset{\text{PHB}}{CH_{1.5}O_{0.5}} + 0.17\,CO_2 + 0.44\,\underset{\text{phosphate}}{H_3PO_4} \quad (2.8)$$

Note that acetate is expressed here as CH_2O which is equal to 1/2 mole of its normally expressed composition of CH_3COOH. This approach was taken to retain a C-mole based model versus only a mole based model.

Meijer notes that the yield of phosphorus released per acetate uptake, $Y_{\mathrm{PO}}^{\mathrm{AN}}$, that is derived from Equation 2.8 is considered to be dependent upon the pH of the bulk solution.[62] Smolders et al. attributes this difference to an increase in electrical potential across the cell membrane with increasing pH.[89] As noted by Meijer, while Smolders et al. found the relationship to be $Y_{\mathrm{PO}}^{\mathrm{AN}} = 0.19\,pH_{out} - 0.85$ P-mol/C-mol, Filipe et al. determined a different linear relationship of $Y_{\mathrm{PO}}^{\mathrm{AN}} = 0.16\,pH_{out} - 0.55$.[26] Meijer hypothesizes that the difference may be caused by the presence of GAOs, which were not measured in the two systems and notes that the presence of propionate and butyrate will also affect the pH dependence. For this reason, Meijer recommends that this yield coefficient be determined experimentally for each system being modeled.

Cellular maintenance in the anaerobic zone is assumed to occur by using ATP generated from a secondary polyphosphate degradation reaction, without acetate uptake:

$$\underset{\text{polyP}}{\mathrm{HPO_3}} + \mathrm{H_2O} \longrightarrow \underset{\text{phosphate}}{\mathrm{H_3PO_4}} \tag{2.9}$$

TUDP Model Aerobic and Anoxic Reactions. The ASM2d and the TUDP models both use a single state variable, $\mathrm{X_{PAO}}$, to model PAOs and dPAOs. To model the activity of dPAOs in an anoxic zone, a factor, $\eta_{\mathrm{NO.PAO}}$, is applied to the anoxic growth process rates of PAOs. A default value of 0.80 is used for $\eta_{\mathrm{NO.PAO}}$ in the TUDP model. This can be interpreted as being the dPAO/PAO fraction in the sludge. In addition, separate yield coefficients for PAOs are used in the TUDP model for aerobic and anoxic growth processes for PAOs due to the different electron acceptor conditions which affects the achievable yields. As described by Murnleitner et al.[67] and Meijer,[62] the TUDP model characterizes the PAO aerobic and anoxic metabolisms using six reactions, four of which are the same in the aerobic and anoxic phases. These reactions are:

1. The degradation of PHB through the TCA cycle for $\mathrm{NADH_2}$ production.
2. Glycogen formation
3. Phosphate uptake
4. Polyphosphate formation

5. ATP production through phosphorylation

6. Biomass Growth and Maintenance

The stoichiometry of reactions 3 (phosphate uptake) and 5 (ATP production through phosphorylation) are dependent upon the type of electron acceptor present (oxygen in an aerobic environment or nitrate in an anoxic environment). A schematic of these reactions within the TUDP model framework is presented in Figure 2.14.

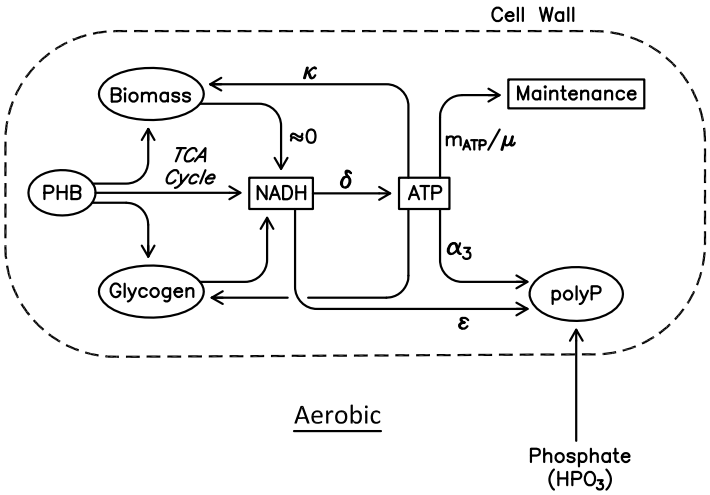

Note: Stoichiometric coefficients refer to moles of substance.

Figure 2.14: PAO aerobic/anoxic metabolic conversions as modeled by the TUDP model (adapted from Smolders et al.[92] and Meijer[62])

The reaction equations for each process are described as follows.

Reaction 1: PHB Degradation

PHB degrades to acetyl-CoA which then enters the TCA cycle which produces reducing equivalents. The model assumes that all $FADH_2$ produced in the TCA cycle is equivalent to $NADH_2$. The following stoichiometric equation is used:

$$\underset{\text{PHB}}{CH_{1.5}O_{0.5}} + 1.5\,H_2O \longrightarrow 2.25\,NADH_2 + 0.5\,ATP + CO_2 \tag{2.10}$$

Note that in Equation 2.10, ATP is produced in the degradation of PHB. This occurs in the conversion of succinyl-CoA to succinate by the *succinate thiokinase* enzyme within the TCA

cycle of bacteria. In contrast, an analogous enzyme within the TCA cycle of mammals produces guanosine triphosphate (GTP) or inosine triphosphate (ITP) instead of ATP at this step.[28]

Reaction 2: Glycogen Formation

Aceytl-CoA from PHB degradation is converted to oxaloacetate through the glyoxylate cycle (the glyoxylate shunt of the TCA cycle). The enzyme *PEP carboxykinase* then produces phosphoenolpyruvate (PEP) from oxaloacetate and ATP.[28] PEP then enters gluconeogenesis to form glycogen. The overall reaction is:

$$\underset{\text{PHB}}{\frac{4}{3}\,CH_{1.5}O_{0.5}} + \frac{5}{6}\,ATP + \frac{5}{6}\,H_2O \longrightarrow \underset{\text{glycogen}}{CH_{10/6}O_{5/6}} + \frac{1}{3}\,CO_2 + NADH_2 \tag{2.11}$$

Reaction 3: Phosphate Uptake

The model assumes that phosphate uptake across the cell membrane occurs against an electric potential in an energy consuming process (due to the negative charge of phosphate).[88] Energy for the process is generated through the proton motive force by oxidation of $NADH_2$ with either oxygen or nitrate as the electron acceptor. Furthermore it is assumed that the positive charged metal cations, Mg^+ and K^+, that are necessary for polyphosphate synthesis are taken up without further energy cost, presumably in symport with phosphorus. The process is analogous to the uptake of phosphorus through a Pit system, as described in Section 2.4.3. The following equations are assumed in the model:

$$\text{Aerobic:} \qquad \underset{\substack{\text{external}\\\text{phosphate}}}{\epsilon_o\,H_3PO_{4(\text{out})}} + NADH_2 + \frac{1}{2}\,O_2 \longrightarrow \underset{\substack{\text{internal}\\\text{phosphate}}}{\epsilon_o\,H_3PO_{4(\text{in})}} + H_2O \tag{2.12}$$

$$\text{Anoxic:} \qquad \underset{\substack{\text{external}\\\text{phosphate}}}{\epsilon_n\,H_3PO_{4(\text{out})}} + NADH_2 + \frac{2}{5}\,HNO_3 \longrightarrow \underset{\substack{\text{internal}\\\text{phosphate}}}{\epsilon_n\,H_3PO_{4(\text{in})}} + \frac{1}{5}\,N_2 + \frac{6}{5}\,H_2O \tag{2.13}$$

The parameters ϵ_o and ϵ_n correspond to the amount of phosphate taken up per $NADH_2$ oxidized in the aerobic and anoxic environments, respectively. The model assumes ϵ_o=7 P-mol/mol $NADH_2$ and ϵ_n=0.5 ϵ_o.[62]

Reaction 4: Polyphosphate Formation

The model uses the following equation for cellular polyphosphate synthesis from internal phosphate:

$$\underset{\substack{\text{internal}\\ \text{phosphate}}}{H_3PO_{4(in)}} + \alpha_3\,ATP \longrightarrow \underset{\text{polyP}}{HPO_3} + H_2O \tag{2.14}$$

The parameter α_3 represents the amount of ATP needed to synthesize 1 mole of polyphosphate. A value of 1 mole ATP per mole of polyphosphate is used in the model.

Reaction 5: ATP Production through Oxidative Phosphorylation

The amount of ATP produced by PAOs will vary according to the electron acceptor present (oxygen or nitrate). In either case, the model assumes ATP production occurs through oxidative phosphorylation which incorporates oxidation of $NADH_2$ according to the following:

$$\text{Aerobic:} \qquad NADH_2 + \frac{1}{2}\,O_2 \longrightarrow \delta_o\,ATP + H_2O \tag{2.15}$$

$$\text{Anoxic:} \qquad NADH_2 + \frac{2}{5}\,HNO_3 \longrightarrow \frac{1}{5}\,N_2 + \delta_n\,ATP + \frac{6}{5}\,H_2O \tag{2.16}$$

Here, δ_o and δ_n are the moles of ATP produced per mole of $NADH_2$ with oxygen and nitrate respectively. Conventionally, δ_o is the P/O ratio. Based on the work of Smolders et al.[88] and Kuba et al.,[44] the model uses values of δ_o=1.85 and $\delta_n = 1/2\,\delta_o$=0.925.

Reaction 6: Biomass Growth and Maintenance

PAO growth occurs on the PAO's internal PHB. The following equation is used to model biomass growth and maintenance:

$$\underset{\text{PHB}}{1.27\,(C_4H_6O_2)_{1/4}} + 0.2\,NH_3 + \underset{\text{phosphate}}{0.015\,H_3PO_4} + 0.385\,H_2O + (K\ + m_{ATP}/\mu)ATP$$

$$\longrightarrow \underset{\text{biomass}}{CH_{2.09}O_{0.54}N_{0.2}P_{0.015}} + 0.615\,NADH_2 + 0.27\,CO_2 \tag{2.17}$$

The parameter K is the ATP requirement for biomass synthesis. A value of 1.72 mol ATP/C-mol is used in the TUDP model, as noted by Meijer. The variable μ is defined as the biomass specific growth rate. The parameter m_{ATP} is the amount of ATP consumed for maintenance purposes. Meijer reports this value as 0.017 mole ATP/C-mol PAO on a theoretical basis.

TUDP Model Kinetics. The anaerobic conversions within the TUDP model are assumed to follow first order kinetics. The model simulates the anaerobic PAO metabolism with an equation for the uptake of acetate and conversion to PHA and an equation describing cellular maintenance. Due to the fixed stoichiometry of these equations, all conversion rates in the anaerobic metabolism can be determined if only one of the rates (e.g. the acetate uptake rate) is given or measured.[62]

Within the aerobic and anoxic metabolism, five conversion rates of interest are identified. These correspond to the consumption of PHA and glycogen and the formation of biomass and polyphosphate in addition to maintenance (r_{pha}, r_x, r_{pp}, r_{gly}, and m_{pha}). By assuming that the concentrations ATP, $NADH_2$, and internal phosphate are in steady state within the cell (their net conversion rates are zero) and by using the stoichiometry of the metabolic processes, a set of interdependent linear relations can be formed in which the yields corresponding to the five identified rates can be determined.

The overall system is underdetermined but one rate can be expressed as a function of the remaining four rates such that the system can be solved if these four rates are given or measured. Within the model, these given kinetic rates are determined by predefined rate equations and kinetic parameters that were formulated and validated by the authors of the model using enriched PAO cultures. Smolders et al. chose to define the kinetic structure of the model such that the PHA degradation rate is expressed as a function of the remaining intercompeting process rates.[88] Hence the model was based on the following linear relation:

$$r_{pha} = \frac{1}{Y_{pha,x}} r_x + \frac{1}{Y_{pha,pp}} r_{pp} + \frac{1}{Y_{pha,gly}} r_{gly} + m_{pha}\, C_x \tag{2.18}$$

The term C_x refers to the active biomass which is defined as the MLSS concentration minus the

concentrations of glycogen, PHA, polyphosphate, and the ash content from nonactive biomass. Approximately 5-10% of the ash content is considered to come from active biomass.[86] The model equation can be visualized as shown in Figure 2.15.

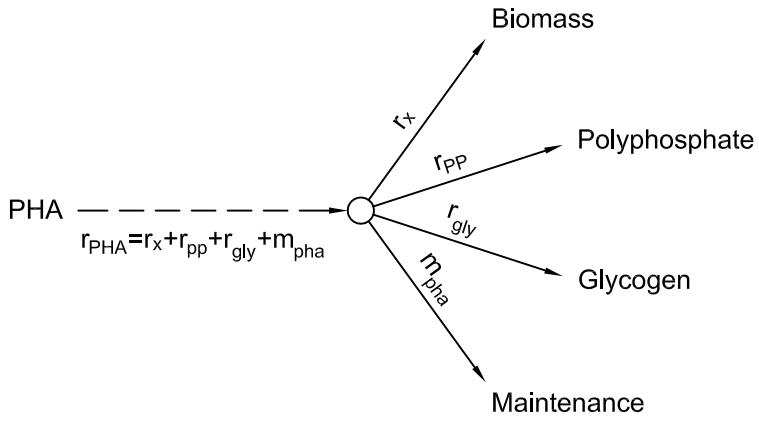

Solid lines represent reaction rates in the model based on predetermined rate equations and kinetic parameters. Dashed lines represent reaction rates determined by the model stoichiometry.

Figure 2.15: Kinetic Structure Proposed by Smolders et al. (adapted from Murnleitner et al,[67] Meijer[62] and Houweling et al.[39])

Here, the rate of PHA degradation can be interpreted to be dependent upon the rates of biomass growth, glycogen formation, and polyphosphate formation. Under this structure, biomass growth is limited by the maximum growth rate.[62] Difficulties with this formulation soon became evident as the model was found to require different kinetic parameters under aerobic and anoxic conditions and was not found to be sufficiently kinetically stable at different SRTs. As Meijer recounts, Filipe et al.[26] also found that the model underpredicted phosphorus concentrations in the continuous flow systems operated in studies by Wentzel et al.[108,109] and subsequently proposed a modified model structure. Murnlietner et al. had proposed a revised kinetic structure previous to the work of Filipe et al., which was able to simulate the PAO metabolism using a single set of model parameters under anaerobic, aerobic, and anoxic conditions and under different SRTs.[67] This model structure for the aerobic and anoxic metabolisms is based on the following equation:

$$r_x = Y_{pha,x}\, r_{pha} - \frac{1}{Y_{x,pp}} r_{pp} - \frac{1}{Y_{x,gly}} r_{gly} - m_x\, C_x \tag{2.19}$$

This redefined kinetic structure formulates the PAO growth rate in terms of the PHA, glycogen, polyphosphate and maintenance rates. This structure is illustrated in Figure 2.16.

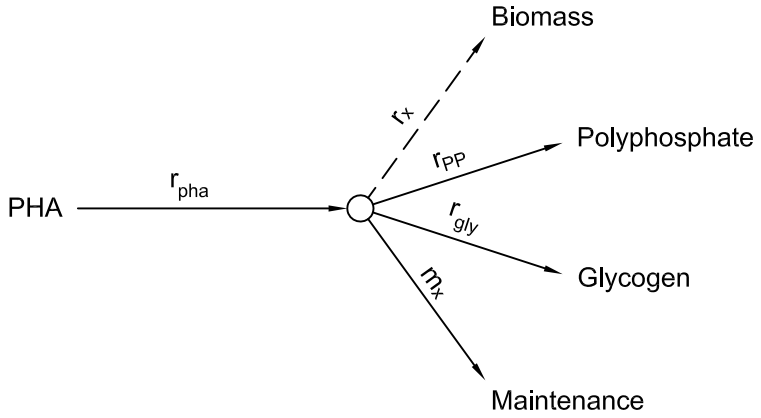

Solid lines represent reaction rates in the model based on predetermined rate equations and kinetic parameters. Dashed lines represent reaction rates determined by the model stoichiometry.

Figure 2.16: Kinetic Structure Proposed by Murnleitner et al. (adapted from Murnleitner et al,[67] Meijer[62] and Houweling et al.[39])

Meijer subsequently refined the TUDP model using the kinetic structure proposed by Murnleitner et al. in order to improve the glycogen kinetics and other parameters. Subsequent testing on lab and full scale systems has shown that the model can successfully simulate many EBPR systems, as previously discussed.

It should be noted that the linear relationship found in equation 2.19 should not be interpreted as consisting of independent processes. The processes in the equation compose a unified metabolism. If these processes are considered to be independent then the form of equation 2.19 may be misinterpreted as indicating that biomass is consumed for polyphosphate and glycogen formation, in addition to supporting maintenance. This interpretation of the metabolism is, of course, incorrect. Indeed, van Loosdrecht et al. notes that equation 2.19 can be rearranged as follows:[99]

$$r_x = Y_{x,pha}\left(r_{pha} - \frac{r_{pp}}{Y_{pp,pha}} - \frac{r_{gly}}{Y_{gly,pha}} - m_{pha}\,C_x\right) \tag{2.20}$$

This form of the model equation indicates that biomass formation occurs on the leftover PHA

after PHA is consumed for glycogen replenishment, polyphosphate formation, and maintenance. This is conceptually more agreeable. As van Loosdrecht et al. notes, however, it is equation 2.19 which is easier to incorporate into the Gujer matrix structure of the TUDP model.

Chapter 3: An Integrated Metabolic Model for Internal Carbon Driven Post-Anoxic Biological Nutrient Removal

3.1 Introduction

Recognizing that the ability to accurately simulate the internal carbon driven post-anoxic B-NR process under different operating conditions and reactor configurations could significantly enhance our understanding of the process and would provide a valuable tool for optimization, a model to simulate this process was created. The particular model processes that are developed in this thesis are focused on the mechanisms underlying the denitrification phase of the internal carbon driven BNR process, i.e. what is occurring in the anoxic zone. In conventional EBPR, an aerobic or anoxic reactor directly follows the anaerobic zone; since PHA is readily available in the aerobic/anoxic zone, PAOs will oxidize PHA reserves for energy. To our knowledge, however, there are currently no published activated sludge models for full scale facilities that specifically include the use of glycogen to drive denitrification when PHA is depleted. Hence, a particular focus of the degradation of these two substrates in the post-anoxic zone was made during the development of the model. In addition, our observations on lab reactors operating in an internal carbon driven post-anoxic BNR configuration has shown that complete ammonia depletion can occur within the anoxic zone without detrimental impact to the process. A second priority in developing the model was to include processes that allowed for the biological activity to continue under nitrate assimilative reduction for biomass growth in the absence of ammonia.

In evaluating modeling approaches, it was noted that a model for biomass which assumes a fixed constitution (an unstructured model) and does not structure the biomass into separate metabolic components can breakdown if the time period in which environmental changes are occurring is within the same order of magnitude as the metabolism's adaptation processes.[81] In the post-anoxic BNR system, the biomass exhibits complete cycling of polymer concentrations within hours while simultaneously experiencing changes in electron acceptor, substrate, and

other conditions. Due to the importance of PHA, glycogen, and polyphosphate cycling within the metabolism of the denitrifiers in this process, a structured metabolic modeling approach was preferred. The ASM 2d and ASM 3 models were considered as candidates for modification in the development of the post-anoxic BNR model. These two models both use a lumped storage parameter that include both PHA and glycogen. Meijer notes, however, that the use of a lumped storage parameter for carbon storage can become problematic since glycogen and PHA have counteracting dynamics (glycogen is generally depleted at the same time that PHA is being synthesized).[62] Lumping both PHA and glycogen into one parameter will thus dampen the counteracting dynamics of PHA and glycogen cycling, which will decrease the accuracy of the storage parameter and its effect in the model. Moreover, as described, PHA and glycogen are independently critical in the WRRF process. As mentioned in Chapter 2.6.3, the TUDP metabolic model has been successfully validated on numerous full scale and lab scale systems and has proven adequate in the simulation of typical EBPR and denitrification systems. This model was therefore used as the backbone of the developed model, with extensions made to the TUDP model that incorporate the degradation of internal glycogen for energy to drive the denitrification process and for BOD, nitrogen, and phosphorus conversions to continue under ammonia limited but nitrate available conditions. The resulting model allows the full reactions and conversions to be simulated, through the anaerobic, aerobic, and anoxic zones, and is easily adaptable to the simulation of full scale facilities.

3.1.1 Model Stoichiometry

Storage Polymer Utilization for Growth and Maintenance. It is hypothesized that in the absence of external substrate, dPAOs and/or dGAOs within the process degrade their internal carbon storage polymers to provide energy to sustain their metabolism, using nitrate and nitrite as the terminal electron acceptor. The TUDP model does not consider GAOs. To avoid unnecessary complexity in the new model, this work also does not consider GAOs in the model processes; denitrification on internal storage products is assumed to occur only by dPAOs. In developing the model stoichiometry for anoxic glycogen degradation, a choice has to be made as to whether the derived energy supports both cellular maintenance and growth or

maintenance processes only. Experimental data (unpublished) on sludge from our SBR reactors fed real wastewater and spiked with ammonia at the end of the aerobic cycle indicated ammonia was being used for biomass synthesis during the processes. In addition, ammonia release from decay of PAOs fed synthetic wastewater was not observed for the first three days in an anoxic long term starvation test performed by Lu et al.[50] The lack of an observed ammonia release (i.e. decay) points to the growth of biomass on glycogen, using ammonia as the nitrogen source for biomass synthesis. Furthermore, Dircks et al. found ammonia uptake occurred during the famine phase of an aerobic SBR reactor and related this uptake to growth and maintenance on internally stored glycogen.[22] Hence, the stoichiometry used to describe the anoxic metabolism of the post-anoxic BNR process will assume that glycogen is utilized for both growth and maintenance.

The developed post-anoxic processes using glycogen as substrate assumes that PAOs will use a portion of the energy from glycogen degradation to support ongoing maintenance processes. In the case when both PHA and glycogen are depleted, it is assumed in this work that PAOs will degrade polyphosphate for maintenance energy within the anoxic zone. In long term starvation experiments on PAO and GAO sludges fed synthetic wastewater, Lopez et al. indicated that in an aerobic environment, PAOs instituted sequential reliance on PHA, glycogen, and polyphosphate for maintenance energy but noted that polyphosphate degradation appeared to be initiated concomitantly with glycogen degradation, after PHA depletion.[49] Lu et al. reported similar results in a nitrate dosed anoxic long term starvation test. They found that PAOs appeared to initially rely on glycogen utilization for maintenance energy after PHA depletion with some energy also produced by hydrolysis of polyphosphate at the same time that glycogen was degraded. After two days, glycogen consumption stabilized at a low concentration and polyphosphate release was substantially increased, indicating that PAOs switched their reliance on glycogen to polyphosphate for their main source of energy. In the anoxic long term starvation test by Lu et al., the reported mixed liquor suspended solids (MLSS) declined over several days, indicating cell decay with little to no growth was occurring during glycogen and polyphosphate degradation. It appears likely that long term starvation, over many hours to days, would induce a change in the microbial metabolism in which growth is suppressed and

energy is conserved to sustain maintenance. In contrast, the microbial environment is clearly different within engineered treatment systems in which microorganisms are continually cycled through relatively short feast and famine conditions. The short time frames between feast and then famine conditions can feasibly inhibit a full acclimation to the new environment and subsequent suppression of growth. Hence, that microbial growth on internal storage polymers in a famine state has been observed in engineered systems is not surprising.

While relatively low rates of polyphosphate degradation for maintenance energy have been observed to occur simultaneous with glycogen utilization, from a practical standpoint, it is proposed to model the utilization of storage polymers for growth and maintenance sequentially such that denitrifiers within the post-anoxic zone will first utilize PHA, then glycogen, and then polyphosphate. This procedure follows that proposed by Lanham et al. in which they modeled PAO and GAO sludge in the aerobic zone of full scale EBPR plants with good results.[46]

Growth and Maintenance From PHA Utilization. The TUDP model uses only PHA as a source of energy and carbon for growth and maintenance of PAOs in both aerobic and anoxic environments. Within the TUDP model structure, the ATP produced to meet growth and maintenance requirements can be interpreted as being met from the difference between the total PHA degraded and the PHA degraded for polyphosphate and glycogen formation, as previously discussed. The stoichiometry of this process is proposed to remain unchanged.

The TUDP model does not account for the case of full PHA depletion, however. In our observations of the post-anoxic EBPR process, PHA depletion almost always occurs by the end of the aerobic cycle, and denitrifiers then appear to rely upon their internal glycogen as a carbon and energy source. In order to model the sequential utilization of storage polymers, Monod type switching functions are proposed to be added to the model's PAO growth and maintenance rate equations. A new process is proposed to be added to the model matrix to simulate glycogen degradation for carbon and energy in the absence of PHA, with a switching function of the form $(\frac{K_{PHA}}{K_{PHA}+X_{PHA}})$ to activate the process as PHA becomes depleted. Similarly, a new process for utilization of polyphosphate for energy to support maintenance as glycogen becomes depleted is also added to the model with similar switching functions to activate the process

upon exhaustion of PHA and glycogen. As long as PHA is present within the PAO cells, it is assumed that the utilization of PHA for energy will be preferred by the cells over glycogen or polyphosphate.

Anoxic Glycogen Utilization. This work assumes that denitrifying activity using glycogen as the substrate is performed by dPAOs. The new integrated model only considers one state variable for PAOs, X_{PAO}, as does the ASM2d and TUDP models. To account for the dPAO fraction, the TUDP model parameter $\eta_{NO.PAO}$ is applied to the glycogen degradation rate equations, with a default value of 0.8. The new model assumes that when PHA is depleted in the post-anoxic BNR process, dPAOs will oxidize glycogen for growth and maintenance which is hypothesized to occur according to the following steps:

1. In the absence of exogenous substrate, glycogen is degraded to glucose-6-phosphate.
2. Some glucose-6-phosphate is degraded to Acetyl-CoA through the EMP pathway for production of reducing equivalents and ATP.
3. Acetyl-CoA enters the TCA cycle for further production of reducing equivalents.
4. Reducing equivalents are oxidized to produce ATP through oxidative phosphorylation using nitrate or nitrite as the electron acceptor.
5. Biomass is formed directly from the glucose-6-phosphate pool.
6. Ammonia is preferentially used as the nitrogen source for biomass synthesis. If ammonia in solution becomes depleted, denitrifiers will reduce available nitrate and nitrite to ammonia for assimilation during synthesis.

A network of the processes can be formed as shown in Fig. 3.1

In considering the specific pathway of glycogen degradation, a choice must be made between the EMP or the ED pathway. In this work, it is assumed that endogenous degradation of glycogen by denitrifying PAOs occurs through the EMP pathway. This choice is based on the following two observations:

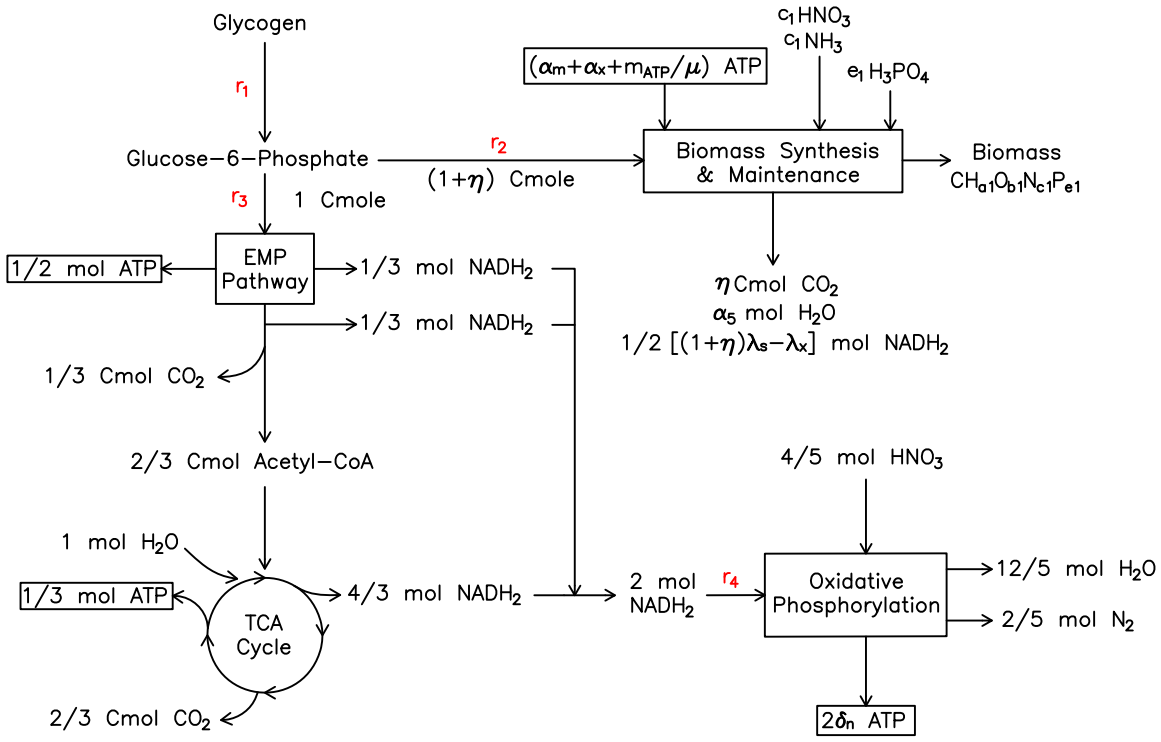

Coefficients

α_m=ATP Required for synthesis of biomass monomers on G6P

α_x=ATP Required for polymerization of monomers

m_{ATP}=ATP Required for maintenance

γ_s=Degree of reduction of substrate (G6P)

γ_x=Degree of reduction of biomass

δ_n=Anoxic biomass P/O ratio

$\alpha_5=[(1+\eta)b_2+4e_1-b_1-2\eta]$

Figure 3.1: Anoxic glycogen degradation metabolism (derived in this work with assistance from Filipe et al.[24] and Dircks et al.[22])

1. The TUDP model assumes anaerobic glycogen degradation occurs solely through the EMP pathway. The TUDP model has been successfully used to simulate many EBPR systems, and the pathway utilized for endogenous glycogen degradation is anticipated to be the same as that for anaerobic glycogen degradation since the machinery for the EMP pathway would already be present within the cell. Use of the EMP pathway for endogenous glycogen degradation will therefore provide consistency with the TUDP model's use of anaerobic glycogen degradation.

2. Metagenomic analysis of sludge dominated by *Accumulibacter* clade IIA (a prevalent

PAO) pointed to the use of the EMP pathway for glycogen degradation for this PAO since the genes required for the EMP pathway were present in the genome but that the genes necessary for the ED pathway were absent.[53] While the specific contribution of *Accumulibacter* to denitrification within the post-anoxic EBPR process has yet to elucidated, *Accumulibacter* has been found within our reactors[113] and the identification of the EMP pathway with *Accumulibacter* provides support for choosing the EMP pathway in the absence of further evidence.

By use of a metabolic flux analysis, the yield of biomass on glycogen as well as the maintenance coefficient for the metabolism can be derived. The procedure consists of identifying the stoichiometry of the relevant metabolic pathways and tracking the steady state flow of carbon from the substrate (glycogen) and intermediate metabolites through the different branches of the metabolic network to the final products. In this case the metabolic network is relatively simple. Glycogen is considered to be the substrate and biomass is considered to be the only product formed. In this procedure, reaction rates that can be measured, e.g. glycogen degradation rate or nitrate consumption rate, will be denoted by the notation r_i. Internal fluxes, or rates, of metabolites along pathways within the cell that generally cannot be measured in vivo will be denoted by the notation v_i. The procedure relies upon the assumption that the fluxes are in steady state, i.e. that there is no net production or decrease of internal metabolites, such as Acetyl-CoA, within the cell. Furthermore, in the foregoing analysis, $NADH_2$ is considered to be the form of reducing equivalent active within the metabolic network, even through other reducing equivalents may in reality be produced and consumed. The validity of this assumption for simple metabolic network analysis was discussed in Section 2.6.3.

Degree of Reduction. The following analysis relies upon the degree of reduction concept, which is described extensively by Roels.[81] The degree of reduction is a measure of the amount of available electrons in a compound and can be used to determine the correct amount of reduction equivalents to apply to the stoichiometric equation for any process in the metabolic network. The concept can be briefly described as follows:[105]

1. For each element in the stoichiometric equation, a redox-neutral reference compound is

described. The degree of reduction of each of these reference compounds is equal to zero. For the elements C,O,H,N,S and P, the compounds CO_2, H_2O, NH_3, H_2SO_4, and H_3PO_4 are typically chosen to be redox neutral.

2. A unit of redox is defined as H = 1.

3. A balance on each redox neutral compound in Item 1 then results in the following redox levels: C = +4, O = -2, H = +1, N = -3, S = +6, P = +5.

4. Nitrogen in biomass is considered a special case, depending on the nitrogen source. If ammonia is used as the nitrogen source, NH_3 is used as the reference compound for nitrogen and degree of reduction for N = -3, whereas if nitrate is used as the nitrogen source, nitrate is used as the reference compound and N = +5.

From these elemental redox levels, the degree of reduction of any compound consisting of these elements can be determined. As an example, the degree of reduction of glycogen, $CH_{10/6}O_{5/6}$ is equal to 4.0. Similarly, a balance of degree of reduction on a stoichiometric equation can be performed to determine the amount of reducing equivalents that must be applied to keep the overall degree of reduction of the process equal to zero, since electrons must be conserved.

3.1.2 Biochemical Reactions Using Glucose-6-Phosphate as Substrate

The degree of reduction for biomass, glucose-6-phosphate, and $NADH_2$ is utilized in the derivation of the yield and maintenance coefficients. Biomass is assumed to have the elemental composition $CH_{2.09}O_{0.54}N_{0.2}P_{0.015}$, which is used in the TUDP model. This formula was originally determined by Smolders et al. from PAO enriched sludge in a sequencing batch reactor fed synthetic wastewater.[89] The elemental composition of biomass, substrate, and metabolic products can generally be expressed as $CH_aO_bN_cS_dP_e$. The phosphoryl group attached to the glucose moiety in glucose-6-phosphate is not tracked in the model. Glucose-6-phosphate (whose full molecular formula is $C_6H_{13}O_9P$) is thus considered to be $C_6H_{12}O_6$. On a C-mole basis, this becomes CH_2O. The elemental composition for biomass and glucose-6-phosphate are itemized as:

Biomass	Glucose-6-Phosphate
$CH_{2.09}O_{0.54}N_{0.20}P_{0.015}$	CH_2O
a_1=2.09	a_2=2
b_1=0.54	b_2=1
c_1=0.20	c_2=0.00
d_1=0.00	d_2=0.00
e_1=0.015	e_2=0.00

In the following analysis, $NADH_2$ is considered to be composed of two hydrogen atoms.

The reference compounds H_2O, CO_2, and H_3PO_4 are defined to have a degree of reduction of zero. When ammonia is used as the nitrogen source for biomass synthesis, NH_3 is used as the reference compound for nitrogen in biomass while HNO_3 is used when nitrate is used as the nitrogen source. The degree of reduction of biomass, glucose-6-phosphate, and $NADH_2$ are therefore:

$$\lambda_x = 4 + a_1 - 2b_1 - 3c_1 + 6d_1 + 5e_1 = \underline{\underline{4.485}} \quad \text{Biomass degree of reduction w/}NH_3\text{ as nitrogen source} \tag{3.1}$$

$$\lambda_{x.\varphi} = 4 + a_1 - 2b_1 + 5c_1 + 6d_1 + 5e_1 = \underline{\underline{6.085}} \quad \text{Biomass degree of reduction w/}NO_3\text{ as nitrogen source} \tag{3.2}$$

$$\lambda_s = 4 + a_2 - 2b_2 - 3c_2 + 6d_2 + 5e_2 = \underline{\underline{4.0}} \quad \text{G6-P degree of reduction} \tag{3.3}$$

$$\lambda_{nadh} = 2(+1) = \underline{\underline{2.0}} \quad NADH_2\text{ degree of reduction} \tag{3.4}$$

Using these concepts, the metabolic fluxes through the network can now be characterized. The total metabolism can be described by six internal reactions which are described below. These reactions are based on the formation and degradation of glucose-6-phosphate through the EMP pathway, similar to the procedure of Dircks et al.[22]

Reaction 1. Glycogen Degradation to Glucose-6-Phosphate

This reaction is denoted r_1 in Figure 3.1. Glycogen is a branched polymer of glucose residues with linear α-1,4-glycosidic linkages and branch points occurring at α-1,6-glycosidic bonds as shown in Figure 3.2.

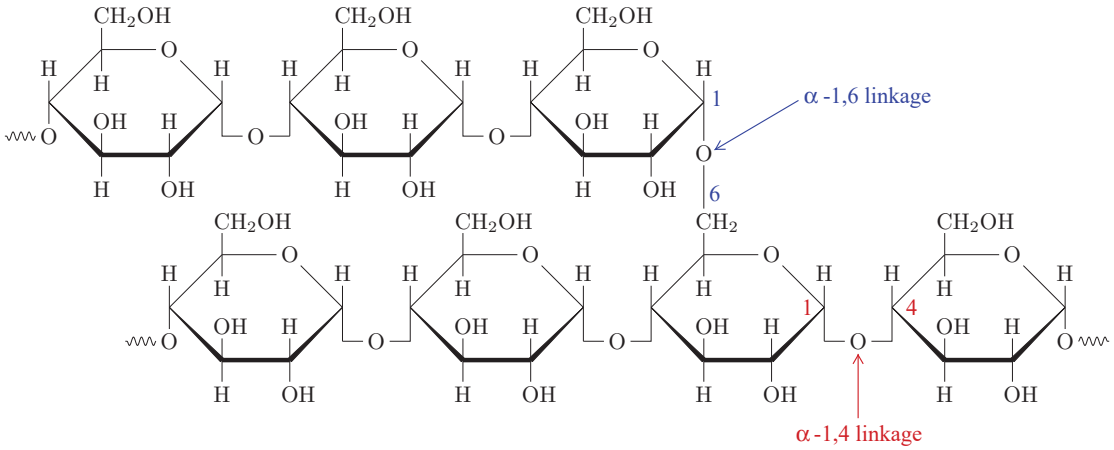

Figure 3.2: Structure of Glycogen Polymer

Glycogen phosphorylase cleaves glycosyl residues from the nonreducing ends of glycogen which are converted to glucose-1-phosphate by the addition of orthophosphate in the process. Glucose-1-phosphate is subsequently converted to glucose-6-phosphate by the enzyme *phosphoglucomutase*.[95] The cleavage of glycosyl residues from the nonreducing ends of glycogen and their subsequent conversion to glucose-6-phosphate does not require the use of ATP since during glycogen formation, the glycosyl residues added to the nonreducing ends of glycogen are of an already activated form of glucose (ADP-glucose). It should be noted that in animals glycogen is synthesized from UDP-glucose instead of ADP-glucose.[28]

Glycogen phosphorylase stops cleaving glycosyl residues a distance of four residues from a branch point. A *transferase* enzyme shifts three of the remaining glycosyl residues to another outer branch for subsequent cleavage by *glycogen phosphorylase*. The final residue in the branch is released by a debranching enzyme, which requires phosphorylation and consumption of ATP when the residue unit is converted to glucose-6-phosphate. Dircks et al. notes that typically one in ten glycosyl residues are branched which results in a net ATP demand of 1/60 mol ATP/C-mol glycogen. Following Dircks et al., this ATP demand is assumed to be inconsequential and is not included in the stoichiometry of the model.

The overall generation of glucose-6-phosphate from glycogen is described as follows (on a C-mole basis):[22]

$$\underset{\text{glycogen}}{CH_{10/6}O_{5/6}} + \frac{1}{6}H_2O \longrightarrow \underset{\text{G6-P}}{CH_2O}$$

Reaction 2. Synthesis of Biomass from Glucose-6-Phosphate

Denitrifiers (considered to be dPAOs) are assumed by the model to degrade internal glycogen storage polymers to glucose-6-phosphate for biomass synthesis in the absence of external carbon substrate and upon depletion of their PHA stores. The formation of biomass on glucose-6-phosphate with ammonia as the nitrogen source can be described as follows:

$$(1+\eta)\underset{\text{substrate}}{CH_{a2}O_{b2}} + \alpha_1 NH_3 + \alpha_2 \underset{\text{phosphate}}{H_3PO_4} + \alpha_3 ATP \longrightarrow \underset{\text{biomass}}{CH_{a1}O_{b1}N_{c1}S_{d1}P_{e1}} + \eta CO_2 + \alpha_4 NADH_2 + \alpha_5 H_2O$$

$$\implies (1+\eta)\underset{\text{G6-P}}{CH_2O} + \alpha_1 NH_3 + \alpha_2 \underset{\text{phosphate}}{H_3PO_4} + \alpha_3 ATP \longrightarrow \underset{\text{biomass}}{CH_{2.09}O_{0.54}N_{0.2}P_{0.015}} + \eta CO_2 + \alpha_4 NADH_2 + \alpha_5 H_2O \quad (3.5)$$

The coefficient, η, is the CO_2 released from the synthesis of one C-mole of biomass on glucose-6-phosphate. A value of 0.131 C-mole is stated by Dircks et al.,[22] which is used here. Therefore:

$$\underline{\underline{\eta = 0.131}}$$

A balance on nitrogen gives:

$$\alpha_1 = c_1 \implies \underline{\underline{\alpha_1 = 0.2}}$$

The coefficient on phosphate is found from a balance on phosphorus:

$$\alpha_2 = e_1 \implies \underline{\underline{\alpha_2 = 0.015}}$$

A balance on oxygen results in:

$$(1+\eta)b_2 + 4\alpha_2 = b_1 + 2\eta + \alpha_5 \implies \alpha_5 = (1+\eta)b_2 + 4\alpha_2 - b_1 - 2\eta$$

$$\implies \alpha_5 = (1)(1.131) + 4(0.015) - 0.54 - 2(0.131) \implies \underline{\underline{\alpha_5 = 0.389}}$$

A balance on the degree of reduction can be used to determine the coefficient on $NADH_2$:

$$(1+\eta)\lambda_s = \lambda_x + \alpha_4\lambda_{nadh} \implies 2\alpha_4 = (1+\eta)\lambda_s - \lambda_x$$

$$\implies \underline{\underline{\alpha_4 = \frac{1}{2}\left[(1+\eta)\lambda_s - \lambda_x\right]}}$$

The coefficient on ATP, α_3, can be expressed in terms of the ATP demand for the formation of biomass monomers, the amount of ATP required for the synthesis of biomass from monomers, and the ATP required to support cellular maintenance. Assumed are:

$\alpha_m = 0.701$ mol ATP/Cmol	ATP required for synthesis of biomass from glucose-6-phosphate[22]
$\alpha_x = 1.5$ mol ATP/Cmol	ATP required for synthesis of biomass from monomers[22]

The ATP demand for maintenance can be expressed as m_{ATP}/μ where m_{ATP} is the specific ATP demand for maintenance and μ is the specific growth rate. Therefore:

$$\alpha_3 = \left(\alpha_m + \alpha_x + \frac{m_{ATP}}{\mu}\right)$$

Substitution of the values obtained for the coefficients into Equation B.1 gives:

$$(1+\eta)\underset{\text{G6-P}}{CH_2O} + 0.2\,NH_3 + 0.015\underset{\text{phosphate}}{H_3PO_4} + \left(\alpha_m + \alpha_x + \frac{m_{ATP}}{\mu}\right)ATP$$

$$\longrightarrow \underset{\text{biomass}}{CH_{2.09}O_{0.54}N_{0.2}P_{0.015}} + \eta\,CO_2 + \frac{1}{2}\left[(1+\eta)\lambda_s - \lambda_x)\right]NADH_2 + 0.389\,H_2O$$

This describes biomass synthesis from glucose-6-phosphate with ammonia as the nitrogen source.

When ammonia is depleted in bulk solution, denitrifiers are assumed to use any available nitrate in solution as their nitrogen source for the synthesis of biomass. Performing a similar balance on nitrogen, phosphorus, and degree of reduction as performed for biomass synthesis with ammonia as the nitrogen source results in:

$$(1+\eta)\underset{\text{G6-P}}{\text{CH}_2\text{O}} + 0.2\,\text{HNO}_3 + 0.015\,\underset{\text{phosphate}}{\text{H}_3\text{PO}_4} + \left(\alpha_m + \alpha_x + \frac{\text{m}_{\text{ATP}}}{\mu}\right)\text{ATP}$$

$$\longrightarrow \underset{\text{biomass}}{\text{CH}_{2.09}\text{O}_{0.54}\text{N}_{0.2}\text{P}_{0.015}} + \eta\,\text{CO}_2 + \frac{1}{2}\left[(1+\eta)\lambda_s - \lambda_{x.\varphi}\right]\text{NADH}_2 + 0.989\,\text{H}_2\text{O}$$

The details of this derivation are included in Appendix B.

Reaction 3. Degradation of Glucose-6-Phosphate through the EMP Pathway

Degradation of glucose-6-phosphate through the EMP pathway occurs as follows (on a C-mole basis):[24]

$$\underset{\text{G6-P}}{\text{CH}_2\text{O}} \longrightarrow \frac{2}{3}\,\text{NADH}_2 + \frac{1}{2}\,\text{ATP} + \frac{1}{3}\,\text{CO}_2 + \frac{2}{3}\,\text{Acetyl}-\text{CoA}$$

Subsequent degradation of Acetyl-CoA through the TCA cycle occurs according to the following stoichiometry (on a C-mole basis):[21]

$$\frac{2}{3}\,\text{AcetylCoA} + \text{H}_2\text{O} \longrightarrow \frac{2}{3}\,\text{CO}_2 + \frac{4}{3}\,\text{NADH}_2 + \frac{1}{3}\,\text{ATP}$$

The TCA cycle is known to produce two molecules of NADH_2, one molecule of NADPH_2, and one molecule of FADH_2 per mole of Acetyl-CoA. NADPH_2, NADH_2, and FADH_2 are assumed to be equivalent in the TUDP model and in this work, as previously discussed. Combining the above two equations results in the following overall equation for glucose-6-phosphate degradation through the TCA cycle:

$$\underset{\text{G6-P}}{\text{CH}_2\text{O}} + \text{H}_2\text{O} \longrightarrow \frac{5}{6}\,\text{ATP} + \text{CO}_2 + 2\,\text{NADH}_2$$

Reaction 4. Oxidative Phosphorylation

The stoichiometry of the production of ATP through oxidative phosphorylation using nitrate as the electron acceptor is as presented by Kuba et al.:[44]

$$\text{NADH}_2 + \frac{2}{5}\,\underset{\text{nitrate}}{\text{HNO}_3} \longrightarrow \frac{1}{5}\,\text{N}_2 + \delta_n\,\text{ATP} + \frac{6}{5}\,\text{H}_2\text{O}$$

As noted in Chapter 2.6.3, the parameter δ_n is the amount of ATP produced per $NADH_2$ molecule (same as the P/O ratio but with nitrate as the electron acceptor). The TUDP model uses a default value of δ_n=0.925 based on work by Kuba et al. The same default value is assumed in this work.

3.2 Yield and Maintenance Coefficients on Glycogen With Ammonia as the Nitrogen Source for Biomass Synthesis

Yield and maintenance coefficients are required in the new model processes for denitrification with glycogen as substrate. The yield and maintenance coefficients with ammonia being used as the nitrogen source for biomass synthesis are derived below. Following this derivation, the coefficients for denitrifiers growing on glycogen with nitrate as the nitrogen source are considered. The biochemical reaction network was previously defined in Section 3.1.1. A simplified schematic of the network is shown in Figure 3.3.

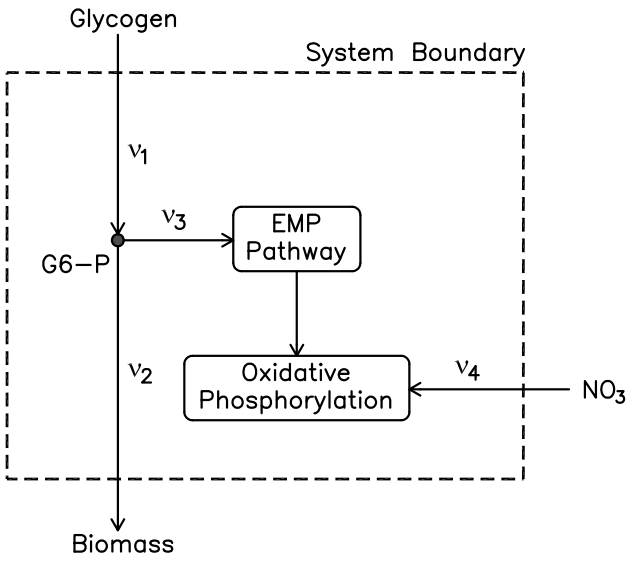

Figure 3.3: Metabolic network schematic for post-anoxic glycogen utilization.

The reactions describing the metabolism presented above are summarized in Table 3.1.

The net conversion rate of substances (the rates of production or consumption of substances) are denoted by r_i. The internal rates of reactions, or flux, are denoted by ν_i. In this case

Table 3.1: Assumed stoichiometric equations for metabolic processes sctive in anoxic glycogen degradation

Reaction	Description	Stoichiometric Equation
R1	Glycogen to G6-P	$CH_{10/6}O_{5/6} + \frac{1}{6}\,H_2O \xrightarrow{\nu_1} CH_2O$
R2a	Synthesis of Biomass (NH_3)	$(1+\eta)CH_2O + 0.2\,NH_3 + 0.015\,H_3PO_4 + (\alpha_m + \alpha_x + m_{ATP}/\mu)\,ATP \xrightarrow{\nu_2} CH_{2.09}O_{0.54}N_{0.2}P_{0.015} + \eta CO_2 + \frac{1}{2}\,[(1+\eta)\lambda_s - \lambda_x)]\;NADH_2 + 0.389\;H_2O$
R2b	Synthesis of Biomass (NO_3)	$(1+\eta)CH_2O + 0.2\,HNO_3 + 0.015\,H_3PO_4 + (\alpha_m + \alpha_x + m_{ATP}/\mu)\,ATP \xrightarrow{\nu_2} CH_{2.09}O_{0.54}N_{0.2}P_{0.015} + \eta CO_2 + \frac{1}{2}\,[(1+\eta)\lambda_s - \lambda_{x.\varphi})]\;NADH_2 + 0.989\;H_2O$
R3	G6-P Degradation	$CH_2O + H_2O \xrightarrow{\nu_3} \frac{5}{6}\,ATP + CO_2 + 2\,NADH_2$
R4	Oxidative Phosphorylation	$NADH_2 + \frac{2}{5}\,HNO_3 \xrightarrow{\nu_4} \frac{1}{5}\,N_2 + \delta_n\,ATP + \frac{6}{5}\,H_2O$

the metabolic network consists of only one substrate (glycogen) and one product (biomass). Carbon from glycogen flows to the glucose-6-phosphate pool at a rate of $-r_s = \nu_1$. Carbon from the glucose-6-phosphate pool then flows toward either biomass production (product) or the EMP pathway for energy (ATP) production.

The glycogen and nitrate degradation rates and the biomass production rate can be related to the internal flux rates through the stoichiometry in Table 3.1. For example, when ammonia is used as the nitrogen source for growth, nitrate is only consumed in the oxidative phosphorylation reaction (Reaction 4). The stoichiometric coefficient on nitrate in this reaction indicates a consumption rate of $2/5\,\nu_4$. Similarly, using the stoichiometric relations in Table 3.1, the following rates are obtained:

$$-r_s = \nu_1 \qquad \text{Glycogen degradation rate} \tag{3.6}$$

$$r_x = \nu_2 \qquad \text{Biomass synthesis rate} \tag{3.7}$$

$$-r_{no3} = \frac{2}{5}v_4 \qquad \text{Denitrification rate} \tag{3.8}$$

The flux analysis relies upon the assumption that internal metabolite concentrations are in a steady-state condition. Therefore, there is no net accumulation or degradation of glucose-6-phosphate, ATP, or $NADH_2$ concentrations within the cell. Referring to the stoichiometric equations in Table 3.1 and performing a balance of each of these constituents across the system, it is seen that their conversion rates can be expressed as:

$$r_{g6p} = \nu_1 - (1+\eta)\nu_2 - \nu_3 = 0 \qquad \text{G6-P balance} \tag{3.9}$$

$$r_{atp} = (\alpha_m + \alpha_x + m_{ATP}/\mu)\,\nu_2 + \frac{5}{6}\nu_3 + \delta_n\nu_4 = 0 \qquad \text{ATP balance} \tag{3.10}$$

$$r_{nadh} = \frac{1}{2}\left[(1+\eta)\lambda_s - \lambda_x\right]\nu_2 + 2\nu_3 - \nu_4 = 0 \qquad \text{NADH}_2 \text{ balance} \tag{3.11}$$

According to the stoichiometry in Table 3.1, the conversion rates can be expressed as a function of the internal flux rates through a stoichiometric reaction matrix as follows:

$$\begin{bmatrix} r_s \\ r_x \\ r_{no3} \\ r_{g6p} \\ r_{atp} \\ r_{nadh} \end{bmatrix} = \begin{bmatrix} -1 & 0 & 0 & 0 \\ 0 & 1 & 0 & 0 \\ 0 & 0 & 0 & -\frac{2}{5} \\ 1 & -(1+\eta) & -1 & 0 \\ 0 & -\left(\alpha_m + \alpha_x + \frac{\mathrm{m_{ATP}}}{\mu}\right) & \frac{5}{6} & \delta_n \\ 0 & \frac{1}{2}\left[(1+\eta)\lambda_s - \lambda_x\right] & 2 & -1 \end{bmatrix} \cdot \begin{bmatrix} \nu_1 \\ \nu_2 \\ \nu_3 \\ \nu_4 \end{bmatrix} \tag{3.12}$$

The system has four unknown flux rates (ν_1-ν_4) which are related through the three linear equations 3.9-3.11. Any three of the flux rates can therefore be defined in terms of the fourth flux rate. It is chosen to define the flux rates in terms of biomass formation, ν_2. To solve the system, a method described by Villadsen et al.[105] is used.

Equation 3.12 is configured so that the first rows of the stoichiometric matrix consist of the reactions for formation/depletion of substrate while the following rows consists of reactions for the formation of products and metabolites. The last three rows consist of the reactions for the internal conserved quantities that exist in steady state. Next, a vector $\mathbf{V_1}$ is defined whose elements are the fluxes in which the remaining flux rates will be defined in terms of. In this case, $\mathbf{V_1}$ consists of only one flux rate, ν_2 (biomass formation). The remaining flux rates make up a vector, $\mathbf{V_2}$.

The stoichiometric matrix is set as $\mathbf{T}$, which is divided into two submatrices. The first, $\mathbf{T_1}$, is the matrix whose columns correspond to $\mathbf{V_2}$, and rows corresponding to the steady-state

reactions (glucose-6-phosphate, ATP, and $NADH_2$ in this case). The second submatrix, $\mathbf{T_2}$, has columns corresponding to vector $\mathbf{V_1}$ and rows corresponding to the steady-state reactions. The vector $\mathbf{V_2}$ is then solved in terms of $\mathbf{V_1}$ by the following:

$$\mathbf{V_2} = -\mathbf{T_1}^{-1} \cdot \mathbf{T_2} \cdot \mathbf{V_1} \tag{3.13}$$

For the system in Equation 3.12 the vectors and matrices are defined as:

$$\mathbf{V_1} = \begin{bmatrix}\nu_2\end{bmatrix} \qquad \mathbf{V_2} = \begin{bmatrix}\nu_1 \\ \nu_3 \\ \nu_4\end{bmatrix} \qquad \mathbf{T_1} = \begin{bmatrix}1 & -1 & 0 \\ 0 & \frac{5}{6} & \delta_n \\ 0 & 2 & -1\end{bmatrix} \qquad \mathbf{T_2} = \begin{bmatrix}-(1+\eta) \\ -\left(\alpha_m + \alpha_x + \mathrm{m_{ATP}}/\mu\right) \\ \frac{1}{2}\left[(1+\epsilon)\lambda_s - \lambda_x\right]\end{bmatrix}$$

From Equation 3.7, r_x is substituted for ν_2 in $\mathbf{V_1}$. $\mathbf{V_2}$ is then found as follows:

$$\mathbf{V_2} = -\mathbf{T_1}^{-1} \cdot \mathbf{T_2} \cdot \mathbf{V_1}$$

$$\implies \mathbf{V_2} = -\begin{bmatrix}1 & -1 & 0 \\ 0 & \frac{5}{6} & \delta_n \\ 0 & 2 & -1\end{bmatrix}^{-1} \cdot \begin{bmatrix}-(1+\eta) \\ -\left(\alpha_m + \alpha_x + \mathrm{m_{ATP}}/\mu\right) \\ \frac{1}{2}\left[(1+\eta)\lambda_s - \lambda_x\right]\end{bmatrix} \cdot r_x$$

$$\implies \begin{bmatrix}\nu_1 \\ \nu_3 \\ \nu_4\end{bmatrix} = \begin{bmatrix} r_x\left[\eta + \dfrac{6\left(\alpha_x + \alpha_m + \dfrac{\mathrm{m_{ATP}}}{\mu}\right)}{12\delta_n + 5} + \dfrac{6\delta_n\left[\dfrac{\lambda_x}{2} - \dfrac{\lambda_s(\eta+1)}{2}\right]}{12\delta_n + 5} + 1\right] \\ r_x\left[\dfrac{6\left(\alpha_x + \alpha_m + \dfrac{\mathrm{m_{ATP}}}{\mu}\right)}{12\delta_n + 5} + \dfrac{6\delta_n\left[\dfrac{\lambda_x}{2} - \dfrac{\lambda_s(\eta+1)}{2}\right]}{12\delta_n + 5}\right] \\ r_x\left[\dfrac{\alpha_x + \alpha_m + \dfrac{\mathrm{m_{ATP}}}{\mu}}{\delta_n + \dfrac{5}{12}} - \dfrac{5\delta_n\left[\dfrac{\lambda_x}{2} - \dfrac{\lambda_s(\eta+1)}{2}\right]}{12\delta_n + \dfrac{5}{12}}\right]\end{bmatrix} \tag{3.14}$$

From Equation 3.6, the glycogen degradation rate can be expressed as $-r_s = \nu_1$. Therefore, from Equation 3.14 the glycogen degradation rate is equivalent to:

$$-r_s = r_x \left[\eta + \frac{6\left(\alpha_x + \alpha_m + \frac{\mathrm{m_{ATP}}}{\mu}\right)}{12\delta_n + 5} + \frac{6\delta_n \left[\frac{\lambda_x}{2} - \frac{\lambda_s(\eta+1)}{2}\right]}{12\delta_n + 5} + 1 \right]$$

$$= (r_x\,\eta)\left(\frac{2\delta_n + \frac{5}{6}}{2\delta_n + \frac{5}{6}}\right) + \frac{\left(\alpha_x + \alpha_m + \frac{\mathrm{m_{ATP}}}{\mu}\right)}{2\delta_n + \frac{5}{6}} r_x + \frac{\frac{1}{2}\delta_n\left[\lambda_x - \lambda_s(\eta+1)\right]}{2\delta_n + \frac{5}{6}}\, r_x + \left(\frac{2\delta_n + \frac{5}{6}}{2\delta_n + \frac{5}{6}}\right) r_x$$

$$= \frac{2\delta_n\eta + \frac{5}{6}\eta + \alpha_x + \alpha_m + \frac{\mathrm{m_{ATP}}}{\mu} + \frac{1}{2}\delta_n\left[\lambda_x - \lambda_s(\eta+1)\right] + 2\delta_n + \frac{5}{6}}{2\delta_n + \frac{5}{6}}\, r_x$$

$$= \frac{\frac{1}{2}\delta_n\left[\lambda_x - \lambda_s(\eta+1) + 4\eta + 4\right] + \left(\alpha_x + \alpha_m + \frac{5}{6}\eta + \frac{5}{6}\right)}{2\delta_n + \frac{5}{6}}\, r_x + \frac{\frac{\mathrm{m_{ATP}}}{\mu}}{2\delta_n + \frac{5}{6}}\, r_x \tag{3.15}$$

By noting that the biomass concentration in the reactor, C_x is equivalent to r_x/μ, the glycogen degradation rate can then be expressed as:

$$-r_s = \frac{\frac{1}{2}\delta_n\left[\lambda_x - \lambda_s(\eta+1) + 4\eta + 4\right] + \left(\alpha_x + \alpha_m + \frac{5}{6}\eta + \frac{5}{6}\right)}{2\delta_n + \frac{5}{6}}\, r_x + \frac{\mathrm{m_{ATP}}}{2\delta_n + \frac{5}{6}}\, C_x \tag{3.16}$$

The term on r_x is the inverse yield coefficient of biomass formation on glycogen while the term on C_x is the maintenance coefficient for biomass on glycogen. Thus:

$$-r_s = \frac{1}{Y_{gx}} r_x + \mathrm{m_{gx}} C_x \tag{3.17}$$

where:

$$Y_{gx} = \frac{\frac{1}{2}\delta_n\left[\lambda_x - \lambda_s(\eta+1) + 4\eta + 4\right] + \left(\alpha_x + \alpha_m + \frac{5}{6}\eta + \frac{5}{6}\right)}{2\delta_n + \frac{5}{6}} \tag{3.18}$$

$$m_{gx} = \frac{\mathrm{m_{ATP}}}{2\delta_n + \frac{5}{6}} \tag{3.19}$$

$$Y_{gx} = \frac{2\delta_n + \frac{5}{6}}{\frac{1}{2}\delta_n\left[\lambda_x - \lambda_s(\eta+1) + 4\eta + 4\right] + \left(\alpha_x + \alpha_m + \frac{5}{6}\eta + \frac{5}{6}\right)} \tag{3.20}$$

$$m_{gx} = \frac{\mathrm{m_{ATP}}}{2\delta_n + \frac{5}{6}} \tag{3.21}$$

The TUDP model uses an anoxic $\mathrm{m_{ATP}}$ value of 0.01 mole ATP/Cmol biomass per hour which was obtained by Kuba et al. for EBPR sludge fed synthetic wastewater in an aerobic-anoxic SBR.[41] Substituting this and the previously stated values for λ_x, λ_s, η, and δ_n into Equations 3.20 and 3.21 results in the following:

$$Y_{gx} = 0.5102 \text{ Cmol biomass/Cmol glycogen} \tag{3.22}$$

$$m_{gx} = 0.0038 \text{ Cmol glycogen/Cmol biomass-hr} \tag{3.23}$$

The parameters must be expressed on a COD basis to be incorporated into the model matrix. Using a value of 32.017 g COD per C-mole of glycogen and 32.017 g COD per C-mole of biomass results in:

$$\boxed{Y_{gx} = 0.5728 \quad \frac{\text{g COD biomass}}{\text{g COD glycogen}}} \qquad (\mathrm{NH_3} \text{ as nitrogen source}) \tag{3.24}$$

$$\boxed{m_{gx} = 0.0812 \quad \frac{\text{g COD glycogen}}{\text{g COD biomass-day}}} \qquad (\mathrm{NH_3} \text{ as nitrogen source}) \tag{3.25}$$

3.3 Yield and Maintenance Coefficients on Glycogen With Nitrate as the Nitrogen Source for Biomass Synthesis

The denitrifying organisms are assumed to assimilate nitrate for biomass synthesis when ammonia is depleted in solution. The assimilation of nitrate requires the transfer of 8 electrons to the nitrate species to reduce it to ammonia form so that it can be incorporated into the biomass. This transfer of electrons reduces the available energy which could otherwise be used for ATP production, reducing the overall biomass yield. Due to the transfer of electrons to the nitrate species, the degree of reduction of nitrogen in biomass is changed from a value of -3 to +5 when nitrate is used as the nitrogen source. Therefore, the degree of reduction of biomass

is calculated to be:

$$\lambda_{x.\varphi} = 4 + a_1 - 2b_1 - 3c_1 + 6d_1 + 5e_1 = \underline{\underline{6.085}} \quad \text{Biomass degree of reduction} \tag{3.26}$$

The degree of reduction of all other components remains the same. The overall metabolic network and reactions for the metabolism are assumed to remain the same as when ammonia is used as the nitrogen source. Therefore Equations 3.20 and 3.21 can be used to calculate the yield and maintenance coefficients with nitrate as the nitrogen source. The new biomass degree of reduction, $\lambda_{x.\varphi}$, is substituted for λ_x in Equation 3.20. The remaining variables in Equations 3.20 and 3.21 are not dependent on the degree of reduction of biomass, and therefore remain unchanged. Furthermore, the internal cellular maintenance processes and thus the ATP demand for cellular maintenance (m_{ATP}) is also assumed to remain unchanged. The following yield and maintenance coefficients are thus obtained:

$$Y_{gx.\varphi} = 0.4477 \quad \frac{\text{Cmol biomass}}{\text{Cmol glycogen}} \tag{3.27}$$

$$m_{gx.\varphi} = 0.0038 \quad \frac{\text{Cmol glycogen}}{\text{Cmol biomas-hour}} \tag{3.28}$$

Conversion to a COD unit basis gives:

$$\boxed{Y_{gx.\varphi} = 0.5027 \quad \frac{\text{g COD biomass}}{\text{g COD glycogen}}} \qquad (NO_3 \text{ as nitrogen source}) \tag{3.29}$$

$$\boxed{m_{gx.\varphi} = 0.0812 \quad \frac{\text{g COD glycogen}}{\text{g COD biomass-day}}} \qquad (NO_3 \text{ as nitrogen source}) \tag{3.30}$$

3.4 Maintenance Coefficient With Polyphosphate as Energy Source

The new model assumes that in the absence of external carbon substrate and depletion of their PHA and glycogen storage polymers, dPAOs will hydrolyze their internal polyphosphate polymers for energy to sustain maintenance activities. Since theoretically no carbon is available

for biomass synthesis, polyphosphate is assumed to support maintenance activities only. Smolders et al. indicates that 1 mole of ATP is produced per mole of polyphosphate hydrolyzed.[89] Therefore, the maintenance coefficient when polyphosphate is used as the energy source, m_{pp}, is derived as $m_{pp} = \mathrm{m_{ATP}}$. Conversion to a gram P per gram COD basis is accomplished by using the molecular weight of phosphorus and a value of 35.948 g COD/Cmol biomass to give:

$$\boxed{m_{gx.pp} = 0.2068 \quad \frac{\text{g P}}{\text{g COD biomass-day}}} \tag{3.31}$$

3.5 PAO and OHO Aerobic and Anoxic Yield Coefficients Under Ammonia Limitation for TUDP Model Processes (Glycogen Not Used as Substrate)

The TUDP model does not consider the case when ammonia is depleted in solution and active bacteria must assimilate nitrate as the nitrogen source to support biomass growth, which thereby lowers their biomass yields. Ammonia is frequently observed to be depleted in the aerobic and anoxic zones of our laboratory reactors operating in a post-anoxic BNR configuration, however. Indeed, it is not uncommon to see ammonia being fully depleted within one hour of a two hour aerobic cycle of an SBR laboratory reactor configured in the post-anoxic BNR configuration. In many cases, PHA depletion is not depleted by the time ammonia limitation occurs. Due to the lower biomass yields that occur under ammonia limited conditions, this condition must be accounted for. In Sections 3.2 and 3.3, biomass yield and maintenance coefficients for denitrifying PAOs growing on internally stored glycogen (after PHA depletion) were derived for the respective case of ammonia and nitrate as the nitrogen source. Yield coefficients for growth with nitrate as the nitrogen source for the PAOs using PHA as their substrate and ordinary heterotrophic organisms (OHOs) simulated in the TUDP model not growing on glycogen are considered here. The case of PAO metabolism under ammonia limited conditions in an aerobic and anoxic reactor are considered first, followed by the growth of OHOs in an aerobic and an anoxic environment. It is assumed that growth does not occur in the anaerobic zone. Additionally, autotrophic organisms in the model rely upon ammonia for operation of their respiratory

metabolism. Due to this, autotrophic growth is considered to not occur if ammonia is limited, even if nitrate is present. Therefore autotrophs are not considered in this section.

3.5.1 PAO Aerobic and Anoxic Metabolism

A metabolic network analysis, analogous to the approach taken in Sections 3.2 and 3.3 may be used to determine the theoretical yield and maintenance coefficients for PAOs in the model. The approach will be to rederive the metabolic yield coefficients for PAOs currently used in the TUDP model, but for growth with nitrate as the nitrogen source. As previously mentioned, only one state variable for PAOs, X_{PAO}, is used in the model. The model parameter $\eta_{NO.PAO}$ is applied to anoxic PAO growth processes to model the activity of the dPAO fraction in the anoxic zone.

In the TUDP model, all PHA species are assumed to be PHB and the model assumes that PAOs grow on PHB as their substrate. The TUDP model also assumes that the metabolism for biomass synthesis is the same under aerobic and anoxic conditions. Under these assumptions, the growth of PAO (and dPAO) biomass using nitrate as the nitrogen source for biomass synthesis may be described by the following formula:

$$\begin{aligned}(1+\eta)\underset{\text{substrate}}{CH_{a2}O_{b2}} + \alpha_1 HNO_3 + \alpha_2 \underset{\text{phosphate}}{H_3PO_4} + \alpha_3 ATP &\longrightarrow \underset{\text{biomass}}{CH_{a1}O_{b1}N_{c1}S_{d1}P_{e1}} \\ &\quad + \eta CO_2 + \alpha_4 NADH_2 + \alpha_5 H_2O \\ \implies (1+\eta)\underset{\text{PHB}}{CH_{1.5}O_{0.5}} + \alpha_1 HNO_3 + \alpha_2 \underset{\text{phosphate}}{H_3PO_4} + \alpha_3 ATP &\longrightarrow \underset{\text{biomass}}{CH_{2.09}O_{0.54}N_{0.2}P_{0.015}} \\ &\quad + \eta CO_2 + \alpha_4 NADH_2 + \alpha_5 H_2O \end{aligned} \quad (3.32)$$

The TUDP model uses an η value of 0.27 C-mole for the amount of CO_2 produced by PAOs during biomass synthesis on acetate. The coefficients on nitrogen and phosphorus can be found from a balance on nitrogen and phosphorus respectively:

$$\underline{\underline{\alpha_1 = 0.2}} \quad (3.33)$$

$$\underline{\underline{\alpha_2 = 0.015}} \tag{3.34}$$

The coefficient on ATP, α_3, represents the amount of ATP consumed during biomass growth, which consists of ATP used for biomass synthesis and ATP used to support biomass maintenance activities. This may be written as $\mathrm{K} + \mathrm{m_{ATP}}/\mu$, where K represents the amount of ATP used for biomass synthesis. Values of K=1.72 mole ATP/Cmol PAO and $\mathrm{m_{ATP}}$=0.017 mole ATP/Cmol-h are used in the TUDP model.

A balance on oxygen then gives:

$$(1+\eta)\mathrm{b}_2 + 3\alpha_1 + 4\alpha_2 = \mathrm{b}_1 + 2\eta + \alpha_5 \implies \alpha_5 = (1+\eta)\mathrm{b}_2 + 3\alpha_1 + 4\alpha_2 - \mathrm{b}_1 - 2\eta$$

$$\implies \alpha_5 = 1.27(0.5) + 3(0.20) + 4(0.015) - 0.54 - 2(0.27) \implies \underline{\underline{\alpha_5 = 0.215}} \tag{3.35}$$

A balance on the degree of reduction is used to find the coefficient on $\mathrm{NADH_2}$:

$$(1+\eta)\lambda_s = \lambda_x + 2\alpha_4 \implies \alpha_4 = \frac{1}{2}\left[(1+\eta)\lambda_s - \lambda_x\right] \tag{3.36}$$

Since nitrate is used as the nitrogen source, $\mathrm{HNO_3}$ is used as the reference for nitrogen in the biomass formula. Therefore, the degree of reduction for $\mathrm{HNO_3}$ is set as zero, resulting in a degree of reduction value for nitrogen of +5. The degree of reduction for biomass and substrate (PHB) is then:

$$\lambda_x = 4 + a_1 - 2b_1 + 5c_1 + 6d_1 + 5e_1 = \underline{\underline{6.085}} \qquad \text{Biomass degree of reduction} \tag{3.37}$$

$$\lambda_s = 4 + a_2 - 2b_2 + 5c_2 + 6d_2 + 5e_2 = \underline{\underline{4.5}} \qquad \text{PHB degree of reduction} \tag{3.38}$$

The coefficient on $\mathrm{NADH_2}$ then becomes:

$$\alpha_4 = \frac{1}{2}\left[(1+\eta)\lambda_s - \lambda_x\right] \implies \alpha_4 = \frac{1}{2}\left[(1.27)4.5 - 6.085\right] \implies \underline{\underline{\alpha_4 = -0.185}} \tag{3.39}$$

The negative sign on $\mathrm{NADH_2}$ indicates that there is a consumption of reducing equivalents during synthesis. A similar balance with ammonia used as the nitrogen source would show a

production of $NADH_2$ during synthesis. The difference is due to the greater degree of reduction of biomass when nitrate is used as the nitrogen source, due to the increased oxidation state of nitrate. The same phenomena is observed for the synthesis of biomass when glycogen is used as the substrate according to the derivations in Section 3.2 and 3.3.

Substituting the determined coefficients into Equation 3.32 gives the following equation for biomass growth with nitrate as the nitrogen source:

$$(1.27)\underset{\text{PHB}}{CH_{1.5}O_{0.5}} + 0.20\,HNO_3 + 0.015\underset{\text{phosphate}}{H_3PO_4} + \left(K + \frac{m_{ATP}}{\mu}\right) ATP \longrightarrow \underset{\text{biomass}}{CH_{2.09}O_{0.54}N_{0.2}P_{0.015}} + \eta\,CO_2 - 0.185\,NADH_2 + 0.215\,H_2O \tag{3.40}$$

The PAO aerobic and anoxic reactions that are incorporated into the TUDP model were presented in Section 2.6.3. These equations along with the just derived equation 3.40 for biomass synthesis using nitrate as the nitrogen source are summarized in Table 3.2.

Table 3.2: TUDP Model Aerobic and Anoxic Reactions

Reaction	Description	Stoichiometric Equation
R1	PHA Degradation	$CH_{1.5}O_{0.5} + 1.5\,H_2O \longrightarrow 2.25\,NADH_2 + 0.5\,ATP + CO_2$
R2a	AE Oxidative Phosphorylation	$NADH_2 + \frac{1}{2}\,O_2 \longrightarrow \delta_o\,ATP + H_2O$
R2b	AX Oxidative Phosphorylation	$NADH_2 + \frac{2}{5}\,HNO_3 \longrightarrow \frac{1}{5}\,N_2 + \delta_n\,ATP + \frac{6}{5}\,H_2O$
R3	PAO Growth (AE & AX)	$1.27\,CH_{1.5}O_{0.5} + 0.2\,HNO_3 + 0.015\,HPO_3 + (K + m_{ATP}/\mu)ATP + 0.185\ NADH2 \longrightarrow CH_{2.09}O_{0.54}N_{0.20}P_{0.015} + 0.215\,H_2O + 0.27\,CO_2$
R4a	AE Phosphate Transport	$\epsilon_o\,H_3PO_{4out} + NADH_2 + \frac{1}{2}\,O_2 \longrightarrow \epsilon_o\,\delta_o\,H_3PO_{4in} + H_2O$
R4b	AX Phosphate Transport	$\epsilon_n\,H_3PO_{4out} + NADH_2 + \frac{2}{5}\,HNO_3 \longrightarrow \epsilon_n\,\delta_n\,H_3PO_{4in} + \frac{1}{5}\,N_2 + \frac{6}{5}\,H_2O$
R5	PolyP Formation	$H_3PO_{4in} + ATP \longrightarrow HPO_3 + H_2O$
R6	Glycogen Formation	$\frac{4}{3}\,CH_{1.5}O_{0.5} + \frac{5}{6}\,ATP + \frac{5}{6}\,H_2O \longrightarrow CH_{10/6}O_{5/6} + \frac{1}{3}\,CO_2 + NADH_2$

Note: AE=Aerobic, AX=Anoxic

The coefficients ϵ_o and ϵ_n represents the ATP required to transfer phosphorus over the cell membrane during phosphate uptake under aerobic and anoxic conditions respectively. The TUDP model uses values of ϵ_o=7 P-mole ATP/mole $NADH_2$ and ϵ_n=3.5 P-mole ATP/mole $NADH_2$. The terms δ_o and δ_n are the P/O ratios (the amount of ATP produced per $NADH_2$ under aerobic and under anoxic conditions). Based on the work of Smolders et al.[86] and Kuba

et al.,[41] values of δ_o=1.85 mole ATP/Cmol $NADH_2$ and δ_n=0.925 mole ATP/Cmol $NADH_2$ are used in the model.

Aerobic Yield and Maintenance Coefficients with Nitrate as the Nitrogen Source. The six aerobic reactions within Table 3.2 define six internal flux rates active within the aerobic zone which can be expressed as an internal flux rate vector, **V**. Twelve conversion rates formed by the system. The conversion rates can be expressed in a conversion rate vector, **r**. The internal flux rates can be related to these conversion rates according to a stoichiometric reaction matrix, **T**, derived from the reactions in Table 3.2, according to $\mathbf{r} = \mathbf{T} \cdot \mathbf{V}$:

$$\begin{bmatrix} r_{phb} \\ r_x \\ r_{gly} \\ r_{pp} \\ r_{no3} \\ r_{p.out} \\ r_{o2} \\ r_{co2} \\ r_{h2o} \\ r_{p.in} \\ r_{atp} \\ r_{nadh} \end{bmatrix} = \begin{bmatrix} -1 & 0 & -1.27 & 0 & 0 & -\frac{4}{3} \\ 0 & 0 & 1 & 0 & 0 & 0 \\ 0 & 0 & 0 & 0 & 0 & 1 \\ 0 & 0 & 0 & 0 & 1 & 0 \\ 0 & 0 & -0.20 & 0 & 0 & 0 \\ 0 & 0 & 0 & -\epsilon_o & 0 & 0 \\ 0 & -\frac{1}{2} & 0 & -\frac{1}{2} & 0 & 0 \\ 1 & 0 & 0.27 & 0 & 0 & \frac{1}{3} \\ -\frac{3}{2} & 1 & 0.215 & 1 & 1 & -\frac{5}{6} \\ 0 & 0 & -0.015 & \epsilon_o & -1 & 0 \\ \frac{1}{2} & \delta_o & -\left(\mathrm{K} + \frac{\mathrm{m_{ATP}}}{\mu}\right) & 0 & -1 & -\frac{5}{6} \\ 2.25 & -1 & -0.185 & -1 & 0 & 1 \end{bmatrix} \cdot \begin{bmatrix} \nu_1 \\ \nu_{2a} \\ \nu_3 \\ \nu_{4a} \\ \nu_5 \\ \nu_6 \end{bmatrix} \tag{3.41}$$

From the stoichiometric reaction matrix it can be seen that:

$$r_x = \nu_3 \tag{3.42}$$

$$r_{pp} = \nu_5 \tag{3.43}$$

$$r_{gly} = \nu_6 \tag{3.44}$$

In addition, it is assumed that the concentrations of ATP, $NADH_2$, and internal phosphate within the cell are in a steady-state condition., i.e. there is no net production or consumption of these concentrations within the metabolism. Therefore:

$$r_{atp} = \frac{1}{2}\,\nu_1 + \delta_o\,\nu_{2a} - \left(K + \frac{\mathrm{m_{ATP}}}{\mu}\right)\nu_3 - \nu_5 - \frac{5}{6}\nu_6 = 0 \tag{3.45}$$

$$r_{nadh} = 2.25\,\nu_1 - \nu_{2a} - 0.185\,\nu_3 - \nu_6 + \nu_5 = 0 \tag{3.46}$$

$$r_{p.in} = -0.015\,\nu_3 + \epsilon_o\,\nu_{4a} - \nu_5 = 0 \tag{3.47}$$

As indicated by Smolders et al.,[88] there are 12 conversion rates, r_i, and 6 internal flux rates, v_i, for a total of 18 rates. With the 3 given steady state equations (r_{atp}, r_{nadh}, $r_{p.in}$), there are a total of 15 unknown rates. The stoichiometric matrix defines 12 linear relations between the production rates and the flux rates. Therefore, the system is underdetermined but may be solved in terms of $15 - 12 = 3$ of the rates if these rates are measured, or given. As discussed in Section 2.6.3, Murnleitner et al. chose to define the model such that the conversion of biomass (r_x) is described by the conversions of PHB (r_{phb}), polyphosphate (r_{pp}), and glycogen (r_{gly}). The yield coefficients for PHB, polyphosphate, and glycogen on biomass with nitrate as the nitrogen source are derived below for use in the model matrix by use of Equation 3.41. With these yield coefficients, the system is able to predict the remaining conversions.

To solve the formulated system of linear equations, a vector, $\mathbf{V_1}$, is defined and composed of the flux rates to be measured or given (ν_3, ν_5, ν_6). A vector, $\mathbf{V_2}$, is composed of the remaining flux rates. A submatrix, $\mathbf{T_2}$ is defined with the last three rows of the stoichiometric matrix which are the constrained, steady-state, reactions (the reactions for ATP, $NADH_2$, and internal phosphate) and with columns corresponding to $\mathbf{V_1}$. The remaining columns of the steady-state reactions in the stoichiometric matrix make up a second submatrix, $\mathbf{T_1}$. The vector $\mathbf{V_2}$ may be solved in terms of $\mathbf{V_1}$ by use of the following formula:

$$\mathbf{V_2} = -\mathbf{T_1}^{-1} \cdot \mathbf{T_2} \cdot \mathbf{V_1} \tag{3.48}$$

The system vectors and submatrices are thus:

$$\mathbf{V_1} = \begin{bmatrix} \nu_3 \\ \nu_5 \\ \nu_6 \end{bmatrix} \quad \mathbf{V_2} = \begin{bmatrix} \nu_1 \\ \nu_{2a} \\ \nu_{4a} \end{bmatrix} \quad \mathbf{T_1} = \begin{bmatrix} 0 & 0 & \epsilon_o \\ \frac{1}{2} & \delta_o & 0 \\ 2.25 & -1 & -1 \end{bmatrix} \quad \mathbf{T_2} = \begin{bmatrix} -0.015 & -1 & 0 \\ -\left(K + \mathrm{m_{ATP}}/\mu\right) & -1 & -\frac{5}{6} \\ -0.185 & 0 & 1 \end{bmatrix}$$

Since $r_x = \nu_3$, $r_{pp} = \nu_5$, and $r_{gly} = \nu_6$, they may be substituted into $\mathbf{V_1}$ resulting in:

$$\mathbf{V_2} = -{\mathbf{T_1}}^{-1} \cdot \mathbf{T_2} \cdot \mathbf{V_1}$$

$$\implies \mathbf{V_2} = -\begin{bmatrix} 0 & 0 & \epsilon_o \\ \frac{1}{2} & \delta_o & 0 \\ 2.25 & -1 & -1 \end{bmatrix}^{-1} \cdot \begin{bmatrix} -0.015 & -1 & 0 \\ -\left(K + \mathrm{m_{ATP}}/\mu\right) & -1 & -\frac{5}{6} \\ -0.185 & 0 & 1 \end{bmatrix} \cdot \begin{bmatrix} r_x \\ r_{pp} \\ r_{gly} \end{bmatrix}$$

$$= \begin{bmatrix} r_x \left[\dfrac{4\left(\mathrm{K} + \dfrac{\mathrm{m_{ATP}}}{\mu}\right) + 0.74\delta_o + \dfrac{0.06}{\epsilon_o}\delta_o}{2 + 9\delta_o} \right] + r_{pp}\left(\dfrac{4 + \dfrac{4\delta_o}{\epsilon_o}}{2 + 9\delta_o}\right) + r_{gly}\left(\dfrac{\dfrac{10}{3} - 4\delta_o}{2 + 9\delta_o}\right) \\ r_x \left[\dfrac{9\left(\mathrm{K} + \dfrac{\mathrm{m_{ATP}}}{\mu}\right) - \dfrac{0.03}{\epsilon_o} - 0.37}{2 + 9\delta_o} \right] + r_{pp}\left(\dfrac{9 - \dfrac{2}{\epsilon_o}}{2 + 9\delta_o}\right) + r_{gly}\left(\dfrac{9.5}{2 + 9\delta_o}\right) \\ r_x\left(\dfrac{0.015}{\epsilon_o}\right) + \dfrac{r_{pp}}{\epsilon_o} \end{bmatrix}$$

Now, the first row of the stoichiometric matrix in Equation 3.41 corresponds to the conversion rate of PHB. Therefore r_{phb} may be found by multiplying this row by vector $\mathbf{V}$. Substituting the values found for $\mathbf{V_1}$ and $\mathbf{V_2}$ into $\mathbf{V}$ and multiplying by the first row of the stoichiometric matrix in Equation 3.41 will define r_{phb} in terms of r_x, r_{pp}, and r_{gly}, as shown below.

$$\mathbf{V} = \begin{bmatrix} r_x \left[\dfrac{4\left(\mathrm{K} + \dfrac{\mathrm{m_{ATP}}}{\mu}\right) + 0.74\delta_o + \dfrac{0.06}{\epsilon_o}\delta_o}{2 + 9\delta_o} \right] + r_{pp}\left(\dfrac{4 + \dfrac{4\delta_o}{\epsilon_o}}{2 + 9\delta_o}\right) + r_{gly}\left(\dfrac{\dfrac{10}{3} - 4\delta_o}{2 + 9\delta_o}\right) \\ r_x \left[\dfrac{9\left(\mathrm{K} + \dfrac{\mathrm{m_{ATP}}}{\mu}\right) - \dfrac{0.03}{\epsilon_o} - 0.37}{2 + 9\delta_o} \right] + r_{pp}\left(\dfrac{9 - \dfrac{2}{\epsilon_o}}{2 + 9\delta_o}\right) + r_{gly}\left(\dfrac{9.5}{2 + 9\delta_o}\right) \\ r_x \\ r_x\left(\dfrac{0.015}{\epsilon_o}\right) + \dfrac{r_{pp}}{\epsilon_o} \\ r_{pp} \\ r_{gly} \end{bmatrix}$$

then:

$$r_{phb} = \begin{bmatrix} -1 & 0 & -1.27 & 0 & 0 & -\dfrac{4}{3} \end{bmatrix} \cdot \mathbf{V} \tag{3.49}$$

$$\implies r_{phb} = -1.27r_x - \frac{4}{3}r_{gly} - r_{pp}\left(\frac{4 + \frac{4}{\epsilon_o}\delta_o}{2 + 9\delta_o}\right) - r_{gly}\left(\frac{\frac{10}{3} - 4\delta_o}{2 + 9\delta_o}\right) - r_x\left(\frac{4\mathrm{K} + \frac{4\mathrm{m_{ATP}}}{\mu} + 0.74\delta_o + \frac{0.06}{\epsilon_o}\delta_o}{2 + 9\delta_o}\right)$$

$$\implies -r_{phb} = 1.27r_x + \frac{4}{3}r_{gly} + r_{pp}\left(\frac{4 + \frac{4}{\epsilon_o}\delta_o}{2 + 9\delta_o}\right) + r_{gly}\left(\frac{\frac{10}{3} - 4\delta_o}{2 + 9\delta_o}\right) + r_x\left(\frac{4\mathrm{K} + \frac{4\mathrm{m_{ATP}}}{\mu} + 0.74\delta_o + \frac{0.06}{\epsilon_o}\delta_o}{2 + 9\delta_o}\right)$$

$$\implies -r_{phb} = 1.27r_x\left(\frac{2 + 9\delta_o}{2 + 9\delta_o}\right) + \frac{4r_{gly}}{3}\left(\frac{2 + 9\delta_o}{2 + 9\delta_o}\right) + r_{pp}\left(\frac{4 + \frac{4}{\epsilon_o}\delta_o}{2 + 9\delta_o}\right) + r_{gly}\left(\frac{\frac{10}{3} - 4\delta_o}{2 + 9\delta_o}\right)$$

$$+ r_x \left(\frac{4\mathrm{K} + \frac{4\mathrm{m_{ATP}}}{\mu} + 0.74\delta_o + \frac{0.06}{\epsilon_o}\delta_o}{2 + 9\delta_o} \right)$$

$$\implies -r_{phb} = r_x \left(\frac{11.43\delta_o + 2.54}{2 + 9\delta_o} \right) + \frac{4r_{gly}}{3} \left(\frac{2 + 9\delta_o}{2 + 9\delta_o} \right) + r_{pp} \left(\frac{4 + \frac{4}{\epsilon_o}\delta_o}{2 + 9\delta_o} \right) + r_{gly} \left(\frac{\frac{10}{3} - 4\delta_o}{2 + 9\delta_o} \right)$$

$$+ r_x \left(\frac{4\mathrm{K} + \frac{4\mathrm{m_{ATP}}}{\mu} + 0.74\delta_o + \frac{0.06}{\epsilon_o}\delta_o}{2 + 9\delta_o} \right)$$

$$\implies -r_{phb} = \frac{4\mathrm{K} + 4\frac{\mathrm{m_{ATP}}}{\mu} + 0.74\delta_o + \frac{0.06}{\epsilon_o}\delta_o + 11.43\delta_o + 2.54}{2 + 9\delta_o} r_x + \frac{4 + \frac{4}{\epsilon_o}\delta_o}{2 + 9\delta_o} r_{pp}$$

$$+ \frac{12\delta_o + \frac{8}{3} + \frac{10}{3} - 4\delta_o}{2 + 9\delta_o} r_{gly}$$

Substituting ϵ_o=7 mol ATP/mol $NADH_2$ and K=1.72 mole ATP/Cmol PAO:

$$\implies -r_{phb} = \frac{9.42 + 12.17857\delta_o}{2 + 9\delta_o} r_x + \frac{4 + \frac{4}{7}\delta_o}{2 + 9\delta_o} r_{pp} + \frac{6 + 8\delta_o}{2 + 9\delta_o} r_{gly} + \frac{4\frac{\mathrm{m_{ATP}}}{\mu}}{2 + 9\delta_o} r_x$$

$$\implies -\frac{9.42 + 12.17587\delta_o}{2 + 9\delta_o} r_x = r_{phb} + \frac{4 + \frac{4}{7}\delta_o}{2 + 9\delta_o} r_{pp} + \frac{6 + 8\delta_o}{2 + 9\delta_o} r_{gly} + \frac{4\frac{\mathrm{m_{ATP}}}{\mu}}{2 + 9\delta_o} r_x$$

$$\implies -r_x = \frac{2 + 9\delta_o}{9.42 + 12.17857\delta_o} r_{phb} + \frac{4 + \frac{4}{7}\delta_o}{2 + 9\delta_o} \cdot \frac{2 + 9\delta_o}{9.42 + 12.17857\delta_o} r_{pp}$$

$$+ \frac{6 + 8\delta_o}{2 + 9\delta_o} \cdot \frac{2 + 9\delta_o}{9.42 + 12.17857\delta_o} r_{gly} + \frac{4\frac{\mathrm{m_{ATP}}}{\mu}}{2 + 9\delta_o} \cdot \frac{2 + 9\delta_o}{9.42 + 12.17857\delta_o} r_x$$

$$\implies -r_x = \frac{2 + 9\delta_o}{9.42 + 12.17857\delta_o} r_{phb} + \frac{4 + \frac{4}{7}\delta_o}{9.42 + 12.17857\delta_o} r_{pp} + \frac{6 + 8\delta_o}{9.42 + 12.17857\delta_o} r_{gly}$$

$$+ \frac{4\frac{\mathrm{m_{ATP}}}{\mu}}{9.42 + 12.17857\delta_o} \tag{3.50}$$

Substituting the active biomass concentration, C_x, for r_x/μ gives the following:

$$-r_x = \frac{2+9\delta_o}{9.42+12.17857\delta_o} r_{phb} + \frac{4+\frac{4}{7}\delta_o}{9.42+12.17857\delta_o} r_{pp} + \frac{6+8\delta_o}{9.42+12.17857\delta_o} r_{gly} + \frac{4\,\mathrm{m_{ATP}}}{9.42+12.17857\delta_o} C_x$$

The terms to the left of r_{phb}, r_{pp}, and r_x are the inverse yield coefficients of PAO biomass on PHB, polyphosphate, and glycogen, respectively. The term to the left of the active biomass concentration, C_x, is the maintenance coefficient for PAOs. Hence, the PAO biomass conversion rate in an aerobic reactor with nitrate as the nitrogen source for biomass growth can be expressed as:

$$-r_x = \frac{1}{Y^{\mathrm{O}}_{\mathrm{PHA}.\varphi}} r_{pha} + \frac{1}{Y^{\mathrm{O}}_{\mathrm{PP}.\varphi}} r_{pp} + \frac{1}{Y^{\mathrm{O}}_{\mathrm{GLY}.\varphi}} r_{gly} + m_{\mathrm{O}.\varphi} C_x \tag{3.51}$$

where:

$$Y^{\mathrm{O}}_{\mathrm{PHA}.\varphi} = \frac{9.42+12.17857\delta_o}{2+9\delta_o} \tag{3.52}$$

$$Y^{\mathrm{O}}_{\mathrm{PP}.\varphi} = \frac{9.42+12.17857\delta_o}{4+\frac{4}{7}\delta_o} \tag{3.53}$$

$$Y^{\mathrm{O}}_{\mathrm{GLY}.\varphi} = \frac{9.42+12.17857\delta_o}{6+8\delta_o} \tag{3.54}$$

$$m_{\mathrm{O}.\varphi} = \frac{4\,\mathrm{m_{ATP}}}{9.42+12.17857\delta_o} \tag{3.55}$$

Note that the TUDP model assumes all PHA species are PHB but uses the notation "PHA" on their yield coefficient. The same notation for the yield coefficient is used in this work. Conversion of the yield coefficients to a COD basis is made by using 35.948 g COD/Cmol PAO biomass, 36.021 g COD/Cmol PHB, 32.017 g COD/Cmol glycogen, and 30.974 g P/mole P. These factors plus the use of the TUDP model's value for δ_o of 1.85 mole ATP/mole $NADH_2$ and $\mathrm{m_{ATP}}$=0.017 mole ATP/Cmol-h gives:

$$\boxed{Y^{O}_{PHA.\varphi} = 1.7166 \quad \frac{\text{g COD PHB}}{\text{g COD PAO}}} \qquad \text{(Aerobic, } NO_3 \text{ as nitrogen source)} \qquad (3.56)$$

$$\boxed{Y^{O}_{PP.\varphi} = 5.4437 \quad \frac{\text{g P}}{\text{g COD PAO}}} \qquad \text{(Aerobic, } NO_3 \text{ as nitrogen source)} \qquad (3.57)$$

$$\boxed{Y^{O}_{GLY.\varphi} = 1.3681 \quad \frac{\text{g COD glycogen}}{\text{g COD PAO}}} \qquad \text{(Aerobic, } NO_3 \text{ as nitrogen source)} \qquad (3.58)$$

$$\boxed{m_{O.\varphi} = 0.0511 \quad \frac{\text{g COD PAO}}{\text{g COD PAO-day}}} \qquad \text{(Aerobic, } NO_3 \text{ as nitrogen source)} \qquad (3.59)$$

As a comparison, the aerobic yield coefficients for PAOs when ammonia is used as the nitrogen source in the TUDP model are:

$$Y^{O}_{PHA} = 1.39 \quad \frac{\text{g COD PHB}}{\text{g COD PAO}}$$

$$Y^{O}_{PP} = 4.42 \quad \frac{\text{g P}}{\text{g COD PAO}}$$

$$Y^{O}_{GLY} = 1.11 \quad \frac{\text{g COD glycogen}}{\text{g COD PAO}}$$

$$m_{O.\varphi} = 0.06 \quad \frac{\text{g COD PAO}}{\text{g COD PAO-day}}$$

It is noted that the yield coefficients are defined in terms of the mass of compound converted per mass of PAO formed; thus an increased amount of compound is required for the same amount of biomass formed when nitrate is used as the nitrogen source versus ammonia. The results indicate an approximate 23% increase in each yield coefficient and an approximate 15% decrease in the maintenance coefficient for PAOs using PHA as their substrate and nitrate as their nitrogen source.

Anoxic Yield and Maintenance Coefficients with Nitrate as the Nitrogen Source. The derivation for the anoxic yield and maintenance coefficients when nitrate is used as the nitrogen source is similar to the derivation of the aerobic coefficients. Using Reactions R1, R2, R3, R4b, R5, and R6 in Table 3.2, the production rates can be related to the internal flux rates according to $\mathbf{r} = \mathbf{T} \cdot \mathbf{V}$:

$$\begin{bmatrix} r_{phb} \\ r_x \\ r_{gly} \\ r_{pp} \\ r_{p.out} \\ r_{no3} \\ r_{co2} \\ r_{h2o} \\ r_{n2} \\ r_{p.in} \\ r_{atp} \\ r_{nadh} \end{bmatrix} = \begin{bmatrix} -1 & 0 & -1.27 & 0 & 0 & -\frac{4}{3} \\ 0 & 0 & 1 & 0 & 0 & 0 \\ 0 & 0 & 0 & 0 & 0 & 1 \\ 0 & 0 & 0 & 0 & 1 & 0 \\ 0 & 0 & 0 & -\epsilon_n & 0 & 0 \\ 0 & -\frac{2}{5} & -0.20 & -\frac{2}{5} & 0 & 0 \\ 1 & 0 & 0.27 & 0 & 0 & \frac{1}{3} \\ -\frac{3}{2} & \frac{6}{5} & 0.215 & \frac{6}{5} & 1 & -\frac{5}{6} \\ 0 & 0 & -0.015 & \epsilon_n & -1 & 0 \\ \frac{1}{2} & \delta_n & -\left(\mathrm{K} + \frac{\mathrm{m_{ATP}}}{\mu}\right) & 0 & -1 & -\frac{5}{6} \\ 2.25 & -1 & -0.185 & -1 & 0 & 1 \end{bmatrix} \cdot \begin{bmatrix} \nu_1 \\ \nu_{2b} \\ \nu_3 \\ \nu_{4b} \\ \nu_5 \\ \nu_6 \end{bmatrix} \tag{3.60}$$

The system is chosen to again be solved in terms of r_{phb}, r_{pp}, and r_{gly}. The production rates, $r_{p.in}$, r_{atp}, and r_{gly} are assumed to be in steady state. Vectors $\mathbf{V_1}$ and $\mathbf{V_2}$ and submatrices $\mathbf{T_1}$ and $\mathbf{T_2}$ are then defined as:

$$\mathbf{V_1} = \begin{bmatrix} \nu_3 \\ \nu_5 \\ \nu_6 \end{bmatrix} \quad \mathbf{V_2} = \begin{bmatrix} \nu_1 \\ \nu_{2b} \\ \nu_{4b} \end{bmatrix} \quad \mathbf{T_1} = \begin{bmatrix} 0 & 0 & \epsilon_n \\ \frac{1}{2} & \delta_n & 0 \\ 2.25 & -1 & -1 \end{bmatrix} \quad \mathbf{T_2} = \begin{bmatrix} -0.015 & -1 & 0 \\ -\left(K + \frac{\mathrm{m_{ATP}}}{\mu}\right) & -1 & -\frac{5}{6} \\ -0.185 & 0 & 1 \end{bmatrix}$$

From the stoichiometric matrix in Equation 3.60, it can be seen that $r_x = \nu_3$, $r_{pp} = \nu_5$, $r_{gly} = \nu_6$. Substituting these values into $\mathbf{V_1}$ and using Equation 3.48 to solve for $\mathbf{V_2}$ results in:

$$\mathbf{V_2} = -\mathbf{T_1}^{-1} \cdot \mathbf{T_2} \cdot \mathbf{V_1}$$

$$\implies \mathbf{V_2} = -\begin{bmatrix} 0 & 0 & \epsilon_n \\ \frac{1}{2} & \delta_n & 0 \\ 2.25 & -1 & -1 \end{bmatrix}^{-1} \cdot \begin{bmatrix} -0.015 & -1 & 0 \\ -\left(K + \frac{\mathrm{m_{ATP}}}{\mu}\right) & -1 & -\frac{5}{6} \\ -0.185 & 0 & 1 \end{bmatrix} \cdot \begin{bmatrix} r_x \\ r_{pp} \\ r_{gly} \end{bmatrix}$$

$$= \begin{bmatrix} r_x \left[\frac{4\left(\mathrm{K} + \frac{\mathrm{m_{ATP}}}{\mu}\right) + 0.74\delta_n + \frac{0.06}{\epsilon_n}\delta_n}{2 + 9\delta_n}\right] + r_{pp}\left(\frac{4 + \frac{4\delta_n}{\epsilon_n}}{2 + 9\delta_n}\right) + r_{gly}\left(\frac{\frac{10}{3} - 4\delta_n}{2 + 9\delta_n}\right) \\ r_x \left[\frac{9\left(\mathrm{K} + \frac{\mathrm{m_{ATP}}}{\mu}\right) - \frac{0.03}{\epsilon_n} - 0.37}{2 + 9\delta_n}\right] + r_{pp}\left(\frac{9 - \frac{2}{\epsilon_n}}{2 + 9\delta_n}\right) + r_{gly}\left(\frac{9.5}{2 + 9\delta_n}\right) \\ r_x\left(\frac{0.015}{\epsilon_n}\right) + \frac{r_{pp}}{\epsilon_n} \end{bmatrix}$$

A linear relation between the conversion rate of PHB and the the rates r_x, r_{pp}, and r_{gly} can be obtained by multiplying the first row in Equation 3.60 (corresponding to r_{phb}) by the flux rate vector, $\mathbf{V}$:

$$\mathbf{V} = \begin{bmatrix} r_x \left[\frac{4\left(\mathrm{K} + \frac{\mathrm{m_{ATP}}}{\mu}\right) + 0.74\delta_n + \frac{0.06}{\epsilon_n}\delta_o}{2 + 9\delta_n}\right] + r_{pp}\left(\frac{4 + \frac{4\delta_n}{\epsilon_n}}{2 + 9\delta_n}\right) + r_{gly}\left[\frac{\frac{10}{3} - 4\delta_n}{2 + 9\delta_n}\right] \\ r_x\left(\frac{9\left(\mathrm{K} + \frac{\mathrm{m_{ATP}}}{\mu}\right) - \frac{0.03}{\epsilon_n} - 0.37}{2 + 9\delta_n}\right) + r_{pp}\left(\frac{9 - \frac{2}{\epsilon_n}}{2 + 9\delta_n}\right) + r_{gly}\left(\frac{9.5}{2 + 9\delta_n}\right) \\ r_x \\ r_x\frac{0.015}{\epsilon_n} + \frac{r_{pp}}{\epsilon_n} \\ r_{pp} \\ r_{gly} \end{bmatrix}$$

then:

$$r_{phb} = \begin{bmatrix} -1 & 0 & -1.27 & 0 & 0 & -\frac{4}{3} \end{bmatrix} \cdot \mathbf{V}$$

$$\implies r_{phb} = -1.27r_x - \frac{4}{3}r_{gly} - r_{pp}\left(\frac{4+\frac{4}{\epsilon_n}\delta_n}{2+9\delta_n}\right) - r_{gly}\left(\frac{\frac{10}{3}-4\delta_n}{2+9\delta_n}\right)$$

$$- r_x\left(\frac{4\mathrm{K}+4\frac{\mathrm{m_{ATP}}}{\mu}+0.74\delta_o+\frac{0.06}{\epsilon_n}\delta_n}{2+9\delta_n}\right)$$

$$\implies -r_{phb} = 1.27r_x + \frac{4}{3}r_{gly} + r_{pp}\left(\frac{4+\frac{4}{\epsilon_n}\delta_n}{2+9\delta_n}\right) + r_{gly}\left(\frac{\frac{10}{3}-4\delta_n}{2+9\delta_n}\right)$$

$$+ r_x\left(\frac{4\mathrm{K}+4\frac{\mathrm{m_{ATP}}}{\mu}+0.74\delta_n+\frac{0.06}{\epsilon_n}\delta_n}{2+9\delta_n}\right)$$

$$\implies -r_{phb} = 1.27r_x\left(\frac{2+9\delta_n}{2+9\delta_n}\right) + \frac{4r_{gly}}{3}\left(\frac{2+9\delta_n}{2+9\delta_n}\right) + r_{pp}\left(\frac{4+\frac{4}{\epsilon_n}\delta_n}{2+9\delta_n}\right) + r_{gly}\left(\frac{\frac{10}{3}-4\delta_n}{2+9\delta_n}\right)$$

$$+ r_x\left(\frac{4\mathrm{K}+4\frac{\mathrm{m_{ATP}}}{\mu}+0.74\delta_n+\frac{0.06}{\epsilon_n}\delta_n}{2+9\delta_n}\right)$$

$$\implies -r_{phb} = r_x\left(\frac{11.43\delta_n+2.54}{2+9\delta_n}\right) + \frac{4r_{gly}}{3}\left(\frac{2+9\delta_n}{2+9\delta_n}\right) + r_{pp}\left(\frac{4+\frac{4}{\epsilon_n}\delta_n}{2+9\delta_n}\right) + r_{gly}\left(\frac{\frac{10}{3}-4\delta_n}{2+9\delta_n}\right)$$

$$+ r_x\left(\frac{4\mathrm{K}+4\frac{\mathrm{m_{ATP}}}{\mu}+0.74\delta_n+\frac{0.06}{\epsilon_n}\delta_n}{2+9\delta_n}\right)$$

$$\implies -r_{phb} = \frac{4\mathrm{K}+4\frac{\mathrm{m_{ATP}}}{\mu}+0.74\delta_n+\frac{0.06}{\epsilon_n}\delta_n+11.43\delta_n+2.54}{2+9\delta_n}r_x + \frac{4+\frac{4}{\epsilon_n}\delta_n}{2+9\delta_n}r_{pp}$$

$$+ \frac{12\delta_n+\frac{8}{3}+\frac{10}{3}-4\delta_n}{2+9\delta_n}r_{gly}$$

Using a value of $\epsilon_n = \epsilon_o/2 = 3.5$ ATP P-mole/$NADH_2$, and K=1.72 mole ATP/Cmol results in:

$$-r_{phb} = \frac{9.42 + 12.18714\delta_n}{2 + 9\delta_n} r_x + \frac{4 + 1.14286\delta_n}{2 + 9\delta_n} r_{pp} + \frac{6 + 8\delta_n}{2 + 9\delta_n} r_{gly} + \frac{4\frac{\mathrm{m_{ATP}}}{\mu}}{2 + 9\delta_n} r_x$$

$$\implies -\frac{9.42 + 12.18714\delta_n}{2 + 9\delta_n} r_x = r_{phb} + \frac{4 + 1.14286\delta_n}{2 + 9\delta_n} r_{pp} + \frac{6 + 8\delta_n}{2 + 9\delta_n} r_{gly} + \frac{4\frac{\mathrm{m_{ATP}}}{\mu}}{2 + 9\delta_n} r_x$$

$$\implies -r_x = \frac{2 + 9\delta_n}{9.42 + 12.18714\delta_n} r_{phb} + \frac{4 + 1.14286\delta_n}{2 + 9\delta_n} \cdot \frac{2 + 9\delta_n}{9.42 + 12.18714\delta_n} r_{pp}$$

$$+ \frac{6 + 8\delta_n}{2 + 9\delta_n} \cdot \frac{2 + 9\delta_n}{9.42 + 12.18714\delta_n} r_{gly} + \frac{4\frac{\mathrm{m_{ATP}}}{\mu}}{2 + 9\delta_n} \cdot \frac{2 + 9\delta_n}{9.42 + 12.18714\delta_n} r_x$$

$$\implies -r_x = \frac{2 + 9\delta_n}{9.42 + 12.18714\delta_n} r_{phb} + \frac{4 + 1.14286\delta_n}{9.42 + 12.18714\delta_n} r_{pp} + \frac{6 + 8\delta_n}{9.42 + 12.18714\delta_n} r_{gly}$$

$$+ \frac{4\frac{\mathrm{m_{ATP}}}{\mu}}{9.42 + 12.187143\delta_n} r_x$$

Substituting the active biomass concentration, C_x, for r_x/μ then gives:

$$-r_x = \frac{2 + 9\delta_n}{9.42 + 12.18714\delta_n} r_{phb} + \frac{4 + 1.14286\delta_n}{9.42 + 12.18714\delta_n} r_{pp} + \frac{6 + 8\delta_n}{9.42 + 12.18714\delta_o} r_{gly}$$

$$+ \frac{4\,\mathrm{m_{ATP}}}{9.42 + 12.18714\delta_n} C_x$$

The conversion rate of PAO biomass under anoxic conditions with nitrate as the nitrogen source can then be written as:

$$-r_x = \frac{1}{Y^{\mathrm{NO}}_{\mathrm{PHA}.\varphi}} r_{pha} + \frac{1}{Y^{\mathrm{NO}}_{\mathrm{PP}.\varphi}} r_{pp} + \frac{1}{Y^{\mathrm{NO}}_{\mathrm{GLY}.\varphi}} r_{gly} + m_{\mathrm{NO}.\varphi} C_x \tag{3.61}$$

where:

$$Y^{\mathrm{NO}}_{\mathrm{PHA}.\varphi} = \frac{9.42 + 12.18714\delta_n}{2 + 9\delta_n} \tag{3.62}$$

$$Y_{\mathrm{PP}.\varphi}^{\mathrm{NO}} = \frac{9.42 + 12.18714\delta_n}{4 + 1.4286\delta_n} \tag{3.63}$$

$$Y_{\mathrm{GLY}.\varphi}^{\mathrm{NO}} = \frac{9.42 + 12.18714\delta_n}{6 + 8\delta_n} \tag{3.64}$$

$$m_{no3}^{no} = \frac{4\mathrm{m}_{\mathrm{ATP}}}{9.42 + 12.18714\delta_n} \tag{3.65}$$

Conversion of the yield and maintenance coefficients to a COD basis and the substitution of the TUDP model's assumed value for δ_n of 0.925 mole ATP/mole $NADH_2$ results in:

$$\boxed{Y_{\mathrm{PHA}.\varphi}^{\mathrm{NO}} = 2.0228 \quad \frac{\text{g COD PHB}}{\text{g COD PAO}}} \qquad \text{(Anoxic, } NO_3 \text{ as nitrogen source)} \tag{3.66}$$

$$\boxed{Y_{\mathrm{PP}.\varphi}^{\mathrm{NO}} = 3.4935 \quad \frac{\text{g P}}{\text{g COD PAO}}} \qquad \text{(Anoxic, } NO_3 \text{ as nitrogen source)} \tag{3.67}$$

$$\boxed{Y_{\mathrm{GLY}.\varphi}^{\mathrm{NO}} = 1.3757 \quad \frac{\text{g COD glycogen}}{\text{g COD PAO}}} \qquad \text{(Anoxic, } NO_3 \text{ as nitrogen source)} \tag{3.68}$$

$$\boxed{m_{no3}^{no} = 0.0800 \quad \frac{\text{g COD PAO}}{\text{g COD PAO-day}}} \qquad \text{(Anoxic, } NO_3 \text{ as nitrogen source)} \tag{3.69}$$

The anoxic yield coefficients for PAOs when ammonia is used as the nitrogen source in the TUDP model are:

$$Y_{\mathrm{PHA}}^{\mathrm{O}} = 1.72 \quad \frac{\text{g COD PHB}}{\text{g COD PAO}}$$

$$Y_{\mathrm{PP}}^{\mathrm{O}} = 3.02 \quad \frac{\text{g P}}{\text{g COD PAO}}$$

$$Y_{\mathrm{GLY}}^{\mathrm{O}} = 1.18 \quad \frac{\text{g COD glycogen}}{\text{g COD PAO}}$$

$$m_{\mathrm{O}.\varphi} = 0.09 \quad \frac{\text{g COD PAO}}{\text{g COD PAO-day}}$$

It is noted that the yield coefficients are defined in terms of the mass of the compound converted per mass of PAO; thus an increased amount of compound is required for the same amount of biomass when nitrate is used as the nitrogen source versus ammonia. The results indicate an approximate 15-16% increase in each yield coefficient and an approximate 11% decrease in the maintenance coefficient for PAOs using PHA as their substrate and nitrate as their nitrogen source.

3.5.2 Ordinary Heterotrophic Organism Aerobic and Anoxic Metabolism

The TUDP model combines the metabolic model derived for PAO metabolism with the ASM2d processes for hydrolysis, COD removal, and nitrogen removal performed by ordinary heterotrophic organisms (OHOs) and autotrophic organisms. The ASM2d (and by extension the TUDP model) stops biomass growth when ammonia is depleted in bulk solution. In reality, OHOs will utilize available nitrate in solution to obtain the nitrogen that is required to be used in biomass synthesis during growth when ammonia is absent. This assimilative reduction of nitrate decreases the potential amount of ATP that can be produced by the cell and lowers the bacterial growth yields. It is important to include this assimilation of nitrate by OHOs for aerobic and anoxic biomass growth into the proposed process model so that the OHO metabolism and yields are adequately predicted. This section derives an aerobic yield coefficient for OHO growth using nitrate as the nitrogen source. In the TUDP model, the same OHO yield coefficient is used in the aerobic and anoxic zones but the anoxic growth rates are multiplied by a factor, $\eta_{\mathrm{NO.H}}$, to account for the slower anoxic growth that occurs. The same approach is used in the new integrated model formulated in this thesis. A default value of 0.8 is used in the TUDP model and in this work for $\eta_{\mathrm{NO.H}}$.

The ASM2d model is based on a gray box modeling approach, as discussed in Section 2.6.1. Therefore, rather than deriving yield coefficients for OHOs under ammonia limited conditions by using a metabolic network analysis, a simpler approach considering thermodynamics will be used in order to maintain a certain consistency with the ASM2d approach for OHOs.

OHO Growth Under Ammonia Limited Conditions. The difference in yield values when ammonia is used as the nitrogen source vs. when nitrate is used arises from the thermodynamics of the metabolic reactions taking place. Several successful thermodynamic methods based on Gibbs energy have been outlined in the literature for estimating bacterial yields on substrate. Two widely applied methods are the Gibbs Energy Dissipation method outlined by Heijnen et al.[35] and the half-reaction approach developed by McCarty.[56] Due to its successful application in the environmental engineering field, McCarty's half-reaction approach is used here.

In the ASM2d and TUDP models, OHOs grow on either acetate or fermentable substrate in the aerobic and anoxic zones. The same OHO yield coefficient, Y_H, is used for growth on both substrates. In the derivation of the OHO yield coefficient using nitrate as the nitrogen source, a choice must be made as to the model substrate used in the derivation. In reality, municipal wastewater contains many different organic compounds in which OHOs will use for growth. In this work, acetate is used as the substrate in the derivation of the OHO yield on nitrate due to the use of acetate as a primary substrate in ASM2d. It should be noted that in an efficiently operating EBPR system, acetate is often depleted in the anaerobic zone. Nevertheless, while acetate may not specifically be available in aerobic and anoxic processes, it is assumed here that the actual organic substrates used for growth by OHOs in the system being modeled have similar energetics to acetate.

OHOs are assumed by the TUDP model to have the same biomass composition as PAOs, $CH_{2.09}O_{0.54}N_{0.20}P_{0.015}$. The degrees of reduction of biomass and substrate are then:

$\lambda_{x.\varphi} = 6.085$	Biomass degree of reduction w/NO_3 as N source
$\lambda_s = 4.0$	Acetate degree of reduction

The average carbon fraction by mass for biomass cells, σ_c, is calculated as follows:

$C = 1$	Number of C atoms in biomass
$\mathrm{MW_x} = 26.023$ g/mole	MW of biomass (Cmol basis)
$\sigma_c = \dfrac{C \cdot 12.011}{\mathrm{MW_x}} = 0.462$ g C/g cells	Average carbon fraction of biomass

Energy values for the appropriate half-reactions are taken from VanBriesen[103] and shown below:

$\Delta G_d^{0'} = 31.06\,\mathrm{KJ/e^-}$	SFE for e^- donor oxidation (acetate)
$\Delta G_a^{0'} = -78.72\,\mathrm{KJ/e^-}$	SFE e^- acceptor reduction (oxygen)
$\Delta G_r^{0'} = \Delta G_a^{0'} - \Delta G_d^{0'} = -109.78\,\mathrm{KJ/e^-}$	SFE for overall reaction
$\Delta G_{\mathrm{CS}}^{0'} = \Delta G_d^{0'} = 31.06\,\mathrm{KJ/e^-}$	Gibbs energy for C-source (acetate) oxidation
$\Delta G_p^{0'} = 35.6\,\mathrm{KJ/e^-}$	Gibbs energy for carbon source to pyruvate

Note: SFE = Standard free energy.

Following McCarty and Rittman,[55] the electron transfer efficiency for the catabolic reaction, K, is taken to be 0.6. The electron transfer efficiency for biomass synthesis, κ, is taken to be equal to K, which is commonly assumed.[103]

According to VanBriesen and Rittmann, the free energy required for the synthesis of macromolecules, $\Delta G_{cells}^{0'}$, depends on the biomass composition and the degree of reduction of the cells.[104] It can be determined from the free energy of ATP hydrolysis and the cell yield on ATP. Values from VanBriesen and Rittmann are assumed:

$\Delta G_{\mathrm{ATP.HYD}}^{0'} = 12.5\,\mathrm{kcal}$	Free Energy for ATP hydrolysis
$Y_{\mathrm{ATP}} = 10.5\,\mathrm{g\ cells/mole\ ATP}$	Cell yield on ATP
$K = 0.6$	Energy capture efficiency

The free energy required for the synthesis of macromolecules is then determined as follows:

$$\Delta G_{cells}^{0'} = \frac{G_{\mathrm{ATP.HYD}}^{0'}}{Y_{\mathrm{ATP}} \cdot 0.9 \cdot \dfrac{\lambda_{x.\varphi}\,\sigma_c}{12}} \cdot 4.184\,\frac{\mathrm{kcal}}{\mathrm{kJ}} = 23.647\,\frac{\mathrm{KJ}}{\mathrm{e^-}}$$

The free energy for synthesis of biomass cells, $\Delta G_{syn}^{0'}$, can be calculated as:

$$\Delta G_{syn}^{0'} = \frac{\Delta G_p^{0'} - \Delta G_{CS}^{0'}}{K^m} + \Delta G_{cells}^{0'} = 31.213\,\mathrm{KJ/e^-}$$

The exponent m=1 in the above equation since the numerator is positive. Conversely, the method calls for m=-1 in the case that the numerator is negative.

The fractions of electrons going to the electron donor and to cellular synthesis are:

$$A = \frac{\Delta G^{0'}_{syn}}{K \cdot \Delta G^{0'}_{r}} = 0.474$$

$$f_{so} = \frac{1}{1+A} = 0.678 \qquad \text{Fraction of } e^- \text{ going to cells}$$

$$f_{eo} = 1 - f_{so} = 0.322 \qquad \text{Fraction of } e^- \text{ going to energy}$$

The aerobic biomass yield on acetate is equal to the fraction of electrons used to produce new cells. The yield value can be expressed in Cmol biomass/Cmol acetate by multiplying the yield by the ratio of the substrate to biomass degree of reduction values:

$$Y_x = f_{so}\frac{\lambda_s}{\lambda_x} = 0.446\,\text{Cmol biomass/Cmol acetate}$$

Conversion of the biomass yield with nitrate as the nitrogen source to COD units is obtained by using 35.948 g COD biomass/Cmol and 32.017 g COD acetate/Cmol:

$$Y_{H.\varphi} = Y_{x.\varphi}\frac{35.948}{32.017} = \underline{\underline{0.501\,\text{COD biomass/COD acetate}}}$$

The default value of the OHO yield, Y_H, used in the TUDP model (with ammonia as the nitrogen source) is 0.63 gCOD biomass/COD substrate. Hence, a decrease of 20% in the yield coefficient is obtained when nitrate is used as the nitrogen source.

The ASM2d and TUDP models simulate OHO growth on acetate and fermentable substrate with a single biomass yield value. The new model in this work makes the same assumption. Therefore, $Y_{H.\varphi}$ is used in the new model processes for both growth on acetate (VFAs) and growth on fermentable substrate under ammonia limited conditions.

3.6 Post-Anoxic Glycogen Degradation Kinetics

There is evidence that internal polymer degradation in EBPR sludge follows first order kinetics.[101] Other studies using aerated, synthetic fed, non-EBPR sludge have found different reaction orders, such as 1.3 for PHA degradation and second order for aerobic glycogen degradation under famine conditions.[6,22] The ASM3 model uses a Monod function to model the degradation of the lumped storage parameter f_{STO}, which is the sum of internally stored PHA and glycogen. A similar Monod function is used to simulate the aerobic and anoxic degradation of PHA by the TUDP model.

In this study, 27 data sets arising from 10 different lab reactors operating in the post-anoxic BNR configuration were analyzed in order to estimate the rate of glycogen degradation for the new model. The data sets used were taken from the work of Coats et al.,[12] Winkler et al.,[113] and unpublished experimental data from our reactors. When determining the glycogen degradation rate from each data set, a choice must be made whether to relate the glycogen degradation rate to the total active biomass fraction (heterotrophs + autotrophs + PAOs) in the reactor or to just the fraction of PAOs in the biomass. In the new model only PAOs are assumed to store and cycle glycogen as part of their metabolism. Further, denitrifying PAOs are the only organisms assumed in the model to denitrify in the absence of external carbon in the anoxic zone. Unfortunately, the PAO fraction is not known for all of the 27 data sets used for determining the glycogen degradation rate. Moreover, the fraction of PAOs can vary widely between systems, even between systems having similar phosphorus removal efficiency. For example, previous qPCR analysis of the biomass from our reactors operating in the post-anoxic EBPR configuration have shown PAO fractions varying widely from 0.9% to 74.1%.[3,113] This wide ranging PAO fraction introduces a large deviation in the estimated glycogen degradation rate.

In the TUDP model, the PHA and glycogen cycling rates were originally estimated using batch tests on enriched EBPR sludge fed synthetic wastewater. These rates were then applied only to PAOs in the model matrix. Upon refinement and calibration of the rates, the model was found to adequately simulate EBPR in full scale plants in which the sludge consists of a highly

mixed consortia of organisms. A similar approach is applied here. Since our reactors are fed real wastewater with a resulting sludge composed of a mixture of organisms and a wide range of PAO fractions, the choice was made to derive the glycogen degradation rate using the total active biomass fraction of the sludge. Since glycogen is degraded only by PAOs in the new model, the glycogen degradation rate is applied only to the PAO fraction, not the total active biomass in the model. The rate derived from these data sets using the active biomass is to be used as a starting point which will need calibration during testing of the model.

Four kinetic models for the degradation of the fraction of glycogen to active biomass, $f_{gly} = C_{gly}/C_x$ were initially evaluated:

1. First order: $r_{gly} = \frac{df_{gly}}{dt} = -k_{gly.px} \cdot f_{gly}$.
2. Second order: $r_{gly} = \frac{df_{gly}}{dt} = -k_{gly.px} \cdot f_{gly}^2$.
3. Monod with Monod constant $K = 1.0$: $r_{gly} = \frac{df_{gly}}{dt} = -q_{gly.px} \cdot \frac{f_{gly}}{1.0+f_{gly}}$.
4. Monod with variable Monod constant, K: $r_{gly} = \frac{df_{gly}}{dt} = -q_{gly.px} \cdot \frac{f_{gly}}{K+f_{gly}}$.

The kinetic coefficients, k_{gly}, $-q_{gly.px}$, and K (for model 4) were estimated through minimization of the sum of squares of the weighted differences between the measured values of each data set and the predicted glycogen fraction from the model according to:

$$\chi^2(\boldsymbol{p}) = \sum_{n=1}^{n} \left(\frac{y_{meas,i} - y_i(\boldsymbol{p})}{\sigma_{meas,i}} \right)^2 \tag{3.70}$$

In which $\boldsymbol{p}$ are the model kinetic coefficients, $y_{meas,i}$ are measured glycogen fractions from the data sets, $y_i(\boldsymbol{p})$ is the calculated glycogen fraction from the model, and $\sigma_{meas,i}$ is the standard deviation of the of data point i. Better model fits are reflected by a lower calculated χ^2 value. The estimation procedure for each data set was automated using the software AQUASIM with use of a secant algorithm for numerical minimization of the sum.[79]

The parameter estimation procedure using a variable K (model 4) allowed for K to vary from 0.001 to 10 along with a variation in $q_{gly.px}$ such that χ^2 is minimized. The minimization of χ^2 for each sample set resulted in a large variations in K (0.001 to 10) and χ^2 (0.01-7.53). Due to these large variations between sample sets, the approach used for model 4 was ultimately

rejected.

The ASM 3 model uses a Monod expression to model biomass growth on lumped internal carbon storage consisting of both PHA and glycogen. The ASM 3 model uses a default value of 1.0 for the Monod half-saturation coefficient, K_{STO}, that is used in this process equation. In analysis using model 3, this value was chosen for K as a starting point with the expectation that K could be adjusted if a better fit is needed. It is notable that the value of 1.0 for K is large compared to f_{gly} and produces an expression resembling first order kinetics.[22] It was found that the resulting χ^2 values for the estimated $q_{gly.px}$ using the assumed K value of 1.0 were sufficiently small that further adjustment to K was deemed unnecessary. The results of the parameter estimation for models 1-3 are shown in Table 3.3.

In Table 3.3, it should be noted that active biomass for reactors PX5 and PX6 were able to be determined directly since PHA and glycogen samples were taken at the same time as the VSS samples. Hence, active biomass could be calculated as the sludge VSS minus PHA and glycogen, plus an assumed 5% active biomass in the ash. The sample times at which VSS samples were taken from the sludge in the other data sets, however, were not recorded. Therefore, the actual concentration of glycogen and PHA in the sludge at the time the VSS sample was taken is unknown and a direct calculation could not be performed for these reactors. The calculated ratios of active biomass to VSS for both PX5 and PX6 was approximately 1.0. This ratio was consistent across both reactors despite the two reactors having different SRTs. Thus, for all of the sample sets, a ratio of 1.0 was multiplied by the recorded VSS to provide an estimated C_x value, which results in the active biomass having the the same concentration as the VSS concentration for these sample sets.

From Table 3.3, it can be seen that across all models, the value of the glycogen degradation rate is significantly smaller for reactors with an SRT of 20 days vs. 10 days, which is largely due to the smaller fraction of glycogen to biomass found at the SRT of 20 days. The average χ^2 values are virtually identical for the estimation of the glycogen degradation rate using all 3 models within the same SRT with an average χ^2=1.3 for an SRT of 10 days and χ^2 = 0.4 for an SRT of 20 days. Therefore a significant advantage of one kinetic model (first order, second order, or Monod kinetics) over another is not apparent and all three models can arguably result

Table 3.3: Post-Anoxic Glycogen Degradation Kinetic Rates

					First Order		Second Order		Monod, K=1.0	
Reactor	Date	SRT (d)	n	C_x (mg/L)	$k_{gly.px}$ (1/h)	χ^2	$k_{gly.px}$ (1/h)	χ^2	$q_{gly.px}$ (mg COD/L-h)	χ^2
PX5	3/14/16	10	6	3091	0.115	0.309	4.372	0.341	0.119	0.308
PX5	3/18/16	10	7	2702	0.255	1.741	10.411	1.493	0.261	1.748
PX5	5/18/16	10	6	2270	0.042	0.610	0.976	0.611	0.043	0.610
PX5	5/25/16	10	6	2523	0.197	0.091	8.451	0.057	0.202	0.092
PX2.1	7/9/15	10	6	2389	0.186	7.535	3.650	7.478	0.196	7.538
PX3.1	7/9/15	10	6	2695	0.113	0.156	2.467	0.194	0.118	0.154
PX2.1	7/30/15	10	6	2346	0.051	1.056	3.090	1.058	0.052	1.055
PX3.1	7/30/15	10	6	2635	0.064	0.045	4.333	0.045	0.065	0.045
PX2.1	8/19/15	10	6	2440	0.192	1.382	6.346	1.252	0.198	1.387
PX3.1	8/19/15	10	6	2465	0.065	0.302	3.002	0.307	0.067	0.302
Mean:					**0.128**	**1.323**	**4.710**	**1.284**	**0.132**	**1.324**
PX6	3/14/16	20	6	4760	0.085	0.040	4.870	0.040	0.086	0.040
PX6	3/18/16	20	7	4257	0.116	0.300	9.862	0.286	0.118	0.300
PX6	5/18/16	20	6	2796	0.000	0.563	0.000	0.563	0.000	0.563
PX6	5/25/16	20	6	3198	0.112	0.199	5.356	0.217	0.114	0.199
PX2	7/9/15	20	6	3120	0.000	2.065	0.000	2.065	0.000	2.065
PX3	7/9/15	20	6	2712	0.082	2.207	1.794	2.202	0.085	2.207
PX2	7/30/15	20	6	3324	0.000	0.263	0.000	0.263	0.000	0.263
PX3	7/30/15	20	6	3162	0.043	0.888	1.923	0.893	0.044	0.888
PX2	8/19/15	20	6	2967	0.000	0.117	0.000	0.117	0.000	0.117
PX3	8/19/15	20	6	3451	0.071	0.082	3.002	0.307	0.073	0.082
A	10/24/08	20	3	2533	0.093	0.055	1.750	0.065	0.098	0.055
A	10/29/08	20	3	2108	0.108	0.045	1.534	0.032	0.116	0.046
B	11/11/08	20	4	1502	0.057	0.101	0.980	0.112	0.061	0.101
I	9/30/10	20	9	4225	0.025	0.052	0.417	0.052	0.027	0.053
J	9/30/10	20	9	4550	0.021	0.022	0.361	0.024	0.022	0.021
I	11/23/10	20	5	1520	0.034	0.034	0.611	0.034	0.037	0.034
J	11/23/10	20	5	1996	0.024	0.009	0.395	0.009	0.026	0.009
Mean:					**0.051**	**0.414**	**1.933**	**0.428**	**0.053**	**0.414**

in adequate simulation of the degradation of glycogen. Monod kinetics (model 3) was thus chosen since it is consistent with the Monod kinetics adopted by the other ASM models. In addition, Monod kinetics allows for greater flexibility during model calibration since both K and the glycogen degradation rate can be adjusted if the glycogen degradation pattern of a specific system is found to not strictly follow first or second order behavior.

From Table 3.3, the average value of q_{gly} is 0.132 h^{-1} for an SRT of 10 days and 0.053 h^{-1} for an SRT of 20 days. The smaller value of 0.05 h^{-1} is chosen as an initial estimate for further comparison in the model evaluation. For implementation in the model matrix, the equivalent expression $q_{gly} = \mu_{gx}/Y_{gx}$ is used in which μ_{gx} is the biomass specific growth rate on glycogen. Using the previously derived value of $Y_{gx} = 0.5728$ g COD/g COD, the following value for μ_{gx} results:

$$\boxed{\mu_{gx} = 0.6874\,\mathrm{d}^{-1}} \tag{3.71}$$

3.7 Model Matrix

The integrated model is presented in Appendix A. The model is presented in the Gujer matrix format used by the ASM models, which was originally proposed by Petersen for representation and modeling of biochemical reactions.[76] A detailed description of the matrix representation may be found elsewhere.[5,29,36,38,94,100] The model is built upon the TUDP model, with added processes and coefficients shown in bold within the matrix. The original TUDP model consists of 22 processes and 18 state variables to describe hydrolysis, carbon, nitrogen, and phosphorus conversions within the wastewater treatment process. The model also simulates alkalinity and TSS concentrations within the wastewater. Seventeen additional processes were added in this work to describe the conversions under ammonia limited conditions, dPAO activity on glycogen when PHA is depleted, and dPAO maintenance on polyphosphate when both PHA and glycogen are limited.

The updated model is balanced on COD, nitrogen, phosphorus, charge, and TSS. When incorporating the yield and stoichiometric structure of each of the new processes into the matrix, the numerical analysis procedure for checking process continuity described by Hauduc et al.[32] was used to ensure a balance was maintained on these constituents. A tabular copy of the continuity check is included in Appendix A. The procedure consists of multiplying the model stoichiometric matrix by a composition matrix for COD, nitrogen, phosphorus, charge, and TSS. If all processes are balanced, a zero matrix should result. Following Hauduc et al., all processes were balanced to a tolerance of 10^{-15}. In their review of seven activated sludge models, Hauduc et al. note that both the New General model and the UCTPHO+ models are not balanced on COD when simulating aerobic and anoxic growth on nitrate under ammonia limited conditions, as these models do not consider the oxygen released from nitrate during the assimilative reduction process. As Hauduc et al. note, the stoichiometric coefficient for the dissolved oxygen state variable will be lower when nitrate is reduced for incorporation into biomass. In essence, a portion of the electrons from the substrate are being used by the bacteria to reduce nitrate for assimilation instead of entering the respiratory system for ATP generation, which results in less oxygen required by the system but lower growth yields. In this work, to balance COD in the aerobic processes using nitrate as the nitrogen source, the stoichiometric coefficient on dissolved oxygen in the matrix is reduced by subtracting the mass of COD of the nitrate incorporated into the biomass, as recommended by Hauduc et al.

Since the stoichiometric coefficient on oxygen cannot be reduced in the anoxic processes, Hauduc et al. recommend considering that more substrate is required under nitrate assimilation to achieve the same amount of growth as when ammonia is used as the nitrogen source. To balance COD in these processes for OHOs, the COD content of the nitrate incorporated into biomass is therefore added to the stoichiometric coefficient on substrate. For PAOs the nitrate content incorporated into biomass is added to the stoichiometric coefficient on PHA when PAOs are not using glycogen as their substrate and to the stoichiometric coefficient on glycogen for the glycogen degradation process.

In addition, a half-saturation coefficient for nitrate assimilation for OHOs, $K_{NO.ASIM}$, and PAOs, $K_{NO.PAO.ASIM}$, is used to control the affinity for nitrate assimilation by use of Monod

functions. The values of the half-saturation coefficients are calibrated during model simulations. Setting the half-saturation coefficient to zero will turn off the nitrate assimilation processes, if the processes are not needed. This may be desired in order to reduce the computation expense to solve the processes equations and to shorten the solve time during simulations when ammonia limitation is not a concern.

Chapter 4: Materials and Methods

4.1 Overview

The developed model presented in Appendix A was tested against lab reactors configured in the post-anoxic BNR configuration. In addition, simulations were performed against data from a similarly configured pilot scale WRRF fed municipal wastewater. Simulations were used to evaluate the adequacy of the model and identify potential improvements that could be made.

Laboratory Bioreactors. Two 2.25L laboratory-scale sequencing batch reactors (SBRs) were operated at room temperature without pH control (over the operational cycle the pH varied between 7.2 and 8.5, and never decreased below 7). One SBR (PX5) was operated to target a 10 day solids residence time (SRT). The second SBR (PX6) was operated to target a 20 day SRT. Each 6-hr SBR cycle included the following periods: feed (5 min), anaerobic (1 hr), aerobic (4 hr, 15 min), settle (30 min), and decant (10 min). A programmable logic controller was used to control operations. Effluent was decanted each cycle and replaced with an equal volume of substrate to maintain an 18 hour hydraulic residence time (HRT). The solids residence time (SRT) was controlled by Garrett wasting of mixed liquor during each aerobic period, once each cycle. Anaerobic conditions were maintained by stopping aeration approximately 30 minutes before the settling period to allow dissolved oxygen (DO) depletion; DO measurements confirmed that anaerobic conditions prevailed. Air was introduced through stone diffusers to create aerobic conditions (DO>2 mg L^{-1}). Reactors were completely mixed with magnetic stir bars. All pumping was performed using peristaltic pumps (Watson Marlow Bredel, Wilmington, MA, USA).

Pilot Scale Facility. A 5,000 gallon continuous flow pilot scale WRRF owned and operated by the University of Idaho Department of Civil and Environmental Engineering and located at the Moscow, Idaho WRRF was operated for additional testing of the developed model. The facility consists of a primary clarifier, three anaerobic continuous stirred-tank reactors (CSTRs), two aerobic CSTRs, an anoxic carousel reactor, and a secondary clarifier. The facility

is continuously fed screened and degritted wastewater from the Moscow WRRF with effluent being directed back to the Moscow WRRF. Additional details of the pilot scale facility are described later.

4.2 Experimental Methods.

Source of Microorganisms for Reactors Inocula for both the lab and pilot scale reactors were obtained from the Moscow, ID, WRRF, an A^2/O (the oxic element being a carousel reactor) EBPR process. For the lab reactors, raw wastewater was obtained from the same facility, downstream of screening and grit removal. VFA-rich fermenter liquor was recovered from a bench-top fermenter fed thickened primary solids from the Pullman, WA, WRRF. All wastewater was stored at 4 °C until used, and raw wastewater was obtained every 5-8 days. Lab bioreactor feed tanks were replenished daily. Icocula for the pilot scale facility was obtained from the return activated sludge (RAS) line of the Moscow, Idaho WRRF.

Analytical Techniques. Samples from all reactors were collected to monitor pH, DO, soluble reactive phosphate (SRP), nitrate (NO_3), ammonia (NH_3), volatile fatty acids (VFAs), mixed-liquor suspended solids (MLSS), mixed liquor volatile suspended solids (MLVSS), glycogen, and PHA. For soluble constituents, samples were first centrifuged to remove biomass and then filtered through a 0.22 µm syringe filter (Millipore Corp., Billerica, MA, USA) prior to testing. SRP was determined in accordance with Hach (Loveland, CO, USA) method 8048 (equivalent to Standard Methods 4500-PE).[2] Soluble NO_3 was determined in accordance with Hach method 10020, while soluble NH_3 testing followed Hach method 10031. A Spectronic 20 Genesys spectrophotometer (Thermo-Fisher Scientific Corp, Waltham, MA, USA) was utilized to measure the absorbance of the reacted sample at a wavelength of 890 nm for SRP, 410 nm for NO_3, and 655 nm for NH_3. Phosphate, NO_3, and NH_3 concentrations were determined utilizing a standard curve (R^2>0.99). Soluble COD was determined by precipitation and settling of colloids and subsequent filtration of the clarified sample through a 0.22 µm filter prior to testing of COD. Colloidal precipitation was achieved by addition of $ZnSO_4$, rapid mixing, pH adjustment, and subsequent flocculation and settling of the sample according to the method

presented by Mamais et al.[52] All COD concentrations were determined in accordance with Standard Methods 5220 D.[2]

MLSS and MLVSS were measured in accordance with Standard Methods 2540 D and 2540 E, respectively.[2] Measurement of pH was accomplished with a Thermo-Fisher Scientific Accumet AP85 Waterproof pH/Conductivity Meter. DO measurements were collected using a Hach HQ30d Meter with a LDO101 DO Probe.

VFAs (acetic, propionic, butyric, isobutyric, valeric, isovaleric, and caproic acids) were quantified using a Hewlett-Packard 6890 series gas chromatograph (Agilent Technologies, Inc., Santa Clara, CA, USA) equipped with a flame-ionization detector and a Hewlett-Packard 7679 series injector. The system was interfaced with the Hewlett-Packard GC ChemStation software version A.06.01. VFA separation was achieved using a capillary column (Heliflex AT-AquaWax-DA , 30 m x 0.25 mm ID, W. R. Grace & Co., Deerfield, IL, USA) which was ramped from an initial 50 °C to 200 °C in three steps (following 2 min at 50 °C, ramp to 95 °C at 30 °C-min^{-1} then to 150 °C at 10 °C-min^{-1} and hold for 3 min; finally, ramp to 200 °C at 25 °C-min^{-1} and hold for 12 min) with helium as the carrier gas (1.2 mL min^{-1}). The split/splitless injector and detector were operated isothermally at 210 and 300 °C, respectively. Prior to analysis, samples were acidified to a pH of 2 using nitric acid. 0.5 µL of each sample was injected in 20:1 split mode. VFA concentrations were determined through retention time matching with known standards (Sigma-Aldrich Co., St. Louis, MO, USA; Thermo Fisher Scientific Inc., Waltham, MA, USA) and linear standard curves (R^2>0.99).

Biomass for PHA and glycogen content was obtained directly from the rectors and centrifuged at 6,000 rpm for 5 minutes. Centrifuged biomass was then rinsed with double deionized water and dried overnight at 105 °C. Dried biomass was then stored in a desiccator until testing for PHA and glycogen content. Biomass PHA content was determined by gas chromatography/mass spectrometry (GC-MS) as described in Coats et al.[12] Total intracellular PHA content was determined on a percent dry weight cell basis (mass PHA/(mass of biomass), w/w). Biomass glycogen concentration was measured using dried biomass samples and enzymatic assay as described by Parrou and Francois, which is postulated to measure glycogen polymers without interference from structural cellular carbohydrates.[75]

Biomass samples to determine the fraction of active biomass in the sludge were taken at the end of the aerobic cycle, when polyphosphate within PAOs are theoretically lowest. As discussed by Smolders et al., MLSS is assumed to consist primarily of a consortia of active biomass, PHA, glycogen, and polyphosphate.[90] The sludge VSS consists of the portion of sludge that is lost by ignition, i.e. PHA, glycogen, and the large part of active biomass as shown in Figure 4.1. What remains is ash, which Smolders indicates will consist of polyphosphate and a small portion of the active biomass. In reality, other inert inorganic particulate material that is present in the sludge will also show up in the ash content.

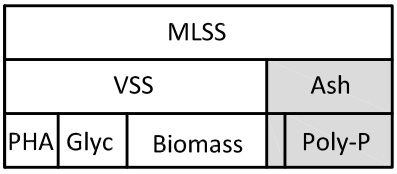

Figure 4.1: Composition of biomass. Adapted from Smolders et al.[90]

Smolders notes that about 5-10% of active biomass consists of ash. Villadsen et al. indicates 4-8%.[105] Active biomass from samples was therefore determined to be the VSS minus PHA and glycogen concentrations of the sludge at the time of the MLSS sample plus an assumed additional 5% of the calculated amount which would form a part of the ash.

Quantitative Polymerase Chain Reaction (qPCR). qPCR was performed on genomic DNA recovered during each system assessment to estimate the relative abundance of Accumulibacter (the model PAO), GAOs, AOBs and NOBs relative to the total eubacterial population. Genomic DNA was extracted using a PowerSoil DNA Extraction Kit (MO BIO Laboratories Inc., Carlsbad, CA USA). Genomic DNA yield and purity was quantified using a Synergy H1 Multi-Mode Reader (BioTek, Winooski, VT). Primer sets used to quantify total bacteria,[68] Accumulibacter,[17,33] and GAOs (by targeting Candidatus Competitbacter phosphatis, a model GAO)[16] are listed in Coats et al.[11] Amplification of AOBs was based on a primer set for the gene ammonia monooxygenase (amoA).[82] For NOBs, Nitrobacter spp. and Nitrospira were amplified using 16S rDNA sequences. qPCR settings were in accordance with Winkler et al.[113] AOB, Nitrobacter, and Nitrospira abundance relative to eubacteria was estimated using the mean

efficiencies for each primer set and the Cq values for the individual samples, assuming average 16S rDNA gene copy numbers of 4.1 for eubacteria, 2.5 for AOB,[47] and 1.0 for both Nitrobacter and Nitrospira.[57] All samples were assessed in triplicate with 5 ng of total genomic DNA per reaction. qPCR melting curves were evaluated to confirm a single melting peak, and agarose gel analysis confirmed a single band for each primer set. Amplification efficiencies were calculated for each primer set using baseline-corrected fluorescence data (StepOne software v2.0), and the LinRegPCR program.[78] The cycle threshold was set at a constant value across all samples based on location within the log-linear region for determination of Cq values (cycle number at which the measured fluorescence exceeds the cycle threshold). Mean amplification efficiencies for the total bacterial, PAO, and GAO primer sets were 95.6±0.085% (n=254), 89.7±0.088% (n=250), and 82.3±0.074% (n=249) respectively. PAO and GAO relative abundances were estimated per Winkler et al.[113]

Chapter 5: Results and Discussion

5.1 Model Performance Against Reactor PX6

In order to test the initial performance of the model, simulations were performed against lab data from SBR reactor PX6 (SRT=20 days). Influent and sludge samples were collected from the SBR reactor over one cycle on each of the days 5/18/16, 5/21/16, and 5/25/16. Sample results over the three days were averaged in order to smooth natural dynamic variations and potential measurement errors.

5.1.1 Wastewater Characterization

The influent samples were used to provide concentrations for the majority of the model's influent state variables. The model consists of 18 state variables as listed in Table 5.1.

Table 5.1: Model state variables

	State Variable	Units	Description
Soluble Components	S_O	gO_2/m^3	Dissolved oxygen
	S_F	$gCOD/m^3$	Fermentable readily biodegradable organic substrate
	S_A	$gCOD/m^3$	Volatile fatty acids (considered to be acetate)
	S_{NH}	gN/m^3	Ammonium plus ammonia
	S_{NO}	gN/m^3	Nitrate plus 3/5 nitrite
	S_{N2}	gN/m^3	Di-nitrogen
	S_{PO}	gP/m^3	Inorganic soluble phosphorus (considered to be orthophosphates)
	S_I	$gCOD/m^3$	Inert soluble organic material
	S_{HCO}	mole HCO_3/m^3	Alkalinity
Particulate Components	X_I	$gCOD/m^3$	Inert particulate organic material
	X_S	$gCOD/m^3$	Slowly biodegradable particulate substrate
	X_H	$gCOD/m^3$	Ordinary heterotrophic organisims
	X_{PAO}	$gCOD/m^3$	Phosphate accumulating organisims
	X_{PP}	gP/m^3	PAO cellular polyphosphate
	X_{PHA}	$gCOD/m^3$	PAO cellular polyhydroxyalkanoates
	X_{GLY}	gCOD/m3	PAO cellular glycogen
	X_A	$gCOD/m^3$	Autotrophic nitrifying organisms
	X_{TSS}	$gTSS/m^3$	Total suspended solids

COD Fractions. The model considers COD to be present as either soluble or particulate COD. Soluble COD consists of VFAs, fermentable COD, and soluble inert material while par-

ticulate COD includes biomass, the cellular polymers PHA and glycogen, slowly biodegradable COD, and particulate inerts. The VFA fraction in the influent, S_A, was determined by gas chromatography as described. Influent soluble inert COD, S_I, was estimated by assuming that VFAs and fermentable COD are completely consumed in the activated sludge process. Under this assumption, S_I is equal to the flocculated and filtered COD in the effluent. The error introduced by this assumption is considered minimal since municipal plants with SRTs greater than approximately three days typically exhibit less than two percent biodegradable effluent COD.[64] The influent soluble COD was determined as the flocculated and filtered influent COD. Influent fermentable COD was then determined as

$$S_F = COD_{inf.sol} - S_A - S_I$$

Roeleveld and van Loosdrecht list typical municipal influent concentrations of autotrophic and PAO biomass in the range of 0.1 - 1.0 gCOD/m^3 based on their work with wastewater characterization in the Netherlands.[80] A value of 0.1 gCOD/m^3 was assumed for the simulations. Influent concentrations of ordinary heterotrophic organisms and the cellular storage polymers were assumed to be zero. The influent X_I was estimated by calibrating the value of $X_I/(X_S+X_I)$ against observed particulate COD in the reactors, after Meijer et al.[60] X_S was determined as the remainder of the influent total COD during calibration of X_I.

Henze, et al. notes that the ASM2d model's TSS value will be larger than the analytical TSS value since the model TSS includes the X_S fraction.[38] A portion of X_S that is colloidal likely passes through the filters used during the analytical test, which will result in a lower TSS value than reflected by the model. This difference may be partially offset, however, if the wastewater contains inert minerals which are not included in the model's state variables.[38] The integrated model uses the same methodology as the TUDP model to model TSS and therefore carries with it the same uncertainties. Due to this, the influent TSS was assumed equal to the ASM2d model default value of 180 gTSS/m^3. The uncertainty inherent in the influent TSS value is incorporated into the calibration of the model's particulate COD through the calibration of the influent $X_I/(X_S+X_I)$ ratio. While differences exist between the analytical results and the model's TSS value in the influent, the error between the analytically measured TSS and

model's predicted TSS value within the reactors is considered to be nominal since the total concentration of X_S in the reactor is an order of magnitude smaller than the concentration of the remaining particulate components.

Table 5.2 summarizes the assumptions and equations used for determination of the influent COD fractions.

Table 5.2: Assumptions and equations used for determination of influent COD fractions

Model Assumptions
X_H, X_{PHA}, X_{GLY}, X_{PP} = 0 gCOD/m^3
X_A, X_{PAO} = 0.1 gCOD/m^3
S_I=$COD_{eff.sol}$
COD Equations
$COD_{inf.sol}$ = Soluble influent COD (flocculated and filtered)
$COD_{eff.sol}$ = Soluble effluent COD (flocculated and filtered)
$COD_{inf.tot}$ = Total unfiltered influent COD
$COD_{inf.tot} = S_A + S_F + S_I + X_S + X_I + X_H + X_A + X_{PAO} + X_{PHA} \approx S_A + S_F + S_I + X_S + X_I$
$COD_{inf.sol} = S_A + S_F + S_I$
$S_F = COD_{inf.sol}$ - $COD_{eff.sol}$ - S_A

Model Inclusion of Nitrate and Nitrite. As discussed in Chapter 2, the reduction of nitrate to nitrogen gas occurs through a multistep process in which nitrate is first reduced to nitrite and then passes through gaseous nitric oxide and nitrous oxide prior to being reduced to nitrogen gas. In the TUDP model nitrate is assumed to be reduced to nitrogen gas in a single step, therefore nitrite is not specifically modeled. The state variable for nitrate, S_{NO}, is considered to be the sum of nitrate and any nitrite species in solution. A more accurate approach is to consider S_{NO} as the sum of $NO_3 + 0.6\,NO_2$. This formulation is derived by considering that 5 electrons from the substrate are required to reduce nitrate to nitrogen gas while only 3 electrons are required to reduce nitrite to nitrogen gas. Thus NO_2 demands 3/5 the electrons from the carbon substrate to be reduced to nitrogen gas as does nitrate. With S_{NO} equal to $NO_3 + 0.6\,NO_2$, S_{NO} can be considered as an equivalent amount of nitrate demanding the same amount of electrons from the substrate as the actual amount of combined nitrate and nitrite in solution.[45] This approach was taken in the model simulations.

Wastewater Characterization. The percent PAOs, GAOs, nitrifiers, and ammonia oxidizing bacteria as determined by qPCR analysis on the sludge in the reactor during the sample period are shown in Table 5.3

Table 5.3: Percent PAOs, GAOs, nitrifiers, and ammonia in PX6

% PAOs	% GAOs	% Nitrobacter	% Nitrosonomas	% Ammonia Oxidizers	n
1.57 ± 0.16	3.37 ± 0.04	3.39 ± 0.25	3.95 ± 0.29	0.11 ± 0.01	3

It is seen that the GAO fraction is larger than the PAO fraction in this reactor, which could indicate a contribution of dGAOs to the observed PHA and glycogen activity in the sludge. Both concentrations are relatively small (less than 5%), however, and the specific contribution of each organism to the observed behavior of the sludge cannot be conclusively determined. In addition, the reactors did not experience a degradation in EBPR activity, which is indicative of GAO enriched sludge.

The average influent characteristics for the three days of sampling of reactor PX6 are summarized in Table 5.4.

5.1.2 Model Calibration.

Simulation Engine. Simulations were performed using the software, Aquasim version 2.1.[79] A minimum operation time of 3 SRTs is generally considered to be required to achieve functional stability in biological wastewater treatment reactors.[29] Reactor PX6 was configured to achieve an effective SRT of 20 days, assuming that negligible biological growth occurs within the anaerobic portion of the cycle. Simulations were therefore performed over a model time of 60 days, which is equivalent to 3 times the target SRT for reactor PX6. Steady state conditions within the model at 60 days were verified by observing negligible changes in state variable concentrations at the ends of each cycle run.

The integrated model considers temperature effects on kinetic rates using Arrhenius correction functions with standard temperature at 20 °C. An average temperature of 22.67 °C was observed in the reactors at the end of the aerobic cycles. This temperature was used in the simulations

Table 5.4: PX6 simulation: influent characterization and model input. Influent characterization values are average of samples taken on 3 different days (n=3).

Tested Parameter	Unit	Average SD
Influent		
Influent Total COD	$gCOD/m^3$	1544.03 ± 308.28
Influent Filtered and flocculated COD	$gCOD/m^3$	517.37 ± 86.06
Soluble undegradable organics (S_I)	$gCOD/m^3$	42.79 ± 17.86
Influent Readily Biodegradable COD (S_S)	$gCOD/m^3$	474.58 ± 103.90
Fermentable COD (S_F)	$gCOD/m^3$	199.19 ± 34.72
Ammonium and ammonia nitrogen	gN/m^3	26.01 ± 6.62
Nitrate Nitrogen (NO_3)	gN/m^3	0.00 ± 0.00
Nitrite Nitrogen (NO_2)	gN/m^3	0.01 ± 0.01
NO_3 + 0.6 NO_2	gN/m^3	0.01 ± 0.01
Orthophosphate (PO_4)	gP/m^3	9.11 ± 1.76
Influent Volatile Fatty Acids (VFAs)		
Acetic Acid	$gCOD/m^3$	94.54 ± 22.11
Propionic Acid	$gCOD/m^3$	71.97 ± 8.36
Butyric Acid	$gCOD/m^3$	25.06 ± 6.39
Isobutyric Acid	$gCOD/m^3$	0.00 ± 0.00
Valeric Acid	$gCOD/m^3$	11.41 ± 0.76
Isovaleric Acid	$gCOD/m^3$	3.03 ± 2.65
Total VFAs	$gCOD/m^3$	206.01 ± 35.93
Reactors		
pH (End aerobic)	-	7.93 ± 0.16
T (End aerobic)	°C	22.67 ± 0.76
MLSS (End aerobic)	g/m^3	3430 ± 269
Effluent		
Effluent filtered and flocculated COD (SI)	$gCOD/m^3$	42.79 ± 17.86
Ammonium and ammonia nitrogen	gN/m^3	0.00 ± 0.00
Nitrate Nitrogen (NO_3)	gN/m^3	0.00 ± 0.00
Nitrite Nitrogen (NO_2)	gN/m^3	0.00 ± 0.00
NO_3 + 0.6 NO_2	gN/m^3	0.00 ± 0.00
Orthophosphate (PO_4)	gP/m^3	0.82 ± 0.47

Model Variable	Description	Unit	Value
Soluble Components			
S_{O2}	Oxygen (negative COD)	g COD/m^3	0
S_F	Fermentable COD	g COD/m^3	199.19
SA	Volatile fatty acids	g COD/m^3	206.01
S_{NH}	Ammonium and ammonia nitrogen	g N/m^3	26.01
S_{NO}	Nitrate and 0.6·nitrite nitrogen	gN/m^3	0.01
S_{N2}	Dissolved nitrogen gas	g N/m^3	0
S_{PO}	Inorganic soluble phosphorus	g P/m^3	9.11
S_I	Soluble inert organic matter	g COD/m^3	42.79
S_{HCO}	Alkalinity	mol/m^3	5
Particulate Components			
X_I	Particulate inert organic matter	g COD/m3	680
X_S	Slowly biodegradable substrate	g COD/m^3	346.66
X_H	Active heterotrophic biomass	g COD/m^3	0
X_A	Active autotrophic biomass	g COD/m^3	0.1
X_{PAO}	Phosphate accumulating organisms	g COD/m3	0.1
X_{PP}	Polyphosphate	g P/m^3	0
X_{PHA}	Polyhydroxyalkanoates	g COD/m^3	0
X_{GLY}	Glycogen	g COD/m^3	0
X_{TSS}	Total suspended solids	g $MLSS/m^3$	180
Bulk Solution Temperature and pH			
T	Temperature	°C	22.67
pH	Average Anaerobic pH	-	7.93

and assumed to be constant throughout the model simulations.

Initial simulation results based on default model values showed unstable PAO polyphosphate concentrations resulting in unstable PAO biomass and significant loss of phosphorus removal. In addition, PAO PHA and glycogen reserves were over predicted while nitrification was underpredicted. Calibration of the model occurred in several steps as further described below.

The calibrated parameters are summarized in Table 5.5

Table 5.5: Calibrated parameters for Reactor PX6 simulations

Parameter	Description	Default	**PX6**	Purpose
b_A	X_A decay rate	0.15	**0.125**	Fit nitrification
$K_{P.A}$	Half-Sat. coeff. for S_{PO}	0.01	**0.0001**	Fit nitrification
$i_{N.BM}$	Biomass N content	0.07	**0.02**	Decrease S_{NH} release
n_{fe}	AN hydrolysis correction factor	0.2	**0**	Decrease S_{NH} release
q_{fe}	Fermentation rate	3	**0.7**	Fit S_{NH} & S_A, decrease PAOs
$Y_{PO.AN}$	AN yield for S_{PO} release/S_A	0.35	**0.1**	Fit AN S_{PO} release
q_{ac}	X_{PAO} AN uptake rate of S_A	4.3	**2.25**	Fit S_A uptake, X_{PAO}, X_{PHA}, & X_{GLY}
K_{ac}	Half-sat. coeff. for growth on S_A	32	**4**	Fit AN S_A, X_{PAO}, X_{PHA}, & X_{GLY}
k_{pp}	X_{pp} formation	0.1	**0.04**	Fit S_{PO} uptake
k_{GLY}	X_{GLY} formation	5.83	**1.2**	Fit glycogen formation
μ_{gx}	AX X_{GLY} degradation rate	0.6874	**0.859**	Fit AX glycogen
k_{PHA}	X_{PHA} consumption	5.51	**8**	Fit X_{PHA} degradation
Kf_{PHA}	Half-sat. ceoff. for X_{PHA}/X_{PAO}	0.2	**0.09**	Fit X_{PHA} degradation
$K_{O.PAO}$	PAO half-sat. coeff. for S_O	0.2	**0.08**	Fit X_{PHA} and X_{GLY} through OHO and PAO
$K_{O.H}$	OHO half-sat. coeff. for S_O	0.2	**0.08**	Fit X_{PHA} and X_{GLY} through OHO and PAO
b_h	X_H decay rate	0.4	**0.2**	Fit X_{PHA} and X_{GLY} through OHO and PAO
$K_{GLY.px}$	Half-sat. coeff. for AX X_{GLY} degradation	1	**0.009**	Fit AX X_{GLY} degradation
$K_{PHA.PX}$	Half-sat. coeff. for AX X_{PHA} switch	-	**0.1**	Implement X_{GLY} degradation
δ_o	Aerobic P/O ratio	1.85	**1.45**	Decrease PAO, PHA, and glycogen
δ_n	Anoxic P/O ratio	0.925	**0.725**	Decrease PAO, PHA, and glycogen

Note: AN=Anaerobic, AE=Aerobic, AX=Anoxic

The calibrated model's simulation results for PHA, glycogen, ammonia, nitrate, and phosphorus are shown in Figure 5.1

Sludge Production. The reactor was simulated with a wasting rate of 21 mL per cycle, indicating an effective SRT of 20 days (assuming no growth in the anaerobic cycle). Sludge production in the reactor was calibrated by adjusting the $X_I/(X_S + X_I)$ ratio to 0.662, which adequately described the solids concentration in the reactor.

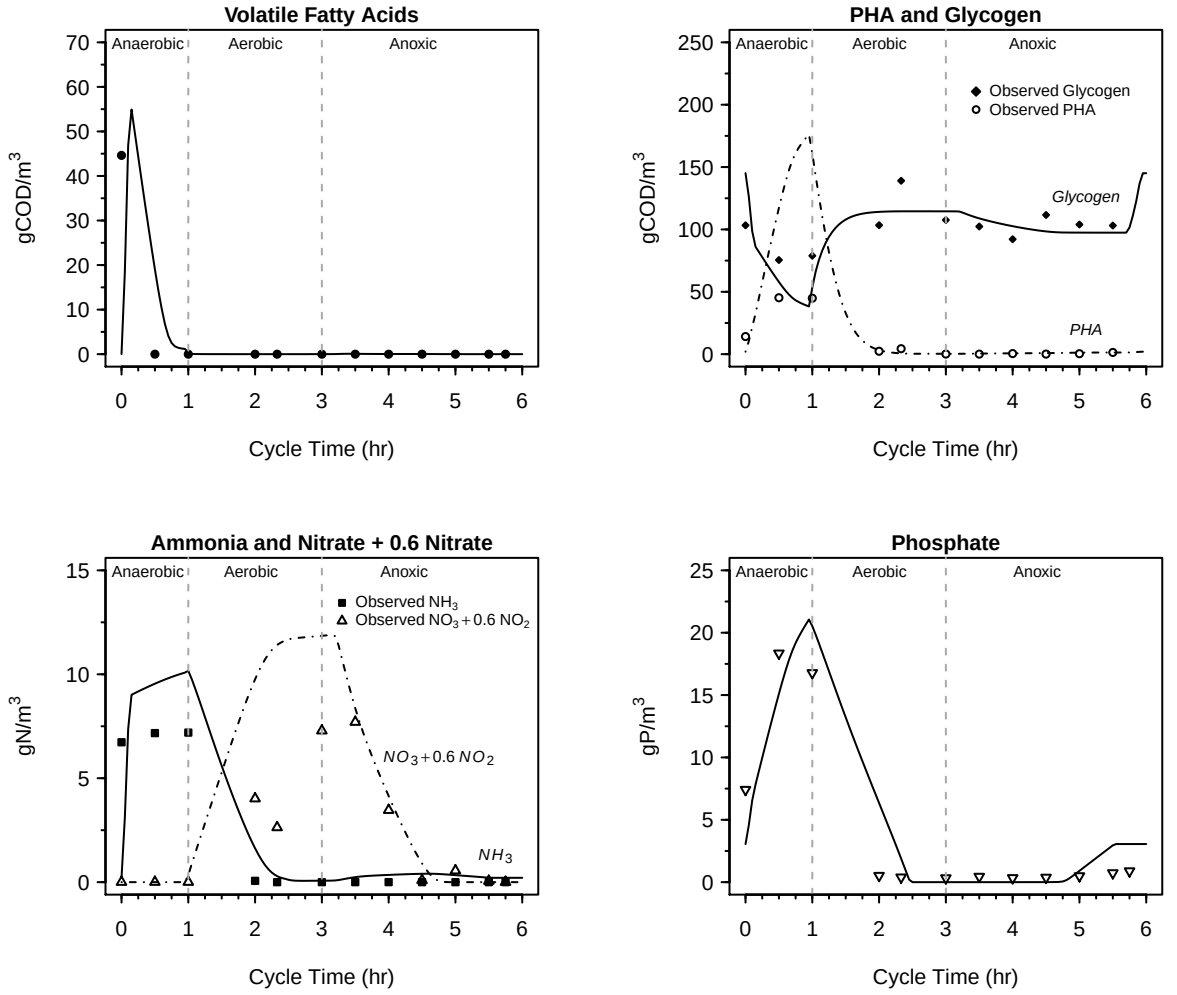

Figure 5.1: PX6 Model vs. experimental results. Observed data from the reactors are shown as points (•). Model simulations are shown as lines (—).

Hydrolysis and Fermentation Processes. The integrated model incorporates the AS-M2d hydrolysis reactions, in which particulate biodegradable organics, X_S, are converted to fermentable organic matter, S_F, while releasing ammonia, phosphorus, and soluble inert material into solution. The hydrolysis reactions are meant to simulate the observed conversion of high molecular weight organic matter and particulates into forms that are able to be used by microbial biomass as substrate. The actual nature of the reactions are not well understood, however, and likely consist of different mechanisms which act on the different types of particulate material found in wastewater sludge. Studies have shown conflicting results regarding the rates of hydrolysis under different electron acceptor conditions. Since several studies have

observed that hydrolysis rates are slower under anoxic and anaerobic environments, the ASM2d hydrolysis processes consist of rate reduction parameters that are individually set for each of the anaerobic and anoxic hydrolysis processes. Initial model simulations showed ammonia and phosphorus increasing in the anaerobic zone faster than was observed in the reactors. The anaerobic hydrolysis reduction factor, η_{fe}, was changed from a default value of 0.2 to zero in order to stop hydrolysis within the anaerobic zone and to decrease the rate of anaerobic ammonia and phosphorus release in the model. As noted by Grady et al., the cessation of hydrolysis under anaerobic conditions is consistent with what has been observed in cyclic aerobic and anoxic systems but may not be accurate for long term anaerobic environments.[29] In addition, the fermentation rate, q_{fe}, was reduced from 3 gCOD/g COD-d to 0.7 gCOD/gCOD-d to fit the effluent ammonia and anaerobic VFA concentrations.

PHA Calibration. The model parameter, δ, represents the PAO's metabolic Phosphorus/Oxygen ratio (P/O ratio) which is the amount of ATP produced per $NADH_2$ in the electron transport chain. The integrated model's aerobic and anoxic yields for PAO PHA, glycogen, and polyphosphate in addition to the PAO maintenance coefficients are dependent upon this value, as shown in the derivation of the yield values presented in Chapter 3. The default value of δ for aerobic conditions (1.85 mole ATP/mole $NADH_2$) and anoxic conditions (0.925 mole ATP/mole $NADH_2$) are based on experiments with EPBR sludge fed synthetic wastewater with acetate as the sole carbon source.[41,88] The P/O ratio is believed to vary depending on the carbon source and the bacterial species.[21] Lower P/O ratios have been observed for propionate fed vs. acetate fed cultures and for GAO vs. PAO enriched cultures.[21] Generally, it has not been recommended to use δ as a calibration parameter without specific knowledge of its value for the system. At the default values of δ, PHA was overpredicted compared to actual values, however. Reduction of the aerobic P/O ratio to 1.45 and a resulting anoxic P/O ratio reduction from 0.925 to 0.500 (1/2 the aerobic P/O ratio) during model calibration resulted in simulated PHA levels in the sludge much closer to observed values, although still predicted to be higher than actual values in the anaerobic cycle. Given that the reactor PX6 was enriched with real wastewater containing a wide variety of carbon substrates, including a significant propionate fraction, and the likely wide variety of organisms, including GAOs, present in the sludge, it is

anticipated that the actual P/O ratio will be lower than the default values of the model that were obtained by Smolders and Kuba on synthetic fed reactors that were highly enriched with PAOs. An aerobic P/O ratio of 1.45 is lower than expected for phosphorus removing sludge, although not completely unrealistic. The aerobic P/O ratio for propionate fed GAO enriched cultures was observed to be 1.29 in one study.[21] Another study found PHA producing cultures in feast/famine reactors enriched with acetate and with propionate were both observed to have P/O ratios near 1.0 when the reactors were fed propionate rich feed.[21] Little data is available regarding typical values for anoxic P/O ratios on mixed microbial sludge fed real wastewater. An anoxic value of 0.725 is likely not unrealistic for reactors fed real wastewater, however. The low P/O values required to calibrate the PHA concentrations in the model could point to a weakness in the model, that will require further investigation.

In order to further reduce simulated PHA concentrations closer to that observed in PX6, the rate constant for PAO acetate uptake in the anaerobic zone, q_{ac}, was reduced from the TUDP default value of 4.3 to 2.25 gCOD PHA/gCOD PAO-d. This resulted an overall better simulation of PHA and glycogen concentrations at the expense of an underprediction of acetate uptake in the anaerobic zone. Grady et al. notes that reported acetate uptake ratios vary widely depending on SRT, pH, and temperature.[29] The ASM2d default value for q_{ac} is 3.0 gCOD PHA/gCOD PAO-d, which is closer to the calibrated value than the TUDP default.

Anoxic Glycogen Degradation. The work in this thesis added processes to the integrated model to degrade glycogen in the anoxic period, when PHA is depleted. The model predicts very low levels of PHA in the anoxic zone ($\approx$ 0.9 gCOD), but not full PHA depletion. Initially, the glycogen degradation process at these very low levels of PHA were not activated. Implementation of a separate kinetic switch in the form of $K_{PHA.px}/(K_{PHA.px} + X_{PHA})$ at low levels of PHA to activate the glycogen degradation and maintenance processes when PHA was near, but not at total depletion, allowed glycogen degradation to be initiated, with a $K_{PHA.px}$ value of 0.1. This makes the modeled processes more realistic as likely the glycogen degradation enzymes in the metabolism begin to become active when PHA becomes low, but not completely consumed. Adjustment of the glycogen affinity constant, $K_{GLY.px}$, from 1.0 gCOD glycogen/gCOD PAO

to 0.1 gCOD glycogen/gCOD PAO and using a PAO specific growth rate on glycogen, μ_{px}, value of 0.859 gCOD PAO/gCOD glycogen resulted in a good prediction of anoxic glycogen concentrations.

Orthophosphate Calibration. Anaerobic phosphate release was overpredicted using model default values. In the TUDP model, the anaerobic yield of phosphate release per VFA consumed, Y_{PO}^{AN} is a function of reactor pH, based upon the work of Smolders et al. on acetate enriched EBPR sludge.[89] Meijer, however, suggests that this yield coefficient be individually calibrated for each system since the yield will vary depending on the presence of propionate and butyrate in the influent and GAOs in the sludge. The average total phosphate release per VFA consumed in the anaerobic zone was found to be approximately 0.21 gP/gCOD. The total amount of phosphate released into solution includes phosphate released from processes that do not release VFAs, including ongoing PAO maintenance, hydrolysis, and fermentation processes. Therefore the model value of Y_{PO}^{AN} should be smaller than the observed 0.21 gP/gCOD. Reduction of Y_{PO}^{AN} to 0.10 gP/gCOD resulted in an acceptable fit for phosphate in the anaerobic zone.

Phosphate removal from solution is sensitive to the model's PAO polyphosphate formation rate, k_{pp}, in addition to the concentration of PAOs in solution. Increasing competition from OHOs reduces PAO concentration and the subsequent phosphate removal rate. Phosphate removal was calibrated by increasing the oxygen affinity of OHOs and PAOs by reducing $K_{O.H}$ and $K_{O.PAO}$, the inhibition coefficients for oxygen for these organisms from the TUDP default of 0.2 gO_2/m^3 to 0.1 gO_2/m^3, and by decreasing the polyphosphate formation rate, k_{pp}, from 0.10 gP/gCOD-d to 0.04 gP/gCOD-d. This resulted in greater OHO competition and adequate effluent phosphate simulation. The lower PAO concentration also contributed to reduction of the overprediction of PHA.

Nitrification and Denitrification Calibration. Ammonia in the reactor was observed to be fully depleted in the aerobic zone and remained depleted throughout the remaining aerobic and anoxic cycles. Calibration was unsuccessful, however, in adequately describing the ammonia profile throughout the SBR cycle. A closer match between simulated and observed

ammonia concentrations was able to obtained by reduction of the autotrophic decay rate, b_A, from the TUDP model default value of 0.15 gCOD/gCOD-d to 0.125 gCOD/gCOD-d. It is observed that the model predicts complete depletion of orthophosphate early in the aerobic zone, causing nutrient phosphate limitation to autotrophs. In reality, the average phosphate concentration profile within the reactor did not drop below 0.3 gP/gCOD. In general, phosphate nutrient limitation in activated sludge systems can occur at concentrations below 0.1 gP/m^3.[94] Therefore, an average minimum value of 0.3 gP/gCOD is not expected to be sufficiently low to impact long term autotrophic growth. In order to mitigate the effects of the predicted phosphate depletion in the aerobic zone, the autotrophic half-saturation coefficient for phosphate, $K_{P.A}$, was reduced from 0.01 gP/gCOD to 0.0001 gP/gCOD. The results in Figure 5.1 reflect this change.

Meijer recommends adjusting the bacteria affinity for oxygen, K_O, to calibrate nitrification. Increasing this constant will decrease the bacterial oxygen affinity and is analogous to decreasing the oxygen penetration into the sludge floc.[62] While these values were adjusted to fit phosphate, as previously mentioned, the simulated ammonia concentrations for reactor PX6 were found to be relatively insensitive to this parameter.

From Figure 5.1, it is seen that the model predicts the initial ammonia concentration at the beginning of the anaerobic cycle higher than the average analytical results over the 3 days of sample collection. Analytical results for ammonia concentrations at the beginning of the anaerobic cycle were lower than the expected concentration based on a mass balance of the tested influent ammonia and the feed volume to the reactor. Table 5.6 compares the analytical results taken within the first minute of the feed cycle to the anticipated results based on a mass balance using 0.75 mL influent feed at the beginning of the anaerobic cycle and a total reactor volume of 2.25 L.

From Table 5.6 the average measured initial ammonia concentration at the start of the anaerobic period is about 2.8 mgN/L lower than expected based on a mass balance of the average influent ammonia concentrations. The cause may be due to a inhomogeneous ammonia concentration in the reactor due to incomplete mixing at the time of sample collection or to other sample or

Table 5.6: Comparison of observed vs. predicted initial ammonia concentrations in PX6

		Analytical Concentration			
Date	Unit	Influent	Reactor	Predicted Reactor Concentration From Mass Balance	Error
5/18/2016	gN/m^3	24.28	6.205	8.09	1.88
5/21/2016	gN/m^3	20.43	5.948	6.81	1.63
5/25/2016	gN/m^3	33.33	8.038	11.11	4.94
	Average	**26.01**	**6.73**	**8.67**	**2.82**

testing errors. The initial ammonia concentration of 8.67 gN/m^3 aligns well with the model's predicted concentration.

Ammonia was observed to be depleted in the aerobic zone and remained depleted throughout the remainder of the SBR cycle. The calibrated model is unable to maintain complete depletion of ammonia throughout the anoxic cycle, however. The integrated model inherits the TUDP and ASM2d lysis-regrowth approach to modeling OHO endogenous respiration. In this approach a portion of OHOs are continually converted to inert particulate organic material, X_I, and slowly biodegradable particulate substrate, X_S, while also releasing ammonia and phosphorus from biomass lysis into solution. The particulate substrate, X_S, originating from the decayed biomass becomes available for bacterial growth. This recycling of decaying biomass for growth complicates the model calibration processes.[62] On the other hand, endogenous respiration of PAOs in the TUDP model are modeled by assuming maintenance processes are fueled by degradation of the internal storage product PHA. The ASM3 model uses a similar approach to modeling endogenous respiration of all bacteria, using degradation of a lumped storage parameter. The integrated model extends the TUDP approach so that degradation of glycogen and polyphosphate provide ATP for PAO maintenance when PHA is depleted. In this approach, the extra production of substrate, X_S, is avoided. In the modeling of a full scale WRRF facility using the TUDP model, Brdjanovic et al. concluded that the lysis-regrowth process of OHOs in the TUDP model overestimated decay of OHOs, leading to higher endogenous phosphorus release in the absence of external substrate than actually observed.[7] The authors further concluded that modeled phosphorus release would most likely be closer to actual observations if OHOs were modeled using an endogenous respiration similar to ASM3.

Similarly, the OHO lysis-regrowth process in the integrated model appears to lead to endogenous ammonia release higher than observed in PX6. Calibration of anoxic ammonia concentration by decreasing the OHO decay rate, b_h, assisted with decreasing the effluent ammonia concentration, but did not lead to sufficiently acceptable results. Too high of a decrease in the decay rate leads to decreased competition of OHOs with PAOs, a resulting proliferation of PAOs, and overprediction of PAO processes such as PHA and glycogen production. To reduce the ammonia release in the anoxic zone, the model's biomass nitrogen content, $i_{N.BM}$, was also decreased from 0.07 gN/gCOD to 0.02 gN/gCOD, thereby reducing the amount of ammonia nitrogen released during endogenous processes and achieving a predicted ammonia concentration of 0.4-0.5 gNH_4 throughout the anoxic cycle. While a biomass nitrogen content of 0.02 gN/gCOD in the sludge is unrealistic, this compromise leads to much closer effluent ammonia prediction to observed values. In agreement with Brdjanovic et al., it is likely that modeling OHO endogenous processes using degradation of stored polymers will improve the model results.

Nitrate formation in the aerobic zone was predicted to be higher than observed due to the overprediction of ammonia. It was decided not to reduce the nitrification rate in order to decrease the rate of nitrate formation, as this would further underpredict the temporal point of ammonia depletion in the aerobic zone. Anoxic denitrification was well described, however, without further calibration.

General Results. Overall the calibrated model predicts anoxic and effluent glycogen, nitrate, and phosphorus concentrations in this data set well. Anoxic and effluent ammonia concentrations are approximately 0.4 gN - 0.5 gN above the full depletion level actually observed. The model's processes, including the anoxic glycogen degradation and the nitrate growth assimilation processes, appear to provide an adequate simulation of the internal carbon driven denitrification process. Anaerobic PHA formation is overpredicted, however. The default anaerobic PHA yield coefficient, Y_{SA}^{AN} controls the amount of PHA produced per VFA consumed in the model. The default value of 1.5 gCOD PHA/gCOD VFA used in the model is based on the work of Smolders et al. which used acetate fed EBPR enriched cultures[89] Reduction of this yield coefficient in the model results immediately in large increases in glycogen formation, making

PHA and glycogen difficult to calibrate simultaneously. It was chosen to keep the anaerobic PHA yield coefficient at the default value, since PHA degradation and PHA concentrations in the aerobic and anoxic zones could be adequately simulated.

It should be noted that the influent VFA concentration of 206 gCOD is much higher than that typically found in systems fed real wastewater. For reference, published work using the TUDP model to simulate treatment facilities using real wastewater reported VFA concentrations in the influent ranges from 47 gCOD/m^3 - 71 gCOD/m^3. It can be hypothesized that at large concentrations of VFA in solution, the efficiency of PHA production in the mixed microbial sludge decreases, thereby decreasing the observed PHA yield on VFA. The specific species of microorganisms in the sludge will also play a role in the actual yield value. From the simulation results of PX6, the TUDP and the integrated model do not well predict this decrease in PHA yield at high influent VFA concentrations. This is an aspect of the models that needs further investigation and refinement.

5.2 Model Performance Against Reactor PX5

5.2.1 Wastewater Characterization

Further evaluation of the model performance was undertaken by comparing the ability of the model to simulate the performance of reactor PX5, which is operated similar to reactor PX6 but is configured to achieve a target SRT of 10 days. Experimental data over one SBR cycle taken on 5/18/16 was used for the evaluation.

Table 5.7 shows the percent PAOs, GAOs, nitrifiers and ammonia oxidizing bacteria found in Reactor PX5 as determined by qPCR analysis on sludge taken during the sampling period.

Table 5.7: Percent PAOs, GAOs, nitrifiers, and ammonia in PX5

% PAOs	% GAOs	% Nitrobacter	% Nitrosonomas	% Ammonia Oxidizers	n
1.86 ± 0.10	3.32 ± 0.29	2.16 ± 0.07	2.36 ± 0.20	0.09 ± 0.01	3

As was the case for Reactor PX6, the sludge contains a GAO fraction larger than the PAO

fraction and which raises the possibility of GAOs contributing to the observed post-anoxic behavior of the sludge.

Influent characteristics and model input for the simulations are summarized in Table 5.8.

5.2.2 Model Calibration

The initial model simulation was performed using the final calibrated values for the Reactor PX6 model analysis. The parameters were then adjusted in several steps, similar to the calibration procedure used for the Reactor PX6 simulation. Final calibration was obtained on the same parameters as were used for Reactor PX6, as shown in Table 5.9. Due to the shorter SRT and resulting different sludge characteristics, some parameters were required to be calibrated to different values then the PX6 reactor.

The results of the simulation of reactor PX5 are shown in Figure 5.2. The solids wasting rate in the model was set to 42.2 mL per cycle to obtain an effective SRT of 10 days. In order to match the observed sludge production, the influent $X_I/(X_S + X_I)$ ratio was adjusted to 0.734, which allowed adequate simulation of the solids concentration in the sludge. In general, the model showed similar strengths and weaknesses in the simulation as was revealed in the simulation of the PX6 data set.

Similar to Reactor PX6, the model overpredicts anaerobic PHA synthesis. The acetate uptake rate, q_{ac}, was reduced to reduce the overprediction of anaerobic PHA. This reduction results in an underprediction of the observed VFA uptake rate, as reflected in Figure 5.2, however. Further reduction in anaerobic PHA was obtained by reducing the aerobic and anoxic P/O ratios, the PAO and OHO affinity for oxygen ($K_{O.H}$ and $K_{O.PAO}$), and other variables as shown in Table 5.9. The observed anoxic glycogen degradation during denitrification appears to be adequately described by the model with adjustment of the $K_{PHA.PX}$ constant to 0.3, the glycogen affinity constant, $K_{GLY.px}$, to 0.1, and the PAO specific growth rate on glycogen, μ_{px}, to 0.859 gCOD PAO/gCOD glycogen.

Table 5.8: PX5 simulation: influent characterization and model input. Influent characterization values were taken on a single day (n=1).

Tested Parameter	Unit	Value
Influent		
Influent Total COD	$gCOD/m^3$	1205.6
Influent Filtered and flocculated COD	$gCOD/m^3$	547.72
Soluble undegradable organics (S_I)	$gCOD/m^3$	39.05
Influent Readily Biodegradable COD (S_S)	$gCOD/m^3$	508.67
Fermentable COD (S_F)	$gCOD/m^3$	343.32
Ammonium and ammonia nitrogen	gN/m^3	24.28
Nitrate Nitrogen (NO_3)	gN/m^3	0.00
Nitrite Nitrogen (NO_2)	gN/m^3	0.024
NO_3 + 0.6 NO_2	gN/m^3	0.015
Orthophosphate (PO_4)	gP/m^3	10.81
Influent Volatile Fatty Acids (VFAs)		
Acetic Acid	$gCOD/m^3$	69.7
Propionic Acid	$gCOD/m^3$	62.57
Butyric Acid	$gCOD/m^3$	18.34
Isobutyric Acid	$gCOD/m^3$	0.00
Valeric Acid	$gCOD/m^3$	10.54
Isovaleric Acid	$gCOD/m^3$	4.20
Total VFAs	$gCOD/m^3$	165.36
Reactors		
pH (End aerobic)	-	7.60
T (End aerobic)	°C	22.1
MLSS (End aerobic)	g/m^3	2690
Effluent		
Effluent filtered and flocculated COD (SI)	$gCOD/m^3$	39.05
Ammonium and ammonia nitrogen	gN/m^3	0.00
Nitrate Nitrogen (NO_3)	gN/m^3	0.00
Nitrite Nitrogen (NO_2)	gN/m^3	0.00
NO_3 + 0.6 NO_2	gN/m^3	0.00
Orthophosphate (PO_4)	gP/m^3	1.35

Model Variable	Description	Unit	Value
Soluble Components			
S_{O2}	Oxygen (negative COD)	g COD/m^3	0
S_F	Fermentable COD	g COD/m^3	343.32
SA	Volatile fatty acids	g COD/m^3	165.36
S_{NH}	Ammonium and ammonia nitrogen	g N/m^3	24.28
S_{NO}	Nitrate and 0.6·nitrite nitrogen	gN/m^3	0.015
S_{N2}	Dissolved nitrogen gas	g N/m^3	0
S_{PO}	Inorganic soluble phosphorus	g P/m^3	10.81
S_I	Soluble inert organic matter	g COD/m^3	39.05
S_{HCO}	Alkalinity	mol/m^3	5
Particulate Components			
X_I	Particulate inert organic matter	g COD/m3	175
X_S	Slowly biodegradable substrate	g COD/m^3	482.88
X_H	Active heterotrophic biomass	g COD/m^3	0
X_A	Active autotrophic biomass	g COD/m^3	0.1
X_{PAO}	Phosphate accumulating organisms	g COD/m3	0.1
X_{PP}	Polyphosphate	g P/m^3	0
X_{PHA}	Polyhydroxyalkanoates	g COD/m^3	0
X_{GLY}	Glycogen	g COD/m^3	0
X_{TSS}	Total suspended solids	g $MLSS/m^3$	180
Bulk Solution Temperature and pH			
T	Temperature	°C	22.1
pH	Average Anaerobic pH	-	7.60

Table 5.9: Calibrated parameters for Reactor PX5 simulations

Parameter	Description	Default	PX6	**PX5**	Purpose
b_A	X_A decay rate	0.15	0.125	**0.10**	Fit nitrification
$K_{P.A}$	Half-Sat. coeff. for S_{PO}	0.01	0.001	**0.0001**	Fit nitrification
$i_{N.BM}$	Biomass N content	0.07	0.02	**0.02**	Decrease S_{NH} release
n_{fe}	AN hydrolysis correction factor	0.2	0	**0**	Decrease S_{NH} release
q_{fe}	Fermentation rate	3	0.7	**1.0**	Fit S_{NH} & S_A, decrease PAOs
$Y_{PO.AN}$	AN yield for S_{PO} release/S_A	0.35	0.1	**0.1**	Fit AN S_{PO} release
q_{ac}	X_{PAO} AN uptake rate of S_A	4.3	2.25	**2.25**	Fit S_A uptake, X_{PAO}, X_{PHA}, & X_{GLY}
K_{ac}	Half-sat. coeff. for growth on S_A	32	4	**4**	Fit AN S_A, X_{PAO}, X_{PHA}, & X_{GLY}
k_{pp}	X_{pp} formation	0.1	0.04	**0.085**	Fit S_{PO} uptake
k_{GLY}	X_{GLY} formation	5.83	1.2	**2.2**	Fit glycogen formation
μ_{gx}	AX X_{GLY} degradation rate	0.6874	0.859	**0.859**	Fit AX glycogen
k_{PHA}	X_{PHA} consumption	5.51	8	**8**	Fit X_{PHA} degradation
Kf_{PHA}	Half-sat. ceoff. for X_{PHA}/X_{PAO}	0.2	0.09	**0.09**	Fit X_{PHA} degradation
$K_{O.PAO}$	PAO half-sat. coeff. for S_O	0.2	0.08	**0.135**	Fit X_{PHA} and X_{GLY} through OHO and PAO
$K_{O.H}$	OHO half-sat. coeff. for S_O	0.2	0.08	**0.135**	Fit X_{PHA} and X_{GLY} through OHO and PAO
b_h	X_H decay rate	0.4	0.2	**0.2**	Fit X_{PHA} and X_{GLY} through OHO and PAO
$K_{GLY.px}$	Half-sat. coeff. for AX X_{GLY} degradation	1	0.009	**0.1**	Fit AX X_{GLY} degradation
$K_{PHA.PX}$	Half-sat. coeff. for AX X_{PHA} switch	-	0.1	**0.3**	Implement X_{GLY} degradation
δ_o	Aerobic P/O ratio	1.85	1.45	**1.25**	Decrease PAO, PHA, and glycogen
δ_n	Anoxic P/O ratio	0.925	0.725	**0.625**	Decrease PAO, PHA, and glycogen

Note: AN=Anaerobic, AE=Aerobic, AX=Anoxic

Ammonia concentrations were overpredicted, likely influenced by an inadequate description of OHO maintenance and decay processes inherited from the ASM2d lysis-regrowth modeling concept for OHOs, and the same parameters were adjusted to fit ammonia as previously described for reactor PX6. An increase in the nitrification rate was obtained by decreasing the autotrophic decay rate, b_A. This resulted in simulated aerobic ammonia concentrations closer to the observed values. An increase in the nitrification rate can result in overprediction of nitrate in the reactor, however. Therefore, a balance must be made in fitting the model between the two constituents. The denitrification rate was found to be adequately close to the observed rate without direct calibration. An overprediction of nitrate at the end of the aerobic cycle results in a later temporal depletion of nitrate in the anoxic cycle compared to the data (5 hours simulated vs. 4.5 hours observed). Phosphorus concentrations were calibrated primarily by adjusting the anaerobic yield coefficient for phosphorus release on acetate to 0.1 gP/gCOD and by adjusting the phosphate uptake rate, k_{pp}, from 0.1 to 0.04 gP/gCOD-d. While anaerobic phosphorus release is underpredicted, aerobic and anoxic phosphorus concentrations could be adequately described for Reactor PX5.

Overall, the model adequately predicts denitrification and phosphorus removal processes well. The simulation results of both reactor PX6 and PX5 indicate that anaerobic PHA and VFA

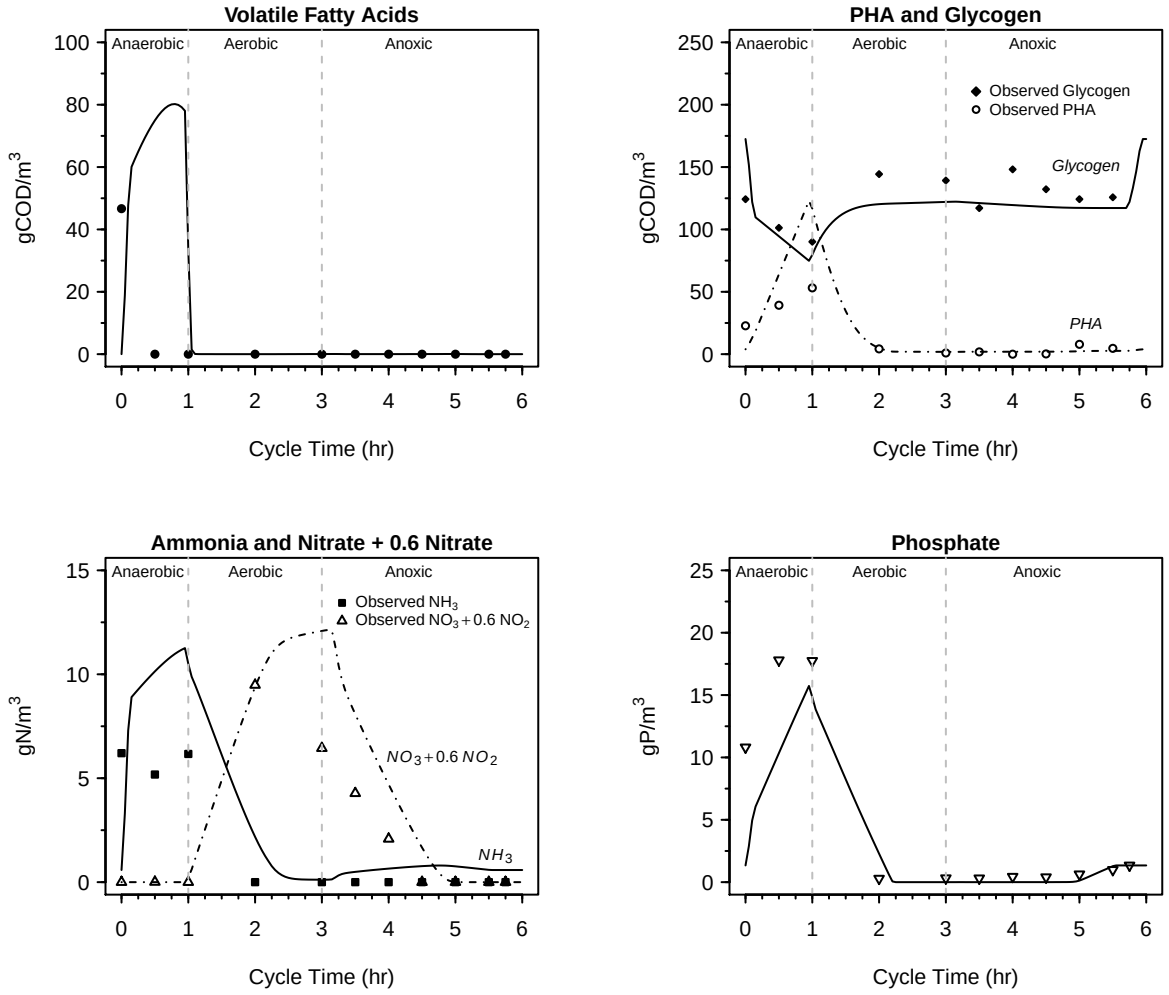

Figure 5.2: PX5 Model vs. experimental results. Observed data from the reactors are shown as points (•). Model simulations are shown as lines (—).

concentrations in addition to overall ammonia concentrations are areas where the model can be improved.

5.3 Simulation of Scale Model.

For further evaluation, the model was compared against data collected from the University of Idaho scale model over 5 days in September 2015. The scale model was placed into operation in March of 2015 by inoculating the system with 40 gallons of return activated sludge from the Moscow, Idaho WRRF facility and subsequently operated by feeding a continuous stream of

degritted and screened wastewater from the Moscow WRRF which feeds the activated sludge reactors. The scale model was originally constructed as a 1/1000th scale configuration of the Moscow WRRF which is configured as a modified A^2/O process. During the 2015 operational season, the scale model configuration was modified to operate in a post-anoxic configuration as shown in Figure 5.3.

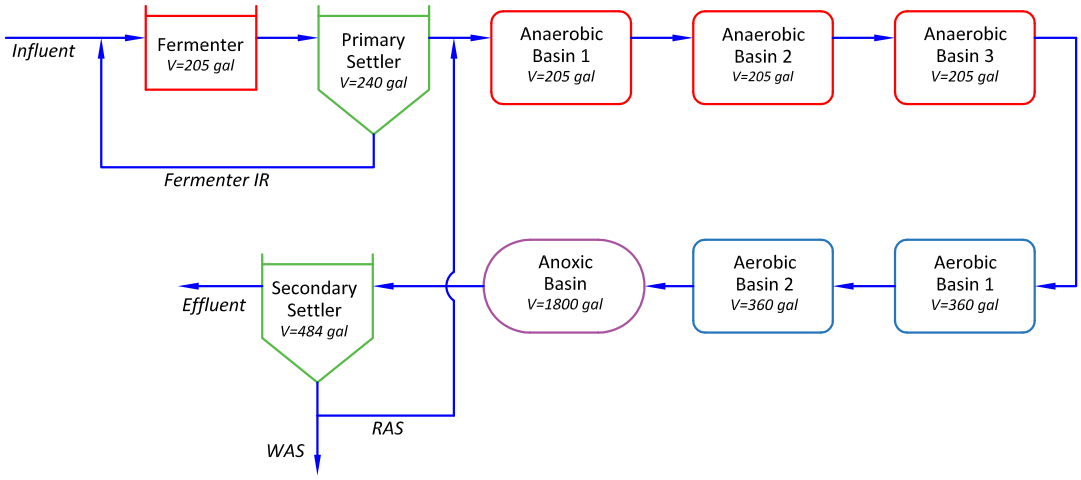

Figure 5.3: University of Idaho scale model process schematic

Influent is pumped to an inline fermenter for production of VFAs prior to flowing to a primary settler. A continuous stream from the bottom of the settler is recycled to the head of the fermenter. Garrett wasting from the fermenter is used to control the fermenter SRT. Three anaerobic continuous stirred tank reactors (CSTRs), two anaerobic CSTRs, and an anoxic carousel reactor provide biological treatment. Effluent from the biological treatment processes is directed to a secondary settler prior to being discharged back to the Moscow WRRF activated sludge intake basin. A recycled activated sludge (RAS) stream taken from the secondary clarifier is directed to the first anaerobic reactor. The system SRT is controlled by wasting from the bottom of the secondary settler.

The system from the primary settler to the anoxic basin effluent was modeled in Aquasim using the average wastewater characteristics obtained over the five day sample record. The anaerobic and aerobic reactors were modeled as completely mixed stirred tank reactors (CSTRs) with the anoxic carousel reactor modeled as four CSTRs in series to simulate the plug flow nature of

the reactor. The influent and RAS flows were input as continuous, steady flows. During the sample period for the data set, the influent flow was estimated at approximately 8.2 m^3/d with RAS flow set at 96% of the influent flow rate. The average system SRT was estimated at 22 days based on the average sludge MLSS and wasting rate during the sample period. Model runs to 300 days allowed for steady state conditions to be reached, confirmed by negligible daily changes in constituent concentrations.

Wastewater Characterization. Table 5.10 shows the percent PAOs, GAOs, nitrifiers and ammonia oxidizing bacteria found in the scale model approximately one month before the model run sample data was collected.

Table 5.10: Percent PAOs, GAOs, nitrifiers, and ammonia in the scale model

% PAOs	% GAOs	% Nitrobacter	% Nitrosonomas	% Ammonia Oxidizers	n
14.14 ± 1.37	0.86 ± 0.15	5.52 ± 1.66	0.30 ± 0.03	0.09 ± 0.00	3

Sufficient sample data to allow estimation of the influent soluble and particulate COD fractions in addition to ammonia, nitrate, and phosphorus were obtained in this data set. Nitrite data was not available for the sample period, however. Historic nitrite sample data collected for the scale model in 2015 are summarized in Table 5.11. Generally, influent nitrite for domestic wastewater is negligible. A nitrite concentration of 0 mg/L was assumed for the simulations due to this and since this concentration is within the error of the historic influent sample results for 2015. In the absence of nitrite data for the sample set, the average historic nitrite data was used for comparison of model's predicted combined nitrate and nitrite profile through the system.

The influent wastewater characterization and model input parameters are shown in Table 5.12. The model was calibrated using a similar stepwise procedure previously described for the laboratory reactors, PX6 and PX5. A summary of the calibrated parameters are shown in Table 5.13. The calibrated parameters from the PX6 and PX5 simulations are also included in Table 5.13 for comparison. Simulation results from the calibrated model are shown in Figure 5.4

Table 5.11: 2015 observed scale model nitrite concentrations

Reactor	Average Concentration	Sample Size (n)
Influent	0.16 ± 0.27	3
AN 3	0.18 ± 0.23	7
AE 1	6.48 ± 6.15	8
AE 2	5.90 ± 7.90	9
AX	0.24 ± 0.10	2
2^o Clarifier	0.23 ± 0.25	15

As shown in Figure 5.4, the actual PHA in the system was not depleted. Therefore, denitrifiers could access internal PHA as a source of energy production in the anoxic zone. Glycogen was thus observed to be replenished in the anoxic zone, according to conventional EBPR theory. The added model processes for simulation of denitrification on glycogen when PHA is depleted could therefore not be directly tested with this data set. The data set is useful, however, to check the integrated model's response to simulate a pilot scale system on real wastewater, check the performance of the added kinetic switches on the new processes to implement anoxic glycogen degradation in the presence of low PHA levels, and to further identify any structural issues that may need to be corrected in the model.

Calibration of Solids Production and SRT. Reduction of the model SRT from 22 days to 20 days and adjustment of the $X_S/(X_S+X_I)$ ratio to 0.85 allowed the solids production to be simulated adequately. It should be noted that calculation of the system SRT based on MLSS concentrations, while being the most common method of SRT calculation, can be prone to large errors. In a comparison of different methodologies for calculating the SRT on a full scale modified University of Cape Town (UCT) BNR plant, Puig et al. found that calculation of SRT using the sludge MLSS resulted in an average SRT of 36.2 days with a standard deviation of 22.2 days.[77] As a comparison, calculation of SRT using a total phosphorus balance based on phosphorus leaving the process resulted in an average SRT of 36.4 days with a standard deviation of 1.5 days. Since total phosphorus data across the system was not available for the scale model, the estimation of SRT is made using the MLSS concentrations with the understanding that the resulting SRT value is prone to large variability. That a better fit of solids production was obtained by reducing the SRT in the model is therefore not surprising.

Table 5.12: Scale model simulation: influent characterization and model input. Influent characterization values are average of samples taken on 5 different days (n=5).

Tested Parameter	Unit	Average SD
Influent		
Influent Total COD	gCOD/m^3	555.92 ± 168.78
Influent Filtered and flocculated COD	gCOD/m^3	434.36 ± 92.77
Soluble undegradable organics (S_I)	gCOD/m^3	20.16 ± 2.82
Influent Readily Biodegradable COD (S_S)	gCOD/m^3	515.73 ± 192.85
Fermentable COD (S_F)	gCOD/m^3	409.80 ± 181.63
Ammonium and ammonia nitrogen	gN/m^3	29.78 ± 4.99
Nitrate Nitrogen (NO_3)	gN/m^3	0.00 ± 0.00
Nitrite Nitrogen (NO_2)	gN/m^3	-
NO_3 + 0.6 NO_2	gN/m^3	-
Orthophosphate (PO_4)	gP/m^3	4.10 ± 0.68
Influent Volatile Fatty Acids (VFAs)		
Acetic Acid	gCOD/m^3	53.80 ± 7.72
Propionic Acid	gCOD/m^3	0.00 ± 0.00
Butyric Acid	gCOD/m^3	0.00 ± 0.00
Isobutyric Acid	gCOD/m^3	0.00 ± 0.00
Valeric Acid	gCOD/m^3	0.00 ± 0.00
Isovaleric Acid	gCOD/m^3	0.00 ± 0.00
Total VFAs	gCOD/m^3	53.80 ± 7.72
Reactors		
pH (End aerobic)	-	7.32 ± 0.05
T (End aerobic)	°C	17.70 ± 2.03
MLSS (End aerobic)	g/m^3	3190 ± 86
Effluent		
Effluent filtered and flocculated COD (SI)	gCOD/m^3	20.16 ± 2.82
Ammonium and ammonia nitrogen	gN/m^3	3.31 ± 4.71
Nitrate Nitrogen (NO_3)	gN/m^3	0.00 ± 0.00
Nitrite Nitrogen (NO_2)	gN/m^3	-
NO_3 + 0.6 NO_2	gN/m^3	-
Orthophosphate (PO_4)	gP/m^3	0.46 ± 0.60

Model Variable	Description	Unit	Value
Soluble Components			
S_{O2}	Oxygen (negative COD)	g COD/m^3	0
S_F	Fermentable COD	g COD/m^3	409.80
SA	Volatile fatty acids	g COD/m^3	53.80
S_{NH}	Ammonium and ammonia nitrogen	g N/m^3	29.78
S_{NO}	Nitrate and 0.6·nitrite nitrogen	gN/m^3	0
S_{N2}	Dissolved nitrogen gas	g N/m^3	0
S_{PO}	Inorganic soluble phosphorus	g P/m^3	4.10
S_I	Soluble inert organic matter	g COD/m^3	20.16
S_{HCO}	Alkalinity	mol/m^3	5
Particulate Components			
X_I	Particulate inert organic matter	g COD/m3	6
X_S	Slowly biodegradable substrate	g COD/m^3	14.03
X_H	Active heterotrophic biomass	g COD/m^3	0
X_A	Active autotrophic biomass	g COD/m^3	0.1
X_{PAO}	Phosphate accumulating organisms	g COD/m3	0.1
X_{PP}	Polyphosphate	g P/m^3	0
X_{PHA}	Polyhydroxyalkanoates	g COD/m^3	0
X_{GLY}	Glycogen	g COD/m^3	0
X_{TSS}	Total suspended solids	g MLSS/m^3	87.2
Bulk Solution Temperature and pH			
T	Temperature	°C	17.70
pH	Average Anaerobic pH	-	7.32

Table 5.13: Calibrated parameters for scale model simulations

Parameter	Description	Default	PX6	PX5	**SM**	Purpose
b_A	X_A decay rate	0.15	0.125	0.10	**0.08**	Fit nitrification
$K_{P.A}$	Half-Sat. coeff. for S_{PO}	0.01	0.0001	0.0001	**-**	Fit nitrification
$i_{N.BM}$	Biomass N content	0.07	0.02	0.02	**0.02**	Decrease S_{NH} release
n_{fe}	AN hydrolysis correction factor	0.2	0	0	**0**	Decrease S_{NH} release
q_{fe}	Fermentation rate	3	0.7	1.0	**1.5**	Fit S_{NH} & S_A, decrease PAOs
Y_{PO}^{AN}	AN yield for S_{PO} release/S_A	0.35	0.1	0.1	**0.32**	Fit AN S_{PO} release
q_{ac}	X_{PAO} AN uptake rate of S_A	4.3	2.25	2.25	**2.7**	Fit S_A uptake, X_{PAO}, X_{PHA}, & X_{GLY}
K_{ac}	Half-sat. coeff. for growth on S_A	32	4	4	**24**	Fit AN S_A, X_{PAO}, X_{PHA}, & X_{GLY}
k_{pp}	X_{pp} formation	0.1	0.04	0.085	**-**	Fit S_{PO} uptake
k_{GLY}	X_{GLY} formation	5.83	1.2	2.2	**-**	Fit glycogen formation
μ_{gx}	AX X_{GLY} degradation rate	0.6874	0.859	0.859	**0.859**	Fit AX glycogen
k_{PHA}	X_{PHA} consumption	5.51	8	8	**-**	Fit X_{PHA} degradation
Kf_{PHA}	Half-sat. ceoff. for X_{PHA}/X_{PAO}	0.2	0.09	0.09	**-**	Fit X_{PHA} degradation
$K_{O.PAO}$	PAO half-sat. coeff. for S_O	0.2	0.08	0.135	**0.6**	Fit X_{PHA} and X_{GLY}
$K_{O.H}$	OHO half-sat. coeff. for S_O	0.2	0.08	0.135	**0.6**	Fit X_{PHA} and X_{GLY}
b_h	X_H decay rate	0.4	0.2	0.2	**0.2**	Fit X_{PHA} and X_{GLY}
$K_{GLY.px}$	Half-sat. coeff. for AX X_{GLY} degradation	1	0.009	0.1	**0.01**	Fit AX X_{GLY} degradation
$K_{PHA.PX}$	Half-sat. coeff. for AX X_{PHA} switch	-	0.1	0.3	**1**	Implement X_{GLY} degradation
δ_o	Aerobic P/O ratio	1.85	1.45	1.25	**-**	Decrease PAO, PHA, and glycogen
δ_n	Anoxic P/O ratio	0.925	0.725	0.625	**-**	Decrease PAO, PHA, and glycogen

Note: AN=Anaerobic, AE=Aerobic, AX=Anoxic, SM=Scale Model

Calibration of Nitrification and Denitrification. The model initially overpredicted nitrification and phosphorus removal in the aerobic reactors, most strongly in reactor AE2. Likely the process in the existing AE2 reactor is not operating optimally, due to short-circuiting in the reactor caused by inadequate mixing, aeration coverage, or other factors. Hydraulic short-circuiting results in a reduction in the overall hydraulic retention time in the reactor. A 30% reduction of the volume of AE2 from 1.363 m^3 to 0.954 m^3 brought ammonia and phosphorus concentrations in the reactor much closer to observed values.

In addition, to better fit ammonia across the system, the anaerobic hydrolysis process was disabled and the fermentation rate was reduced in the model. This is justified given that the upstream fermenter will ferment much of the fermentable substrate in the wastewater prior to the wastewater entering the anaerobic zone. The biomass nitrogen content had to be dramatically reduced from 0.07 gN/gCOD to 0.02 gN/gCOD, as was done for the laboratory reactor simulations, in order to provide a closer fit to effluent ammonia concentrations. While this value is unrealistic, it is a compromise made to better simulate actual OHO death and ammonia release processes given the lysis-decay concept used by the model for OHOs, inherited from the ASM2d model structure.

Nitrate was found to be non-detectable across all reactors over the 5 days of data, with the

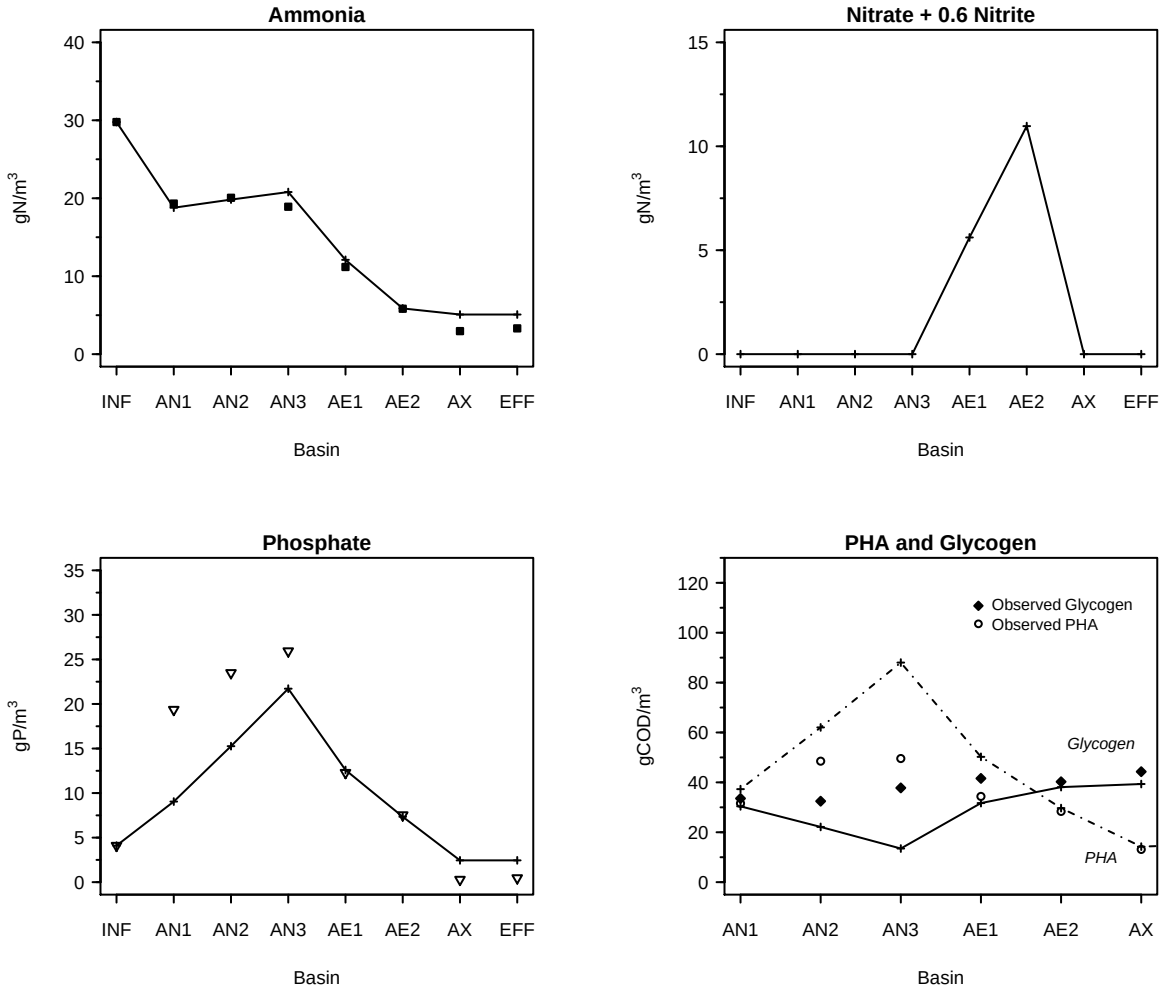

Figure 5.4: Scale Model simulation vs. experimental results. Observed data from the reactors are shown as points (•). Model simulations are shown as marked lines (+).

exception of AE2 which showed an average nitrate concentration of 0.18 gN/m^3. The average historic nitrite concentration in AE2 was 5.90 gN/m^3. Assuming this nitrite concentration occurs in AE2 during the sample period results in a calculated S_{NO} of 0.18 + 0.6 (5.90) = 3.72 gN/m^3 which is much smaller than the 10.97 gN/m^3 predicted to occur in AE2 by the model. Ammonia reduction across AE1 and AE2 are adequately simulated, however. This points to a significant level of nitrate reduction in the aerated basins, likely from simultaneous nitrification/denitrification occurring within the biomass floc that is not being simulated.

Calibration of Phosphorus, PHA, and Glycogen. Phosphate was calibrated by reduction of the anaerobic phosphate to VFA yield coefficient and the anaerobic acetate uptake rate for PAOs. Anaerobic phosphorus release and anaerobic acetate uptake rate (not shown) were both underpredicted. Indeed, the model predicts VFAs persisting through Reactor AE1 before being depleted, while observations showed complete VFA depletion in AN1.

The calibrated model was able to predict aerobic phosphorus concentrations well, while effluent phosphorus is slightly overpredicted. In addition, anaerobic PHA was found to be overpredicted by the model, as occurred in the simulations of PX6 and PX5. The model was able to predict sufficient glycogen replenishment at the expense of PHA with a PAO specific growth rate on glycogen, μ_{px},value of 0.859 gCOD PAO/gCOD glycogen and a half-saturation coefficient, $K_{PHA.PX}$, value of 1.0. It was found that the simulation was sensitive to glycogen degradation in the post-anoxic zone, even though a net glycogen replenishment was observed in the anoxic reactor. The post-anoxic glycogen degradation rate in the model can be controlled by adjusting the specific growth rate on glycogen or the half-saturation coefficient, $K_{PHA.PX}$. Increasing $K_{PHA.PX}$ in the model increases the activity of the post-anoxic glycogen degradation process. Adjustment of $K_{PHA.PX}$ from a value of 0.1 used in the PX6 reactor to 1.0 indicates that some glycogen degradation may be occurring in the floc even though a net PHA concentration in the biomass is still available. It can be theorized that a subset of dPAOs and/or dGAOs within the overall biomass may have depleted their PHA stores while adequate stores are still available for the majority of dPAOs and/or dGAOs in the overall biomass. Alternatively, a different set of calibration parameters which has not been identified but that includes no active post-anoxic glycogen degradation may be possible. Future testing of the model against pilot scale data can provide further insight into this issue and if improvements to the model glycogen degradation processes need to be made.

Further calibration efforts of the model against the data set was not deemed to be productive as overall, as the model could predict the effluent ammonia, nitrate, and phosphate concentrations at a reasonable level while issues for further investigation to improve the model had been identified.

5.4 General Observations and Recommendations for Future Research

Commentary on Modeling of Laboratory SBR Reactors. Due to their cyclic nature, SBRs are never in a steady state condition. This property makes accurate long term simulations of an SBR reactor difficult to achieve. The summation of small deviations of simulated concentrations of the model's sensitive parameters can increase dramatically over a large number of cycles, making long term simulation difficult. For example, Murnleitner et al. notes that the TUDP model was found sensitive to influent substrate concentrations, such that small errors compounded from cycle to cycle, essentially making the influent substrate concentration a model parameter in SBR simulation.[67] This feature of SBRs makes calibration of a model complex, as one or even several parameters may need to be adjusted to tight tolerances to keep the system close to the observed data. In addition, it was found that the model was sensitive to the balance of OHOs and PAOs. As an example, a slight adjustment to the OHO affinity for oxygen, $K_{O.H}$, may lead to decreased OHOs and a resulting proliferation of PAOs and extremely large and unrealistic PHA concentrations after many cycles. This type of behavior was significantly less noticeable in the modeling of the continuous flow scale model simulations as was found with the laboratory SBRs PX6 and PX5.

In addition, modeling of an SBR can require significantly more computational resources than modeling a steady state continuous flow system. The original TUDP model has 22 process equations. The integrated model, developed in this work, expands the number of process equations to 39. Use of the full model to simulate an SBR, which is constantly in a dynamic state, demands significant computational resources and can lead to significantly long computation times, particularly at long SRTs. During the model calibration phase, when dozens of model runs can be required, the cumulative modeling time can become significant. Modeling of a continuous flow system can be much quicker, as once the model approaches steady state conditions, the computational time to solve the system speeds up rapidly during each model run. Despite these disadvantages, the use of the developed model to simulate potential configurations of laboratory SBRs can be an important tool to optimize the process and to save significant amount of laboratory time testing configurations that may not be optimal.

Model Performance and Recommendations for Future Research The processes added to the model to simulate post-anoxic denitrification on glycogen were found to work well against the laboratory data sets examined. In addition, the model switch to inhibit the use of glycogen as substrate in the presence of PHA was found to be able to be adjusted to simulate post-anoxic glycogen concentrations satisfactorily. In depth testing of the added nitrate assimilative reduction processes during ammonia limitation was not extensively performed and is left for future work. It was observed, however, that the new model predicts greater growth of OHOs and PAOs under ammonia limitation due to the addition of the nitrate assimilation processes in the model (data not shown). Future work is needed to verify that these processes are working to simulate actual growth on nitrate adequately.

The integrated model inherits several processes from the ASM2d and TUDP model structure. Anaerobically, VFA uptake and PHA production were found to be inadequately described by the model. Overprediction of PHA was also observed for all three data sets. Reduction of the metabolic P/O ratio was found to bring PHA levels much closer to observed concentrations, but an overprediction of anaerobic PHA could not be completely rectified without adversely affecting other model processes. It is noted that the TUDP model kinetics, including PHA and glycogen cycling kinetics, were performed using synthetic fed batch reactors with highly enriched EBPR sludge.[41,67,88,89] Although the TUDP model has been verified to be able to perform well in simulating overall COD, nitrogen, and phosphorus conversions within EBPR processes, specific validation of the TUDP model to predict the observed PHA and glycogen concentrations in full scale EBPR sludge has not been extensively performed. Our use of real wastewater, supplemented by fermenter liquor for supply of VFAs, provides an influent with a more complex mixture of organic substrates than supplied to synthetic fed laboratory cultivated cultures. This may explain the discrepancies in observed versus predicted VFA and PHA concentrations and the required adjustment of the P/O ratio in the simulations performed in this work. Future work to compare and improve the new model kinetics against real wastewater fed systems is recommended.

Further, it was observed that the use of the lysis-regrowth concept for OHO endogenous metabolism appears to result in overprediction of ammonia and phosphorus release in the data

sets examined. Decreasing the OHO decay rate in the model also affects the PAO/OHO balance and can lead to a proliferation of PAOs that will negatively affect other model processes. A structural change to the model so that OHO metabolism is simulated using the maintenance concept, similar to that used in ASM3 is warranted further investigation to fix this issue.

Finally, given the significant nitrite fraction that can accumulate in the aerobic reactors of the post-anoxic BNR configuration, it is recommended that nitrite be incorporated as a state variable in a future version of the model. This will allow for evaluation of options aimed at achieving nitritation, which can provide significant energy savings to the post-anoxic BNR process.

References

[1] Kootenai Environmental Alliance. Fernan lake blue-green algae bloom comes early. http://kealliance.org/2014/07/09/fernan-lake-blue-green-algae-bloom-comes-early/. Accessed 02-17-16.

[2] American Public Health Association. *Standard methods for the examination of water and wastewater*. American Public Health Association, Water Environment Federation Washington, 1998.

[3] Felicity Appel. Advancing a post-anoxic biological nutrient removal process selecting for nitritation. Master's thesis, University of Idaho, 2015.

[4] Viswanath Arun, Takashi Mino, and Tomonori Matsuo. Biological mechanism of acetate uptake mediated by carbohydrate consumption in excess phosphorus removal systems. *Water Research*, 22(5):565–570, 1988.

[5] Danielle Baetens. *Enhanced Biological Phosphorus Removal: Modelling and Experimental Design Gestimuleerde Biologische Fosfaatverwijdering: Modelbouw en Experimenteel Ontwerp*. PhD thesis, Faculty of Agricultural and Applied Sciences, Ghent University, Belgium, 2001.

[6] JJ Beun, F Paletta, MC Van Loosdrecht, and JJ Heijnen. Stoichiometry and kinetics of poly-β-hydroxybutyrate metabolism in aerobic, slow growing, activated sludge cultures. *Biotechnology and Bioengineering*, 67(4):379–389, 2000.

[7] Damir Brdjanovic, Mark C. M. van Loosdrecht, Paul Versteeg, Christine M. Hooijmans, Guy J. Alaerts, and Joseph J. Heijnen. Modeling COD, N and P removal in a full-scale WWTP Haarlem Waarderpolder. *Water Research*, 34(3):846–858, 2000.

[8] Hong-bo Chen, Qi Yang, Xiao-ming Li, Yan Wang, Kun Luo, and Guang-ming Zeng. Post-anoxic denitrification via nitrite driven by PHB in feast-famine sequencing batch reactor. *Chemosphere*, 92(10):1349–1355, 2013.

[9] Ingrid Chorus and Jamie Bartram. *Toxic Cyanobacteria in Water: A guide to their public health consequences, monitoring and management.* E & FN Spon, London and New York, 1999.

[10] E.R. Coats. Lecture, University of Idaho. CE 512 Advanced Topics in Waste Management (unpublished). Lecture Notes, 2015.

[11] Erik R Coats, Cynthia K Brinkman, and Stephen Lee. Characterizing and contrasting the microbial ecology of laboratory and full-scale ebpr systems cultured on synthetic and real wastewaters. *Water Research*, 108:124–136, 2017.

[12] Erik R. Coats, Alexander Mockos, and Frank J. Loge. Post-anoxic denitrification driven by PHA and glycogen within enhanced biological phosphorus removal. *Bioresource Technology*, 102(2):1019–1027, 2011.

[13] Erik R Coats, David L Watkins, and Dan Kranenburg. A comparative environmental life-cycle analysis for removing phosphorus from wastewater: Biological versus physical/chemical processes. *Water Environment Research*, 83(8):750–760, 2011.

[14] Y. Comeau, K. J. Hall, R. E. W. Hancock, and W. K. Oldham. Biochemical model for enhanced biological phosphorus removal. *Water Research*, 20(12):1511–1521, 1986.

[15] Engrcia Costa, Julio Prez, and Jan-Ulrich Kreft. Why is metabolic labour divided in nitrification? *Trends in Microbiology*, 14(5):213 – 219, 2006.

[16] Gregory R Crocetti, Jillian F Banfield, Jürg Keller, Philip L Bond, and Linda L Blackall. Glycogen-accumulating organisms in laboratory-scale and full-scale wastewater treatment processesb. *Microbiology*, 148(11):3353–3364, 2002.

[17] Gregory R Crocetti, Philip Hugenholtz, Philip L Bond, Andrew Schuler, Jürg Keller, David Jenkins, and Linda L Blackall. Identification of polyphosphate-accumulating organisms and design of 16s rrna-directed probes for their detection and quantitation. *Applied and Environmental Microbiology*, 66(3):1175–1182, 2000.

[18] Glen T. Daigger. Oxygen and carbon requirements for biological nitrogen removal processes accomplishing nitrification, nitritation, and anammox. *Water Environment Research*, 86(3),

2014.

[19] Holger Daims, Elena V. Lebedeva, Petra Pjevac, Ping Han, Craig Herbold, Mads Albertsen, Nico Jehmlich, Marton Palatinszky, Julia Vierheilig, Alexandr Bulaev, Rasmus H. Kirkegaard, Martin von Bergen, Thomas Rattei, Bernd Bendinger, Per H. Nielsen, and Michael Wagner. Complete nitrification by nitrospira bacteria. *Nature*, 528(7583):504–509, Dec 2015.

[20] Holger Daims and Michael Wagner. The microbiology of nitrogen removal. In R. J. Seviour and Per Halkjr Nielsen, editors, *Microbial ecology of activated sludge*, London, 2010. IWA Publishing.

[21] Joo M. L. Dias, Adrian Oehmen, Lusa S. Serafim, Paulo C. Lemos, Maria A. M. Reis, and Rui Oliveira. Metabolic modelling of polyhydroxyalkanoate copolymers production by mixed microbial cultures. *BMC Systems Biology*, 2(1):1–21, 2008.

[22] Klaus Dircks, JJ Beun, M Van Loosdrecht, JJ Heijnen, and Mogens Henze. Glycogen metabolism in aerobic mixed cultures. *Biotechnology and Bioengineering*, 73(2):85–94, 2001.

[23] Water Environment Federation. *Nutrient removal, Manual of Practice No. 34*. McGraw-Hill, New York, 2011.

[24] Carlos D. M. Filipe and Glen T. Daigger. Development of a revised metabolic model for the growth of phosphorus-accumulating organisms. *Water Environment Research*, 70(1):67–79, 1998.

[25] Carlos D. M. Filipe, Glen T. Daigger, and C. P. Leslie Grady. A metabolic model for acetate uptake under anaerobic conditions by glycogen accumulating organisms: Stoichiometry, kinetics, and the effect of pH. *Biotechnology and Bioengineering*, 76(1):17–31, 2001.

[26] Carlos D. M. Filipe, Glen T. Daigger, and C. P. Leslie Grady. Stoichiometry and kinetics of acetate uptake under anaerobic conditions by an enriched culture of phosphorus-accumulating organisms at different pHs. *Biotechnology and Bioengineering*, 76(1):32–43, 2001.

[27] Krist V. Gernaey, Mark C. M. van Loosdrecht, Mogens Henze, Morten Lind, and Sten B. Jrgensen. Activated sludge wastewater treatment plant modelling and simulation: state of the art. *Environmental Modelling & Software*, 19(9):763–783, 2004.

[28] Gerhard Gottschalk. *Bacterial Metabolism*. Springer, New York, 2nd ed. edition, 1986.

[29] Jr. Grady, C.P. Leslie Grady, Glen T. Daigger, Nancy G. Love, and Carlos D.M. Filipe. *Biological Wastewater Treatment*. IWA Publishing/CRC Press, Boca Raton, FL, third edition, 2011.

[30] W. Gujer, M. Henze, T. Mino, and M.C.M. Van Loosdrecht. Activated Sludge Model No. 3. *IAWPRC Scientific and Technical Reports*, No. 9. Report, London: International Water Association, 2000.

[31] Willi Gujer and Tove A. Larsen. The implementation of biokinetics and conservation principles in {ASIM}. *Water Science and Technology*, 31(2):257 – 266, 1995. Modelling and Control of Activated Sludge ProcessesSelected Proceedings of the {IAWQ} International Specialized Seminar on Modelling and Control of Activated Sludge Processes.

[32] H. Hauduc, L. Rieger, I. Takacs, A. Heduit, P. A. Vanrolleghem, and S. Gillot. A systematic approach for model verification: application on seven published activated sludge models. *Water Science and Technology*, 61(4):825–839, 2010.

[33] Shaomei He, Daniel L Gall, and Katherine D McMahon. candidatus accumulibacter population structure in enhanced biological phosphorus removal sludges as revealed by polyphosphate kinase genes. *Applied and environmental microbiology*, 73(18):5865–5874, 2007.

[34] Shaomei He and Katherine D. McMahon. Microbiology of candidatus accumulibacter in activated sludge. *Microbial Biotechnology*, 4(5):603–619, 2011.

[35] J. J. Heijnen, M. C. M. van Loosdrecht, and L. Tijhuis. A black box mathematical model to calculate auto- and heterotrophic biomass yields based on gibbs energy dissipation. *Biotechnology and Bioengineering*, 40(10):1139–1154, 1992.

[36] M. Henze, C.P.L. Jr. Grady, W. Gujer, G.v.R. Marais, and T. Matsuo. Activated Sludge Model No. 1. *IAWPRC Scientific and Technical Reports*, No. 1. Report, London: Interna-

tional Water Association, 1987.

[37] M. Henze, W. Gujer, T. Mino, T. Matsuo, M. C. Wentzel, and G. v R. Marais. Activated Sludge Model No. 2. *IAWPRC Scientific and Technical Reports*, No. 3. Report, London: International Water Association, 1995.

[38] Mogens Henze, Willi Gujer, Takahashi Mino, Tomonori Matsuo, Mark C. Wentzel, Gerrit v R. Marais, and Mark C. M. Van Loosdrecht. Activated Sludge Model no. 2D, ASM2D. *Water Science and Technology*, 39(1):165–182, 1999.

[39] Dwight Houweling, Yves Comeau, Imre Takcs, and Peter Dold. Comment on modelling the PAO-GAO competition: Effects of carbon source, pH and temperature by Lopez-Vazquez, C.M., Oehmen, A., Hooijmans, C.M., Brdjanovic, D., Gijzen, H.J., Yuan, Z., van Loosdrecht, M.C.M. Water Res. (2009). *Water Research*, 43(11):2947–2949, 2009.

[40] Andreas Kroll. Grey box models: concepts and application. In Masoud Mohammadian, editor, *New Frontiers in Computational Intelligence and its Applications*, pages 42–51, Amsterdam; Washington, DC, 2000. International Conference on Computational Intelligence for Modelling, Control and Automation, IOS Press.

[41] T. Kuba, E. Murnleitner, M. C. M. Van Loosdrecht, and J. J. Heijnen. A metabolic model for biological phosphorus removal by denitrifying organisms. *Biotechnology and Bioengineering*, 52(6):685–695, 1996.

[42] T. Kuba and M.C.M. van Loosdrechtt. Effect of cyclic oxygen exposure on the activity of denitrifying phosphorus removing bacteria. *Water Science and Technology*, 34(12):33 – 40, 1996. Water Quality International '96 Part 1: Nutrient Removal; Selected Proceedings of the 18th Biennial Conference of the International Association on Water Quality.

[43] T. Kuba, A. Wachtmeister, M. C. M. van Loosdrecht, and J. J. Heijnen. Effect of nitrate on phosphorus release in biological phosphorus removal systems. *Water Science and Technology*, 30(6):263–269, 1994.

[44] T. Kuba, A. Wachtmeister, M. C. M. Van Loosdrecht, and J. J. Heijnen. Effect of nitrate on phosphorus release in biological phosphorus removal systems. In *Proceedings of the 17th*

Biennial Conference of the International Association on Water Quality. Part 1, July 24, 1994 - July 30, 1994, volume 30 of *Water Science and Technology*, pages 263–269. Pergamon Press Inc, 1994.

[45] Katarzyna Kujawa and Bram Klapwijk. A method to estimate denitrification potential for predenitrification systems using NUR batch test. *Water Research*, 33(10):2291 – 2300, 1999.

[46] Ana B. Lanham, Adrian Oehmen, Aaron M. Saunders, Gilda Carvalho, Per H. Nielsen, and Maria A. M. Reis. Metabolic modelling of full-scale enhanced biological phosphorus removal sludge. *Water Research*, 66:283 – 295, 2014.

[47] S Leininger, T Urich, M Schloter, L Schwark, J Qi, GW Nicol, JI Prosser, SC Schuster, and C Schleper. Archaea predominate among ammonia-oxidizing prokaryotes in soils. *Nature*, 442(7104):806–809, 2006.

[48] Zhongming Li, Shuying Wang, Weitang Zhang, Lei Miao, Tianhao Cao, and Yongzhen Peng. Nitrogen removal from medium-age landfill leachate via post-denitrification driven by PHAs and glycogen in a single sequencing batch reactor. *Bioresource Technology*, 169:773 – 777, 2014.

[49] C. Lopez, M.N. Pons, and E. Morgenroth. Endogenous processes during long-term starvation in activated sludge performing enhanced biological phosphorus removal. *Water Research*, 40(8):1519 – 1530, 2006.

[50] Huabing Lu, Jrg Keller, and Zhiguo Yuan. Endogenous metabolism of candidatus accumulibacter phosphatis under various starvation conditions. *Water Research*, 41(20):4646–4656, 2007.

[51] Jacek Makinia. *Mathmatical modeling and computer simulation of activated sludge systems.* IWA Publishing, London, 2010.

[52] Daniel Mamais, David Jenkins, and Paul Prrr. A rapid physical-chemical method for the determination of readily biodegradable soluble COD in municipal wastewater. *Water Research*, 27(1):195 – 197, 1993.

[53] Hector Garcia Martin, Natalia Ivanova, Victor Kunin, Falk Warnecke, Kerrie W. Barry, Alice C. McHardy, Christine Yeates, Shaomei He, Asaf A. Salamov, Ernest Szeto, Eileen Dalin, Nik H. Putnam, Harris J. Shapiro, Jasmyn L. Pangilinan, Isidore Rigoutsos, Nikos C. Kyrpides, Linda Louise Blackall, Katherine D. McMahon, and Philip Hugenholtz. Metagenomic analysis of two enhanced biological phosphorus removal (EBPR) sludge communities. *Nat Biotech*, 24(10):1263–1269, 2006.

[54] M. Maurer, D. Abramovich, H. Siegrist, and W. Gujer. Kinetics of biologically induced phosphorus precipitation in waste-water treatment. *Water Research*, 33(2):484 – 493, 1999.

[55] Perry L McCarty and Bruce E Rittmann. *Environmental biotechnology : principles and applications*. Boston : McGraw-Hill, Boston, 2001.

[56] PL McCarty. Energetics and bacterial growth. In SD Hunter and JV Faust, editors, *Organic Compounds in Aquatic Environments*. Marcel Dekker, Inc., New York, 1971.

[57] Simon Jon McIlroy, Aaron Marc Saunders, Mads Albertsen, Marta Nierychlo, Bianca McIlroy, Aviaja Anna Hansen, Søren Michael Karst, Jeppe Lund Nielsen, and Per Halkjær Nielsen. Midas: the field guide to the microbes of activated sludge. *Database*, 2015:bav062, 2015.

[58] Katherine D. McMahon, Shaomei He, and Adrian Oehmen. The microbiology of phosphorus removal. In R. J. Seviour and Per Halkjr Nielsen, editors, *Microbial ecology of activated sludge*, London, 2010. IWA Publishing.

[59] S. C. F. Meijer, H. van der Spoel, S. Susanti, J. J. Heijnen, and M. C. M. van Loosdrecht. Error diagnostics and data reconciliation for activated sludge modelling using mass balances. *Water Science and Technology*, 45(6):145–156, 2002.

[60] S. C. F. Meijer, M. C. M. van Loosdrecht, and J. J. Heijnen. Metabolic modelling of full-scale biological nitrogen and phosphorus removing WWTP's. *Water Research*, 35(11):2711–2723, 2001.

[61] S. C. F. Meijer, M. C. M. Van Loosdrecht, and J. J. Heijnen. Modelling the start-up of a full-scale biological phosphorous and nitrogen removing WWTP. *Water Research*,

36(19):4667–4682, 2002.

[62] S.C.F. Meijer. *Theoretical and practical aspects of modelling activated sludge processes*. Thesis, Delft University of Technology, 2004.

[63] S.C.F. Meijer and P. Piekema. *Use of models to explain deterioration of effluent quality under wet weather conditions*, Book Section 14. IWA Publishing, London, U.K., 2015.

[64] Henryk Melcer and Water Environment Federation. *Methods for wastewater characterization in activated sludge modeling*. Water Environment Federation ; IWA Pub., Alexandria, VA; London, U.K., 2003.

[65] Arnold B. Menar and David Jenkins. Fate of phosphorus in waste treatment processes: enhanced removal of phosphate by activated sludge. *Environmental Science & Technology*, 4(12):1115–1121, 1970.

[66] Takashi Mino, Viswanath Arun, Yoshiaki Tsuzuki, and Tomonori Matsuo. *Effect of Phosphorus Accumulation on Acetate Metabolism in Biological Phosphorus Removal Process*, pages 27–38. Pergamon, 1987.

[67] E. Murnleitner, T. Kuba, M. C. M. Van Loosdrecht, and J. J. Heijnen. An integrated metabolic model for the aerobic and denitrifying biological phosphorus removal. *Biotechnology and Bioengineering*, 54(5):434–450, 1997.

[68] Gerard Muyzer, Ellen C De Waal, and Andre G Uitterlinden. Profiling of complex microbial populations by denaturing gradient gel electrophoresis analysis of polymerase chain reaction-amplified genes coding for 16s rrna. *Applied and environmental microbiology*, 59(3):695–700, 1993.

[69] Jens Hiriis Nielsen, John Villadsen, and Gunnar Liden. *Bioreaction engineering principles*. Kluwer Academic/Plenum Publishers, New York :, 2nd ed. / edition, 2003.

[70] Masaru K. Nobu, Hideyuki Tamaki, Kengo Kubota, and Wen-Tso Liu. Metagenomic characterization of CandidatusDefluviicoccus tetraformis strain TFo71,a tetrad-forming organism, predominant in an anaerobic-aerobic membrane bioreactor with deteriorated biological phosphorus removal. *Environmental Microbiology*, 16(9):2739–2751, 2014.

[71] Adrian Oehmen, Paulo C. Lemos, Gilda Carvalho, Zhiguo Yuan, Jurg Keller, Linda L. Blackall, and Maria A. M. Reis. Advances in enhanced biological phosphorus removal: From micro to macro scale. *Water Research*, 41(11):2271–2300, 2007.

[72] Oregon Department of Environmental Quality (Joe Eilers). Harmful algal blooms. http://www.deq.state.or.us/wq/algae/algae.htm. Accessed 02-17-16.

[73] State of Washington Department of Ecology. Late summer at the lake? Watch for blue-green algae. http://ecologywa.blogspot.com/2011/09/late-summer-at-lake-watch-for-blue.html, 2011. Accessed 02-17-2016.

[74] State of Washington Department of Ecology. What does an algae bloom look like? http://www.ecy.wa.gov/programs/wq/plants/algae/monitoring/AlgaeBlooms.html, 2016. Accessed 02-17-2016.

[75] Jean Luc Parrou and Jean Franois. A simplified procedure for a rapid and reliable assay of both glycogen and trehalose in whole yeast cells. *Analytical Biochemistry*, 248(1):186 – 188, 1997.

[76] E.E. Petersen. *Chemical Reaction Analysis*. Premtice Hall.

[77] S. Puig, M.C.M. van Loosdrecht, J. Colprim, and S.C.F. Meijer. Data evaluation of full-scale wastewater treatment plants by mass balance. *Water Research*, 42(18):4645 – 4655, 2008.

[78] Christian Ramakers, Jan M Ruijter, Ronald H Lekanne Deprez, and Antoon FM Moorman. Assumption-free analysis of quantitative real-time polymerase chain reaction (pcr) data. *Neuroscience letters*, 339(1):62–66, 2003.

[79] Peter Reichert. Aquasim – a tool for simulation and data analysis of aquatic systems. *Water Science and Technology*, 30(2):21–30, 1994.

[80] PJ Roeleveld and MCM van Loosdrecht. Experience with guidelines for wastewater characterisation in The Netherlands.

[81] J. A. Roels. *Energetics and kinetics in biotechnology*. Elsevier Biomedical Press B.V., 1983.

[82] Jan-Henrich Rotthauwe, Karl-Paul Witzel, and Werner Liesack. The ammonia monooxygenase structural gene amoa as a functional marker: molecular fine-scale analysis of natural ammonia-oxidizing populations. *Applied and environmental microbiology*, 63(12):4704–4712, 1997.

[83] S. Salem, D. Berends, J. J. Heijnen, and M. C. M. van Loosdrecht. Model-based evaluation of a new upgrading concept for N-removal. *Water Science and Technology*, 45(6):169–176, 2002.

[84] A.M. Saunders. *The physiology of microorganisims in enhanced biological phosphorus removal*. Thesis, University of Queensland, 2005.

[85] Robert J. Seviour, Takashi Mino, and Motoharu Onuki. The microbiology of biological phosphorus removal in activated sludge systems. *FEMS Microbiology Reviews*, 27(1):99–127, 2003.

[86] G. J. F. Smolders, D. J. Bulstra, R. Jacobs, M. C. M. Van Lossdrecht, and J. J. Heijnen. A metabolic model of the biological phosphorus removal process: II. validation during start-up conditions. *Biotechnology and Bioengineering*, 48(3):234–245, 1995.

[87] G. J. F. Smolders, J. M. Klop, M. C. M. Van Loosdrecht, and J. J. Heijnen. A metabolic model of the biological phosphorus removal process: I. effect of the sludge retention time. *Biotechnology and Bioengineering*, 48(3):222–233, 1995.

[88] G. J. F. Smolders, J. Van Der Meij, M. C. M. Van Loosdrecht, and J. J. Heijen. Stoichiometric model of the aerobic metabolism of the biological phosphorus removal process. *Biotechnology and Bioengineering*, 44(7):837–848, 1994.

[89] G. J. F. Smolders, J. Van der Meij, M. C. M. Van Loosdrecht, and J. J. Heijnen. Model of the anaerobic metabolism of the biological phosphorus removal process: Stoichiometry and pH influence. *BIT Biotechnology and Bioengineering*, 43(6):461–470, 1994.

[90] G. J. F. Smolders, J. Van der Meij, M. C. M. Van Loosdrecht, and J. J. Heijnen. A structured metabolic model for anaerobic and aerobic stoichiometry and kinetics of the

biological phosphorus removal process. *Biotechnology and Bioengineering*, 47(3):277–287, 1995.

[91] G.J.F. Smolders. *A metabolic model of the biological phosphorus removal - stoichiometry, kinetics and dynamic behavior*. Thesis, Delft University of Technology, 1995.

[92] G.J.F. Smolders, M.C.M. van Loosdrecht, and J.J. Heijnen. A metabolic model for the biological phosphorus removal process. *Water Science and Technology*, 31(2):79–93, 1995.

[93] Edris Taher and Kartik Chandran. High-rate, high-yield production of methanol by ammonia-oxidizing bacteria. *Environmental Science & Technology*, 47(7):3167–3173, 2013.

[94] George Tchobanoglous, David H. Stensel, Ryujiro Tsuchihashi, and Franklin Burton. *Wastewater engineering: treatment and resource recovery*. Metcalf and Eddy, AECOM: Mcgraw-Hill Education, New York, NY, fifth edition, 2014.

[95] John L. Tymoczko, Lubert Stryer, and Jeremy M. Berg. *Biochemistry*. New York : W.H. Freeman, New York, 5th ed. edition, 2002.

[96] USEPA. Preventing eutrophication: Scientific support for dual nutrient criteria. Technical report, United States Environmental Protection Agency, 2015.

[97] Maartje A. H. J. van Kessel, Daan R. Speth, Mads Albertsen, Per H. Nielsen, Huub J. M. Op den Camp, Boran Kartal, Mike S. M. Jetten, and Sebastian Lücker. Complete nitrification by a single microorganism. *Nature*, 528(7583):555–559, Dec 2015. Letter.

[98] M. C. M. Van Loosdrecht, C. M. Lopez-Vazquez, S. C. F. Meijer, C. M. Hooijmans, and D. Brdjanovic. Twenty-five years of asm1: past, present and future of wastewater treatment modelling. *Journal of Hydroinformatics*, 17(5):697–718, 2015.

[99] Mark C. M. Van Loosdrecht, Adrian Oehmen, Christine M. Hooijmans, Damir Brdjanovic, Huub J. Gijzen, Zhiguo Yuan, and Carlos M. Lopez-Vazquez. Response to the comment on modelling the PAO-GAO competition: Effects of carbon source, pH and temperature by Dwight Houweling et al. *Water Research*, 43(11):2950–2951, 2009.

[100] Mark C.M. Van Loosdrecht, George A. Ekama, Mark C. Wentzel, Damir Brdjanovic, and Christine M. Hooijmans. *Modelling Activated Sludge Processes*, book Section 14. IWA Publishing, London, UK, 2008.

[101] M.C.M. van Loosdrecht and J.J. Heijnen. Modelling of activated sludge processes with structured biomass. *Water Science and Technology*, 45(6):13–23, 2002.

[102] H. M. Van Veldhuizen, M. C. M. Van Loosdrecht, and J. J. Heijnen. Modelling biological phosphorus and nitrogen removal in a full scale activated sludge process. *Water Research*, 33(16):3459–3468, 1999.

[103] Jeanne M. VanBriesen. Evaluation of methods to predict bacterial yield using thermodynamics. *Biodegradation*, 13(3):171–190, 2002.

[104] JM VanBriesen and BE Rittmann. Mathematical description of microbiological reactions involving intermediates. *Biotechnology and Bioengineering*, 67(1):35–52, JAN 5 2000.

[105] John Villadsen, Jens Hoiriis Nielsen, and Gunnar Liden. *Bioreaction engineering principles.* New York : Springer, New York, 3rd ed. edition, 2011.

[106] M. Vocks, C. Adam, B. Lesjean, R. Gnirss, and M. Kraume. Enhanced post-denitrification without addition of an external carbon source in membrane bioreactors. *Water Research*, 39(14):3360–3368, 2005.

[107] Federation Water Environment, Force Biological Nutrient Removal Operation in Wastewater Treatment Plants Task, Environmental, and Institute Water Resources. *Biological nutrient removal (BNR) operation in wastewater treatment plants.* McGraw-Hill, New York, 2006.

[108] M. C. Wentzel, P. L. Dold, G. A. Ekama, and R. Marais Gv. Enhanced polyphosphate organism cultures in activated sludge systems. Part iii: Kinetic model. *Water S.A.*, 15(2):89–102, 1989.

[109] M. C. Wentzel, G. A. Ekama, R. E. Loewenthal, P. L. Dold, and R. Marais Gv. Enhanced polyphosphate organism cultures in activated sludge systems. Part II: Experimental behavior. *Water S.A.*, 15(2):71–88, 1989.

[110] M. C. Wentzel, L. H. Lotter, R. E. Loewenthal, and G. V. Marais. Metabolic behavior of acinetobacter spp in enhanced biological phosphorus removal - a biochemical-model. *Water Sa*, 12(4):209–224, 1986.

[111] David White. *The physiology and biochemistry of prokaryotes*. New York : Oxford University Press, New York, 3rd ed. edition, 2007.

[112] J. W. T. Wimpenny. The validity of models. *Advances in Dental Research*, 11(1):150–159, 1997.

[113] Matt Winkler, Erik R. Coats, and Cynthia K. Brinkman. Advancing post-anoxic denitrification for biological nutrient removal. *Water Research*, 45(18):6119–6130, 2011.

[114] Raymond Zeng, Zhiguo Yuan, Mark C. M. van Loosdrecht, and Jrg Keller. Proposed modifications to metabolic model for glycogen-accumulating organisms under anaerobic conditions. *Biotechnology and Bioengineering*, 80(3):277–279, 2002.

[115] Raymond J. Zeng, Mark C. M. van Loosdrecht, Zhiguo Yuan, and Jrg Keller. Metabolic model for glycogen-accumulating organisms in anaerobic/aerobic activated sludge systems. *Biotechnology and Bioengineering*, 81(1):92–105, 2003.

[116] Raymond J. Zeng, Zhiguo Yuan, and Jrg Keller. Enrichment of denitrifying glycogen-accumulating organisms in anaerobic/anoxic activated sludge system. *Biotechnology and Bioengineering*, 81(4):397–404, 2003.

[117] Yan Zhou, Maite Pijuan, Raymond J. Zeng, and Zhiguo Yuan. Involvement of the tca cycle in the anaerobic metabolism of polyphosphate accumulating organisms (PAOs). *Water Research*, 43(5):1330–1340, 2009.

Appendix A: The Integrated Metabolic Model

Table A1: Model Stoichiometric Matrix

	Process	Component:	1 S_O gO_2/m^3	2 S_F $gCOD/m^3$	3 S_A $gCOD/m^3$	4 S_{NH} gN/m^3	5 S_{NO} gN/m^3
1	Aerobic Hydrolysis	$gCOD_{XS}/d$		$1-f_{SI}$		$c_{1.NH}$	
2	Anoxic Hydrolysis	$gCOD_{XS}/d$		$1-f_{SI}$		$c_{2.NH}$	
3	Anaerobic Hydrolysis	$gCOD_{XS}/d$		$1-f_{SI}$		$c_{3.NH}$	
Ordinary Heterotrophic Organisms (OHOs)							
4	Aerobic Growth on S_F	$gCOD_{XH}/d$	$-(1-Y_H)/Y_H$	$-1/Y_H$		$c_{4.NH}$	
4b	**Aerobic Growth on S_F w/NO_3**	$\mathbf{gCOD_{XH}/d}$	$\mathbf{-(1-Y_{H.\varphi})/Y_{H\varphi} - i_{COD.NO3}\cdot i_{N.BM}}$	$\mathbf{-1/Y_{H.\varphi}}$		$\mathbf{c_{4b.NH}}$	$\mathbf{-i_{N,BM}}$
5	Aerobic Growth on S_A	$gCOD_{XH}/d$	$-(1-Y_H)/Y_H$		$-1/Y_H$	$c_{5.NH}$	
5b	**Aerobic Growth on S_A w/NO_3**	$\mathbf{gCOD_{XH}/d}$	$\mathbf{-(1-Y_{H.\varphi})/Y_{H\varphi} - i_{COD.NO3}\cdot i_{N.BM}}$		$\mathbf{-1/Y_{H.\varphi}}$	$\mathbf{c_{5b.NH}}$	$\mathbf{-i_{N,BM}}$
6	Anoxic Growth on S_F	$gCOD_{XH}/d$		$-1/Y_H$		$c_{6.NH}$	$-(1-Y_H)/(i_{NO3.N2}\cdot Y_H)$
6b	**Anoxic Growth on S_F w/NO_3**	$\mathbf{gCOD_{XH}/d}$		$\mathbf{-1/Y_{H.\varphi} + i_{COD.NO3}\cdot i_{N.BM}}$		$\mathbf{c_{6b.NH}}$	$\mathbf{-\frac{1-Y_{H.\varphi}}{i_{NO3.N2}Y_{H.\varphi}} - i_{N,BM}}$
7	Anoxic Growth on S_A	$gCOD_{XH}/d$			$-1/Y_H$	$c_{7.NH}$	$-\frac{1-Y_H}{i_{NO3.N2}Y_H}$
7b	**Anoxic Growth on S_A w/NO_3**	$\mathbf{gCOD_{XH}/d}$			$\mathbf{-1/Y_{H.\varphi} + i_{COD.NO3}\cdot i_{N.BM}}$	$\mathbf{c_{7b.NH}}$	$\mathbf{-\frac{1-Y_{H.\varphi}}{i_{NO3.N2}Y_{H.\varphi}} - i_{N,BM}}$
8	Fermentation	$gCOD_{SF}/d$		-1	1	$c_{8.NH}$	
9	Heterotrophic Lysis	$gCOD_{XH}/d$				$c_{9.NH}$	
Phosphorus Accumulating Organisms (PAOs)							
10	Anaerobic Storage of S_A	$gCOD_{SA}/d$			-1	$c_{10.NH}$	
11	Anaerobic Maintenance	gP/d				$c_{11.NH}$	
12	Anoxic Storage of S_A	$gCOD_{SA}/d$			-1	$c_{12.NH}$	$-(1-Y_{SA}^{NO})/i_{NO3.N2}$
13	Anoxic PHA Consumption	$gCOD_{PHA}/d$				$c_{13.NH}$	$-(1-1/Y_{PHA}^{NO})/i_{NO3.N2}$
13b	**Anoxic PHA Consumption w/NO_3**	$\mathbf{gCOD_{PHA}/d}$				$\mathbf{c_{13b.NH}}$	$\mathbf{-(1-1/Y_{PHA.\varphi}^{NO})/i_{NO3.N2} - i_{N.BM}/Y_{PHA.\varphi}^{NO}}$
14	Anoxic Storage of X_{PP}	gP/d				$c_{14.NH}$	$-(1/Y_{PP}^{NO})/i_{NO3.N2}$
14b	**Anoxic Storage of X_{PP} w/NO_3**	$\mathbf{gP/d}$				$\mathbf{c_{14b.NH}}$	$\mathbf{-\frac{1/Y_{PP.\varphi}^{NO}}{i_{NO3.N2}}}$
15	Anoxic Glycogen Formation	$gCOD_{GLY}/d$				$c_{15.NH}$	$-\frac{1/Y_{GLY}^{NO}-1}{i_{NO3.N2}}$
15b	**Anoxic Glycogen Formation w/NO_3**	$\mathbf{gCOD_{GLY}/d}$				$\mathbf{c_{15b.NH}}$	$\mathbf{-\frac{1/Y_{GLY.\varphi}^{NO}-1}{i_{NO3.N2}}}$
16	Anoxic Maintenance	$gCOD_{PAO}/d$				$c_{16.NH}$	$-1/i_{NO3,N2}$
16b	**Anoxic Maintenance w/NO_3**	$\mathbf{gCOD_{PAO}/d}$				$\mathbf{c_{16b.NH}}$	$\mathbf{-1/i_{NO3,N2}}$
17	Aerobic PHA Consumption	$gCOD_{PHA}/d$	$-1+1/Y_{PHA}^{O}$			$c_{17.NH}$	
17b	**Aerobic PHA Consumption w/NO_3**	$\mathbf{gCOD_{PHA}/d}$	$\mathbf{-1+1/Y_{PHA.\varphi}^{O} - i_{COD.NO3}\cdot i_{N.BM}/Y_{PHA.\varphi}^{O}}$			$\mathbf{c_{17b.NH}}$	$-i_{N.BM}/Y_{PHA.\varphi}^{O}$
18	Aerobic Storage of X_{PP}	gP/d	$-1/Y_{PP}^{O}$			$c_{18.NH}$	
18b	**Aerobic Storage of X_{PP} w/NO_3**	$\mathbf{gP/d}$	$\mathbf{-1/Y_{PP.\varphi}^{O}}$			$\mathbf{c_{18b.NH}}$	
19	Aerobic Glycogen Formation	$gCOD_{GLY}/d$	$-(1-Y_{GLY}^{O})/Y_{GLY}^{O}$			$c_{19.NH}$	
19b	**Aerobic Glycogen Formation w/NO_3**	$\mathbf{gCOD_{GLY}/d}$	$\mathbf{-(1-Y_{GLY.\varphi}^{O})/Y_{GLY\varphi}^{O}}$			$\mathbf{c_{19b.NH}}$	
20	Aerobic Maintenance	$gCOD_{PAO}/d$	-1			$c_{20.NH}$	
20b	**Aerobic Maintenance w/NO_3**	$\mathbf{gCOD_{PAO}/d}$	$\mathbf{-1}$			$\mathbf{c_{20b.NH}}$	
Autotrophic Nitrifying Organisms							
21	Aerobic Growth on X_A	$gCOD_{XA}/d$	$-(i_{COD.NO3}-Y_A)/Y_A$			$c_{21.NH}$	$1/Y_A$
22	Autotrophic Lysis	$gCOD_{XA}/d$				$c_{22.NH}$	
Denitrifying PAOs without External Substrate							
23	**Anoxic Glycogen Degradation**	$\mathbf{gCOD_{PAO}/d}$				$\mathbf{c_{23.NH}}$	$\mathbf{-\frac{1-Y_{gx}^{NO}}{Y_{gx}^{NO}\cdot i_{NO3.N2}}}$
24	**Anoxic Glycogen Degradation w/NO_3**	$\mathbf{gCOD_{PAO}/d}$				$\mathbf{c_{24.NH}}$	$\mathbf{-\frac{1-Y_{gx.\varphi}^{NO}}{Y_{gx.\varphi}^{NO}\cdot i_{NO3.N2}} - i_{N.BM}}$
25	**Anoxic Maintenance on Glycogen**	$\mathbf{gCOD_{PAO}/d}$				$\mathbf{c_{25.NH}}$	$\mathbf{-1/i_{NO3.N2}}$
26	**Anoxic Maintenance on Glycogen w/NO_3**	$\mathbf{gCOD_{PAO}/d}$				$\mathbf{c_{26.NH}}$	$\mathbf{-1/i_{NO3.N2}}$
27	**Anoxic Maintenance on X_{PP}**	$\mathbf{gCOD_{PAO}/d}$				$\mathbf{c_{27.NH}}$	

Table A1: Model Stoichiometric Matrix

6 S_{N2} gN/m^3	7 S_{PO} gP/m^3	8 S_I $gCOD/m^3$	9 S_{HCO} $mole/m^3$	10 X_I $gCOD/m^3$	11 X_S $gCOD/m^3$	12 X_H $gCOD/m^3$	13 X_{PAO} $gCOD/m^3$	14 X_{PP} gP/m^3	15 X_{PHA} $gCOD/m^3$	16 X_{GLY} $gCOD/m^3$	17 X_A $gCOD/m^3$	18 X_{TSS} g/m^3	
	$c_{1.PO}$	f_{SI}	$c_{1.HCO}$		-1							$c_{1.TSS}$	r_H^O
	$c_{2.PO}$	f_{SI}	$c_{2.HCO}$		-1							$c_{2.TSS}$	r_H^{NO}
	$c_{3.PO}$	f_{SI}	$c_{3.HCO}$		-1							$c_{3.TSS}$	r_H^{AN}
	$c_{4.PO}$		$c_{4.HCO}$			1						$c_{4.TSS}$	r_{SF}^O
	$\mathbf{c_{4b.PO}}$		$\mathbf{c_{4b.HCO}}$			**1**						$\mathbf{c_{4b.TSS}}$	$\mathbf{r_{SF.\varphi}^O}$
	$c_{5.PO}$		$c_{5.HCO}$			1						$c_{5.TSS}$	r_{SA}^O
	$\mathbf{c_{5b.PO}}$		$\mathbf{c_{5b.HCO}}$			**1**						$\mathbf{c_{5b.TSS}}$	$\mathbf{r_{SA.\varphi}^O}$
$(1-Y_H)/(i_{NO3.N2}\cdot Y_H)$	$c_{6.PO}$		$c_{6.HCO}$			1						$c_{6.TSS}$	r_{SF}^{NO}
$\mathbf{\frac{1-Y_{H.\varphi}}{i_{NO3.N2}Y_{H.\varphi}}}$	$\mathbf{c_{6b.PO}}$		$\mathbf{c_{6b.HCO}}$			**1**						$\mathbf{c_{6b.TSS}}$	$\mathbf{r_{SF.\varphi}^{NO}}$
$\frac{1-Y_H}{i_{NO3.N2}Y_H}$	$c_{7.PO}$		$c_{7.HCO}$			1						$c_{7.TSS}$	r_{SA}^{NO}
$\mathbf{\frac{1-Y_{H.\varphi}}{i_{NO3.N2}Y_{H.\varphi}}}$	$\mathbf{c_{7b.PO}}$		$\mathbf{c_{7b.HCO}}$			**1**						$\mathbf{c_{7b.TSS}}$	$\mathbf{r_{SA.\varphi}^{NO}}$
	$c_{8.PO}$		$c_{8.HCO}$									$c_{8.TSS}$	r_{fe}^{AN}
	$c_{9.PO}$		$c_{9.HCO}$	$f_{XI,H}$	$1-f_{XI,H}$	-1						$c_{9.TSS}$	r_{HL}
	$c_{10.PO}$		$c_{10.HCO}$					$-Y_{PO}^{AN}$	Y_{SA}^{AN}	$1-Y_{SA}^{AN}$		$c_{10.TSS}$	r_{SA}^{AN}
	$c_{11.PO}$		$c_{11.HCO}$					-1				$c_{11.TSS}$	r_M^{AN}
$(1-Y_{SA}^{NO})/i_{NO3.N2}$	$c_{12.PO}$		$c_{12.HCO}$					$-Y_{PO}^{NO}$	Y_{SA}^{NO}			$c_{12.TSS}$	r_{SA}^{NO}
$(1-Y_{PHA}^{NO})/i_{NO3.N2}$	$c_{13.PO}$		$c_{13.HCO}$				$1/Y_{PHA}^{NO}$		-1			$c_{13.TSS}$	r_{PHA}^{NO}
$\mathbf{(1-Y_{PHA.\varphi}^{NO})/i_{NO3.N2}}$	$\mathbf{c_{13b.PO}}$		$\mathbf{c_{13b.HCO}}$				$\mathbf{1/Y_{PHA.\varphi}^{NO}}$		$\mathbf{-1+i_{COD.NO3}\cdot i_{N.BM}/Y_{PHA.\varphi}^{NO}}$			$\mathbf{c_{13b.TSS}}$	$\mathbf{r_{PHA.\varphi}^{NO}}$
$(1/Y_{PP}^{NO})/i_{NO3.N2}$	$c_{14.PO}$		$c_{14.HCO}$				$-1/Y_{PP}^{NO}$	1				$c_{14.TSS}$	r_{PP}^{NO}
$\mathbf{\frac{1/Y_{PP.\varphi}^{NO}}{i_{NO3.N2}}}$	$\mathbf{c_{14b.PO}}$		$\mathbf{c_{14b.HCO}}$				$\mathbf{-1/Y_{PP.\varphi}^{NO}}$	**1**				$\mathbf{c_{14b.TSS}}$	$\mathbf{r_{PP.\varphi}^{NO}}$
$\frac{1/Y_{GLY}^{NO}-1}{i_{NO3.N2}}$	$c_{15.PO}$		$c_{15.HCO}$				$-1/Y_{GLY}^{NO}$			1		$c_{15.TSS}$	r_{GLY}^{NO}
$\mathbf{\frac{1/Y_{GLY.\varphi}^{NO}-1}{i_{NO3.N2}}}$	$\mathbf{c_{15b.PO}}$		$\mathbf{c_{15b.HCO}}$				$\mathbf{-1/Y_{GLY.\varphi}^{NO}}$			**1**		$\mathbf{c_{15b.TSS}}$	$\mathbf{r_{GLY.\varphi}^{NO}}$
$1/i_{NO3,N2}$	$c_{16.PO}$		$c_{16.HCO}$				-1					$c_{16.TSS}$	r_M^{NO}
$\mathbf{1/i_{NO3,N2}}$	$\mathbf{c_{16b.PO}}$		$\mathbf{c_{16b.HCO}}$				$\mathbf{-1}$					$\mathbf{c_{16b.TSS}}$	$\mathbf{r_{M.\varphi}^{NO}}$
	$c_{17.PO}$		$c_{17.HCO}$				$1/Y_{PHA}^{O}$		-1			$c_{17.TSS}$	r_{PHA}^{o}
	$\mathbf{c_{17b.PO}}$		$\mathbf{c_{17b.HCO}}$				$\mathbf{1/Y_{PHA.\varphi}^{O}}$		$\mathbf{-1}$			$\mathbf{c_{17b.TSS}}$	$\mathbf{r_{PHA.\varphi}^{O}}$
	$c_{18.PO}$		$c_{18.HCO}$				$-1/Y_{PP}^{O}$	1				$c_{18.TSS}$	r_{PP}^{O}
	$\mathbf{c_{18b.PO}}$		$\mathbf{c_{18b.HCO}}$				$\mathbf{-1/Y_{PP.\varphi}^{O}}$	**1**				$\mathbf{c_{18b.TSS}}$	$\mathbf{r_{PP.\varphi}^{O}}$
	$c_{19.PO}$		$c_{19.HCO}$				$-1/Y_{GLY}^{O}$			1		$c_{19.TSS}$	r_{GLY}^{O}
	$\mathbf{c_{19b.PO}}$		$\mathbf{c_{19b.HCO}}$				$\mathbf{-1/Y_{GLY.\varphi}^{O}}$			**1**		$\mathbf{c_{19b.TSS}}$	$\mathbf{r_{GLY.\varphi}^{O}}$
	$c_{20.PO}$		$c_{20.HCO}$				-1					$c_{20.TSS}$	r_M^{O}
	$\mathbf{c_{20b.PO}}$		$\mathbf{c_{20b.HCO}}$				$\mathbf{-1}$					$\mathbf{c_{20b.TSS}}$	$\mathbf{r_{M.\varphi}^{O}}$
	$c_{21.PO}$		$c_{21.HCO}$								1	$c_{21.TSS}$	r_A^{O}
	$c_{22.PO}$		$c_{22.HCO}$	$f_{XI,A}$	$1-f_{XI,A}$						-1	$c_{22.TSS}$	r_{AL}
$\mathbf{\frac{1-Y_{gx}^{NO}}{Y_{gx}^{NO}\cdot i_{NO3.N2}}}$	$\mathbf{c_{23.PO}}$		$\mathbf{c_{23.HCO}}$				**1**			$\mathbf{-1/Y_{gx}^{NO}}$		$\mathbf{c_{23.TSS}}$	$\mathbf{r_{GLY.PX}^{NO}}$
$\mathbf{\frac{1-Y_{gx.\varphi}^{NO}}{Y_{gx.\varphi}^{NO}\cdot i_{NO3.N2}}}$	$\mathbf{c_{24.PO}}$		$\mathbf{c_{24.HCO}}$				**1**			$\mathbf{-1/Y_{gx.\varphi}^{NO}+i_{COD.NO3}\cdot i_{N.BM}}$		$\mathbf{c_{24.TSS}}$	$\mathbf{r_{GLY.PX.\varphi}^{NO}}$
$\mathbf{1/i_{NO3.N2}}$	$\mathbf{c_{25.PO}}$		$\mathbf{c_{25.HCO}}$							$\mathbf{-1}$		$\mathbf{c_{25.TSS}}$	$\mathbf{r_{m.gx}^{NO}}$
$\mathbf{1/i_{NO3.N2}}$	$\mathbf{c_{26.PO}}$		$\mathbf{c_{26.HCO}}$							$\mathbf{-1}$		$\mathbf{c_{26.TSS}}$	$\mathbf{r_{m.gx.\varphi}^{NO}}$
	$\mathbf{c_{27.PO}}$		$\mathbf{c_{27.HCO}}$					$\mathbf{-1}$				$\mathbf{c_{27.TSS}}$	$\mathbf{r_{m.gx.pp}^{NO}}$

Table A2: State Variables

Component	Description	Units
Dissolved Components		
S_F	Fermentable organic matter	g COD/m^3
S_A	Fermentation products (acetate)	g COD/m^3
S_I	Soluble inert, non-biodegradable organics	g COD/m^3
S_O	Dissolved oxygen	g O_2/m^3
S_{NH}	Ammonia ($NH_4^+ + NO_3$)	g N/m^3
S_{NO}	Nitrate and nitrite ($NO_3 + NO_2$)	g N/m^3
S_{N2}	Dissolved nitrogen gas	g N/m^3
S_{PO}	Inorganic soluble phosphorus	g P/m^3
S_{HCO}	Alkalinity (HCO_3)	g P/m^3
Particulate Components		
X_I	Particulate inert, non-biodegradable organics	g COD/m^3
X_S	Particulate biodegradable organics	g COD/m^3
X_H	Ordinary heterotrophic organisms	g COD/m^3
X_A	Autotrophic, nitrifying organisms	g COD/m^3
X_{PAO}	Phosphorus accumulating organisms	g COD/m^3
X_{PHA}	Stored PHA in PAOs	g COD/m^3
X_{GLY}	Stored glycogen in PAOs	g COD/m^3
X_{PP}	Stored polyphosphates in PAOs	g P/m^3
X_{TSS}	Total suspended solids	g TSS/m^3

Table A3: Stoichiometric Matrix Composition Factors for S_{NH} and S_{PO}

S_{NH} (gN/m^3)	S_{PO} (gP/m^3)
$c_{1.NH} = i_{N.XS} - i_{N.SI} \cdot f_{SI} - i_{N.SF}(1 - f_{SI})$	$c_{1.PO} = i_{P.XS} - i_{P.SI} \cdot f_{SI} - i_{P.SF}(1 - f_{SI})$
$c_{2.NH} = i_{N.XS} - i_{N.SI} \cdot f_{SI} - i_{N.SF}(1 - f_{SI})$	$c_{2.PO} = i_{P.XS} - i_{P.SI} \cdot f_{SI} - i_{P.SF}(1 - f_{SI})$
$c_{3.NH} = i_{N.XS} - i_{N.SI} \cdot f_{SI} - i_{N.SF}(1 - f_{SI})$	$c_{3.PO} = i_{P.XS} - i_{P.SI} \cdot f_{SI} - i_{P.SF}(1 - f_{SI})$
$c_{4.NH} = i_{N.SF}/Y_H - i_{N.BM}$	$c_{4.PO} = i_{P.SF}/Y_H - i_{P.BM}$
$\mathbf{c_{4b.NH} = i_{N.SF}/Y_{H.\varphi}}$	$\mathbf{c_{4b.PO} = i_{P.SF}/Y_{H.\varphi} - i_{P.BM}}$
$c_{5.NH} = -i_{N.BM}$	$c_{5.PO} = -i_{P.BM}$
$\mathbf{c_{5b.NH} = 0}$	$\mathbf{c_{5b.PO} = -i_{P.BM}}$
$c_{6.NH} = i_{N.SF}/Y_H - i_{N.BM}$	$c_{6.PO} = i_{P.SF}/Y_H - i_{P.BM}$
$\mathbf{c_{6b.NH} = i_{N.SF}/Y_{H.\varphi} - i_{COD.NO3} \cdot i_{N.BM} \cdot i_{N.SF}}$	$\mathbf{c_{6b.PO} = i_{P.SF}/Y_{H.\varphi} - i_{P.BM} - i_{COD.NO3} \cdot i_{N.BM} \cdot i_{P.SF}}$
$c_{7.NH} = -i_{N.BM}$	$c_{7.PO} = -i_{P.BM}$
$\mathbf{c_{7b.NH} = 0}$	$\mathbf{c_{7b.PO} = -i_{P.BM}}$
$c_{8.NH} = i_{N.SF}$	$c_{8.PO} = i_{P.SF}$
$c_{9.NH} = i_{N.BM} - i_{N.XI} \cdot f_{XI.H} - i_{N.XS}(1 - f_{XI.H})$	$c_{9.PO} = i_{P.BM} - i_{P.XI} \cdot f_{XI.H} - i_{P.XS}(1 - f_{XI.H})$
$c_{10.NH} = 0$	$c_{10.PO} = Y_{PO.AN}$
$c_{11.NH} = 0$	$c_{11.PO} = 1$
$c_{12.NH} = 0$	$c_{12.PO} = Y_{PO}^{NO}$
$c_{13.NH} = -i_{N.BM}/Y_{PHA}^{NO}$	$c_{13.PO} = -i_{P.BM}/Y_{PHA}^{NO}$
$\mathbf{c_{13b.NH} = 0}$	$\mathbf{c_{13b.PO} = -i_{P.BM}/Y_{PHA.\varphi}^{NO}}$
$c_{14.NH} = i_{N.BM}/Y_{PP}^{NO}$	$c_{14.PO} = i_{P.BM}/Y_{PP}^{NO} - 1$
$\mathbf{c_{14b.NH} = i_{N.BM}/Y_{PP.\varphi}^{NO}}$	$\mathbf{c_{14b.PO} = i_{P.BM}/Y_{PP.\varphi}^{NO} - 1}$
$c_{15.NH} = i_{N.BM}/Y_{GLY}^{NO}$	$c_{15.PO} = i_{P.BM}/Y_{GLY}^{NO}$
$\mathbf{c_{15b.NH} = i_{N.BM}/Y_{GLY.\varphi}^{NO}}$	$\mathbf{c_{15b.PO} = i_{P.BM}/Y_{GLY.\varphi}^{NO}}$
$c_{16.NH} = i_{N.BM}$	$c_{16.PO} = i_{P.BM}$
$\mathbf{c_{16b.NH} = i_{N.BM}}$	$\mathbf{c_{16b.PO} = i_{P.BM}}$
$c_{17.NH} = -i_{N.BM}/Y_{PHA}^{O}$	$c_{17.PO} = -i_{P.BM}/Y_{PHA}^{O}$
$\mathbf{c_{17b.NH} = 0}$	$\mathbf{c_{17b.PO} = -i_{P.BM}/Y_{PHA.\varphi}^{O}}$
$c_{18.NH} = i_{N.BM}/Y_{PP}^{O}$	$c_{18.PO} = i_{P.BM}/Y_{PP}^{O} - 1$
$\mathbf{c_{18b.NH} = i_{N.BM}/Y_{PP.\varphi}^{O}}$	$\mathbf{c_{18b.PO} = i_{P.BM}/Y_{PP.\varphi}^{O} - 1}$
$c_{19.NH} = i_{N.BM}/Y_{GLY}^{O}$	$c_{19.PO} = i_{P.BM}/Y_{GLY}^{O}$
$\mathbf{c_{19b.NH} = i_{N.BM}/Y_{GLY.\varphi}^{O}}$	$\mathbf{c_{19b.PO} = i_{P.BM}/Y_{GLY.\varphi}^{O}}$
$c_{20.NH} = i_{N.BM}$	$c_{20.PO} = i_{P.BM}$
$\mathbf{c_{20b.NH} = i_{N.BM}}$	$\mathbf{c_{20b.PO} = i_{P.BM}}$
$c_{21.NH} = -i_{N.BM} - 1/Y_A$	$c_{21.PO} = -i_{P.BM}$
$c_{22.NH} = i_{N.BM} - i_{N.XI} \cdot f_{XI.A} - i_{N.XS}(1 - f_{XI.A})$	$c_{22.PO} = i_{P.BM} - i_{P.XI} \cdot f_{XI.A} - i_{P.XS}(1 - f_{XI.A})$
$\mathbf{c_{23.NH} = -i_{N.BM}}$	$\mathbf{c_{23.PO} = -i_{P.BM}}$
$\mathbf{c_{24.NH} = 0}$	$\mathbf{c_{24.PO} = -i_{P.BM}}$
$\mathbf{c_{25.NH} = 0}$	$\mathbf{c_{25.PO} = 0}$
$\mathbf{c_{26.NH} = 0}$	$\mathbf{c_{26.PO} = 0}$
$\mathbf{c_{27.NH} = 0}$	$\mathbf{c_{27.PO} = 1}$

Note: Composition factors in bold from this thesis. Remaining composition factors from Meijer (2004).

Table A4: Stoichiometric Matrix Composition Factors for S_{HCO}

$\mathbf{S_{HCO}\ (gN/m^3)}$
$c_{1.HCO} = c_{1.NH} \cdot i_{Charge.SNHx} + c_{1.PO} \cdot i_{Charge.PO4}$
$c_{2.HCO} = c_{2.NH} \cdot i_{Charge.SNHx} + c_{2.PO} \cdot i_{Charge.PO4}$
$c_{3.HCO} = c_{3.NH} \cdot i_{Charge.SNHx} + c_{3.PO} \cdot i_{Charge.PO4}$
$c_{4.HCO} = c_{4.NH} \cdot i_{Charge.SNHx} + c_{4.PO} \cdot i_{Charge.SPO4}$
$\mathbf{c_{4b.HCO} = c_{4b.NH} \cdot i_{Charge.SNHx} + c_{4b.PO} \cdot i_{Charge.SPO4} + c_{4b.NO} \cdot i_{Charge.SNO3}}$
$c_{5.HCO} = c_{5.NH} \cdot i_{Charge.SNHx} + c_{5.PO} \cdot i_{Charge.SPO4} - (1/Y_H) \cdot i_{Charge.SVFA}$
$\mathbf{c_{5b.HCO} = c_{5b.NO} \cdot i_{Charge.SNO3} + c_{5b.PO} \cdot i_{Charge.SPO4} - (1/Y_{H.\phi}) \cdot i_{Charge.SVFA}}$
$c_{6.HCO} = c_{6.NH} \cdot i_{Charge.SNHx} + c_{6.PO} \cdot i_{Charge.SPO4} + c_{6.NO} \cdot i_{Charge.SNO3}$
$\mathbf{c_{6b.HCO} = c_{6b.NH} \cdot i_{Charge.SNHx} + c_{6b.PO} \cdot i_{Charge.SPO4} + c_{6b.NO} \cdot i_{Charge.SNO3}}$
$c_{7.HCO} = c_{7.NH} \cdot i_{Charge.SNHx} + c_{7.PO} \cdot i_{Charge.SPO4} + c_{7.NO} \cdot i_{Charge.SNO3} - (1/Y_H) \cdot i_{Charge.SVFA}$
$\mathbf{c_{7b.HCO} = c_{7b.NO} \cdot i_{Charge.SNO3} + c_{7b.PO} \cdot i_{Charge.SPO4} - (1/Y_{H.\phi}) \cdot i_{Charge.SVFA}}$
$c_{8.HCO} = c_{8.NH} \cdot i_{Charge.SNHx} + c_{8.PO} \cdot i_{Charge.SPO4} + i_{Charge.SVFA}$
$c_{9.HCO} = c_{9.NH} \cdot i_{Charge.SNHx} + c_{9.PO} \cdot i_{Charge.SPO4}$
$c_{10.HCO} = c_{10.PO} \cdot i_{Charge.SPO4} - i_{Charge.SVFA} - Y_{PO}^{AN} \cdot i_{Charge.XPAO.PP}$
$c_{11.HCO} = i_{Charge.SPO4} - i_{Charge.XPAO.PP}$
$c_{12.HCO} = c_{12.PO} \cdot i_{Charge.SPO4} - i_{Charge.SVFA} - Y_{PO}^{NO} \cdot i_{Charge.XPAO.PP} + c_{12.NO} \cdot i_{Charge.SNO3}$
$c_{13.HCO} = c_{13.NH} \cdot i_{Charge.SNHx} + c_{13.PO} \cdot i_{Charge.SPO4} + c_{13.NO} \cdot i_{Charge.SNO3}$
$\mathbf{c_{13b.HCO} = c_{13b.PO} \cdot i_{Charge.SPO4} + c_{13b.NO} \cdot i_{Charge.SNO3}}$
$c_{14.HCO} = c_{14.NH} \cdot i_{Charge.SNHx} + c_{14.PO} \cdot i_{Charge.SPO4} + c_{14.NO} \cdot i_{Charge.SNO3} + i_{Charge.XPAO.PP}$
$\mathbf{c_{14b.HCO} = c_{14b.NH} \cdot i_{Charge.SNHx} + c_{14b.PO} \cdot i_{Charge.SPO4} + c_{14b.NO} \cdot i_{Charge.SNO3} + i_{Charge.XPAO.PP}}$
$c_{15.HCO} = c_{15.NH} \cdot i_{Charge.SNHx} + c_{15.PO} \cdot i_{Charge.SPO4} + c_{15.NO} \cdot i_{Charge.SNO3}$
$\mathbf{c_{15b.HCO} = c_{15b.NH} \cdot i_{Charge.SNHx} + c_{15b.PO} \cdot i_{Charge.SPO4} + c_{15b.NO} \cdot i_{Charge.SNO3}}$
$c_{16.HCO} = c_{16.NH} \cdot i_{Charge.SNHx} + c_{16.PO} \cdot i_{Charge.SPO4} + c_{16.NO} \cdot i_{Charge.SNO3}$
$\mathbf{c_{16b.HCO} = c_{16b.NH} \cdot i_{Charge.SNHx} + c_{16b.PO} \cdot i_{Charge.SPO4} + c_{16b.NO} \cdot i_{Charge.SNO3}}$
$c_{17.HCO} = c_{17.NH} \cdot i_{Charge.SNHx} + c_{17.PO} \cdot i_{Charge.SPO4}$
$\mathbf{c_{17b.HCO} = c_{17b.NO} \cdot i_{Charge.SNO3} + c_{17b.PO} \cdot i_{Charge.SPO4}}$
$c_{18.HCO} = c_{18.NH} \cdot i_{Charge.SNHx} + c_{18.PO} \cdot i_{Charge.SPO4} + i_{Charge.XPAO.PP}$
$\mathbf{c_{18b.HCO} = c_{18b.NH} \cdot i_{Charge.SNHx} + c_{18b.PO} \cdot i_{Charge.SPO4} + i_{Charge.XPAO.PP}}$
$c_{19.HCO} = c_{19.NH} \cdot i_{Charge.SNHx} + c_{19.PO} \cdot i_{Charge.SPO4}$
$\mathbf{c_{19b.HCO} = c_{19b.NH} \cdot i_{Charge.SNHx} + c_{19b.PO} \cdot i_{Charge.SPO4}}$
$c_{20.HCO} = c_{20.NH} \cdot i_{Charge.SNHx} + c_{20.PO} \cdot i_{Charge.SPO4}$
$\mathbf{c_{20b.HCO} = c_{20b.NH} \cdot i_{Charge.SNHx} + c_{20b.PO} \cdot i_{Charge.SPO4}}$
$c_{21.HCO} = c_{21.NH} \cdot i_{Charge.SNHx} + c_{21.PO} \cdot i_{Charge.SPO4} + c_{21.NO} \cdot i_{Charge.SNO3}$
$c_{22.HCO} = c_{22.NH} \cdot i_{Charge.SNHx} + c_{22.PO} \cdot i_{Charge.SPO4}$
$\mathbf{c_{23.HCO} = c_{23.NH} \cdot i_{Charge.SNHx} + c_{23.PO} \cdot i_{Charge.SPO4} + c_{23.NO} \cdot i_{Charge.SNO3}}$
$\mathbf{c_{24.HCO} = c_{24.NO} \cdot i_{Charge.SNO3} + c_{24.PO} \cdot i_{Charge.SPO4}}$
$\mathbf{c_{25.HCO} = c_{25.NH} \cdot i_{Charge.SNHx} + c_{25.PO} \cdot i_{Charge.SPO4} + c_{25.NO} \cdot i_{Charge.SNO3}}$
$\mathbf{c_{26.HCO} = c_{26.NH} \cdot i_{Charge.SNHx} + c_{26.PO} \cdot i_{Charge.SPO4} + c_{26.NO} \cdot i_{Charge.SNO3}}$
$\mathbf{c_{27.HCO} = i_{Charge.SPO4} - i_{Charge.XPAO.PP}}$

Note: Composition factors in bold from this thesis. Remaining composition factors from Meijer (2004).

Table A5: Stoichiometric Matrix Composition Factors for X_{TSS}

	$\mathbf{X_{TSS}\ (mole/m^3)}$
$c_{1.TSS}$	$= -i_{TSS.XS}$
$c_{2.TSS}$	$= -i_{TSS.XS}$
$c_{3.TSS}$	$= -i_{TSS.XS}$
$c_{4.TSS}$	$= i_{TSS.BM}$
$\mathbf{c_{4b.TSS}}$	$\mathbf{= i_{TSS.BM}}$
$c_{5.TSS}$	$= i_{TSS.BM}$
$\mathbf{c_{5b.TSS}}$	$\mathbf{= i_{TSS.BM}}$
$c_{6.TSS}$	$= i_{TSS.BM}$
$\mathbf{c_{6b.TSS}}$	$\mathbf{= i_{TSS.BM}}$
$c_{7.TSS}$	$= i_{TSS.BM}$
$\mathbf{c_{7b.TSS}}$	$\mathbf{= i_{TSS.BM}}$
$c_{8.TSS}$	$= 0$
$c_{9.TSS}$	$= i_{TSS.XI} \cdot f_{XI.H} + i_{TSS.XS}(1 - f_{XI.H}) - i_{TSS.BM}$
$c_{10.TSS}$	$= i_{TSS.PP}\left(-Y_{PO}^{AN}\right) + i_{TSS.PHA} \cdot Y_{SA}^{AN} + i_{TSS.GLY}(1 - Y_{SA}^{AN})$
$c_{11.TSS}$	$= -i_{TSS.PP}$
$c_{12.TSS}$	$= i_{TSS.PP}\left(-Y_{PO}^{NO}\right) + i_{TSS.PHA} \cdot Y_{SA}^{NO}$
$c_{13.TSS}$	$= i_{TSS.BM}/Y_{PHA}^{NO} - i_{TSS.PHA}$
$\mathbf{c_{13b.TSS}}$	$\mathbf{= i_{TSS.BM}/Y_{PHA.\varphi}^{NO} + i_{TSS.PHA} \cdot (i_{N.BM} \cdot i_{COD.NO3}/Y_{PHA.\varphi}^{NO} - 1)}$
$c_{14.TSS}$	$= -i_{TSS.BM}/Y_{PP}^{NO} + i_{TSS.PP}$
$\mathbf{c_{14b.TSS}}$	$\mathbf{= -i_{TSS.BM}/Y_{PP.\varphi}^{NO} + i_{TSS.PP}}$
$c_{15.PO}$	$= -i_{TSS.BM}/Y_{GLY}^{NO} + i_{TSS.GLY}$
$\mathbf{c_{15b.TSS}}$	$\mathbf{= -i_{TSS.BM}/Y_{GLY.\varphi}^{NO} + i_{TSS.GLY}}$
$c_{16.TSS}$	$= -i_{TSS.BM}$
$\mathbf{c_{16b.TSS}}$	$\mathbf{= -i_{TSS.BM}}$
$c_{17.TSS}$	$= i_{TSS.BM}/Y_{PHA}^{O} - i_{TSS.PHA}$
$\mathbf{c_{17b.TSS}}$	$\mathbf{= i_{TSS.BM}/Y_{PHA.\varphi}^{O} - i_{TSS.PHA}}$
$c_{18.TSS}$	$= -i_{TSS.BM}/Y_{PP}^{O} + i_{TSS.PP}$
$\mathbf{c_{18b.TSS}}$	$\mathbf{= -i_{TSS.BM}/Y_{PP.\varphi}^{O} + i_{TSS.PP}}$
$c_{19.TSS}$	$= -i_{TSS.BM}/Y_{GLY}^{O} + i_{TSS.GLY}$
$\mathbf{c_{19b.TSS}}$	$\mathbf{= -i_{TSS.BM}/Y_{GLY.\varphi}^{O} + i_{TSS.GLY}}$
$c_{20.TSS}$	$= -i_{TSS.BM}$
$\mathbf{c_{20b.TSS}}$	$\mathbf{= -i_{TSS.BM}}$
$c_{21.TSS}$	$= i_{TSS.BM}$
$c_{22.TSS}$	$= i_{TSS.XI} \cdot f_{XI.A} + i_{TSS.XS}(1 - f_{XI.A}) - i_{TSS.BM}$
$\mathbf{c_{23.TSS}}$	$\mathbf{= i_{TSS.BM} - i_{TSS.GLY}/Y_{gx}^{NO}}$
$\mathbf{c_{24.TSS}}$	$\mathbf{= i_{TSS.BM} + i_{TSS.GLY}(-1/Y_{gx.\varphi}^{NO} + i_{COD.NO3} \cdot i_{N.BM})}$
$\mathbf{c_{25.TSS}}$	$\mathbf{= -i_{TSS.GLY}}$
$\mathbf{c_{26.TSS}}$	$\mathbf{= -i_{TSS.GLY}}$
$\mathbf{c_{27.TSS}}$	$\mathbf{= -i_{TSS.PP}}$

Note: Composition factors in bold from this thesis. Remaining composition factors from Meijer (2004).

Table A6: Stoichiometric Matrix Composition Factors for S_{NH} and S_{PO}

Process	Kinetic Rate ($M\ L^{-3}\ T^{-1}$)
1. Aerobic Hydrolysis	$r_h^O = k_h \cdot \frac{X_S/(X_H + X_{PAO})}{K_X + X_S/(X_H + X_{PAO})} \cdot \frac{S_O}{K_{O.HYD} + S_O} \cdot (X_H + X_{PAO})$
2. Anoxic Hydrolysis	$r_H^{NO} = k_h \cdot \eta_{NO.HYD} \cdot \frac{K_{O.HYD}}{K_{O.HYD} + S_O} \cdot \frac{X_S/(X_H + X_{PAO})}{K_X + X_S/(X_H + X_{PAO})} \cdot \frac{S_{NO}}{K_{NO.HYD} + S_{NO}} \cdot (X_H + X_{PAO})$
3. Anaerobic Hydrolysis	$r_H^{AN} = k_h \cdot \eta_{fe} \cdot \frac{K_{O.HYD}}{K_{O.HYD} + S_O} \cdot \frac{X_S/(X_H + X_{PAO})}{K_X + X_S/(X_H + X_{PAO})} \cdot \frac{K_{NO.HYD}}{K_{NO.HYD} + S_{NO}} \cdot (X_H + X_{PAO})$
4. Aerobic Growth on S_F	$r_{SF}^O = \mu_H \cdot \frac{S_O}{K_{O.H} + S_O} \cdot \frac{S_F}{K_F + S_F} \cdot \frac{S_F}{S_F + S_A} \cdot \frac{S_{N.H}}{K_{N.H} + S_{NH}} \cdot \frac{S_{PO}}{K_{P.H} + S_{PO}} \cdot \frac{S_{HCO}}{K_{HCO.H} + S_{HCO}} \cdot X_H$
4b. Aerobic Growth on S_F w/NO_3	$\mathbf{r_{SF.\varphi}^O = \mu_H \cdot \frac{S_O}{K_{O.H} + S_O} \cdot \frac{S_F}{K_F + S_F} \cdot \frac{S_F}{S_F + S_A} \cdot \frac{K_{N.H}}{K_{N.H} + S_{NH}} \cdot \frac{S_{NO}}{K_{NO} + S_{NO}} \cdot \frac{S_{PO}}{K_{P.H} + S_{PO}} \cdot \frac{S_{HCO}}{K_{HCO.H} + S_{HCO}} \cdot \frac{S_{NO}}{K_{NO.ASIM} + S_{NO}} \cdot X_H}$
5. Aerobic Growth on S_A	$r_{SA}^O = \mu_H \cdot \frac{S_O}{K_{O.H} + S_O} \cdot \frac{S_A}{K_{Ac} + S_A} \cdot \frac{S_A}{S_F + S_A} \cdot \frac{S_{N.H}}{K_{N.H} + S_{NH}} \cdot \frac{S_{PO}}{K_{P.H} + S_{PO}} \cdot \frac{S_{HCO}}{K_{HCO.H} + S_{HCO}} \cdot X_H$
5b. Aerobic Growth on S_A w/NO_3	$\mathbf{r_{SA.\varphi}^O = \mu_H \cdot \frac{S_O}{K_{O.H} + S_O} \cdot \frac{S_A}{K_{Ac} + S_A} \cdot \frac{S_A}{S_F + S_A} \cdot \frac{K_{N.H}}{K_{N.H} + S_{NH}} \cdot \frac{S_{NO}}{K_{NO} + S_{NO}} \cdot \frac{S_{PO}}{K_{P.H} + S_{PO}} \cdot \frac{S_{HCO}}{K_{HCO.H} + S_{HCO}} \cdot \frac{S_{NO}}{K_{NO.ASIM} + S_{NO}} X_H}$
6. Anoxic Growth on S_F	$r_{SF}^{NO} = \mu_H \cdot \eta_{NO.H} \cdot \frac{K_{O.H}}{K_{O.H} + S_O} \cdot \frac{S_{NO}}{K_{NO.H} + S_{NO}} \cdot \frac{S_F}{K_F + S_F} \cdot \frac{S_F}{S_F + S_A} \cdot \frac{S_{NH}}{K_{NH.H} + S_{NH}} \cdot \frac{S_{PO}}{K_{P.H} + S_{PO}} \cdot \frac{S_{HCO}}{K_{HCO.H} + S_{HCO}} \cdot X_H$
6b. Anoxic Growth on S_F w/NO_3	$\mathbf{r_{SF.\varphi}^{NO} = \mu_H \cdot \eta_{NO.H} \cdot \frac{S_O}{K_{O.H} + S_O} \cdot \frac{S_{NO}}{K_{NO.H} + S_{NO}} \cdot \frac{S_F}{K_F + S_F} \cdot \frac{S_F}{S_F + S_A} \cdot \frac{K_{NH.H}}{K_{NH.H} + S_{NH}} \cdot \frac{S_{PO}}{K_{P.H} + S_{PO}} \cdot \frac{S_{HCO}}{K_{HCO.H} + S_{HCO}} \cdot \frac{S_{NO}}{K_{NO.ASIM} + S_{NO}} X_H}$
7. Anoxic Growth on S_A	$r_{SA}^{NO} = \mu_H \cdot \eta_{NO.H} \cdot \frac{K_{O.H}}{K_{O.H} + S_O} \cdot \frac{S_{NO}}{K_{NO.H} + S_{NO}} \cdot \frac{S_A}{K_{Ac} + S_A} \cdot \frac{S_A}{S_F + S_A} \cdot \frac{S_{NH}}{K_{NH} + S_{NH}} \cdot \frac{S_{PO}}{K_{P.H} + S_{PO}} \cdot \frac{S_{HCO}}{K_{HCO.H} + S_{HCO}} \cdot X_H$
7b. Anoxic Growth on S_A w/NO_3	$\mathbf{r_{SA.\varphi}^{NO} = \mu_H \cdot \eta_{NO.H} \cdot \frac{S_O}{K_{O.H} + S_O} \cdot \frac{S_{NO}}{K_{NO.H} + S_{NO}} \cdot \frac{S_A}{K_{Ac} + S_A} \cdot \frac{S_A}{S_F + S_A} \cdot \frac{K_{NH.H}}{K_{NH.H} + S_{NH}} \cdot \frac{S_{PO}}{K_{P.H} + S_{PO}} \cdot \frac{S_{HCO}}{K_{HCO.H} + S_{HCO}} \cdot \frac{S_{NO}}{K_{NO.ASIM} + S_{NO}} X_H}$
8. Fermentation	$r_{fe}^{AN} = q_{fe} \cdot \frac{K_{O.H}}{K_{O.H} + S_O} \cdot \frac{K_{NO.H}}{K_{NO.H} + S_{NO}} \cdot \frac{S_F}{K_{fe} + S_F} \cdot \frac{S_{HCO}}{K_{HCO.H} + S_{HCO}} \cdot X_H$
9. Heterotrophic Lysis	$r_{HL} = b_H \cdot X_H$
10. Anaerobic Storage of S_A	$r_{SA}^{AN} = q_{Ac} \cdot \frac{S_A}{K_{Ac} + S_A} \cdot \frac{K_{O.PAO}}{K_{O.PAO} + S_O} \cdot \frac{K_{NO.PAO}}{K_{NO.PAO} + S_{NO}} \cdot \frac{X_{GLY}}{K_{GLY} + X_{GLY}} \cdot \frac{X_{PP}}{K_{PP} + X_{PP}} \cdot X_{PAO}$
11. Anaerobic Maintenance	$r_M^{AN} = m_{AN} \cdot \frac{K_{O.PAO}}{K_{O.PAO} + S_O} \cdot \frac{K_{NO.PAO}}{K_{NO.PAO} + S_{NO}} \cdot \frac{X_{PP}}{K_{PP} + X_{PP}} \cdot X_{PAO}$
12. Anoxic Storage of S_A	$r_{SA}^{NO} = q_{Ac}^{NO} \cdot \frac{S_A}{K_{Ac} + S_A} \cdot \frac{K_{O.PAO}}{K_{O.PAO} + S_O} \cdot \frac{S_{NO}}{K_{NO.PAO} + S_{NO}} \cdot \frac{X_{PP}}{K_{PP} + X_{PP}} \cdot X_{PAO}$
13. Anoxic PHA Consumption	$r_{PHA}^{NO} = k_{PHA} \cdot \eta_{NO.PAO} \cdot \frac{K_{O.PAO}}{K_{O.PAO} + S_O} \cdot \frac{S_{NH}}{K_{N.PAO} + S_{NH}} \cdot \frac{S_{NO}}{K_{NO.PAO} + S_{NO}} \cdot \frac{S_{PO}}{K_{P.PAO} + S_{PO}} \cdot \frac{S_{HCO}}{K_{HCO.PAO} + S_{HCO}} \cdot \frac{X_{PHA}/X_{PAO}}{K_{fPHA} + X_{PHA}/X_{PAO}} \cdot X_{PAO}$
13b. Anoxic PHA Consumption w/NO_3	$\mathbf{r_{PHA.\varphi}^{NO} = k_{PHA} \cdot \eta_{NO.PAO} \cdot \frac{S_O}{K_{O.PAO} + S_O} \cdot \frac{K_{N.PAO}}{K_{N.PAO} + S_{NH}} \cdot \frac{S_{NO}}{K_{NO.PAO} + S_{NO}} \cdot \frac{S_{PO}}{K_{P.PAO} + S_{PO}} \cdot \frac{S_{HCO}}{K_{HCO.PAO} + S_{HCO}} \cdot \frac{X_{PHA}/X_{PAO}}{K_{fPHA} + X_{PHA}/X_{PAO}} \cdot \frac{S_{NO}}{K_{NO.ASIM} + S_{NO}} \cdot X_{PAO}}$
14. Anoxic Storage of X_{PP}	$r_{PP}^{NO} = k_{PP} \cdot \eta_{NO.PAO} \cdot \frac{X_{PAO}}{X_{PP}} \cdot \frac{K_{O.PAO}}{K_{O.PAO} + S_O} \cdot \frac{S_{NH}}{K_{N.PAO} + S_{NH}} \cdot \frac{S_{NO}}{g_{PP} \cdot K_{NO.PAO} + S_{NO}} \cdot \frac{S_{PO}}{K_{P.PAO} + S_{PO}} \cdot \frac{X_{PHA}}{K_{PHA} + X_{PHA}} \cdot \frac{f_{PP.max} \cdot X_{PP}/X_{PAO}}{K_{fPP} + (f_{pp.max} - X_{PP}/X_{PAO})} \cdot X_{PAO}$

Process	Kinetic Rate ($M\ L^{-3}\ T^{-1}$)
14b. Anoxic Storage of X_{PP} w/NO_3	$\mathbf{r_{PP.\varphi}^{NO} = k_{PP} \cdot \eta_{NO.PAO} \cdot \frac{X_{PAO}}{X_{PP}} \cdot \frac{K_{O.PAO}}{K_{O.PAO} + S_O} \cdot \frac{S_{NO}}{g_{PP} \cdot K_{NO.PAO} + S_{NO}} \cdot \frac{K_{N.PAO}}{K_{N.PAO} + S_{NH}} \cdot \frac{S_{PO}}{K_{P.PAO} + S_{PO}} \cdot \frac{X_{PHA}}{K_{PHA} + X_{PHA}} \cdot \frac{f_{PP.max} \cdot \frac{X_{PP}}{X_{PAO}}}{K_{fPP} + (f_{pp.max} - X_{PP}/X_{PAO})} \cdot \frac{S_{NO}}{K_{NO.ASIM} + S_{NO}} \cdot X_{PAO}}$
15. Anoxic Glycogen Formation	$r_{GLY}^{NO} = k_{GLY} \cdot \eta_{NO.PAO} \cdot \frac{X_{PHA}}{X_{GLY}} \cdot \frac{K_{O.PAO}}{K_{O.PAO} + S_O} \cdot \frac{S_{NH}}{K_{N.PAO} + S_{NH}} \cdot \frac{S_{NO}}{K_{NO.PAO} + S_{NO}} \cdot \frac{X_{PHA}}{K_{PHA} + X_{PHA}} \cdot \frac{f_{GLY}^{max} - X_{GLY}/X_{PAO}}{K_{fGLY} + (f_{GLY}^{max} - X_{GLY}/X_{PAO})} \cdot \frac{S_{HCO}}{K_{HCO.PAO} + S_{HCO}} \cdot X_{PAO}$
15b. Anoxic Glyc. Form. w/NO_3	$\mathbf{r_{GLY.\varphi}^{NO} = k_{GLY} \cdot \eta_{NO.PAO} \cdot \frac{X_{PHA}}{X_{GLY}} \cdot \frac{K_{O.PAO}}{K_{O.PAO} + S_O} \cdot \frac{K_{N.PAO}}{K_{N.PAO} + S_{NH}} \cdot \frac{S_{NO}}{K_{NO.PAO} + S_{NO}} \cdot \frac{X_{PHA}}{K_{PHA} + X_{PHA}} \cdot \frac{f_{GLY}^{max} - \frac{X_{GLY}}{X_{PAO}}}{K_{fGLY} + (f_{GLY}^{max} - X_{GLY}/X_{PAO})} \cdot \frac{S_{HCO}}{K_{HCO.PAO} + S_{HCO}} \cdot \frac{S_{NO}}{K_{NO.ASIM} + S_{NO}} \cdot X_{PAO}}$
16. Anoxic Maintenance	$r_M^{NO} = m_{NO} \cdot \frac{K_{O.PAO}}{K_{O.PAO} + S_O} \cdot \frac{S_{NO}}{K_{NO.PAO} + S_{NO}} \cdot \frac{S_{NH}}{K_{N.PAO} + S_{NH}} \cdot X_{PAO}$
16b. Anoxic Maintenance w/NO_3	$\mathbf{r_{M.\varphi}^{NO} = m_{NO.\varphi} \cdot \frac{K_{O.PAO}}{K_{O.PAO} + S_O} \cdot \frac{S_{NO}}{K_{NO.PAO} + S_{NO}} \cdot \frac{K_{N.PAO}}{K_{N.PAO} + S_{NH}} \cdot \frac{S_{NO}}{K_{NO.ASIM} + S_{NO}} \cdot X_{PAO}}$
17. Aerobic PHA Consumption	$r_{PHA}^{O} = k_{PHA} \cdot \frac{S_O}{K_{O.PAO} + S_O} \cdot \frac{S_{NH}}{K_{N.PAO} + S_{NH}} \cdot \frac{S_{PO}}{K_{P.PAO} + S_{PO}} \cdot \frac{S_{HCO}}{K_{HCO.PAO} + S_{HCO}} \cdot \frac{X_{PHA}/X_{PAO}}{K_{fPHA} + X_{PHA}/X_{PAO}} \cdot X_{PAO}$
17b. Aerobic PHA Consumption w/NO_3	$\mathbf{r_{PHA.\varphi}^{O} = k_{PHA} \cdot \frac{S_O}{K_{O.PAO} + S_O} \cdot \frac{K_{N.PAO}}{K_{N.PAO} + S_{NH}} \cdot \frac{S_{PO}}{K_{P.PAO} + S_{PO}} \cdot \frac{S_{HCO}}{K_{HCO.PAO} + S_{HCO}} \cdot \frac{X_{PHA}/X_{PAO}}{K_{fPHA} + X_{PHA}/X_{PAO}} \cdot \frac{S_{NO}}{K_{NO.ASIM} + S_{NO}} \cdot X_{PAO}}$
18. Aerobic Storage of X_{PP}	$r_{PP}^{O} = k_{PP} \cdot \frac{X_{PAO}}{X_{PP}} \cdot \frac{S_O}{g_{PP} \cdot K_{O.PAO} + S_O} \cdot \frac{S_{NH}}{K_{N.PAO} + S_{NH}} \cdot \frac{S_{PO}}{K_{P.PAO} + S_{PO}} \cdot \frac{X_{PHA}}{K_{PHA} + X_{PHA}} \cdot \frac{f_{PP}^{max} - \frac{X_{PP}}{X_{PAO}}}{K_{fPP} + \left(f_{PP.max} - \frac{X_{PP}}{X_{PAO}}\right)} \cdot X_{PAO}$
18b. Aerobic Storage of X_{PP} w/NO_3	$\mathbf{r_{PP.\varphi}^{O} = k_{PP} \cdot \frac{X_{PAO}}{X_{PP}} \cdot \frac{S_O}{g_{PP} \cdot K_{O.PAO} + S_O} \cdot \frac{S_{PO}}{K_{P.PAO} + S_{PO}} \cdot \frac{K_{N.PAO}}{K_{N.PAO} + S_{NH}} \cdot \frac{X_{PHA}}{K_{PHA} + X_{PHA}} \cdot \frac{f_{PP}^{max} - \frac{X_{PP}}{X_{PAO}}}{K_{fPP} + \left(f_{PP.max} - \frac{X_{PP}}{X_{PAO}}\right)} \cdot \frac{S_{NO}}{K_{NO.ASIM} + S_{NO}} \cdot X_{PAO}}$
19. Aerobic Glycogen Formation	$r_{GLY}^{O} = k_{GLY} \cdot \frac{X_{PHA}}{X_{GLY}} \cdot \frac{S_O}{K_{O.PAO} + S_O} \cdot \frac{S_{NH}}{K_{N.PAO} + S_{NH}} \cdot \frac{X_{PHA}}{K_{PHA} + X_{PHA}} \cdot \frac{f_{GLY}^{max} - X_{GLY}/X_{PAO}}{K_{fGLY} - (f_{GLY}^{max} - X_{GLY}/X_{PAO})} \cdot X_{PAO}$
19b. Aerobic Glycogen Formation w/NO_3	$\mathbf{r_{GLY.\varphi}^{O} = k_{GLY} \cdot \frac{X_{PHA}}{X_{GLY}} \cdot \frac{S_O}{K_{O.PAO} + S_O} \cdot \frac{K_{N.PAO}}{K_{N.PAO} + S_{NH}} \cdot \frac{X_{PHA}}{K_{PHA} + X_{PHA}} \cdot \frac{f_{GLY}^{max} - X_{GLY}/X_{PAO}}{K_{fGLY} - (f_{GLY}^{max} - X_{GLY}/X_{PAO})} \cdot \frac{S_{NO}}{K_{NO.ASIM} + S_{NO}} \cdot X_{PAO}}$
20. Aerobic Maintenance	$r_M^{O} = m_O \cdot \frac{S_O}{K_{O.PAO} + S_O} \cdot \frac{S_{NH}}{K_{N.PAO} + S_{NH}} \cdot X_{PAO}$
20b. Aerobic Maintenance w/NO_3	$\mathbf{r_{M.\varphi}^{O} = m_{O.\varphi} \cdot \frac{S_O}{K_{O.PAO} + S_O} \cdot \frac{K_{N.PAO}}{K_{N.PAO} + S_{NH}} \cdot X_{PAO}}$
21. Aerobic Growth on X_A	$r_A^{O} = \mu_A \cdot \frac{S_O}{K_{O.A} + S_O} \cdot \frac{S_{NH}}{K_{NH.A} + S_{NH}} \cdot \frac{S_{PO}}{K_{P.A} + S_{PO}} \cdot \frac{S_{HCO}}{K_{HCO.A} + S_{HCO}} \cdot X_A$
22. Autotrophic Lysis	$r_{AL} = b_A \cdot X_A$

Process	Kinetic Rate ($M\ L^{-3}\ T^{-1}$)
23. Anoxic Glycogen Degradation	$\mathbf{r^{NO}_{GLY.PX} = \mu_{px} \cdot \eta_{NO.PAO} \cdot \frac{X_{GLY}/X_{PAO}}{K_{GLY.PX} + X_{GLY}/C_X} \cdot \frac{K_{O.PAO}}{K_{O.PAO} + S_O} \cdot \frac{S_{NH}}{K_{N.PAO} + S_{NH}} \cdot \frac{S_{NO}}{K_{NO.PAO} + S_{NO}} \cdot \frac{K_{PHA.PX}}{K_{PHA.PX} + X_{PHA}} \cdot \frac{X_{GLY}}{K_{GLY} + X_{GLY}} \cdot \frac{S_{HCO}}{K_{HCO.PAO} + S_{HCO}} \cdot \frac{S_{NO}}{K_{NO.ASIM} + S_{NO}} \cdot X_{PAO}}$
24. Anoxic Glycogen Deg. w/NO_3	$\mathbf{r^{NO}_{GLY.PX.\varphi} = \mu_{px} \cdot \eta_{NO.PAO} \cdot \frac{X_{GLY}/X_{PAO}}{K_{GLY.PX} + X_{GLY}/C_X} \cdot \frac{K_{O.PAO}}{K_{O.PAO} + S_O} \cdot \frac{K_{N.PAO}}{K_{N.PAO} + S_{NH}} \cdot \frac{S_{NO}}{K_{NO.PAO} + S_{NO}} \cdot \frac{K_{PHA.PX}}{K_{PHA.PX} + X_{PHA}} \cdot \frac{X_{GLY}}{K_{GLY} + X_{GLY}} \cdot \frac{S_{HCO}}{K_{HCO.PAO} + S_{HCO}} \cdot \frac{S_{NO}}{K_{NO.ASIM} + S_{NO}} \cdot X_{PAO}}$
25. Anoxic Maintenance on Glycogen	$\mathbf{r^{NO}_{m.gx} = m_{gx} \cdot \frac{K_{O.PAO}}{K_{O.PAO} + S_O} \cdot \frac{S_{NO}}{K_{NO.PAO} + S_{NO}} \cdot \frac{S_{NH}}{K_{N.PAO} + S_{NH}} \cdot \frac{K_{PHA.PX}}{K_{PHA.PX} + X_{PHA}} \cdot \frac{X_{GLY}}{K_{GLY} + X_{GLY}} \cdot \frac{S_{NO}}{K_{NO.ASIM} + S_{NO}} \cdot X_{PAO}}$
26. Anoxic Maintenance on Glycogen w/NO_3	$\mathbf{r^{NO}_{m.gx.\varphi} = m_{gx.\varphi} \cdot \frac{K_{O.PAO}}{K_{O.PAO} + S_O} \cdot \frac{K_{N.PAO}}{K_{N.PAO} + S_{NH}} \cdot \frac{S_{NO}}{K_{NO.PAO} + S_{NO}} \cdot \frac{K_{PHA.PX}}{K_{PHA.PX} + X_{PHA}} \cdot \frac{X_{GLY}}{K_{GLY.PX} + X_{GLY}} \cdot \frac{S_{NO}}{K_{NO.ASIM} + S_{NO}} \cdot X_{PAO}}$
27. Anoxic Maintenance on X_{PP}	$\mathbf{r^{NO}_{m.gx.pp} = m_{gx.pp} \cdot \frac{K_{O.PAO}}{K_{O.PAO} + S_O} \cdot \frac{S_{NO}}{K_{NO.PAO} + S_{NO}} \cdot \frac{X_{PP}}{K_{PP} + X_{PP}} \cdot \frac{K_{PHA.PX}}{K_{PHA.PX} + X_{PHA}} \cdot \frac{K_{GLY}}{K_{GLY} + X_{GLY}} \cdot \frac{S_{NO}}{K_{NO.ASIM} + S_{NO}} \cdot X_{PAO}}$

Note: Kinetic rates and functions in bold from this thesis. Remaining rates and functions from Meijer (2004).

Table A7: Stoichiometric Coefficients

Parameter	Definition	Value	Unit
Hydrolysis			
f_{SI}	Fraction of inert COD generated in hydrolysis	0	g COD S_I/g COD (X_H+X_{PAO})
Ordinary Heterotrophic Organisms			
Y_H	Yield for X_H growth w/NH_4 as N source	0.625	g COD X_H/g COD
$\mathbf{Y_{H.\varphi}}$	**Yield for X_H growth w/NO_3 as N source**	**0.501**	**g COD X_H/g COD**
$f_{XI.H}$	Fraction of X_I generated in heterotrophic biomass decay	0.10	g COD X_I/g COD X_H
Phosphorus Accumulating Organisms			
Y^{O}_{PHA}	Aerobic yield for degradation of X_{PHA} w/NH_4 as N source	1.39	g COD X_{PHB}/g COD X_{PAO}
$\mathbf{Y^{O}_{PHA.\varphi}}$	**Aerobic yield for degradation of X_{PHA} w/NO_3 as N source**	**1.717**	**g COD X_{PHB}/g COD X_{PAO}**
Y^{NO}_{PHA}	Anoxic yield for degradation of X_{PHA} w/NH_4 as N source	1.72	g COD X_{PHB}/g COD X_{PAO}
$\mathbf{Y^{NO}_{PHA.\varphi}}$	**Anoxic yield for degradation of X_{PHA} w/NO_3 as N source**	**2.023**	**g COD X_{PHB}/g COD X_{PAO}**
Y^{O}_{PP}	Aerobic yield for formation of X_{PP} w/NH_4 as N source	4.42	g P/g COD X_{PAO}
$\mathbf{Y^{O}_{PP.\varphi}}$	**Aerobic yield for formation of X_{PP} w/NH_4 as N source**	**5.444**	**g P/g COD X_{PAO}**
Y^{NO}_{PP}	Anoxic yield for formation of X_{PP} w/NH_4 as N source	3.02	g P/g COD X_{PAO}
$\mathbf{Y^{NO}_{PP.\varphi}}$	**Anoxic yield for formation of X_{PP} w/NO_3 as N source**	**3.494**	**g P/g COD X_{PAO}**
Y^{AN}_{SA}	Yield for anaerobic formation of PHA from S_A	1.50	g COD X_{PHB}/g COD S_A
Y^{NO}_{SA}	Yield for anoxic formation of PHA from S_A	0.71	g COD X_{PHB}/g COD S_A
Y^{AN}_{PO}	Anaerobic yield for phosphate release	0.35	g P/g COD S_A
Y^{NO}_{PO}	Observed yield for anoxic phosphate release	0.23	g P/g COD S_A
Y^{O}_{GLY}	Aerobic yield for formation of X_{GLY} w/NH_4 as N source	1.11	g COD X_{GLY}/g COD X_{PAO}
$\mathbf{Y^{O}_{GLY.\varphi}}$	**Aerobic yield for formation of X_{GLY} w/NO_3 as N source**	**1.368**	**g COD X_{GLY}/g COD X_{PAO}**
Y^{NO}_{GLY}	Anoxic yield for formation of X_{GLY} w/NH_4 as N source	1.18	g COD X_{GLY}/g COD X_{PAO}
$\mathbf{Y^{NO}_{GLY.\varphi}}$	**Anoxic yield for formation of X_{GLY} w/NO_3 as N source**	**1.376**	**g COD X_{GLY}/g COD X_{PAO}**
$\mathbf{Y^{NO}_{gx}}$	**Yield for X_{PAO} growth on glycogen w/NH_4 as N source**	**0.573**	**g COD X_{PAO}/g COD X_{GLY}**
$\mathbf{Y^{NO}_{gx.\varphi}}$	**Yield for X_{PAO} growth on glycogen w/NO_3 as N source**	**0.503**	**g COD X_{PAO}/g COD X_{GLY}**
Autotrophic Organisms			
Y_A	Yield of X_A growth	0.24	g COD X_A/g N S_{NH}
$f_{XI.A}$	Fraction of X_I generated in autotrophic biomass decay	0.10	g COD X_I/g COD X_A
Composition Factors			
$i_{N.SF}$	Nitrogen content of S_F	0.03	g N/g COD S_F
$i_{N.SI}$	Nitrogen content of S_I	0.01	g N/g COD S_I
$i_{N.XI}$	Nitrogen content of X_I	0.03	g N/g COD X_I
$i_{N.XS}$	Nitrogen content of X_S	0.03	g N/g COD X_s
$i_{N.BM}$	Nitrogen content of biomass; X_H, X_{PAO}, X_A	0.07	g N/g COD biomass
$i_{P.SF}$	Phosphorus content of S_F	0.01	g P/g COD S_F
$i_{P.SI}$	Phosphorus content of S_I	0	g P/g COD S_I
$i_{P.XI}$	Phosphorus content of X_I	0.01	g P/g COD X_I
$i_{P.XS}$	Phosphorus content of X_S	0.01	g P/g COD X_S
$i_{P.BM}$	Phosphorus content of biomass; X_H, X_{PAO}, X_A	0.02	g P/g COD biomass
$i_{TSS.XI}$	Ratio of TSS to X_I	0.75	g TSS/g COD X_I
$i_{TSS.XS}$	Ratio of TSS to X_S	0.75	g TSS/g COD X_S
$i_{TSS.PHA}$	Ratio of TSS to X_{PHA}	0.6	g TSS/g COD X_I
$i_{TSS.BM}$	Ratio of TSS to biomass; X_H, X_{PAO}, X_A $(CH_{2.09}O_{0.54}N_{0.2}P_{0.015})_n$	0.90	g TSS/g COD biomass
$i_{TSS.PP}$	Ratio of TSS to X_{PP}	3.23	g TSS/g P X_{PP}
$i_{TSS.GLY}$	Ratio of TSS to X_{GLY}	0.84	g TSS/g COD X_I
$i_{NO3.N2}$	COD equivalence of NO_3 reduction to N_2	40/14	g COD/g N
$i_{COD.NO3}$	Ratio of COD to nitrate	−64/14	g COD/g N S_{NO}
$i_{COD.N2}$	Ratio of COD to dinitrogen	−24/14	g COD/g N S_{N2}
$i_{Charge.SVFA}$	Ratio of charge to COD S_A (CH_3COO^-)	−1/64	Charge/g COD
$i_{Charge.SNHx}$	Ratio of charge to NH_x	1/14	Charge/g N S_{NH}
$i_{Charge.SNO3}$	Ratio of charge to nitrate	−1/14	Charge/g N S_{NO}
$i_{Charge.SPO4}$	Ratio of charge to PO_4	−1.5/31	Charge/g P S_{PO}
$i_{Charge.XPAO.PP}$	Ratio of charge to X_{PP}	−1/31	Charge/g P X_{PP}

Note: Parameters in bold from this thesis. See Meijer (2004) for source of remaining parameters.

Table A8: Kinetic Coefficients

Parameter	Description	Value	Unit
Hydrolysis			
k_h	Hydrolysis rate	$3.0 \cdot e^{0.0406(T-20)}$	
K_X	Half-saturation coefficient for particulate COD	$0.1 \cdot e^{-0.110(T-20)}$	g COD X_S/g COD $X_H + X_{PAO}$
$\eta_{NO.HYD}$	Reduction coefficient for hydrolysis under anoxic conditions	0.8	-
η_{fe}	Reduction coefficient for anaerobic hydrolysis	0.2	-
q_{fe}	Fermentation rate	3	g S_F/g X_H - d
$K_{O.HYD}$	Half-saturation/inhibition coefficient for S_O	0.2	g O_2/m^3
$K_{NO.HYD}$	Half-saturation/inhibition coefficient for S_{NO}	0.5	g N S_{NO}/m^3
Ordinary Heterotrophic Organisms			
μ_H	Maximum heterotrophic growth rate	$6.0 \cdot e^{0.069(T-20)}$	g COD X_H/g COD X_H - d
$\eta_{NO.H}$	Reduction coefficient for anoxic growth of X_H	0.8	-
q_{fe}	Maximum fermentation rate	$3.0 \cdot e^{0.069(T-20)}$	g COD S_F/g COD X_H - d
K_F	Half-saturation coefficient for growth on S_F	4.0	g COD S_F/m^3
K_{Ac}	Half-saturation coefficient for growth on S_A	4.0	g COD S_A/m^3
b_H	Rate constant for decay and lysis of X_H	$0.4 \cdot e^{0.069(T-20)}$	g COD X_H/g COD X_H - d
K_{fe}	Half-saturation coefficient for fermentation of S_F	20.0	g COD X_{SF}/m^3
$K_{O.H}$	Half-saturation/inhibition coefficient for S_O	0.2	g O_2/m^3
$K_{NO.H}$	Half-saturation/inhibition coefficient for S_{NO}	0.5	g N S_{NO}/m^3
$K_{N.H}$	Half-saturation coefficient for ammonium (nutrient)	0.05	g N S_N/m^3
$K_{P.H}$	Half-saturation coefficient for phosphate (nutrient)	0.01	g P S_{PO}/m^3
$K_{HCO.H}$	Saturation coefficient for alkalinity (HCO_3^-)	0.1	mole HCO_3/m^3
Phosphorus Accumulating Organisms			
q_{Ac}	Maximum anaerobic acetate uptake rate	$8.0 \cdot e^{0.090(T-20)}$	g COD S_A/g COD X_{PAO} - d
$q_{Ac.NO}$	Maximum anoxic acetate uptake rate	$1.5 \cdot q_{Ac} \cdot e^{0.090(T-20)}$	g COD S_A/g COD X_{PAO} - d
k_{PP}	Rate constant for polyphosphate formation	$0.10 \cdot e^{0.031(T-20)}$	g P X_{PP}/g COD X_{PAO} - d
g_{PP}	Saturation reduction factor for polyphosphate formation	0.22	-
$f_{PP.max}$	Maximum ratio of X_{PP}/X_{PAO}	0.35	g P X_{PP}/g COD X_{PAO}
K_{fPP}	Half-saturation coefficient for f_{PP} (switch)	0.01	g P X_{PP}/g COD X_{PAO}
k_{GLY}	Glycogen formation rate constant	$0.93 \cdot e^{0.118(T-20)}$	g COD X_{GLY}/g COD X_{PAO} - d
μ_{PX}	**PAO specific growth rate on glycogen**	$\mathbf{0.687 \cdot e^{0.069(T-20)}}$	**g COD X_{PAO}/g COD X_{PAO} - d**
$K_{GLY.PX}$	**Half-saturation coefficient for anoxic glycogen degradation**	**1.0**	**g COD X_{GLY}/g COD X_{PAO}**
$f_{GLY.max}$	Maximum ratio of X_{GLY}/X_{PAO}	0.5	g COD X_{GLY}/g COD X_{PAO}
$K_{PHA.PX}$	**Half-saturation coefficient for anoxic PHA switch**	0.1	**g COD X_{PHA}/g COD X_{PAO}**
K_{fGLY}	Half-saturation coefficient for X_{GLY}/X_{PAO} (switch)	0.01	g COD X_{GLY}/g COD X_{PAO}
K_{fPHA}	Half-saturation coefficient for X_{PHA}/X_{PAO}	0.2	g COD X_{PHA}/g COD X_{PAO}
k_{PHA}	PHA degradation rate constant	$5.51 \cdot e^{0.121(T-20)}$	g COD X_{PHA}/g COD X_{PAO} - d
$\eta_{NO.PAO}$	Reduction factor for denitrifying P removal	0.8	-
m_{OC}	Observed oxygen consumption for maintenance	0.096	g O_2/g COD X_{PAO} - d
m_O	Aerobic maintenance rate (non-NH_4 limited)	$0.06 \cdot e^{0.069(T-20)}$	g COD X_{PAO}/g COD X_{PAO} - d
$m_{O.\varphi}$	**Aerobic maintenance rate (NH_4 limited)**	$\mathbf{0.051 \cdot e^{0.069(T-20)}}$	**g COD X_{PAO}/g COD X_{PAO} - d**
m_{NO}	Anoxic maintenance rate (non-NH_4 limited)	$0.09 \cdot e^{0.069(T-20)}$	g COD X_{PAO}/g COD X_{PAO} - d
$m_{NO.\varphi}$	**Anoxic maintenance rate (NH_4 limited)**	$\mathbf{0.080 \cdot e^{0.069(T-20)}}$	**g COD X_{PAO}/g COD X_{PAO} - d**
m_{AN}	Anaerobic maintenance rate	$0.05 \cdot e^{0.069(T-20)}$	g COD X_{GLY}/g COD X_{PAO} - d
m_{gx}	**Anoxic maintenance rate on glycogen (non-NH_4 limited)**	$\mathbf{0.081 \cdot e^{0.069(T-20)}}$	**g COD X_{GLY}/g COD X_{PAO} - d**
$m_{gx.\varphi}$	**Anoxic maintenance rate on glycogen (NH_4 limited)**	$\mathbf{0.081 \cdot e^{0.069(T-20)}}$	**g COD X_{GLY}/g COD X_{PAO} - d**
$m_{gx.pp}$	**Anoxic maintenance rate on polyphosphate**	$\mathbf{0.207 \cdot e^{0.069(T-20)}}$	**g P X_{PP}/g COD X_{PAO} - d**
K_{Ac}	Half-saturation coefficient for growth on S_A	4.0	g COD S_A/m^3
$K_{O.PAO}$	Half-saturation coefficient for S_O	0.2	g COD S_O/m^3
$K_{NO.PAO}$	Half-saturation coefficient for S_{NO}	0.5	g N S_{NO}/m^3
$K_{NO.PAO.ASIM}$	Half-saturation coefficient for S_{NO} in biomass assmilation	0.5	g N S_{NO}/m^3
$K_{N.PAO}$	Half-saturation coefficient for S_{NH} (nutrient)	0.5	g N S_{NH}/m^3
K_{PO}	Half-saturation coefficient for Poly-P formation	1.0	g P S_{PO}/m^3
$K_{P.PAO}$	Half-saturation coefficient for PO_4 (nutrient)	0.02	g P S_{PO}/m^3
K_{PP}	Half-saturation coefficient for X_{PP} (switch)	0.01	g P/m^3
K_{PHA}	Half-saturation coefficient for X_{PHA} (switch)	0.01	g COD X_{PHA}/m^3
K_{GLY}	Half-saturation coefficient for X_{GLY} (switch)	0.01	g COD X_{GLY}/m^3
$K_{HCO.PAO}$	Half-saturation coefficient for S_{HCO} (switch)	0.01	mole HCO_3/m^3
Autotrophic Organisms			
μ_A	Autotrophic growth rate	$1.0 \cdot e^{0.105(T-20)}$	g COD X_A/g COD X_A - d
b_A	Autotrophic decay rate	$0.15 \cdot e^{0.110(T-20)}$	g COD X_A/g COD X_A - d
$K_{O.A}$	Half-saturation coefficient for oxygen	0.5	g O_2/m^3
$K_{NH.A}$	Half-saturation coefficient for S_{NH}	1.0	g N S_{NH}/m^3
$K_{P.A}$	Half-saturation coefficient for S_{PO}	0.01	g P S_{PO}/m^3
$K_{HCO.A}$	Half-saturation coefficient for S_{HCO}	0.5	g P S_{PO}/m^3

Note: Parameters in bold from this thesis. See Meijer (2004) for source of remaining parameters.

Model Continuity Check

Stoichiometric Parameters

f_{SI}	0
Y_H	0.63
$f_{XI,H}$	0.1
$Y_{PHA,O}$	1.39500088
$Y_{PHA,NO}$	1.72478288
$Y_{PP,NO}$	3.01837004
$Y_{PP,O}$	4.42657059
$Y_{SA,AN}$	1.5
$Y_{SA,NO}$	0.70924925
$Y_{PO,AN}$	0.3480
$Y_{PO,NO}$	0.23
$Y_{GLY,NO}$	1.1780022
$Y_{GLY,O}$	1.11396438
δ	1.85
α	0.334
Y_A	0.24
$f_{XI,A}$	0.1
$i_{N,SF}$	0.03
$i_{N,SI}$	0.01
$i_{N,XI}$	0.03
$i_{N,XS}$	0.03
$i_{N,BM}$	0.07
$i_{P,SF}$	0.01
$i_{P,SI}$	0
$i_{P,XI}$	0.01
$i_{P,XS}$	0.01
$i_{P,BM}$	0.02
$i_{TSS,XI}$	0.75
$i_{TSS,XS}$	0.75
$i_{TSS,PHA}$	0.6
$i_{TSS,BM}$	0.9
$i_{TSS,PP}$	3.23
$i_{TSS,GLY}$	0.84
$i_{NO3,N2}$	2.85714
i_{COD_NO3}	-4.57143
i_{COD_N2}	-1.71429
i_{Charge_SVFA}	-0.01563
i_{Charge_SNHx}	0.07143
i_{Charge_SNO3}	-0.07143
i_{Charge_SPO4}	-0.04839
$i_{Charge\_XPAO,PP}$	-0.03226
Y_{gx}	0.57581
$Y_{gx.no3}$	0.50500
$Y_{PHA,O,NO3}$	2.23190
$Y_{PP,O,NO3}$	7.08410
$Y_{GLY,O,NO3}$	1.11330
$Y_{PHA,NO,NO3}$	1.68900
$Y_{PP,NO,NO3}$	2.90400
$Y_{GLY,NO,NO3}$	1.14900
$Y_{H,NO3}$	0.50400

Stoichiometric Matrix

		S_O	S_F	S_A	S_{NH}	S_{NO}	S_{N2}	S_{PO}	S_I	S_{HCO}	X_I	X_S	X_H	X_{PAO}	X_{PP}	X_{PHA}	X_{GLY}	X_A	X_{TSS}
1	Aerobic hydrolysis		1		0			0	0	*0*		-1							-0.75
2	Anoxic hydrolysis		1		0			0	0	0		-1							-0.75
3	Anaerobic hydrolysis		1		0			0	0	0		-1							-0.75
4	Aerobic growth of X_H on S_F	-0.5873	-1.5873		-0.02238			-0.00413		-0.0014			1						0.9
4b	Aerobic growth of X_H on S_F with NO_3	-0.66413	-1.98413		0.059524	-0.07		-0.00016		0.009259			1						0.9
5	Aerobic growth of X_H on S_A	-0.5873		-1.5873	-0.07			-0.02		0.020769			1						0.9
5b	Aerobic growth of X_H on S_A with NO_3	-0.66413		-1.98413		-0.07		-0.02		0.03697			1						0.9
6	Anoxic growth of X_H on S_F		-1.5873		-0.02238	-0.20556	0.205556	-0.00413		0.013284			1						0.9
6b	Anoxic growth of X_H on S_F with NO_3		-2.30413		0.069124	-0.41444	0.344444	0.003041		0.034393			1						0.9
7	Anoxic growth of X_H on S_A			-1.5873	-0.07	-0.20556	0.205556	-0.02		0.035452			1						0.9
7b	Anoxic growth of X_H on S_A with NO_3			-2.30413		-0.41444	0.344444	-0.02		0.066573			1						0.9
8	Fermentation		-1	1	0.03			0.01		-0.01397									
9	Lysis				0.04			0.01		0.002373	0.1	0.9	-1						-0.15
10	Anaerobic Storage of S_A			-1				0.348		0.010012					-0.348	1.5	-0.5		-0.64404
11	Anaerobic Maintenance							1		-0.01613					-1				-3.23
12	Anoxic storage of S_A			-1		-0.10176	0.101763	0.23		0.019184					-0.23	0.709249			-0.31735
13	Anoxic PHA consumption				-0.04058	-0.14708	0.147076	-0.0116		0.008168				0.579783		-1			-0.0782
13b	Anoxic PHA consumption with NO_3					-0.18422	0.142777	-0.01184		0.013732				0.592066		-1.18946			-0.18082
14	Anoxic Storage of X_{PP}				0.023191	-0.11596	0.115957	-0.99337		0.025748				-0.3313	1				2.931826
14b	Anoxic Storage of X_{PP} with NO_3				0.024105	-0.12052	0.120523	-0.99311		0.026126				-0.34435	1				2.920083
15	Anoxic glycogen formation				0.059423	0.052887	-0.05289	0.016978		-0.00035				-0.84889			1		0.075995
15b	Anoxic glycogen formation with NO_3				0.060923	0.045387	-0.04539	0.017406		0.000267				-0.87032			1		0.05671
16	Anoxic maintenance				0.07	-0.35	0.35	0.02		0.029032				-1					-0.9
16b	Anoxic maintenance w NO_3				0.07	-0.35	0.35	0.02		0.029032				-1					-0.9
17	Aerobic PHA consumption	-0.28315			-0.05018			-0.01434		-0.00289				0.716845		-1			0.045161
17b	Aerobic PHA consumption with NO_3	-0.40858				-0.03136		-0.00896		0.002674				0.448049		-1			-0.19676
18	Aerobic Storage of X_{PP}	-0.22591			0.015814			-0.99548		0.01704				-0.22591	1				3.026682
18b	Aerobic Storage of X_{PP} with NO_3	-0.14116			0.009881			-0.99718		0.016698				-0.14116	1				3.102955
19	Aerobic glycogen formation	0.102305			0.062839			0.017954		0.00362				-0.89769			1		0.032075
19b	Aerobic glycogen formation with NO_3	0.10177			0.062876			0.017965		0.003622				-0.89823			1		0.031593
20	Aerobic maintenance	-1			0.07			0.02		0.004032				-1					-0.9
20b	Aerobic maintenance with NO_3	-1			0.07			0.02		0.004032				-1					-0.9
21	Aerobic growth of X_A	-18.0476			-4.23667	4.166667		-0.02		-0.59927								1	0.9
22	Lysis				0.04			0.01		0.002373	0.1	0.9						-1	-0.15
23	Anoxic glycogen degradation				-0.07	-0.25784	0.257837	-0.02		0.014385				1			-1.73668		-0.55881
24	Anoxic glycogen degradation with NO_3					-0.41307	0.343069	-0.02		0.030473				1			-2.3002		-1.03217
25	Anoxic maintenance on glycogen					-0.35	0.35			0.025							-1		-0.84
26	Anoxic maintenance on glycogen w/NO3					-0.35	0.35			0.025							-1		-0.84
27	Anoxic maintenance on PolyP							1		-0.01613					-1				-3.23

Composition Matrix

	COD	N	P	Charge	TSS
S_{O2}	-1				
S_F	1	0.03	0.01		
S_A	1			-0.01563	
S_{NH}		1		0.071429	
S_{NO}	-4.57143	1		-0.07143	
S_{N2}	-1.71429	1			
S_{PO}			1	-0.04839	
S_I	1	0.01	0		
S_{HCO}				-1	
X_I	1	0.03	0.01		0.75
X_S	1	0.03	0.01		0.75
X_H	1	0.07	0.02		0.9
X_{PAO}	1	0.07	0.02		0.9
X_{PP}			1	-0.03226	3.23
X_{PHA}	1				0.6
X_{GLY}	1				0.84
X_A	1	0.07	0.02		0.9
X_{TSS}					-1

Resulting Matrix

COD	N	P	Charge	TSS
0.00E+00	0.00E+00	0.00E+00	0.00E+00	0.00E+00
0.00E+00	0.00E+00	0.00E+00	0.00E+00	0.00E+00
0.00E+00	0.00E+00	0.00E+00	0.00E+00	0.00E+00
1.11E-16	0.00E+00	0.00E+00	0.00E+00	0.00E+00
0.00E+00	0.00E+00	-3.47E-18	-1.73E-18	0.00E+00
1.11E-16	0.00E+00	0.00E+00	0.00E+00	0.00E+00
0.00E+00	0.00E+00	0.00E+00	0.00E+00	0.00E+00
0.00E+00	0.00E+00	0.00E+00	0.00E+00	0.00E+00
1.11E-16	0.00E+00	0.00E+00	0.00E+00	0.00E+00
0.00E+00	0.00E+00	0.00E+00	0.00E+00	0.00E+00
1.11E-16	0.00E+00	0.00E+00	0.00E+00	0.00E+00
0.00E+00	0.00E+00	0.00E+00	0.00E+00	0.00E+00
0.00E+00	0.00E+00	0.00E+00	0.00E+00	0.00E+00
0.00E+00	0.00E+00	0.00E+00	0.00E+00	0.00E+00
0.00E+00	0.00E+00	0.00E+00	0.00E+00	0.00E+00
0.00E+00	0.00E+00	0.00E+00	1.73E-18	0.00E+00
-1.11E-16	6.94E-18	0.00E+00	0.00E+00	0.00E+00
0.00E+00	6.94E-18	0.00E+00	0.00E+00	0.00E+00
0.00E+00	-1.04E-17	0.00E+00	0.00E+00	0.00E+00
0.00E+00	3.47E-18	0.00E+00	-6.94E-18	0.00E+00
0.00E+00	-6.94E-18	0.00E+00	1.08E-19	0.00E+00
0.00E+00	6.94E-18	0.00E+00	-1.08E-19	0.00E+00
-1.11E-16	0.00E+00	0.00E+00	0.00E+00	0.00E+00
-1.11E-16	0.00E+00	0.00E+00	0.00E+00	0.00E+00
0.00E+00	0.00E+00	0.00E+00	0.00E+00	0.00E+00
0.00E+00	0.00E+00	1.73E-18	0.00E+00	0.00E+00
0.00E+00	0.00E+00	0.00E+00	0.00E+00	0.00E+00
0.00E+00	0.00E+00	0.00E+00	0.00E+00	0.00E+00
0.00E+00	0.00E+00	0.00E+00	0.00E+00	0.00E+00
0.00E+00	0.00E+00	0.00E+00	0.00E+00	0.00E+00
0.00E+00	0.00E+00	0.00E+00	0.00E+00	0.00E+00
0.00E+00	0.00E+00	0.00E+00	0.00E+00	0.00E+00
0.00E+00	-2.78E-16	0.00E+00	0.00E+00	0.00E+00
0.00E+00	0.00E+00	0.00E+00	0.00E+00	0.00E+00
0.00E+00	0.00E+00	0.00E+00	-1.73E-18	0.00E+00
4.44E-16	0.00E+00	0.00E+00	0.00E+00	0.00E+00
-1.11E-16	0.00E+00	0.00E+00	0.00E+00	0.00E+00
-1.11E-16	0.00E+00	0.00E+00	0.00E+00	0.00E+00
0.00E+00	0.00E+00	0.00E+00	0.00E+00	0.00E+00

Appendix B: Synthesis of Biomass from Glucose-6-Phosphate With Nitrate as the Nitrogen Source

The synthesis of biomass by dPAOs on glucose-6-phosphate using nitrate as the nitrogen source is assumed to occur as follows:

$$(1+\eta)\underset{\text{substrate}}{\mathrm{CH_{a2}O_{b2}}} + \alpha_1\,\mathrm{HNO_3} + \alpha_2\,\underset{\text{phosphate}}{\mathrm{H_3PO_4}} + \alpha_3\,\mathrm{ATP} \longrightarrow \underset{\text{biomass}}{\mathrm{CH_{a1}O_{b1}N_{c1}S_{d1}P_{e1}}} + \eta\,\mathrm{CO_2} + \alpha_4\,\mathrm{NADH_2} + \alpha_5\,\mathrm{H_2O}$$

$$\implies (1+\eta)\underset{\text{G6-P}}{\mathrm{CH_2O}} + \alpha_1\,\mathrm{HNO_3} + \alpha_2\,\underset{\text{phosphate}}{\mathrm{H_3PO_4}} + \alpha_3\,\mathrm{ATP} \longrightarrow \underset{\text{biomass}}{\mathrm{CH_{2.09}O_{0.54}N_{0.2}P_{0.015}}} + \eta\,\mathrm{CO_2} + \alpha_4\,\mathrm{NADH_2} + \alpha_5\,\mathrm{H_2O} \quad \text{(B.1)}$$

The coefficient, η, is the CO_2 released from the synthesis of one C-mole of biomass on glucose-6-phosphate. The value of 0.131 C-mole that was used in Section 3.1.2 for growth with ammonia as the substrate is assumed. Therefore:

$$\underline{\underline{\eta = 0.131}}$$

A balance on nitrogen gives:

$$\alpha_1 = \mathrm{c_1} \implies \underline{\underline{\alpha_1 = 0.2}}$$

The coefficient on phosphate is found from a balance on phosphorus:

$$\alpha_2 = \mathrm{e_1} \implies \underline{\underline{\alpha_2 = 0.015}}$$

A balance on oxygen results in:

$$(1+\eta)\mathrm{b_2} + 3\alpha_1 + 4\alpha_2 = \mathrm{b_1} + 2\eta + \alpha_5 \implies \alpha_5 = (1+\eta)\mathrm{b_2} + 3\alpha_1 + 4\alpha_2 - \mathrm{b_1} - 2\eta$$

$$\implies \alpha_5 = (1)(1.131) + 3(0.2) + 4(0.015) - 0.54 - 2(0.131) \implies \underline{\underline{\alpha_5 = 0.989}}$$

A balance on the degree of reduction is used to determine the coefficient on $NADH_2$:

$$(1+\eta)\lambda_s = \lambda_x + \alpha_4\lambda_{nadh} \implies 2\alpha_4 = (1+\eta)\lambda_s - \lambda_x$$

$$\implies \underline{\underline{\alpha_4 = \frac{1}{2}\left[(1+\eta)\lambda_s - \lambda_x\right]}}$$

As was done in Section 3.1.2 for growth using ammonia as the nitrogen source, the coefficient on ATP, α_3 is be expressed in terms of the ATP demand for the formation of biomass monomers, the amount of ATP required for the synthesis of biomass from monomers, and the ATP required to support cellular maintenance. The same values assumed for growth with ammonia as the nitrogen source are used:

$\alpha_m = 0.701$ mol ATP/Cmol	ATP required for synthesis of biomass from glucose-6-phosphate[22]
$\alpha_x = 1.5$ mol ATP/Cmol	ATP required for synthesis of biomass from monomers[22]

The ATP demand for maintenance can be expressed as $\mathrm{m_{ATP}}/\mu$ where $\mathrm{m_{ATP}}$ is the specific ATP demand for maintenance and μ is the specific growth rate. Therefore:

$$\alpha_3 = \left(\alpha_m + \alpha_x + \frac{\mathrm{m_{ATP}}}{\mu}\right)$$

Substitution of the values obtained for the coefficients into Equation B.1 gives:

$$(1+\eta)\underset{\text{G6-P}}{\mathrm{CH_2O}} + 0.2\,\mathrm{HNO_3} + 0.015\underset{\text{phosphate}}{\mathrm{H_3PO_4}} + \left(\alpha_m + \alpha_x + \frac{\mathrm{m_{ATP}}}{\mu}\right)\mathrm{ATP}$$

$$\longrightarrow \underset{\text{biomass}}{\mathrm{CH_{2.09}O_{0.54}N_{0.2}P_{0.015}}} + \eta\,\mathrm{CO_2} + \frac{1}{2}\left[(1+\eta)\lambda_s - \lambda_{x.\varphi})\right]\mathrm{NADH_2} + 0.989\,\mathrm{H_2O}$$